Analysis of sequestration mechanisms in the large milkweed bug, *Oncopeltus fasciatus* (DALLAS, 1852)

Dissertation

zur Erlangung des Doktorgrades der

Naturwissenschaften (Dr. rer. nat.)

Fachbereich Biologie der Fakultät für Mathematik,

Informatik und Naturwissenschaften

an der Universität Hamburg

vorgelegt von

Fee Larika Eleonore Margaretha Meinzer

aus Graben-Neudorf

Hamburg, Januar 2026



Vorsitzender der Prüfungskommission: Prof. Dr. Tobias Lenz

Erstgutachterin: Prof. Dr. Susanne Dobler

Zweitgutachter: Prof. Dr. Christian Lohr

Datum der Disputation: 08. Mai 2026

Table of contents

Abstract 1

Zusammenfassung 2

General Introduction 5

- Plant-herbivore coevolution 5
- Secondary plant metabolites: Cardenolides 5
- Adaptations to cardenolides 9
  - Tolerance mechanism: Target-site insensitivity 9
  - Tolerance mechanism: Permeability barriers 9
  - Resistance mechanism: Biotransformation 10
  - Resistance mechanism: Sequestration 10
- Cardenolide sequestration 11
- The large milkweed bug, *Oncopeltus fasciatus* 12
  - The Na,K-ATPase of *O. fasciatus* 12
  - Cardenolide sequestration in *O. fasciatus* 14
- The ATP-binding cassette (ABC) transporter superfamily 17
  - ABC subfamily B transporter 18
- Objectives of this dissertation 21

Chapter 1

Robust reference gene design and validation for expression studies in the large milkweed bug, *Oncopeltus fasciatus*, upon cardiac glycoside stress 24

- Abstract 24
- Introduction 25
- Material & Methods 27
  - Milkweed bugs and cardiac glycoside injection assay 27
  - RNA extraction and cDNA synthesis 28
  - Reference gene homolog transcriptome search, primer design and evaluation 28
  - Quantitative real-time PCR 31
  - Data analysis and reference gene stability evaluation 31
  - Statistical analysis 32
- Results 33
  - Identification of candidate reference genes and RT-qPCR primer evaluation 33
  - Candidate reference gene expression upon cardiac glycoside challenge over different exposure periods 33

Comprehensive gene expression stability evaluation 35
Discussion 38
Conclusions 42
Chapter 2
Molecular basis of cardenolide sequestration in the large milkweed bug, *Oncopeltus fasciatus* 43
Abstract 43
Introduction 43
Material & Methods 47
Experimental animals 47
Tissue dissections 47
Immunohistochemical staining 48
Monoclonal antibodies 48
Protein extraction and Western blot 49
De novo transcriptome assembly 49
In silico identification of putative ABCB full transporters in *O. fasciatus* 50
Phylogenetic inference 51
Cardenolide injections 51
DNA extraction, RNA extraction and cDNA synthesis 51
Primer design and specificity 52
Standard PCR, sequencing and cloning of putative ABCB full transporter in *O. fasciatus* 52
Quantitative real-time PCR 53
RNA interference 54
Sampling and cardenolide extraction of defensive fluids for HPLC analysis 54
Internal standard multi-level calibration for ouabain quantification 55
High-performance liquid chromatography 55
Data Analysis 56
Results 56
Immuno-detection and subcellular localization of putative ABCB full transporters in *O. fasciatus* 56
Identification of putative ABCB transporters in *O. fasciatus* 58
ABCB-like transcript identification in different transcriptome assemblies 59
Putative OfABCB full transporters in *O. fasciatus* 59
OfABCB1 59
OfABCB2 62
Phylogenetic inference of ABCB proteins 65
Revalidation of reference gene stability 67

Differential systemic and tissue-specific *Ofabcb* transporter expression....68
Constitutive *Ofabcb* transporter gene expression in the presence of cardenolides....70
Efficient knockdown of *Ofabcb* transporter gene expression by RNA interference....70
Functional trade-off between OfABCB transporters with respect to cardenolide sequestration....73
Discussion....75
Conclusion....81
Chapter 3
Insights into sequestration dynamics and related factors in the large milkweed bug, *Oncopeltus fasciatus* (DALLAS, 1852)....83
Abstract....83
Introduction....84
Material and Methods....87
Laboratory animals....87
Defensive fluid sampling and volume quantification....88
Ouabain sequestration assay....88
Cardenolide extraction....88
Cardenolide preparation....89
High-performance liquid chromatography....89
HPLC system I....90
HPLC system II....91
HPLC system III....91
Determination of factors related to the volume of released defensive fluid....91
Immunofluorescence staining and fluorescence quantification of defensive fluids....92
Na,K-ATPase gene expression analysis and immunohistochemistry....92
Statistics....93
Ouabain quantification accuracy by HPLC system I....93
Temporal ouabain sequestration dynamics....94
Analysis of factors possibly related to defensive fluid volume....94
Results....95
Ouabain peak resolution is a function of HPLC starting acetonitrile concentration....95
Dietary cardenolides accumulated in defensive fluids....96
Temporal dynamics of ouabain sequestration....100
Factors related to fluid levels in the thoracic storage compartment....103

Proteins related to cardenolide adaptations in milkweed bug laboratory lines with different diet histories 105
Na,K-ATPase tissue localization and expression response to ouabain 107
Discussion 109
General Discussion and outlook 116
Role of ABC transporter in the sequestration of phytochemicals 117
OfABCB full transporter functions in *O. fasciatus* 121
Function of OfABCB full transporter in the cardenolide transport network of *O. fasciatus* 121
Alternative splicing of *Ofabcb2* 124
Putative substrates of OfABCB full transporters 124
Synthesis on possible sequestration mechanisms mediated by OfABCB full transporters 126
Transcriptional changes by feeding on toxic plants 129
Cardenolide sequestration dynamics in *O. fasciatus* 130
Chemical defense by defensive fluid release in *O. fasciatus* 132
From gene expression to physiological function: Methodological aspects 134
Adaptation strategies to cope with toxic cardenolides: Who needs whom? 136
Interrelation of cardenolide sequestration and Na,K-ATPase insensitivity 137
Outlook 139
References 143
List of abbreviations 168
List of tables 171
Tables 171
Supplementary tables 171
List of figures 173
Figures 173
Supplementary figures 174
Appendix 177
Supplementary tables 177
Supplementary figures 223
Additional files 246
List of publications 246
Acknowledgments 246
Contribution and Declaration on Oath 248

Abstract

The coevolution of plants and herbivorous insects over several hundred million years has driven an astonishing diversity of plant defense strategies and counterstrategies of their herbivores. Herbivore adaptations to toxic cardenolide-producing plants involve tolerance mechanisms like target-site (Na,K-ATPase) insensitivity or permeability barriers as well as resistance mechanisms like biotransformation, excretion and sequestration. Sequestration into compartments is a widespread strategy in insects to cope with the chemical defenses of their host plants and is the crucial adaptation that escalates the evolutionary arms race to the third trophic level. While sequestration has evolved convergently in members of all six insect orders that have specialized on cardiac glycoside-producing plants, little is known about the underlying molecular mechanisms. *Oncopeltus fasciatus* (DALLAS, 1852) is among the best-characterized species with regard to its adaptation to cardenolides, especially in terms of target-site insensitivity, biotransformation, and sequestration physiology. However, even in this species the molecular key components and mechanisms for sequestration are unknown. Yet, characterization of molecular components of the sequestration system is crucial for understanding its evolution, and the list of plant defense compound transporters in specialized insects is still extremely short.

In this dissertation, I characterize the presence and function of ATP-binding cassette (ABC) subfamily B full transporters in cardenolide sequestration in *O. fasciatus*, which have long been considered prime candidates for cardenolide transport. Recently, it was shown that insect ABCB full transporters are activated by and transport cardenolides in vitro. Transcriptome, gene expression, and immunohistochemical analyses were combined with RNA interference in this thesis to define the role of ABCB full transporters in cardenolide sequestration, which had remained unaddressed to date. In a first step towards this characterization, ten reference genes, which were lacking for the milkweed-bug-system at that time, were identified. *Ofef1a* and *Oftubulin* were evaluated as the most suitable normalizers upon temporal cardenolide challenge by comprehensive stability algorithm analysis (Bestkeeper, Normfinder, geNorm, comparative ΔCt method). While there are no universal stable reference genes, revalidation across multiple treatments, like diet or tissues, shows that the *Ofef1a* gene comes very close to this state. Along these lines, a robust approach to RT-qPCR primer design for organisms with unannotated genomes is shown. In addition, insights into stability evaluation in multifactorial experimental designs are given, as time-scaled analyses can be particularly important in ABC transporter research.

My combined in vivo and in vitro analyses provide the first evidence that ABCB full transporters are tightly associated with cardenolide sequestration in *O. fasciatus*. Of the two OfABCB full transporters identified in *O. fasciatus*, OfABCB1 was indispensable for ouabain sequestration capacity, unlike OfABCB2. The knockdown of *Ofabcb1* by RNA interference resulted in a significant drop in sequestration capacity by up to 70 % in vivo. Its enrichment in tissues important for tolerance to and resistance against cardenolides suggests a pleiotropic role: on the one hand as the evolutionarily conserved chemoprotective barrier, and on the other hand through the acquisition of a new function in sequestration. The enigmatic role of its homolog, OfABCB2, in the cardenolide transport network is an open question to be addressed. Yet, my data suggest that this gene is under complex transcriptional control, potentially diversifying its functions and enabling adaptive flexibility.

Subsequent investigations on ouabain sequestration capacity and dynamics in milkweed bug lines long-term acclimatized to different diets (cardenolide-free and -containing) suggest robustness, but also plasticity of cardenolide storage in *O. fasciatus*, which is to a certain degree detached from defensive fluid accumulation. Chemical and pilot immunohistological analyses suggest that this plasticity in sequestration is related to nutritional and molecular mechanisms involving ABCB full transporter proteins. Yet, the two OfABCB transporters as well as dietary cardenolides were not mandatory for defensive fluid accumulation, the underlying mechanism of which remains poorly understood. My investigations show that factors like biomass, sex, female age and to some degree also stored cardenolide amount are associated with released defensive fluid volumes and hence likely with defensive efficacy of *O. fasciatus*. The extensive absence of cardenolide target-sites (Na,K-ATPase) in defensive fluid cells indicated by immunohistochemistry suggests further a safe toxin storage by removal from the metabolism. This likely releases *O. fasciatus* from toxicity constraints in sequestration known for certain cardenolides. These findings along with the overexpression of one of its insensitive Na,K-ATPase paralogs (α1A) on the total mRNA level upon ouabain accumulation suggest a close interrelation between sequestration and Na,K-ATPase insensitivity in *O. fasciatus*.

Zusammenfassung

Die Koevolution zwischen Pflanzen und herbivoren Insekten über Millionen von Jahren führte zu einer erstaunlichen Vielfalt an Abwehrstrategien bei Pflanzen und entsprechenden Gegenanpassungen von Herbivoren. Anpassungen an giftige cardenolidhaltige Pflanzen beinhalten sowohl Toleranzmechanismen, wie die Wirkort-Unempfindlichkeit (der Na,K-

ATPase) gegenüber dem Toxin oder Permeabilitätsbarrieren, als auch Resistenzmechanismen, wie Biotransformation, Exkretion und Sequestration. Die Sequestration in Körperkompartimente ist eine weitverbreitete Strategie bei Insekten, um die chemische Wirtspflanzenabwehr zu überwinden und stellt die kritische Anpassung dar, die das evolutionäre Wettrüsten auf die dritte trophische Ebene eskalieren lässt. Trotz der konvergenten Evolution von Sequestration in Mitgliedern aller sechs Insektenordnungen, die sich auf herzglykosidhaltige Pflanzen spezialisiert haben, sind die zugrundeliegenden molekularen Mechanismen noch unzureichend verstanden. *Oncopeltus fasciatus* (DALLAS, 1852) gehört zu den am besten charakterisierten Arten in Hinblick auf seine Anpassungen an Cardenolide, besonders bezüglich der Wirkort-Unempfindlichkeit, der Biotransformation und der Speicherungsphysiologie. Jedoch selbst in dieser Art sind die molekularen Schlüsselkomponenten der Sequestration bislang unbekannt. Gleichzeitig ist die Charakterisierung solcher Sequestrations-System-Komponenten essentiell für das Verständnis ihrer Entstehung und die Liste an Pflanzenabwehrstoff-transportierenden Proteinen in spezialisierten Insekten ist insgesamt immer noch überaus kurz.

In dieser Dissertation charakterisiere ich das Vorhandensein von „ATP-binding cassette“ (ABC) Volltransportern der Unterfamilie B, welche schon länger als Spitzenkandidaten für den Cardenolid-Transport angesehen werden, und deren Funktion in der Cardenolidspeicherung bei *O. fasciatus*. Kürzlich wurde in vitro gezeigt, dass ABCB-Volltransporter von Insekten durch Cardenolide aktiviert werden und diese transportieren. Um die noch ausstehende Rolle von ABCB-Volltransportern im Cardenolid-Sequestrationsprozess zu bestimmen, wurden in dieser Thesis Transkriptom-, Genexpression- und immunhistochemische Untersuchungen mit RNA-Interferenz kombiniert. Als einen ersten Schritt hin zu dieser Charakterisierung wurden zehn Referenzgene identifiziert, die bis zu diesem Zeitpunkt für das Milchkrautwanzen-System fehlten. *Ofef1a* und *Oftubulin* wurden als die am besten geeigneten Referenzgene zur Normalisierung der Expression bei unterschiedlicher Cardenolid-Expositions-Dauer mittels umfassenden Stabilitäts-Algorithmen-Analysen bestimmt (Bestkeeper, Normfinder, geNorm, komparative ΔCt Methode). Während es keine universell gültigen Referenzgene gibt, kommt das *Ofef1a*-Gen dem schon sehr nahe, wie die Revalidierung über weitere verschiedene Zustände, einschließlich Nahrung und Gewebe, zeigt. In diesem Zusammenhang wird auch ein robuster Ansatz für das RT-qPCR-Primer-Design in Organismen mit noch nicht annotierten Genomen gezeigt. Ein zusätzlicher Fokus richtet sich auf die Stabilitätsevaluation in multifaktoriellen Versuchen, da zeitlich skalierte Untersuchungen bei der Forschung zu ABC-Transportern von besonderer Bedeutung sein können.

Meine Kombination aus in vivo und in vitro Untersuchungen liefert erste Beweise, dass ABCB-Volltransporter eng mit der Cardenolid-Sequestration in *O. fasciatus* in Verbindung stehen. Von den beiden identifizierten OfABCB-Transportern war OfABCB1 für die Speicherkapazität von Ouabain unersetzlich im Gegensatz zu OfABCB2. Die Herunterregulation der *Ofabcb1*-Expression mittels RNA-Interferenz bedingte Abfälle in der Speicherkapazität bis zu 70 % in vivo. Seine Dominanz in Geweben, die wichtig für die Toleranz für und die Resistenz gegen Cardenolide sind, deutet auf eine pleiotrope Rolle dieses Gens hin: Zum einen als evolutionär konservierte biochemische Schutzbarriere und zum anderen mit neuer Funktion in der Sequestration. Die rätselhafte Rolle des homologen Gens, OfABCB2, im Cardenolid-Transport-Netzwerk ist eine offene Frage, die noch geklärt werden muss. Gleichzeitig deuten meine Daten darauf hin, dass dieses Gen unter einer komplexen transkriptionellen Kontrolle steht, was möglicherweise Funktionen diversifiziert und adaptive Flexibilität ermöglicht.

Nachfolgende Untersuchungen zu Ouabain-Speicherkapazität und -dynamiken in zwei an unterschiedliche Nahrung langzeitakklimatisierten Milchkrautwanzen-Laborlinien (cardenolid-frei und -beinhaltend) legen die Robustheit des Sequestrationsprozesses nahe, aber gleichzeitig auch dessen Plastizität, was bis zu einem gewissen Grad von der Akkumulation des Abwehrsekretes losgelöst ist. Chemische Analysen und ein immunhistochemischer Pilotversuch deuten darauf hin, dass die Sequestrationsplastizität in Zusammenhang mit nahrungsbedingten und molekularen Mechanismen unter Beteiligung von ABCB-Volltransportern steht. Beide OfABCB-Transporter, wie auch Cardenolide aus der Nahrung, waren aber nicht für die Ansammlung von Abwehrflüssigkeit zwingend erforderlich, deren zugrundeliegender Mechanismus nach wie vor unzureichend verstanden ist. Meine Untersuchungen zeigen, dass mehrere Faktoren, wie Biomasse, Geschlecht, das Alter von Weibchen und bis zu einem gewissen Grad auch die gespeicherte Cardenolidmenge in Verbindung mit dem freigesetzten Abwehrsekretvolumen stehen. Damit stehen sie wahrscheinlich auch mit der Wirksamkeit der Abwehr von *O. fasciatus* in Zusammenhang. Die weitgehend immunhistochemische Abwesenheit des Cardenolid-Wirkortes (der Na,K-ATPase) in den Zellen des Abwehrsekrets deutet des Weiteren auf eine kompartimentierte und somit sichere Toxin-Speicherung durch den Entzug aus dem Metabolismus hin. Das vermeidet in *O. fasciatus* wahrscheinlich bestimmte Toxizitätsbeschränkungen in der Sequestration wie es für bestimmte Cardenolide bekannt ist. Zusammen mit der Überexpression des unempfindlichen Na,K-ATPase-Paralogs, α1A, auf Gesamt-mRNA-Niveau bei Ouabain-Akkumulation, deuten diese Erkenntnisse auf eine enge Verbindung zwischen Sequestration und Na,K-ATPase-Unempfindlichkeit in *O. fasciatus* hin.

General Introduction

Plant-herbivore coevolution

Insects are predicted to be the most diverse terrestrial group of the eukaryotic kingdom on earth (~5,000,000) followed by fungi (~611,000) and plants (~298,000) (Chapman, 2009; Mora et al., 2011). More than one third of known insect species share a common feeding strategy, namely phytophagy (Chapman, 2009; Mitter et al., 1991), which is especially prominent in the orders Lepidoptera, Orthoptera and Hemiptera (Wiens et al., 2015) and in the largest groups within the Coleoptera (Farrell, 1998). The coevolution of herbivorous insects and plants for several hundred million years has been suggested as one of the main drivers of their radiation. According to Misof et al. (2014), for example, diversifications within three insect orders (Diptera, Lepidoptera, Hymenoptera) occurred concurrently with the radiation of angiosperms. While the driving role of herbivorous-insect-plant-coevolution on species radiation is still the subject of controversial debate, plants clearly evolved a magnificent array of defenses to deter herbivores from feeding (Farrell, 1998; Mithöfer and Boland, 2012; Mitter et al., 1991; War et al., 2012; Wiens et al., 2015). Those encompass “escape in time and space” strategies (Ralph, 1976), changes in morphology, physiology and biochemistry within plants themselves, and also conspecific warnings or enticement of their herbivores' enemies by volatiles (for review see Mithöfer and Boland, 2012; War et al., 2012).

Challenged by the defensive battery of their hosts, phytophagous insects evolved at the same time “counter-adaptations” to circumvent their hosts’ elaborate defensive systems (Ehrlich and Raven, 1964). Behavioral switches to overcome morphological barriers or physiological ones, like indigestibility or toxicity, can be considered the most rapid and obvious adaptations. However, those might be limited in terms of energetic value, being essential for species persistence. Hence, it is hardly surprising that insects evolved profound molecular, physiological, and morphological adaptations to cope with their host plants' defenses (reviewed by Després et al., 2007; Futuyma and Keese, 1992).

Secondary plant metabolites: Cardenolides

The chemical plant defense by secondary metabolites is especially intriguing given the fact that plants synthesize more than 51 thousand different compounds belonging to diverse chemical classes, often associated with toxic effects (Mithöfer and Boland, 2012). Cardiac glycosides, also referred to as heart poisons, are one class of potent toxins among those

(Brower, 1969; Euw et al., 1967; Sticher, 2010). Cardiac glycosides comprise two different compound classes: cardenolides and bufadienolides. Both share an androstane backbone (more precisely, a perhydrophenanthrene nucleus) but differ in the lactone ring bound at C17 (cardenolides: β-bound butanolide ring, bufadienolides: β-bound pentadienolide ring) and hence in their aglycone (cardenolide (C_{23}-steroids) versus bufanolide (C_{24}-steroids)) (Agrawal et al., 2012; Krenn and Kopp, 1998; Luckner and Wichtl, 2000; Malcolm, 1991; Steyn and van Heerden, 1998; Sticher, 2010) (Figure 1).

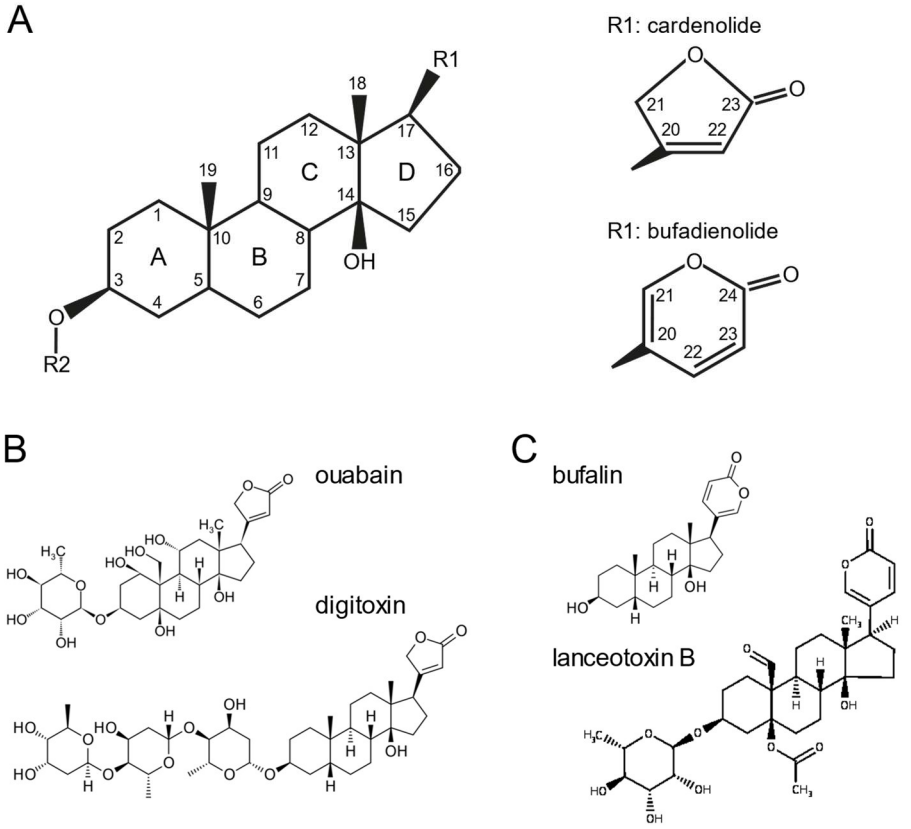


Figure 1 Chemical structure of cardiac glycosides. A: Basic cardiac glycoside structure. In the aglycone (= four-cyclic steroid backbone plus monounsaturated five-membered or diunsaturated six-membered lactone ring (R1) bound at C17) A and B rings are either cis or trans configured while C and D rings have a cis-conformation. In genins, R2 corresponds to a bound hydrogen atom and hence a conjugated hydroxyl group, while in glycosides one or more sugar molecules are conjugated with the aglycone. B illustrates cardenolide glycoside examples as follows: ouabain with its α-L-rhamnoside bound at C3 and digitoxin conjugated with three sugar residues with β-D stereochemistry (digitoxose) at C3 of its aglycone digoxigenin. C shows examples of bufadienolides: the genin, bufalin, and the glycoside, lanceotoxin B. Note that A represents the common chemical structure of cardiac glycosides. Conjugations with different chemical atoms or groups (e.g. hydrogen, aldehyde-, acetoxy-, epoxy-, hydroxy-, hydroxymethyl-, oxo-, or methoxide groups) have been observed at multiple positions of the aglycone (e.g. C1, C2, C5, C6, C8, C10, C11, C12, C15, C16, C19) as well as different double bonds within cyclic rings resulting in an extraordinary diversity of more than 500 different compounds (Agrawal et al., 2012; Krenn and Kopp, 1998; Luckner and Wichtl, 2000; Malcolm, 1991; Steyn and van Heerden, 1998; Sticher, 2010).

In general, synthesis of these highly diverse chemicals (> 500) occurs predominantly, but not exclusively in plants (at least 14 families, 73 genera). In fact, cardiac glycosides are de novo synthesized also in animals, yet this is restricted to fewer taxa (at least three families, 11 genera). While cardenolide synthesis is more widespread compared to bufadienolides (Table 1), both compound classes reveal similar chemical diversities (cardenolides: ~200, bufadienolides: > 250) (Agrawal et al., 2012; Krenn and Kopp, 1998; Luckner and Wichtl, 2000; Malcolm, 1991; Mithöfer and Boland, 2012; Pasteels, 1993; Pasteels et al., 1995; Steyn and van Heerden, 1998; Sticher, 2010). More importantly, they share similar physiological effects on animals, tightly associated with their toxicity: the selective inhibition of the sodium-potassium pump (Na,K-ATPase) (Agrawal et al., 2012; Horisberger, 2004; Lingrel et al., 1990; Steyn and van Heerden, 1998; Sticher, 2010). The Na,K-ATPase is an essential energy-driven ion-antiporter in animals, maintaining the neurons' resting potential and hence excitability, but is also involved in many further cellular signaling and regulatory processes (for a current review, see Blaustein and Hamlyn, 2024). Inhibition of this enzyme induces profound molecular, biochemical, and physiological alterations, which can be fatal (Brower, 1969; Klimanova et al., 2017; Koltsova et al., 2012; Perne et al., 2009; Sticher, 2010).

Nonetheless, more than 100 specialized herbivores belonging to six insect orders (Orthoptera, Hemiptera, Hymenoptera, Coleoptera, Diptera, Lepidoptera) naturally explore these noxious plants (for a recent review, see Agrawal et al., 2024b). Yet, these insect orders span 290 million years or more of independent evolution (Orthoptera ~390 Myr, Hemiptera ~373 Myr, Hymenoptera ~350 Myr, Coleoptera ~330 Myr, Diptera & Lepidoptera ~290 Myr) (Misof et al., 2014). Hence, the "cardiac glycoside herbivore system" has become one of the most intensively studied models to understand specific adaptations evolved by insects to cope with their host plants' chemical defense (for a review, see also Birnbaum and Abbot, 2018; Dobler et al., 2015).

Table 1 Overview of cardiac glycoside occurrence in different plant and animal families. Bufadienolides occur in 6 angiosperm plant families (11 genera)[a,b,f,g] while cardenolides occur in at least 10 families (62 genera; > 50 % in Apocynaceae)[e-h]. In contrast, de novo cardiac glycoside production is limited to a few animal taxa[a-d]. Note that only taxa in which autogenous synthesis has been previously described in the context of chemical defense are listed. Hence, snakes and mammals were excluded: Bufadienolides in snakes (*Rhabdophis* sp.)[a,b] have been exclusively linked to dietary accumulation so far[i,j]; in mammals, endogenous cardiac glycosides serve a different purpose (e.g. endocrine functions)[h]. Species names and systematic classifications were checked using the Global Biodiversity Information Facility database (December 2025) and were adjusted if applicable.

	Taxon	Family	Genera	
Bufadienolides	Vertebrata[a,b]	Bufonidae	6	*Anaxyrus, Bufo, Bufotes, Duttaphrynus, Phrynoidis, Rhinella*
	Insecta[a,b]	Lampyridae	1	*Photinus*
	Angiosperms[a,b,f,g]	Asparagaceae	3	*Bowiea, Drimia, Fusifilum*
		Crassulaceae	3	*Cotyledon, Tylecodon, Kalanchoe*
		Iridaceae	1	*Moraea*
		Melianthaceae	2	*Bersama, Melianthus*
		Ranunculaceae	1	*Helleborus*
		Thesiaceae	1	*Thesium*
Cardenolides	Insecta[c,d]	Chrysomelidae	4	*Calligrapha, Chrysolina, Oreina, Zygogramma*
	Angiosperms[e-h]	Apocynaceae	38	*Adenium, Acokanthera, Anodendron, Apocynum, Asclepias, Aspidoglossum, Alstonia, Beaumontia, Calotropis, Carissa, Cerbera, Cryptolepis, Cryptostegia, Glossostelma, Gomphocarpus, Gongronema, Gonolobus, Holarrhena, Kanahia, Leptadenia, Matelea, Marsdenia, Mandevilla, Melodinus, Nerium, Pachycarpus, Parquetina, Pentalinon, Pentopetia, Pergularia, Periploca, Pervillaea, Plumeria, Picralima, Rauvolfia, Strophantus, Thevetia, Vallaris, Xysmalobium*
		Asparagaceae	4	*Convallaria, Polygonatum, Rohdea, Ornithogalum*
		Brassicaceae	4	*Conringia, Erysimum, Hesperis, Syrenia*
		Celastraceae	3	*Elaeodendron, Euonymus, Lophopetalum*
		Euphorbiaceae	1	*Mallotus*
		Fabaceae	1	*Coronilla*
		Malvaceae	2	*Corchorus, Mansonia*
		Moraceae	7	*Antiaris, Antiaropsis, Castilla, Dorstenia, Maquira, Naucleopsis, Ogcodeia, Streblus*
		Plantaginaceae	1	*Digitalis*
		Ranunculaceae	1	*Adonis*

[a] Krenn and Kopp (1998); [b] Steyn and van Heerden (1998); [c] Pasteels (1993); [d] Pasteels et al. (1995); [e] Agrawal et al. (2012); [f] Luckner and Wichtl (2000); [g] Malcolm (1991); [h] Sticher (2010); [i] Mori et al. (2012); [j] Mohammadi, pers. communication.

Adaptations to cardenolides

Specialization on cardenolide-synthesizing host plants has 28 origins across six insect orders: Orthoptera, Hemiptera, Hymenoptera, Coleoptera, Diptera, Lepidoptera. The research on insects' adaptations to dietary cardenolides over more than 100 years has unraveled a complex diversity of adaptations with sometimes striking parallelism. Adaptations evolved to cope with the potent neurotoxicity of host-plant-derived cardenolides include target-site insensitivity, permeability barriers, biotransformation, and sequestration (Agrawal et al., 2024b; Birnbaum and Abbot, 2018; Dobler et al., 2015; Petschenka et al., 2013b). These adaptations are classified as either tolerance or resistance mechanisms dependent on chemical cardenolide modification and transport degree (Jeckel et al., 2022).

Tolerance mechanism: Target-site insensitivity

The nervous systems of several specialized insect species are highly insensitive to cardenolides (Bramer et al., 2015; Moore and Scudder, 1986; Petschenka et al., 2013a; Vaughan and Jungreis, 1977). Molecular studies of the Na,K-ATPase α-subunit, where the "binding pocket" for cardenolides is located (Laursen et al., 2015; Qiu et al., 2005; Yatime et al., 2011), revealed that this is attributable to distinct amino acid exchanges paired with Na,K-ATPase gene duplication events in four of the six insect orders specialized on cardiac glycoside-producing plants (Coleoptera, Diptera, Orthoptera, and Hemiptera) (Agrawal et al., 2024b; Dalla et al., 2013; Dobler et al., 2012; Dobler et al., 2015; Petschenka et al., 2013a; Petschenka et al., 2017; Zhen et al., 2012). In addition, tissue distribution of such paralogs varies intra- and interspecifically indicating different requirements for toxin insensitivities (Dobler et al., 2019; Lohr et al., 2017; Yang et al., 2019; Zhen et al., 2012).

Tolerance mechanism: Permeability barriers

The intestine is the first barrier which ingested cardenolides must overcome to unfold their toxicity within organisms. Dietary cardenolides are not only spatio-temporally diverse in number and quantity, but also in their polarity (Agrawal et al., 2012; Moore and Scudder, 1985; Rasmann and Agrawal, 2011). The polarity of a cardenolide determines its ability to passively cross the cellular lipid bilayer: the less polar it is, the higher is its presumed passive diffusion capacity (Agrawal et al., 2012; Malcolm, 1991; Sticher, 2010). Hence, especially apolar cardenolides have been deemed toxic as those cannot be trapped by cellular compartmentalization (Agrawal et al., 2012; Malcolm, 1991; Rasmann and Agrawal, 2011). A measure of the apolarity of a substance is the LogP value, which can be directly determined

or predicted (XLogP3), and is available in databases such as PubChem. It is calculated as the logarithm of the n-octanol-water partition coefficient, whereby positive values indicate lipophilicity and negative hydrophilicity. It can therefore be used to estimate the passive diffusivity of cardenolides, which can be an important factor for their biological activity (Kim et al., 2025; Pádua et al., 2022; Rutkowska et al., 2013). Despite the wide cardenolide polarity range in *Asclepias* species (Agrawal et al., 2012; Moore and Scudder, 1985; Rasmann and Agrawal, 2011), several specialized and generalized insects have been shown to possess impermeable intestines that limit the neurotoxic effects of cardenolides (Groen et al., 2017; Petschenka and Agrawal, 2015; Scudder and Meredith, 1982b; Wink and Schneider, 1990). While impermeable guts might be the first barrier for cardenolides in several insects, it is not the only one. Previous studies also suggest that the blood-brain barrier, or more precisely the hemolymph-brain barrier, is an effective diffusion barrier protecting sensitive nervous systems against cardenolides with varying efficacy across insect species (Moore and Scudder, 1986; Petschenka et al., 2012; Petschenka et al., 2013b).

Resistance mechanism: Biotransformation

Biotransformation is often used by specialized insects to detoxify noxious secondary plant metabolites. In addition, metabolic alterations can also facilitate toxin transport for excretion or sequestration (Birnbaum and Abbot, 2018; Després et al., 2007; Dobler et al., 2011). Biotransformation is thus closely linked to the transport of cardenolides.

Resistance mechanism: Sequestration

Sequestration refers to complex processes including secondary plant metabolite absorption, biotransformation, accumulation and storage (Duffey, 1980; Erb and Robert, 2016; Opitz and Müller, 2009; Petschenka and Agrawal, 2016). The ability to sequester toxins has been repeatedly observed among phytophagous insects. To date, more than 275 insect species are known to store host-plant-derived phytochemicals, while the sequestration purpose and adjunctive fate are tightly connected with their chemical nature (Agrawal et al., 2024b; Beran and Petschenka, 2022; Després et al., 2007; Opitz and Müller, 2009). In the first instance, toxin accumulation at specific sites can be considered an effective avoidance mechanism. However, toxin accumulation within the body provides a major additional advantage: unpalatability to predators (Després et al., 2007; Duffey, 1980; Opitz and Müller, 2009). It is therefore an important physiological ability for the escalation at the tritrophic level during coevolution (Malcolm, 1991; Petschenka and Agrawal, 2015, 2016).

Cardenolide sequestration

The sequestration of cardiac glycosides has been demonstrated in members belonging to all six insect orders which exploit plants synthesizing these noxious substances (Coleoptera, Diptera, Lepidoptera, Orthoptera, Hemiptera, Hymenoptera) and is tightly associated with aposematic coloration and interrelated with target-site insensitivity (Agrawal et al., 2024b; Beran and Petschenka, 2022). The so-called cardenolide "sequestering specialist syndrome" is a prime example of convergent evolution. It describes that cardenolide-sequestering species are aposematically colored and a certain degree of Na,K-ATPase insensitivity seems to be a prerequisite for sequestration, though one exception of that rule exists (*Diabrotica nummularis* (Harold 1877): Chrysomelidae: Coleoptera). Along these lines, it is important to note that this interrelation is not bi-directional, as some non-sequestering species also accommodate target-site insensitivities (Agrawal et al., 2024b).

Within the Hemiptera, this syndrome is ancestral to the subfamily Lygaeinae (about 550 species; also known as milkweed, seed, or ground bugs) (Bramer et al., 2015). This subfamily belongs to the family Lygaeidae (SCHILLING, 1829; about 1033 species (GIBF September 2023)), a family where chemical ecology is a key part of biology and which is furthermore characterized by many pest species and a diverse predator spectrum (summarized by Burdfield-Steel and Shuker, 2014). Many insects of the Lygaeinae are brilliantly, aposematically colored, and almost half of the described genera include at least one member for which cardenolide accumulation has been demonstrated (Beran and Petschenka, 2022; Bramer et al., 2015; Scudder and Duffey, 1972). The sequestration of host-plant-derived cardenolides is an effective chemical protection for milkweed bugs against various predators like spiders, mantids, lacewings, and birds (Berenbaum and Miliczky, 1984; Bramer et al., 2018; Hill, 2006; Newcombe et al., 2013; Petschenka et al., 2022; Pokharel et al., 2020). The degree of chemical protection is related to the quality and source of stored toxins in milkweed bugs, in which varying degrees of dietary specialization and host plant switches are known (Bramer et al., 2015; Petschenka et al., 2022; Pokharel et al., 2020). Some lygaeids have been found to accumulate the highest amounts of ingested dietary cardenolides (up to 900 µg) known in sequestering insects (Agrawal et al., 2012; Scudder et al., 1986). Among those, the large milkweed bug, *Oncopeltus fasciatus* (DALLAS, 1852), is the best-studied species in chemical ecology and most other evolutionary and developmental biology fields (Burdfield-Steel and Shuker, 2014). Moreover, this species is a prime example for cardenolide-associated adaptations besides the monarch butterfly, *Danaus plexippus* (LINNAEUS, 1758; Nymphalidae: Lepidoptera) (Beran and Heckel, 2024).

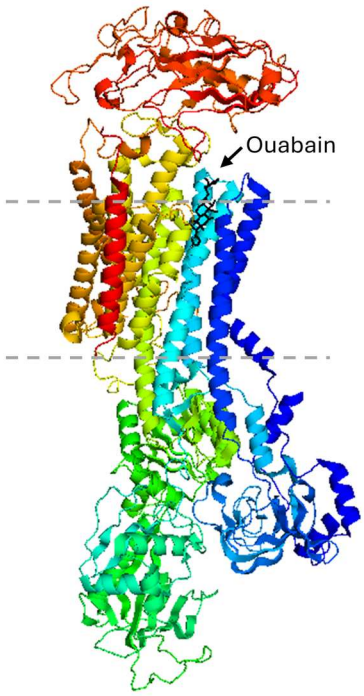
The large milkweed bug, *Oncopeltus fasciatus*

The large milkweed bug, *Oncopeltus fasciatus* (DALLAS, 1852), is distributed in North, Central and South America (summarized by Feir, 1974). The species is a laboratory model animal with long tradition. It is easy to rear and amenable to a diversity of molecular techniques such as RNA interference (RNAi). Furthermore, it has been regarded as a representative of Hemimetabola and its genome has been sequenced (Feir, 1974; Liu and Kaufman, 2009; Panfilio et al., 2019). More importantly, the life cycle of this hemimetabolous insect is tightly connected with its milkweed hosts of the genus *Asclepias* spp. (Apocynaceae: Angiosperms). In contrast to monarch butterflies, whose caterpillars exclusively feed on the poisonous host plants, the large milkweed bug feeds on milkweeds throughout its life, i.e. from nymph to adult (Miller and Dingle, 1982; Ralph, 1976). On their milkweed hosts, insects preferentially feed on seeds (Chaplin, 1980; Eggermann and Bongers, 1971; Ralph, 1976), which contain especially high cardenolide amounts (Agrawal et al., 2012; Duffey, 1970; Vaughan, 1979).

The Na,K-ATPase of *O. fasciatus*

The large milkweed bug is thus highly insensitive to these bitter-tasting, noxious substances, tolerating more than thousandfold the LD_{50} dose of ouabain for non-adapted insects (Moore and Scudder, 1986). The resistance of its nervous system, the major target-site for cardenolide neurotoxic actions, even exceeds that of the monarch butterfly tenfold (Bramer et al., 2015). As outlined before, target-site insensitivity to cardenolides is mediated by amino acid alterations of the Na,K-ATPase. Significant alterations shared with other insects associated with Apocynaceae members, like *D. plexippus*, include, for example, the amino acid substitutions at positions 111 and 122 in the extracellular loop of the Na,K-ATPase α1-subunits (Figure 2) (Agrawal et al., 2024b; Dobler et al., 2012; Yang et al., 2019; Zhen et al., 2012). In vitro analyses of *Drosophila* Na,K-ATPase α1-subunit mimics showed that the single exchange at position 122 (asparagine → histidine) for example potentiates resistance up to 25-fold and synergistically, with that at position 111 (glutamine → valine), even more (> 2000-fold) (Dalla et al., 2013). Moreover, *O. fasciatus'* Na,K-ATPase underwent three gene duplication events, resulting in four Na,K-ATPase α1-subunit paralogs in total (α1D → α1C → α1A, α1B). Each paralog acquired additional substitutions compared to its ancestor, α1D (Yang et al., 2019; Zhen et al., 2012) (Figure 2). These mediate different insensitivities (α1C < α1A < α1B) and ion-pumping activities (α1A ≤ α1B < α1C) of the α1-subunits, which are further fine-tuned by combination with one of the four Na,K-ATPase β-subunit paralogs in *O. fasciatus* (β1, β2, β3, βx) (Figure 2) (Dalla et al., 2013; Dalla et al., 2017; Dalla and Dobler, 2016; Herbertz et al.,

2024). The cardenolide insensitive Na,K-ATPase α1-subunit paralogs (α1A, α1B) are essential for *O. fasciatus* to be able to tolerate and survive exposures to cardenolides (Lohr et al., 2017). A further physiological role of this enzyme in *O. fasciatus* is suggested in the formation of septate junctions (Herbertz et al., 2025) and hence in the regulation of tissue tightness and compartmentalization.



		Amino acid positions with confirmed function in cardenolide insensitivity[a]					
Paralog[b,c]	Mya[c]	111	122	786	797	IC_{50} (ouabain)[d]	Tissue with major expression[e]
α1B	60	T	H	N	T	2.1E-03 - 7.1E-03	Ovary, Malpighian Tubules
α1A	60	T	H	N	A	3.5E-04 - 2.6E-05	Malpighian Tubules
α1C	125	Q	H	F	S	4.3E-04 - 7.6E-04	Nervous system
α1D		Q	H	F	T		

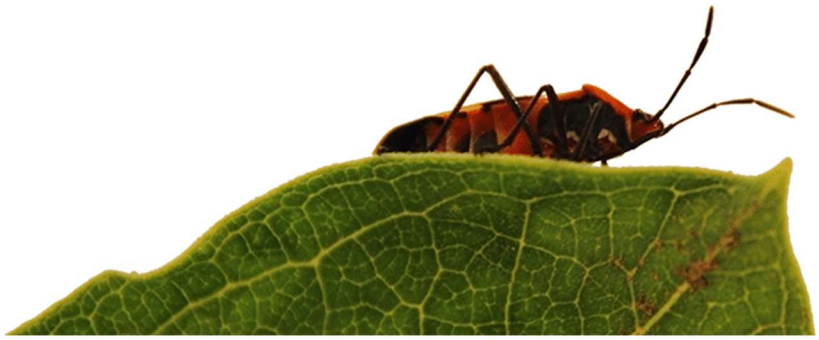


Figure 2 Ouabain binding in pig Na,K-ATPase (left) and characteristics of Na,K-ATPase paralogs in *O. fasciatus* (right). Pig Na,K-ATPase 3D secondary structure (entry: 7WYT, Kanai et al. (2022)) was retrieved from Research Collaboratory for Structural Bioinformatics RCSB database (Berman et al., 2000). Visualization was conducted with PyMOL (Version 3.0) (Schrödinger). Grey dashed lines represent the cell membrane. Table on the right-hand side summarizes characteristics of *O. fasciatus* Na,K-ATPase paralogs as follows: Mya stands for "million years ago" and gives the estimated time of the gene duplication event. Amino acid exchanges for each paralog derived from gene duplication (ancestral α1D → α1C → α1A, α1B) are listed for in vitro confirmed functional sites in *Drosophila* Na,K-ATPase mimics. IC_{50} ranges correspond to the range observed when a given α1-subunit paralog is heterologously co-expressed with one of the four Na,K-ATPase β-subunit paralogs of *O. fasciatus* in cell culture. [a]Dalla et al. (2013), Dalla et al. (2017); [b]Dobler et al. (2012), Zhen et al. (2012); [c]Yang et al. (2019), [d]Herbertz et al. (2024); [e]Lohr et al. (2017).

Cardenolide sequestration in *O. fasciatus*

It is not surprising that *O. fasciatus* is one of the top sequestering species known in terms of cardenolide quantity (Agrawal et al., 2012; Scudder et al., 1986). This milkweed specialist transports, concentrates and sequesters cardenolides from its milkweed host plants in all life stages (Duffey and Scudder, 1974; Isman et al., 1977; Vaughan, 1979). Once accumulated, the loss of sequestered cardenolides is negligible (Duffey, 1980). Hence, feeding on cardenolide-containing host plants must not permanently occur to give this specialist a long-term chemical protection. The accumulation capacity differs between its life stages and peaks from the fourth instar nymphs to adults in terms of stored cardenolide quantity (Duffey and Scudder, 1974). The underlying sequestration mechanism is highly sensitive and selective, yet not well understood. *O. fasciatus* enriches cardenolides far above levels present in its host plants, with minute amounts sufficient to be accumulated (Agrawal et al., 2012; Agrawal et al., 2022; Duffey et al., 1978; Rubiano-Buitrago et al., 2023; Vaughan, 1979). Furthermore, the sequestered cardenolide spectrum does not coincide in quality and quantity with the spectrum in the host plants (Agrawal et al., 2022; Duffey et al., 1978; Duffey and Scudder, 1974; Isman et al., 1977; Moore and Scudder, 1985; Rubiano-Buitrago et al., 2023; Rubiano-Buitrago et al., 2024; Scudder and Meredith, 1982a; Vaughan, 1979). While host plants produce cardenolides across a broad polarity range (Agrawal et al., 2012; Rasmann and Agrawal, 2011), *O. fasciatus* particularly concentrates polar to intermediate-polar ones (Agrawal et al., 2022; Duffey et al., 1978; Duffey and Scudder, 1974; Moore and Scudder, 1985; Rubiano-Buitrago et al., 2023; Rubiano-Buitrago et al., 2024). Furthermore, the metabolization of apolar cardenolides, like labriformin (a milkweed seed cardenolide) or digitoxin (a foxglove cardenolide), into more polar cardenolides is part of selective storage and differential cardenolide excretion. The same applies to highly polar cardenolides of the host plant spectrum, which become less polar through deglycosylation (Agrawal et al., 2022; Duffey and Scudder, 1974; Rubiano-Buitrago et al., 2023; Rubiano-Buitrago et al., 2024; Scudder and Meredith, 1982b). The vast majority of these transformed and untransformed polar and intermediate-polar cardenolides are stored in adults in a specialized storage compartment. In this compartment, a cardenolide-enriched defensive fluid is stored with cardenolide concentrations far higher than those of the hemolymph and all other body organs or glands (Duffey et al., 1978; Duffey and Scudder, 1974; Rubiano-Buitrago et al., 2024; Scudder and Duffey, 1972; Scudder and Meredith, 1982b). Hence, there is a steep electrochemical cardenolide gradient across the compartment's basal lamina. The compartment is functionally different from the scent glands and is concentrated in the thoracic region with three parts, each in one thoracic segment (Bramer et al., 2017; Duffey and Scudder, 1974; Scudder and Meredith, 1982a). It is therefore

referred to as the thoracic storage compartment in the following, since there is no uniform name yet (Bramer et al., 2017; Rubiano-Buitrago et al., 2024; Scudder et al., 1986; Scudder and Meredith, 1982a). Cardenolides are suggested to be stored in the inner vacuolated cells of the double-layered integument which lines the thoracic storage compartment and is separated by a thick basal lamina from the hemolymph (Scudder and Meredith, 1982a). Yet, the exact cellular composition of the compartment is not yet fully settled (Bramer et al., 2017; Scudder et al., 1986). The thoracic storage compartment is a synapomorphy of the Lygaeinae subfamily, with *O. fasciatus* having the most sophisticated type in terms of the releasing mechanism (Bramer et al., 2017). Due to pressure, such as that exerted during a predator attack, the compartment cuticle breaks at thin, predefined points (releasing sites) at the dorsolateral margins of the thoracic and abdominal segments (Bramer et al., 2017; Scudder and Meredith, 1982a). The ability to release sequestered toxins on its body surface is a nonlethal way for predator deterrence restricted to the adult stage (Berenbaum and Miliczky, 1984; Eisner and Meinwald, 1966; Scudder and Meredith, 1982a). However, how exactly cardenolides get from the site of ingestion to the site of release is still unclear and the main question of this thesis.

In plants, cardenolides occur as aglycones or glycosides (Luckner and Wichtl, 2000). Glycosides are (more) hydrophilic and, as outlined before, under physiological conditions rather impermeable to membranes (Wink and Schneider, 1990). On the other hand, lipophilic (apolar) aglycones tend to get stuck in lipophilic areas like membranes (Duffey, 1980). However, cardenolide distribution in the body of *O. fasciatus* differs considerably from a simple polarity-related distribution (Duffey and Scudder, 1974; Moore and Scudder, 1985). Previous physiological studies showed that there are indeed different cardenolide transfer kinetics and hence permeabilities across different body-compartment membranes (intestine, Malpighian tubules, thoracic storage compartment). The gut is the first barrier to be passed by cardenolides after ingestion. Non-polar cardenolides, like digitoxin (foxglove, *Digitalis* sp. (Luckner and Wichtl, 2000), a cardenolide often used as a standard cardenolide), and their more polar metabolites rapidly penetrate the intestine. In contrast, polar ouabain (g-strophanthin), also a commercial standard cardenolide from *Strophanthus* and *Acokanthera* sp. (Cassels, 1985) (Figure 1), is taken up much more slowly into the insects' hemolymph. Transport mechanisms at the intestine are suggested to exclusively rely on simple diffusion (Scudder and Meredith, 1982b; Yoder et al., 1976) or a combination with facilitated diffusion by an unknown carrier-mediated mechanism (Detzel and Wink, 1995). In contrast to the intestine, the Malpighian tubules are impermeable to digitoxin, its more polar metabolites, and metabolized ouabain (Meredith et al., 1984; Scudder and Meredith, 1982b). However, the

tubules excrete and reabsorb ouabain ex vivo. While the excretion is suggested to be passive, the reabsorption is suggested to rely on an active-transport “rescue mechanism” for efficient ouabain sequestration (Meredith et al., 1984). The major site of cardenolide sequestration, the thoracic storage compartment, has a selective cardenolide permeability that is reversed compared to that of the intestine. Apolar cardenolides are rarely or not found at all in the compartment. In contrast, ouabain is rapidly translocated into the storage compartment against its concentration gradient once in the hemolymph (Duffey et al., 1978; Duffey and Scudder, 1974; Scudder and Meredith, 1982b). Nonetheless, several mechanisms for passive cardenolide transfer into the storage compartment have been suggested based on uptake kinetics and tissue histology observed in previous studies (Duffey et al., 1978; Scudder et al., 1986; Scudder and Meredith, 1982a; Scudder and Meredith, 1982b). Duffey et al. (1978) suggest that chemical activity is reduced by a physical emulsion-particle-based mechanism whereby the transport across the membrane actually occurs along the electrochemical gradient. Scudder and Meredith (1982a) suggest that this could rather be achieved by protein emulsion formation or by protein-binding in the inner vacuolated epidermal cells within the thoracic storage compartment. A protein-involved encapsulation and sieving function of the basal lamina was also suggested in this context. Scudder et al. (1986) also suggested a mechanism that involves protein-binding for sequestration into the thoracic storage compartment. Yet, no further evidence for either of these mechanisms or any related key player protein has been found to date (Bramer et al., 2017; Scudder and Meredith, 1982a). In general, knowledge about the sequestration mechanism is so far limited to the chemical and physiological level in *O. fasciatus*.

The lack of identified molecular key players for secondary plant metabolite transport in general has been deemed a bottleneck for understanding the evolution of sequestration and its mechanisms (Beran and Petschenka, 2022). Up to now, proteins that are involved in secondary plant compound transport have only been identified in four of the known 275 sequestering species. These proteins belong to three different ubiquitous protein superfamilies: the cytochrome P450 superfamily, the major facilitator superfamily and the **A**TP-**b**inding **c**assette (**ABC**) transporter superfamily (Beran and Petschenka, 2022; Kowalski et al., 2020; Kumar et al., 2014; Strauss et al., 2013; Yang et al., 2021).

The ATP-binding cassette (ABC) transporter superfamily

ATP-**b**inding **c**assette (**ABC**) transporters are ubiquitous in all living organisms and are important for many physiological processes in vertebrates and invertebrates. The ABC superfamily is therefore very ancient and is suggested to have originated from the ancestors of today's prokaryotes and eukaryotes. Their tasks can be classified into three major biological functions: molecule import, molecule export, and cellular regulation (Dassa and Bouige, 2001; Higgins, 1992; Igarashi, 2004; Xiong et al., 2015). The essential and eponymous commonality of all ABC transporters is their highly conserved nucleotide-binding domain (NBD), which provides energy through ATP hydrolysis. It is characterized by several conserved motifs: the Walker A and B motifs are typical for ATPase domains, while the Q-loop and the ABC signature motif (LSGGQ) are unique characteristics of ABC transporter polypeptides. Most ABC transporters have one or more transmembrane domains (TMDs) with five to six transmembrane helices, where substrate binding takes place. This structure underlines their physiological roles as cellular transport proteins (Culbertson and Liao, 2025; Dassa and Bouige, 2001; Dean et al., 2001; Dean and Annilo, 2005; Denecke et al., 2021; Dermauw and van Leeuwen, 2014; Higgins, 1992; Hwang et al., 2016; Igarashi, 2004; Linton and Higgins, 2007; Xiong et al., 2015). The typical ABC transporter consists of two NBDs and TMDs in alternating order. Yet, there are diverse protein architectures depending on kingdom and protein function. Prokaryotic ABC importer domains are encoded separately by distinct polypeptides. In contrast, exporter domains are encoded by one protein and are hence fused. Eukaryotic ABC transporters always have fused functional domains and are usually organized as either full transporter proteins (FT; typical ABC transporter structure: TMD-NBD-TMD-NBD) or half transporter (HT; one NBD, one TMD) that homo- or heterodimerize to function (Dassa and Bouige, 2001; Higgins, 1992; Igarashi, 2004; Xiong et al., 2015). Based on their domain structures and sequence similarities, ABC proteins in eukaryotes have been classified into nine ABC transporter subfamilies (A - I). Seven subfamilies, ABCA to ABCG, are ancient and present in most eukaryotes. Arthropods have an additional subfamily (ABCH, also found in zebrafish), as do plants (ABCI). Subfamily-specific domain architectures are partially associated with significantly different functions (Dassa and Bouige, 2001; Dean et al., 2001; Dean and Annilo, 2005; Denecke et al., 2021; Dermauw and van Leeuwen, 2014; Hwang et al., 2016; Xiong et al., 2015). Mammalian members of the seven ancient subfamilies (ABCA-G) have a long research history and are thus best studied (for review, see Theodoulou and Kerr, 2015). Members of subfamily E and F are cytosolic ABC proteins without transport function as they lack transmembrane domains (Dean et al., 2001; Dean and Annilo, 2005).

The other subfamily members (A, B, C, D, G) and hence the majority of ABC transporters are mostly versatile primary active efflux pumps that transport hundreds of molecules, usually against their electrochemical gradient, across membranes of organelles or cells (Borst and Elferink, 2002; Marquez and van Bambeke, 2011; Schinkel and Jonker, 2003; Vasiliou et al., 2009). Along these lines, it is important to note that efflux refers to transport out of the cell's cytosol, where ATP as energy source is present. Depending on the transporter location, the substrate can be transported out of cells or within cells. Mammalian ABCD half transporters, for example, move fatty acids into peroxisomes (Dassa and Bouige, 2001). Meanwhile, there is also evidence for the ability of a few plant ABC transporters to import substrates into cells (Kamimoto et al., 2012; Lee et al., 2008). In contrast, members of the mammalian ABCA, ABCB, ABCC, and ABCG subfamilies export xenobiotics besides their physiological substrates, which can lead to multidrug resistance in humans (see overviews by Borst and Elferink, 2002; Dean et al., 2001; Dean and Annilo, 2005; Marquez and van Bambeke, 2011; Schinkel and Jonker, 2003; Scotto, 2003). Also in insects, ABCB, ABCC and ABCG transporters have been implicated in resistance mechanisms against insecticides and toxic allelochemicals (Amezian et al., 2024; Dermauw and van Leeuwen, 2014; Dobler et al., 2015; Groen et al., 2017; Jin et al., 2020; Li et al., 2025; Merzendorfer, 2014; Petschenka et al., 2013b; Seong et al., 2016; You et al., 2025). Furthermore, ABCB and C subfamily members have been shown to transport phytochemicals in mammals and insects, indicating a certain substrate and/or functional conservation (Chen et al., 2021; Katti et al., 2025; Kowalski et al., 2020; Strauss et al., 2013). Strauss et al. (2013) demonstrated that an ABCC transporter is indeed involved in the salicin sequestration mechanism in the poplar leaf beetle, *Chrysomela populi* (LINNAEUS, 1758, Chrysomelidae: Coleoptera). In a pioneering work, Kowalski et al. (2020) recently characterized the cardenolide substrate spectra of three ABC subfamily B transporters of a cardenolide-sequestering leaf beetle species in vitro. Thus, the ABC subfamily B is of special interest in terms of cardenolide transport and their sequestration.

ABC subfamily B transporter

The human ABCB subfamily consists of 11 genes encoding four full transporters (ABCB1, ABCB4, ABCB5, ABCB11) and seven half transporters (ABCB2, ABCB3, ABCB5, ABCB6, ABCB8, ABCB9, ABCB10) (Dean et al., 2001; Vasiliou et al., 2009). ABCB5 is the only one of the four ABCB full transporters whose physiological function and role in multidrug resistance in humans is still largely unclear (Gerard and Gillet, 2024). ABCB4 (alias MDR3) and ABCB11 are liver-specific and have a primary role in bile secretion (Dean et al., 2001; van der Bliek et al., 1988; van Helvoort et al., 1996).

Human ABCB1, better known as MDR1 or Pgp1, is the most famous ABC transporter to date. This typical full transporter has gained notoriety because it was the first ABC protein found to confer a multidrug resistance (MDR) phenotype on cancer cells (Juliano and Ling, 1976), and many others have followed. Extensive research revealed that human ABCB1 is the most versatile of all ABC transporters, and also the best studied (Dean et al., 2001; Marquez and van Bambeke, 2011; Schinkel and Jonker, 2003; Theodoulou and Kerr, 2015). The physiological role of human ABCB1 is the protection of the organism from xenobiotics by barrier, plasma-clearing, and excretory functions (see for example reviews by Marquez and van Bambeke, 2011; Schinkel and Jonker, 2003). Hence, it is especially prominent at interfaces with strong contact to exogenous substances, such as the digestive tract, at interfaces to sensitive and particularly vulnerable tissues, such as the brain, testes, or placenta, and at interfaces for excretion, like the kidney or liver (Cordon-Cardo et al., 1989; Langmann et al., 2003; Thiebaut et al., 1987).

Human ABCB1 transports a vast array of chemically different substrates (> 80) including clinical drugs, pesticides and also secondary plant metabolites like certain alkaloids as well as some cardenolides (Dean et al., 2001; Marquez and van Bambeke, 2011; Schinkel and Jonker, 2003). Thanks to its therapeutic use (Soldin, 1986), foxglove cardenolide digoxin is also included in this heterogeneous substrate list. This toxin has long been studied in the context of insect specialization on cardenolide-producing plants and is also sequestered by *O. fasciatus* (Agrawal et al., 2012; Bramer et al., 2015).

ABCB1 transporter homologs have therefore long been considered prime candidates for cardenolide transport in specialized insects (Agrawal et al., 2012; Dobler et al., 2015). They have been previously linked to tolerance and resistance mechanisms in at least five insect orders (Coleoptera, Diptera, Lepidoptera, Orthoptera) including recently also the order Hemiptera (Amezian et al., 2024; Denecke et al., 2017; Denecke et al., 2022; Dermauw and van Leeuwen, 2014; Groen et al., 2017; Kowalski et al., 2020; Lanning et al., 1996; Li et al., 2025; Mayer et al., 2009; Murray et al., 1994; Pauchet et al., 2016; Petschenka et al., 2013b; Ricardo and Lehmann, 2009; Rossi et al., 2019; Seong et al., 2016; Wu et al., 1991). Their function is best understood in the fruit fly *Drosophila melanogaster* (MEIGEN, 1830; Drosophilidae: Diptera) (Dermauw and van Leeuwen, 2014). The four ABCB full transporters of this species (MDR49, MDR50, MDR65, CG10226 (FBgn0035695, AMT)) act as gatekeepers in terms of oral availability, elimination, and chemoprotection against pesticides and allelochemicals like the foxglove cardenolide digoxin (Denecke et al., 2017; Denecke et al., 2022; Dermauw and van Leeuwen, 2014; Gerrard et al., 1993; Groen et al., 2017; Mayer

et al., 2009; Pignatelli et al., 2018; Seong et al., 2016; Wu et al., 1991). A transporter-specific physiological role in germ cell attraction has further been described (Ricardo and Lehmann, 2009).

Homologous functions and substrate specificities of ABC transporters have been demonstrated over large evolutionary distances (Mayer et al., 2009; Szeri et al., 2009). The chemoprotective role of ABCB1 homologs in the blood-brain barrier is evolutionarily conserved. While the cellular locations differ due to differences in blood-brain barrier structures and circulatory systems, ABCB1 homologs have been shown to be gatekeepers in shielding the brain from apolar cardenolide accumulation in mammals and insects (Mayer et al., 1996; Mayer et al., 2009; Murray et al., 1994; Petschenka et al., 2013a). Protection against polar cardenolides is supposedly achieved by cellular tightness of the barrier, whereby the functional components, like tight or septate junctions, are taxon-specific (Dunton et al., 2021; Petschenka et al., 2013a). Another conserved gatekeeper function is suggested at the intestinal barrier (Dobler et al., 2015; Groen et al., 2017). In mammals, ABCB1 homologs are expressed in the lumen-facing apical region of digestive tract cells, thereby determining the degree of passive intestinal digoxin uptake and its excretion route (Hoffmeyer et al., 2000; Mayer et al., 1996). A conserved cell polarization has been demonstrated in the gut of insects (Denecke et al., 2022; Dobler et al., 2015), but functional studies are so far limited to *D. melanogaster*. A recent study by Denecke et al. (2022) indicates that the midgut expressed homologs (MDR49, MDR50) and their subcellular localization could be one of the pivotal factors that determines sensitivity or tolerance to pesticides in *D. melanogaster*. Groen et al. (2017) previously demonstrated that knockdowns of both homologs increase susceptibility to cardenolides. In summary, this highlights the crucial and evolutionarily conserved role of ABCB1 homologs in the compartmentalization within animals.

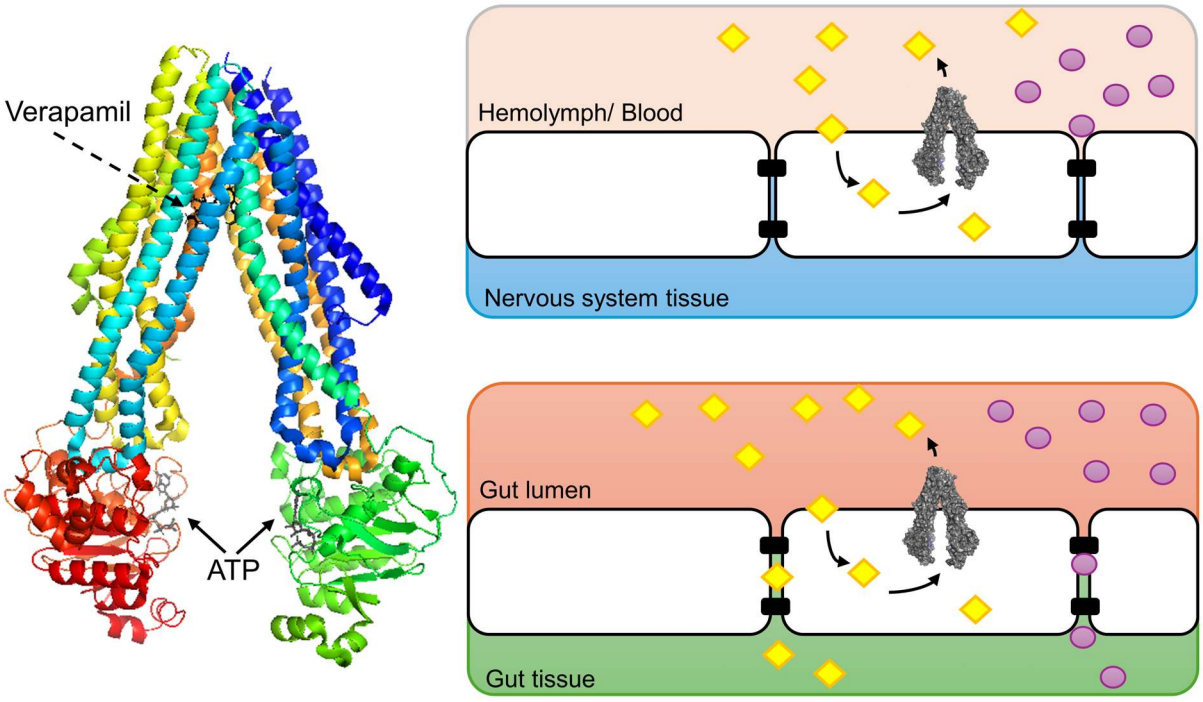


Figure 3 3D structure of human ABCB1 (left) and its localization for protective compartment function in tissues (right). 3D secondary structure shows inward-facing in state 1 under turnover conditions with substrate verapamil and binding of ATP. It was retrieved from the Research Collaboratory for Structural Bioinformatics RCSB database (Berman et al., 2000): entry 8SB7, Culbertson and Liao (2025). Visualization was conducted with PyMOL (Version 3.0) (Schrödinger). A simplified schematic localization of ABCB1 homologs in the blood-brain barrier and in the gut of mammals and insects is shown on the right-hand side. Yellow diamonds = apolar cardenolides, purple circles = polar cardenolides.

Objectives of this dissertation

Sequestration itself can be considered a type of compartmentalization (Després et al., 2007; Jeckel et al., 2022). As outlined above, ABCB1 homologs are therefore prime candidates for molecular origins of adaptive evolution for specialization on cardenolide-containing plants, and furthermore, for escalation to the tritrophic level. Recently, Kowalski et al. (2020) demonstrated in a pioneering study conducted in parallel to this dissertation the ability of insect ABCB full transporters to activate and likely transport several cardenolides in vitro. However, a direct functional association with sequestration in vivo is pending.

This dissertation therefore specifically focuses on investigating the role of ABCB full transporters in the cardenolide transport network of *O. fasciatus*. A major objective of this thesis was to characterize their function regarding cardenolide sequestration in vivo to provide this still missing functional association in the complex, living organism. The accessibility of *O. fasciatus* to a variety of molecular techniques including RNA interference, its natural

specialization on cardenolide-containing plants, and its physiologically characterized sequestration process make this species a perfect model to do so.

Among the research methodologies used to characterize ABC transporter functions (see review by Lv et al., 2025), gene expression profiles and dynamics by quantitative real-time PCR (RT-qPCR) provide indirect links to physiological transporter function and substrate transport (Amezian et al., 2024; Hoffmeyer et al., 2000; Marquez and van Bambeke, 2011; Mayer et al., 1996). More importantly, distribution within and between tissues can be crucial in determining whether toxin tolerance or susceptibility develops (Denecke et al., 2022). Ten reference genes were identified in an assembled transcriptome of *O. fasciatus* and evaluated for their stability by four common algorithms in Chapter 1 as an important step for accurate relative gene expression quantification of ABCB full transporters in this thesis and other candidate genes in future studies. An experimental setup for evaluation was chosen that addresses several important aspects of this thesis and our research group: the temporal gene expression in *O. fasciatus* during ouabain exposure since no universal normalizers exist (Chapman and Waldenström, 2015; Kozera and Rapacz, 2013; Shakeel et al., 2018; Shi et al., 2015).

In Chapter 2 this basis was used and also reevaluated to characterize the role of ABCB full transporters in the cardenolide transport network in *O. fasciatus*. Assembled transcriptomes were specifically searched for ABCB full transporter homologs whose tissue distributions were then studied on the mRNA level. Immunohistochemistry was furthermore conducted, which provides links between ABC transporter expressions and their physiological tissue functions (Amezian et al., 2024; Denecke et al., 2022). To test the function of these transporters in cardenolide sequestration, knockdowns by RNA interference were established and sequestration capacity of ouabain analyzed. While certain knockdowns showed an impaired sequestration capacity, *O. fasciatus* was still able to release defensive fluids. That was a clear contrast to the previously described ABCC-mediated glandular sequestration system in the poplar leaf beetle, *C. populi* (Strauss et al., 2013), and sparked my interest in the formation of defensive fluids and the factors associated with them. As little research had been done on this topic to date, I conducted experiments examining factors such as biomass, gender, age, and stored cardenolide content as described in Chapter 3. That also included an examination of whether dietary changes, such as those associated with common rearing practices of *O. fasciatus*, affect the sequestration capacity.

Since it was shown in Chapter 3 that such changes can shape the sequestration capacity, I collected initial immunohistochemical data on ABCB full transporter occurrence comparing our

laboratory lines, which are long-term acclimatized to different diets and were previously examined at the mRNA level in Chapter 2. In addition, immunohistochemical staining of the Na,K-ATPase was performed to see how this basal adaptation (Bramer et al., 2015) is interrelated at the tissue level with ABCB full transporters, which are linked to sequestration by the results of Chapter 2. Lastly, I re-examine the expression response of the most abundant and highly insensitive Na,K-ATPase α1A paralog (Dalla et al., 2017; Dalla and Dobler, 2016; Herbertz et al., 2024; Lohr et al., 2017) to ouabain on a finely tuned timescale to detect both early and late responsiveness.

Chapter 1

Robust reference gene design and validation for expression studies in the large milkweed bug, *Oncopeltus fasciatus*, upon cardiac glycoside stress

The work presented in this chapter was published 2019 in Gene, Volume 710, Pages 66-75

https://doi.org/10.1016/j.gene.2019.05.032

Highlights

- Ten potential references genes were identified in *O. fasciatus*
- *Ef1a* and *tubulin* are suitable normalizers upon temporal cardiac glycoside challenge
- Robust RT-qPCR primer design is also feasible in non-model organisms
- Multifactorial designs allow for detailed reference gene stability exploration

Abstract

Despite its history as a developmental and evolutionary model organism, gene expression analysis in the large milkweed bug, *Oncopeltus fasciatus*, has rarely been explored using quantitative real-time PCR. The strength of this method depends greatly on the endogenous controls used for normalization, which are lacking for the milkweed bug system. Here, to fill in this gap in our knowledge, we validated the stability of a set of ten candidate reference genes identified from the *O. fasciatus* transcriptome, and did so upon exposure to a dietary toxin, a cardiac glycoside, and across four different exposure periods. To increase robustness against gDNA contaminants, genome resources were used to design intron-bridging primers. A comprehensive stability validation by the Bestkeeper, Normfinder, geNorm and comparative ΔCt methods identified *ef1a* and *tubulin* as the most stable genes across treatments and time points, whereas *18S rRNA* was the most unstable. However, accounting for the temporal scale indicated that time point confined normalizers might enable higher quantification accuracy for treatment comparison. Overall this study demonstrates: (i) a robust RT-qPCR primer design approach is possible for non-model organisms where genome annotation is often incomplete, and (ii) the importance of detailed reference gene stability exploration in multifactorial experimental designs.

Introduction

The large milkweed bug, *Oncopeltus fasciatus* (DALLAS, 1852), is an important model organism in both developmental and evolutionary biology, due to its simple culture maintenance, phylogenetic status (reviewed by Chipman, 2017; Feir, 1974), and ease of use for genetic manipulation via RNA interference (Aspiras et al., 2011; Lohr et al., 2017). Furthermore, this species is a prime example of how herbivorous insects can circumvent the chemical defense of their host plants (Duffey and Scudder, 1974; Moore and Scudder, 1986). All life stages of *O. fasciatus* feed on milkweed plants (*Asclepias* sp.), which synthesize secondary plant metabolites called cardiac glycosides to deter herbivores (Agrawal et al., 2012; Brower, 1969; Duffey and Scudder, 1972; Duffey and Scudder, 1974). Cardiac glycosides are highly toxic because they bind to and thereby inhibit the Na,K-ATPase, an essential enzyme of animal cells (Agrawal et al., 2012; Horisberger, 2004; Lingrel et al., 1990). However, these insects have evolved two adaptations to prevent these toxic effects: (i) insensitive paralogs of the Na,K-ATPase gene (Moore and Scudder, 1986; Zhen et al., 2012) and (ii) sequestration of the ingested toxins in a storage compartment (Bramer et al., 2017; Duffey and Scudder, 1974; Scudder and Meredith, 1982a). Interestingly, duplications of the Na,K-ATPase gene and cardiac glycoside tolerance have evolved independently across several insect orders (Agrawal et al., 2012; Dobler et al., 2012; Dobler et al., 2015; Petschenka et al., 2017; Zhen et al., 2012). Although increasing progress has been made in understanding the molecular mechanisms underlying these cardiac glycoside tolerance adaptations in the large milkweed bug, gene expression studies by quantitative real-time PCR (RT-qPCR) have rarely been exploited (Lohr et al., 2017; Zhen et al., 2012).

RT-qPCR has been the method of choice for gene expression quantification over the last twenty years (Bustin, 2000), and remains the most accurate and sensitive method in conjunction with low analysis times and costs (Everaert et al., 2017; Nonis et al., 2014; van Heetvelde et al., 2017). In relative RT-qPCR, normalizing the expression of a gene of interest (GOI) by the expression of reference genes allows, when properly employed, highly accurate measurements reflecting biological differences minimally skewed by technical variance (Huggett et al., 2005; Livak and Schmittgen, 2001; Nolan et al., 2006; Pfaffl, 2001; Vandesompele et al., 2002). Unfortunately, such reference genes can be a major pitfall if their stability has not been carefully validated (e.g. see Cameron et al., 2013; Dheda et al., 2005). The misconception that so called “housekeeping genes”, like *18S rRNA* or *GAPDH*, are expressed constitutively under all experimental conditions has been disproven in a variety of studies and across many taxa (reviewed by Kozera and Rapacz, 2013; see further also

Chapman and Waldenström, 2015; Shakeel et al., 2018; Shi et al., 2015). In fact, such "housekeeping genes" are actually less likely to be chosen as normalizers when multiple genes are evaluated for their stability (Chapman and Waldenström, 2015).

Addressing this need, the number of publications reporting reference gene stability for GOI quantification by RT-qPCR has increased in recent years (Chapman and Waldenström, 2015). For arthropods, some 93 reference genes across 54 species have now been analyzed under various experimental conditions; for which expression across developmental stages and tissues makes up the bulk of those studies (reviewed by Shakeel et al., 2018; Shi et al., 2015). In the large milkweed bug, however, only a handful of studies have used relative RT-qPCR for gene expression analysis, and these have only used single gene normalization (Dean et al., 2016; Ginzburg et al., 2017; Lohr et al., 2017), or lack any normalization to independent references genes (Zhen et al., 2012). Normalization by at least two or three reference genes is recommended (Bustin et al., 2010; Vandesompele et al., 2002) as single reference gene normalization errors can be as high as 20-fold (Vandesompele et al., 2002). This highlights the need for a proper validation analysis in *O. fasciatus*, to improve the reliability of future expression analyses and their accordance with the MIQE guidelines (Bustin et al., 2009).

Given the large milkweed bugs' use as a model system for insect-plant interactions and adaptations to host-plant derived dietary toxins, we specifically assessed expression stability at the systemic level, i.e. whole body, upon exposure to the cardiac glycoside ouabain. Ouabain is a highly polar cardiac glycoside, which is routinely used to investigate the mechanisms mediating insensitivity to cardiac glycosides across insect species (Moore and Scudder, 1986; Petschenka et al., 2013b; Petschenka et al., 2013a; Vaughan and Jungreis, 1977). In the large milkweed bug, cardiac glycoside transport within the body is highly complex (Detzel and Wink, 1995; Duffey et al., 1978; Duffey and Scudder, 1974; Meredith et al., 1984; Scudder and Meredith, 1982b; Yoder et al., 1976) and is not fully understood. As such, we are explicitly interested in studying gene expression patterns of potential candidates, like the ATP-binding cassette or solute carrier organic anion superfamily members (Agrawal et al., 2012; Dobler et al., 2015; Groen et al., 2017; Petschenka et al., 2013b; Strauss et al., 2013; Torrie et al., 2004) upon cardiac glycoside exposure to elucidate their role in cardiac glycoside transport, accumulation and insensitivity in *O. fasciatus*. This is essential, as hypotheses on accumulation facilitating mechanisms are still based on contradicting physiological evidence (Detzel and Wink, 1995; Duffey et al., 1978; Duffey and Scudder, 1974; Scudder and Meredith, 1982b; Yoder et al., 1976) and underlying molecular mechanisms are unknown in the majority

of toxin accumulating insect species (Duffey and Scudder, 1972; Erb and Robert, 2016; Opitz and Müller, 2009).

A useful method to study toxin handling is via gene expression and for this we need properly validated references upon cardiac glycoside challenge. In fact, a recent study in *O. fasciatus* found ouabain's toxic action to be severely reduced by insensitive paralogs of the Na,K-ATPase, (α1A and α1B: Lohr et al., 2017), an adaptation closely linked to accumulation (Bramer et al., 2015; see further also review by Erb and Robert, 2016). Yet, the same paralogs did not show a cardiac glycoside regulated expression pattern in *O. fasciatus* (Lohr et al., 2017). Temporal dynamics were not considered in previous studies and may be an important factor to consider. Indeed, screening across different time points after a treatment might not only increase the likelihood of detecting responsiveness per se, but can also enable a more detailed biological interpretation, e.g. identification of early and late response genes (Sørensen et al., 2010).

Here, we identified 10 putative reference genes previously investigated in other insect species (Shakeel et al., 2018; Shi et al., 2015) and evaluated the stability of 7 of these genes by four commonly used algorithms (Bestkeeper, Normfinder, geNorm and comparative ΔCt) in milkweed bugs exposed to ouabain over different time periods. In our fully-crossed 2 × 4 experimental design, we also examined if treatment response, i.e. expression stability, changed dependent on exposure duration. Further, we used in silico resources to design intron-bridging primers, a method used to enhance the reliability of expression data (Cui et al., 2007), and one which is often not feasible in non-model organisms where the underlying gene structure is uncertain. In addition, the methods and findings established here bring us further in applying RT-qPCR to elucidate the molecular mechanisms, patterns and key players of the large milkweed bug's adaptations against cardiac glycoside toxins in more detail.

Material & Methods

Milkweed bugs and cardiac glycoside injection assay

Milkweed bugs (*Oncopeltus fasciatus*) were obtained from our laboratory culture maintained at 25 °C under 16 h light : 8 h dark conditions (for further information see Lohr et al., 2017). For use in experiments, last instar individuals (L5 stage) were separated and molting to the adult stage was checked daily. Freshly molted females (reared on *Helianthus annuus* seeds) were transferred individually to vials and maintained as described above. Seven days after molting the insects were injected laterally between the 4th and 5th abdominal segment with

either 2 µl of 5 mg/ml ouabain (Sigma, Taufkirchen, Germany) in 0.9 % NaCl (saline) (Carl Roth, Karlsruhe, Germany) or with 2 µl of saline only, using a 10 µl syringe with a 34 gauge needle (Hamilton®, Romania). To assess the effect of toxin exposure over time, animals were kept at the conditions described above and sacrificed 1 h, 6 h, 16 h and 32 h *post* injection by freezing in liquid nitrogen. Each treatment (ouabain or control = saline) consisted of three biological replicates at each time interval. All samples were stored at -80 °C until RNA extraction.

RNA extraction and cDNA synthesis

Extraction of injected insects was conducted as described in Lohr et al. (2017) with the RNeasy Plus Mini Kit (Qiagen, Hilden, Germany) including gDNA Eliminator columns for genomic DNA removal. RNA quantity was measured using a NanoDrop™ 2000 spectrophotometer (Thermo Scientific, Thermo Fisher Scientific). All samples had 260/280 ratios ≥ 1.95 and 260/230 ratios ≥ 1.75. 1 µg of total RNA was reverse transcribed by adding 1× ProtoScript®II buffer, 200 U ProtoScript®II RT Enzyme, 10 mM DTT (all New England BioLabs, Frankfurt, Germany), 5 µM T17 primer (eurofins Genomics, Ebersberg, Germany), 5 µM random hexamer primer, 0.5 mM dNTP each (both Thermo Scientific) and nuclease-free water (Carl Roth) to a final volume of 20 µl. Mixtures were incubated at room temperature for 10 min, 42 °C for 50 min, 80 °C for 5 min and diluted 1:5 for RT-qPCR. For initial primer tests pooled cDNA (25 ng) from female and male milkweed bugs reared on sunflower and milkweed seeds was used to mimic cardiac glycoside presence. Furthermore, 100 ng of each cDNA was analyzed on a 1 % agarose gel stained with ethidium bromide (1× TAE buffer, 100 V, 40 min) to spot synthesis errors *prior* to RT-qPCR measurement. In addition, an exemplary set of RNA samples (n = 6, 1 µg each) was also analyzed and showed no major quality differences (Figure S 1).

Reference gene homolog transcriptome search, primer design and evaluation

RNA-seq data of *O. fasciatus* was obtained from http://genomics-pubs.princeton.edu/insect_genomics/data.shtml (Zhen et al., 2012). Low quality bases were trimmed using sickle v1.290 (Joshi and Fass, 2011). To rigorously discard reads of low quality, we increased the quality threshold to 33 (-q 33) and kept only those reads which were longer than 50 bp after trimming (-l 50). All reads that survived trimming were employed in a de novo transcriptome assembly using Trinity r2014-041-3p1 (Grabherr et al., 2011). E-value cut-offs of tblastn (blastn for *18S*) (BLAST+) homology searches in the *O. fasciatus* transcriptome with respective *D. melanogaster* queries (Table 2) were 1e-50. Coding potential was predicted by Transdecoder (http://transdecoder.github.io) (Haas et al., 2013) and sequence identity

confirmed by blastx/n searches via Blast2GO v4.1.9 (Götz et al., 2008) (Table S 1). Furthermore, we combined two bioinformatic tools to predict exon-intron junctions for our reference gene transcripts in silico: (i) Blastn searches were conducted with the i5k Workspace@NAL blast tool (https://i5k.nal.usda.gov/webapp/blast) in the *O. fasciatus* genome, sequenced by the Baylor College of Medicine Human Genome Sequencing Center (Murali et al., 2015; Panfilio et al., 2017; Poelchau et al., 2015). (ii) Using NCBI Splign (Kapustin et al., 2008; https://www.ncbi.nlm.nih.gov/sutils/splign/splign.cgi) the best scaffold hit (lowest E-value) and the respective contigs were aligned to identify potential splice sites. Using the obtained positional information, primers were designed to bind in two neighboring exons and thereby span a predicted intron. Primer design and evaluation were conducted using BioEdit (Hall, 1999), Primer3 (Koressaar and Remm, 2007; Untergasser et al., 2012; http://primer3.ut.ee), Beacon Designer™ Free Edition (http://www.premierbiosoft.com/qpcr) and UNAFold software (available online e.g. at the Integrated DNA Technologies website https://eu.idtdna.com/UNAFold) following the recommendations of Thornton and Basu (2011).

Primer pairs were first tested in standard PCR reactions of 25 µl containing 1× PCR buffer Minus Mg^{++}, 2 mM $MgCl_2$, 0.04 U μl^{-1} Taq polymerase (all Invitrogen, Thermo Fisher Scientific), 0.2 mM dNTP each (Thermo Scientific), 0.4 µM of each primer (eurofins Genomics), 0.5 µg μl^{-1} BSA (Fermentas, Thermo Fisher Scientific), sterile water and 20 ng cDNA or 69 ng gDNA (extracted by DNeasy Blood & Tissue Kit (Qiagen) according to manufacturer instructions). Cycling conditions were: 95 °C for 1 min followed by 35 cycles of 95 °C for 1 min, 60 °C for 30 s, 72 °C for 3 min and a final elongation for 5 min at 72 °C (Eppendorf Mastercylcer gradient, Hamburg, Germany). PCR products (5 µl) were analyzed on agarose gels as described above.

Table 2 Designed primer pairs for ten reference genes identified in the assembled transcriptome of *Oncopeltus fasciatus* by homology search. Predicted gDNA amplicon size ranges were conditioned by N-stretches in the genomic scaffold: Lower range = without N, higher range = N included. R^2 = coefficient of determination of standard curves used for RT-qPCR efficiency determination.

Reference gene	*D. melanogaster* query for homolog search (Genbank)	predicted protein [aa]	identity to query [%]	Primer			cDNA product size [bp]	gDNA product size [bp]	Efficiency [%]	R^2
				Name	Type	Sequence (5' → 3')				
18S ribosomal RNA	NR_133559.1		84	*18S*[a]	fwd	AGGGACAGGCGGCTCTTAG	113	113	100.9	0.997
					rev	CAGGGGAGCACACGCTGATT				
Actin5C	NP_001284915.1	376	100	*actin5C*	fwd	GAACATCCTGTCCTCCTTACAGAA	121	242	105.8	0.996
					rev	GTACTGCCTGGATAGCGACA				
Arginine kinase	NP_729446.1	417	84	*AK*	fwd	AAAGCGGACCAGTGAATCCC	119	1198-1363		
					rev	TGCAGCGTCAACCATTCTAGTTTT				
Elongation factor 1 alpha	NP_477375.1; NP_524611.1	462	92	*ef1a*[a]	fwd	CCACCAAGGGCTGCTTCTGA	110	201	102.4	0.994
					rev	GCAATATGGGCTGTGTGGCAAT				
Glyceraldehyde 3-phosphate dehydrogenase	NP_001033936.1; NP_542445.1	333	78	*GAPDH*	fwd	TAATGGATTTGGAAGAATCGGGCGT	99	8159-11135	104.8	0.999
					rev	TACTCTACATTGATGAAAGGGTCGTTG				
Ribosomal protein 49	P04359.3; P84323.1	134	82	*rp49*	fwd	GGCATCAAAGTGACCGATATGTGAA	86	215	104.0	0.999
					rev	CTTAAACCTCCTTCTGACTCTGTTGT				
Ribosomal protein L11	P46222.2	197	92	*RPL11*	fwd	GGTTTCGGTATCCAAGAACATATTGATTT	126	2521-2875		
					rev	TTTCCTTCTCCTATGGGCAACG				
Ribosomal protein S3	NP_476632.1	249	79	*RPS3*	fwd	TGGAGAACCCTGTAATGAGTATGT	120	1599-1740	112.3	0.998
					rev	GGACCATTCTTGCCAGTAGGA				
TATA box-binding protein	P20227.1	297	88	*TBP*	fwd	TATGGTTGGAAGTTGTGATGTGAAG	112	3984		
					rev	TCTGTAAATAAGACCAGGGAAGAGT				
Tubulin56D	NP_523795.2	447	99	*tubulin*[a]	fwd	TGCCTGGTTTTGCACCACTGAC	115	1267	107.1	0.999
					rev	GGGTCACAAGCGGCCATCAT				

[a] Lohr et al. (2017)

Quantitative real-time PCR

All samples were measured in technical duplicates on a StepOne™ Real-Time PCR System (MicroAmp® Fast Optical 48-Well Reaction Plate and Adhesive Film; Applied Biosystems, Thermo Fisher Scientific). Plate setup was based on the sample maximization strategy recommended by Hellemans et al. (2007) (for further details see Table S 2, Figure S 2). One biological replicate was run as an inter-plate calibrator (IPC). RT-qPCR reactions were adjusted to 10 µl with nuclease-free water (Carl Roth) and contained 1× EvaGreen® QPCR-Mix II (ROX) (Bio-Budget Technologies GmbH, Krefeld, Germany), 0.2 µM of each primer (eurofins Genomics) and 1 µl cDNA. The cycling conditions were: 95 °C for 15 min, 40 cycles of 15 s at 95 °C, 30 s at 63 °C and 30 s at 72 °C followed by melting curve analysis. Furthermore, the length of the PCR product for each primer pair (1 µl) was checked once on a 2 % agarose gel. Primer efficiencies were determined for each primer pair by a 5-point dilution series of pooled cDNA derived from both treatments separately (ouabain and control) to account for any potential treatment-specific inhibitory effects. In accordance with the MIQE guidelines (Bustin et al., 2009), signals in negative controls were ignored if they revealed differing melting temperatures and Cp values were at least 5 cycles higher than all sample Cps.

Data analysis and reference gene stability evaluation

The threshold cycle value (Cp) was determined at the same threshold for all amplicons in all plates and corrected for inter-run variation (Cp_c) according to Kubista et al. (2007). Flagged wells were excluded from analyses. As a result, 14 out of 336 measurements relied on only one technical replicate. Cp_c values or efficiency corrected relative quantities ($E^{Cp(min)-Cp}$) were analyzed using Bestkeeper (Pfaffl et al., 2004), Normfinder (Andersen et al., 2004), geNorm (Vandesompele et al., 2002) and the comparative ΔCt method (ΔCt) (Silver et al., 2006) to evaluate candidate gene expression stability. We then ranked the results for all genes and calculated geometric averages ($rank_{geo}$) to determine which genes were the most stable as illustrated in Table 3. Stability rankings by Bestkeeper (rank(BK)) were based on geometric averages of individual ranks obtained by Cp value standard deviation (sd) and Pearson´s correlation coefficient (r) with the Bestkeeper Index (BKI; geometric mean of all genes). Genes with divergent expression (*p* value of $r > 0.05$) or violating the assumptions of Pearson's correlation analysis were excluded from calculations (Pfaffl et al., 2004) and manually ranked last. If multiple genes had to be excluded from the index calculation, these were differentiated by sd. We conducted two different rankings by Normfinder (experimental group assigned

or not) and geNorm (M values before = M_i or *post* step-wise exclusions of the most unstable genes = M_e). This enabled us also to evaluate the influence of group assignment and successive unstable gene elimination on the stability assessment values by these methods.

Table 3 Overview of the methods and ranking strategies used to evaluate candidate reference gene expression comprehensively. For each algorithm the respective stability parameter is listed with its associated measure of expression stability, i.e. least or most stable if parameter is high or low. Analysis refers to the different analysis modes used for stability evaluations via Normfinder and geNorm. Asterisks indicate that if respective cut-offs or assumptions were not met, genes were either excluded from analyses for this algorithm or manually ranked last: *Genes showing M_i > 1.5 (geNorm M value calculation based on expression of all reference genes) were excluded from analyses. **Genes with Bestkeeper sd > 1 were also excluded *prior* to analyses. ***Genes for which Pearson correlation coefficient with the Bestkeeper Index was p > 0.05 or respective statistical assumptions were not met, were excluded (manually ranked last) and r was re-calculated. Multiple excluded genes were differentiated by sd. By geometric averaging of ranks obtained by Bestkeeper sd and r, the combined measure BK(rank) was determined. Concurrent numbers in ranking column indicate that ranks obtained by these analyses were used to rank gene expression comprehensively by geometric averaging. Last row shows the interpretation of stability by the obtained comprehensive ranks. Abbreviation: SV = Normfinder stability value, M_e = geNorm M values calculation based one step-wise exclusion of least stable genes, mean sd = average sd of all pairwise gene expression comparisons as calculated by comparative ΔCt.

	Analysis		Stability			Ranking
			Parameter	Least	Most	
Normfinder	Experimental groups assigned	No	SV	High	Low	1
		Yes	SV	High	Low	2
geNorm	Least stable gene step-wise excluded	No	M_i*	High	Low	1
		Yes	M_e	High	Low	2
Comparative ΔCt			Mean sd	High	Low	1/2
Bestkeeper			sd**	High	Low	
			r***	Low	High	
			BK(rank)	High	Low	1/2
Comprehensive rank				High	Low	

Statistical analysis

Cp_cs from the complete dataset and subgroups were tested for fit to a normal distribution and homogeneity of variances using Shapiro-Wilk and Levene's tests. Both are preconditions for calculation of Pearson's correlation coefficient, which is conducted by Bestkeeper (Pfaffl et al., 2004). Post hoc pairwise F-tests with Bonferroni corrections were conducted to identify genes exhibiting different variances. The effect of treatment and exposure time on transcript levels was analyzed by two-way analysis of variance (ANOVA). Diagnostic plots of the parametric ANOVA models indicated that part of our results might be less reliable (Figure S 3 to Figure S 6). Hence, we chose to use permutational ANOVAs (aovp function of the lmperm package

(Wheeler and Torchiano, 2016)) to infer expression changes. Note that the permutation and parametric ANOVAs produced consistent results in terms of significance, i.e. $p < 0.05$ (Table S 3). All analyses were conducted using R (R Core Team, 2017).

Results

Identification of candidate reference genes and RT-qPCR primer evaluation

We identified 10 putative commonly used reference genes belonging to different functional classes (reviewed by Shakeel et al., 2018; Shi et al., 2015) including previously used references (Dean et al., 2016; Ginzburg et al., 2017; Lohr et al., 2017) from the transcriptome of *Oncopeltus fasciatus* (see additional file S1). Translated sequences (see additional file S2) revealed 78 to 100 % identity to their respective *Drosophila melanogaster* proteins used as tblastn (blastn) queries (Table 2): Actin5C, Arginine kinase (AK), Elongation factor 1 alpha (ef1a), Glyceraldehyde 3-phosphate dehydrogenase (GAPDH), TATA box-binding protein (TBP), Tubulin56D (tubulin), 18S ribosomal RNA (18S), Ribosomal protein 49 (rp49), L11 (RPL11) and S3 (RPS3). We were able to locate exon-exon borders for all nine protein-coding reference genes and designed intron-bridging primers (Table 2, Figure S 2) by sequence comparison with the publicly available genome assembly of *O. fasciatus*. Although all designed primer pairs yielded clean melting curves, i.e. one peak, and thus confirmed their presence in adult milkweed bugs in initial RT-qPCR tests, three candidates were excluded from subsequent analyses (*RPL11* = “abnormal” amplification curves indicating unsuitable amplification efficiency; *TBP* = low expression level (≥ 25 cycles); *AK* = gender-specific amplification with low and inconsistent amplifications (Ct ≥ 34) in female insects (Figure S 8, Figure S 9)). Tests of the remaining primer pairs (*tubulin*, *actin5C, rp49*, *ef1a*, *RPS3*, *GAPDH*) in standard PCRs enabled differentiation of cDNA and gDNA templates based on amplicon length and thus confirmed the presence of the in silico predicted exon-exon boundaries (Figure S 10). However, no distinction could be made for the intron-free *18S rRNA* gene. Primer sets displayed efficiencies in RT-qPCR ranging from 2.01 to 2.12 with $R^2 \geq 0.994$ (Table 2).

Candidate reference gene expression upon cardiac glycoside challenge over different exposure periods

All six protein-coding genes had similar raw expression levels to each other, whereas the *18S* gene had an extraordinarily high transcript abundance (*18S* ($Cp_{mean} = 6.22$) followed by *actin5C* (17.95), then *ef1a* (18.56), *tubulin* (19.10), *RPS3* (19.49), *rp49* (19.70) and lastly *GAPDH* (20.92)) (Figure 4, Table S 4). Furthermore, the expression variability of the *18S* gene was

much lower ($\Delta Cp_{max\text{-}min}$ = 0.6, sd = 0.147), significantly diverged from all other genes ($p < p_{Bonferroni} = 0.0024$), and was the only gene not affected by either exposure time or ouabain challenge ($p > 0.05$) (Figure 4, Table S 3, Table S 4). In contrast, we found indications of exposure time related treatment effects for all mRNA coding genes (interaction $F_{3,16}$ treatment : time $p < 0.05$, Table S 3). The expression levels of all mRNA genes revealed differential time related differences between treatments while an explicit trend across all time intervals was not present (Table S 5). Furthermore, all expression levels, except that of *actin5C* and *rp49*, were significantly lower in ouabain exposed animals 16 h *post* injection (Tukey HSD control vs. ouabain 16 h: *ef1a* $p = 0.019$, *GAPDH* $p = 0.003$, *RPS3* $p = 0.025$, *tubulin* $p = 0.013$) (Table S 5). Unfortunately, due to the low sample size of $N = 3$ of the time $*$ treatment interaction for ouabain, the level of variation level is high and prevents us from drawing solid conclusions about this data set.

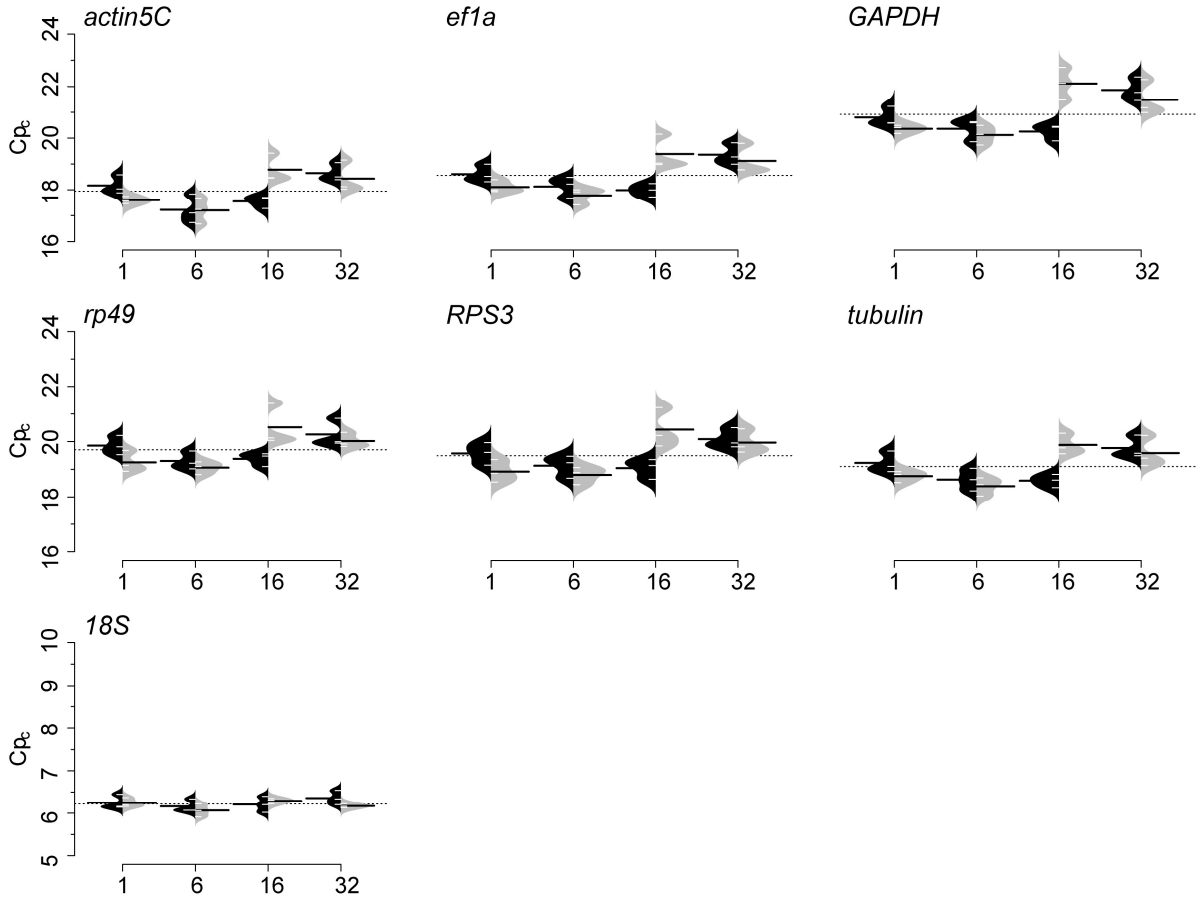


Figure 4 Cp_c values (interplate calibrated Cp values) of the seven tested reference genes upon control (black) or cardiac glycoside (ouabain, grey) treatment at different exposure periods (1 – 32 h) represented as beanplots. Dashed lines represent the mean of all samples ($n = 24$), solid black lines the mean and solid white lines are the respective values within treatment groups per time interval ($n = 3$ each).

Comprehensive gene expression stability evaluation

All seven candidate genes had acceptable gene stability values, i.e. lower than recommended analysis inclusion cut-offs (Bestkeeper sd < 1 (Pfaffl et al., 2004); M value < 1.5 (Vandesompele et al., 2002)). The most stable genes were determined by the geometric averages of ranks obtained by the different algorithms (Table 3). This analysis identified *tubulin* and *ef1a* (both $rank_{geo}$ = 1.41) as the most stably expressed genes (Figure 5, Table S 6). Both genes were consistently ranked first or second by all four algorithms. Thus, these genes were least affected by our treatments over the monitored time range. *Rp49* ($rank_{geo}$ = 2.63) was also identified as exhibiting low variability (ranked 2nd overall). However, individual ranking positions differed more widely, i.e. by more than one rank. Bestkeeper determined *rp49*, based on high r (0.972, p = 0.001) and low sd (0.472), as most stable along with *tubulin* (Figure 5, Table S 6). In contrast, Normfinder ranked *rp49* as 3rd and geNorm and the comparative ∆Ct method as the 4th most stable gene. *RPS3*, having a moderate stability ($rank_{geo}$ = 3.22), showed only minor ranking differences across methods, i.e. one rank difference, being ranked either as the 3rd (geNorm, ∆Ct and Bestkeeper) or 4th most stable gene (Normfinder). Overall, the least stable genes were *actin5C* ($rank_{geo}$ = 5), followed by *GAPDH* ($rank_{geo}$ = 5.42) and *18S* ($rank_{geo}$ = 6.74), and were consistently determined as genes showing the highest expression variability. Although the actual ranking conformity (identical ranks) by the four algorithms was consequently 14.3 %, no major discrepancies in stability assessments were observed overall (≤ 1 rank difference = 71.4 %).

It is important to note here, that during an initial ranking with the Bestkeeper algorithm, we observed opposing stability rankings when stability was ranked either by Cp standard variation (sd) or by the Pearson correlation coefficient (r) with the Bestkeeper Index. This was most prominent for the *18S* gene: ranked 1st by sd, but last by r (Table S 6). Therefore, stabilities were ranked separately by sd and r and both rankings were then combined by geometric rank averaging in a common stability measure: rank(BK) (Table 3). Hence, this measure included the information of both parameters in stability assessments (sd: overall expression variability, r: highest general expression pattern contribution (Pfaffl et al., 2004)).

Normfinder and geNorm identify not only the most stably expressed genes, but also the combination of genes exhibiting the lowest variation for normalization: Normfinder by comparing intra- and inter-experimental group variation (Andersen et al., 2004) and geNorm by excluding the least stable genes in a step-wise manner (referred to as M_e hereafter; (Vandesompele et al., 2002)) (Table 3). Both algorithms identified different gene combinations as most suitable for normalization among one another as well as in comparison with the

preceding ranking. Normfinder determined the stability of *tubulin* and *rp49* in combination as superior to the best single normalizer, because their opposing intergroup variations (Figure S 11) reduced the stability value to 0.071 (vs. 0.097 for *ef1a*) (Figure 5, Figure 6, Table S 6, Table S 7). In contrast to Normfinder, geNorm recommended normalization to *ef1a* combined with *RPS3* (M_e = 0.168), these genes being ranked 1st and 3rd by the initial M value (referred to as M_i hereafter) *prior* to successive exclusion of least stable genes (Figure 5, Figure 6, Table S 6, Table S 7). Furthermore, normalization with these two genes was indicated to be adequate, as the pairwise variation ($V_{2/3}$ = 0.06), which is a measure to determine the optimal reference gene number needed, was lower than the recommended cut-off (0.15) (Vandesompele et al., 2002).

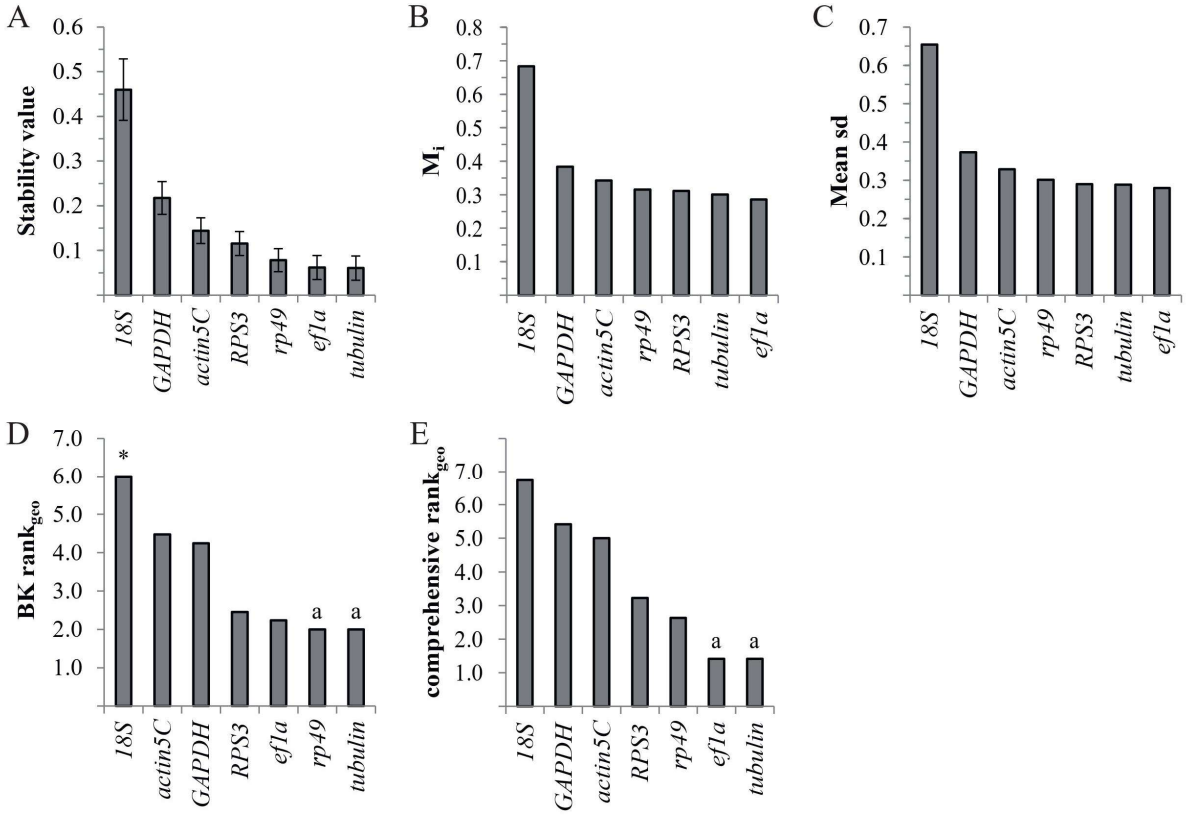


Figure 5 Expression stabilities of the seven candidate reference genes as determined by Normfinder (A – without experimental group assignment), geNorm (B – *prior* to step-wise exclusion of the least stable genes), the comparative ΔCt method (C), Bestkeeper (D) and the comprehensive stability by all four methods (E). Genes are sorted from least to most stable. Asterisk indicates manual ranking and same letters indicate concordant stabilities. Error bars in A = standard error of Normfinder stability values.

We furthermore observed that the influence of analysis mode in Normfinder, i.e. inclusion of experimental group information, had no influence on the identity of the top three most stable normalizers (both *ef1a*, *tubulin*, *rp49*), in contrast to the two different geNorm stability measures (M_i (*ef1a, tubulin*, *rp49*) vs. M_e (*ef1a, RPS3, rp49*)). However, including the stability

values of the comparative ΔCt and Bestkeeper methods, this comprehensive stability ranking was in agreement with the preceding ranking where *ef1a* and *tubulin* were differentiated as 1st and 2nd most stable.

As our preliminary statistical analysis of the raw expression values indicated the importance of exposure duration between treatments, we repeated these analyses for each subgroup: (i) exposure to the control solution (saline) for different time periods, (ii) exposure to the toxin ouabain for different time periods, or (iii–vi) the exposure to these solutions per time interval. We found that the overall most stable single genes (*ef1a* and *tubulin*) were not consistently ranked as the genes with the highest expression stability within the different subgroups (Table S 6, Table S 7). In contrast to *ef1a* which was always among the three most stable genes, *tubulin* was moderate to highly unstable in most exposure periods (1h: 5th (3rd), 16h: 5th (4th), 32h: 4th (3rd)) and in control injected animals (4th or 5th). Conversely, the stability of *actin5C* was higher for these exposure periods and in ouabain treated animals (1st to 3rd). Similar changes in stability assessments were also observed for *GAPDH* (global scale = all samples = 5th (6th) vs. 1 h =3rd (2nd)) and *RPS3* (global scale = 3rd (4th), 32h = 1st). Consequently, the reference genes displayed different degrees of variation between treatments depending on the exposure time interval and may, thereby, differ in their suitability for normalization. Furthermore, contrary to the global analysis, the most stable gene combinations recommended by geNorm and Normfinder consistently shared one gene per subgroup (Table S 6, Table S 7).

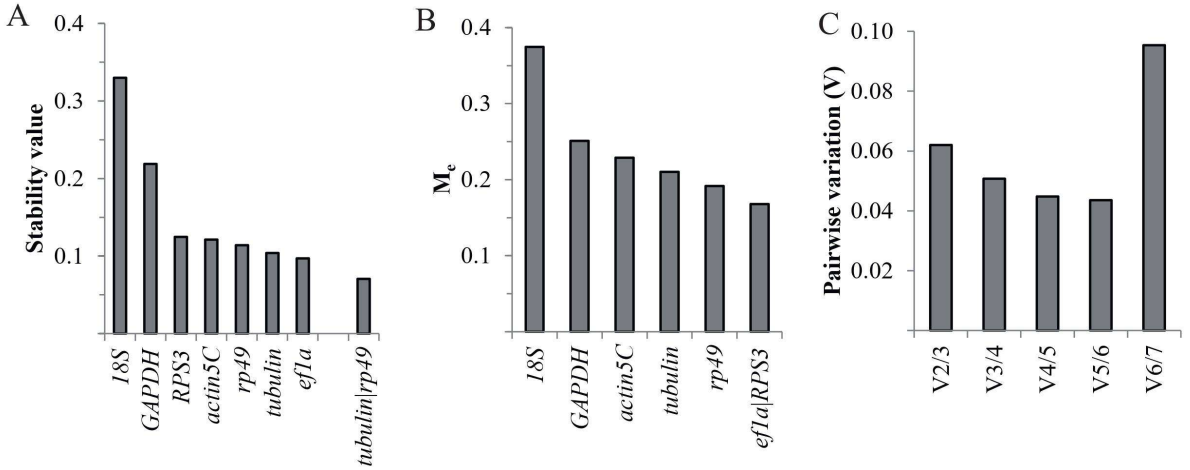


Figure 6 Expression stabilities of the seven candidate reference genes as determined by Normfinder (A) when experimental group information was included into analysis and by geNorm (B) when most unstable genes were successively excluded from M value calculation (M_e). Genes are sorted from least to most stable. Far right column in A represents the stability value of the best recommended gene combination by Normfinder. C: pairwise variation values (V) calculated by geNorm at which genes (n) were stepwise added ($V_{n/n+1}$) to the most stable gene combination (V_n = 2). This identified the minimum gene number required for reliable normalization: if $V_{n/n+1}$ < 0.15 then (n-1) genes are considered adequate (Vandesompele et al., 2002).

Discussion

Quantitative real time PCR (RT-qPCR) can be an indispensable technique for elucidating the molecular pathways involved in biological processes. However, a prerequisite for accurate and reliable relative quantification is the validation of stable endogenous normalizers (Andersen et al., 2004; Bustin, 2002; Bustin et al., 2009; Bustin et al., 2010; Bustin and Nolan, 2004; Bustin and Nolan, 2017; Dheda et al., 2005; Huggett et al., 2005; Kozera and Rapacz, 2013; Nolan et al., 2006; Pfaffl et al., 2004; Silver et al., 2006; Vandesompele et al., 2002). Here, we analyzed how strongly the temporal expression of candidate reference genes for RT-qPCR in *O. fasciatus* is affected by exposure to cardiac glycosides, dietary toxins that these hemipterans are naturally confronted with (Agrawal et al., 2012; Duffey and Scudder, 1972; Duffey and Scudder, 1974).

In total, we designed primers for and evaluated the temporal stability of seven out of ten candidate reference genes in *O. fasciatus* upon cardiac glycoside challenge. We particularly chose ouabain injections here, based on three major considerations: (i) Facilitated transport can be assumed based on its polarity (Agrawal et al., 2012) and various previous accumulation studies with this cardiac glycoside (Detzel and Wink, 1995; Duffey et al., 1978; Duffey and Scudder, 1974; Meredith et al., 1984; Scudder and Meredith, 1982a; Scudder and Meredith, 1982b; Yoder et al., 1976) provide excellent preconditions to connect physiological with gene expression changes. (ii) Especially the selective uptake of polar cardiac glycosides from the hemolymph into its specialized accumulation sites (Duffey et al., 1978; Duffey and Scudder, 1974; Scudder and Meredith, 1982b) suggests active transport mechanisms here, in contrast to the gut (Detzel and Wink, 1995; Scudder and Meredith, 1982b; Yoder et al., 1976). Injections have also been applied in other insect species to study secondary plant metabolite transport in vivo (Discher et al., 2009; Narberhaus et al., 2003; Nickisch-Rosenegk et al., 1990b) and can be considered the most reliable approach to identify active transport related expression changes without any potential undefined spatiotemporal delay. (iii) Along the same lines, as accumulation necessitates appropriate tolerance strategies (Erb and Robert, 2016), injections enable furthermore a non-biased examination of its Na,K-ATPase paralogs expression.

In fact, assuming a hemolymph volume of 5–10 µl (Duffey and Scudder, 1974), the final ouabain concentrations in the hemocoel of the *O. fasciatus* specimens studied here correspond to a range where neural Na,K-ATPase activity inhibition is approximately 50 % in vitro (Bramer et al., 2015). Na,K-ATPase inhibition by ouabain induces profound gene expression changes in mammalian cells including protein translation regulators (Klimanova et al., 2017; Koltsova et al., 2012). In contrast, all candidate reference genes tested here had

acceptable stabilities below the recommended Bestkeeper and geNorm cut-offs for subsequent stability analyses (Bestkeeper sd < 1 (Pfaffl, 2004); geNorm M < 1.5 (Vandesompele et al., 2002) or the previously refined M < 1.0 (Hellemans et al., 2007)). The lack of expression change seen here, especially for the protein synthesis related genes, *ef1a* and *rp49*, could be a further indicator of the high extent to which this species is adapted to cardiac glycosides and profits from its triplicated Na,K-ATPase α-subunits (Dalla and Dobler, 2016; Lohr et al., 2017; Zhen et al., 2012). However, as yet none of these paralogs have shown a change in expression upon cardiac glycoside exposure, despite being essential for survival (Lohr et al., 2017). A physiological response to ouabain, however, was verified in our animals (Bramer et al., 2015; Lohr et al., 2017). If the latter is accompanied by changes on the level of gene expression requires future research, which will be facilitated by the reference genes validated here.

Even though the candidate reference gene stabilities found here were acceptable, our stability analysis using four established methods (Bestkeeper, Normfinder, geNorm and the comparative ΔCt) emphasized how certain genes allow more accurate expression quantifications than others. All of the stability algorithms identified the *18S rRNA* gene as the most inappropriate endogenous normalizer. The suitability of this “historic” normalizer remains controversial and its use should be case dependent, as for all reference genes (Chapman and Waldenström, 2015; Huggett et al., 2005; Kozera and Rapacz, 2013). Here, for the quantification of GOI expression upon cardiac glycosides challenge in whole body samples, we consider the *18S* gene unsuitable because of its (i) diverging expression pattern from all mRNA coding genes, (ii) the potential susceptibility to inaccurate baseline corrections in analysis software due to its high abundance (Vandesompele et al., 2002) and (iii) because of the known differential transcription and degradation of rRNA and mRNA (Kozera and Rapacz, 2013 and references therein). Furthermore, although several studies inferring reference gene stability in insects (e.g. Bansal et al., 2016; Pan et al., 2015; Yuan et al., 2014; Zhai et al., 2014) have used Bestkeepers’ sd for stability ranking, our results for *18S* demonstrate the need for careful ranking parameter selection, as recently addressed (Olias et al., 2014; Spiegelaere et al., 2015). In principle, we agree with Spiegelaere et al. (2015) that the correlation coefficient rather than sd should be used for stability assessment. Our ranking strategy used here (similar to that conducted by Olias et al., 2014) is more appropriate when correlation coefficient differences are minor, such as is the case in this study (all datasets ≤ 0.091 except saline (0.295)). A major advantage of this algorithm is, that target gene expression can be easily included to infer their differential expression or consideration as further potential reference genes (Pfaffl et al., 2004). A preliminary screening of target genes

indeed indicates that an ABCB protein (*Ofabcb1*) as wells as the α1A Na,K-ATPase paralog might be valuable reference gene candidates (Meinzer, unpublished data).

The acceptable level of variability in endogenous normalizers depends on the accuracy needed to draw reliable biological conclusions (Hellemans et al., 2007; Huggett et al., 2005). GOI quantifications at the systemic level, as measured here upon cardiac glycoside exposure, are likely to entail reduced GOI responses due to opposing tissue-specific reactions. Consequently, selecting the most accurate normalizers is essential to maximize quantification reliability for subtle expression changes. To explore these issues we used different stability algorithms and also investigated the impact of different analysis modes and treatment subsets on stability assessments. Based on our results we recommend normalization by *ef1a*, *tubulin* and *rp49* in future studies concerning cardiac glycoside stress at the systemic level in the large milkweed bug based on the following considerations: (i) a prerequisite of pairwise comparison approaches like geNorm is the assumption that genes are not co-regulated (Vandesompele et al., 2002). However, we observed a clustering of the protein synthesis related genes *ef1a* (aminoacyl-tRNA transfer catalyzer), *rp49* (60S ribosomal subunit) and *RPS3* (40S subunit) after stepwise exclusion in contrast to their initial ranking. Thus, a potential co-regulated favored stability assessment by this algorithm could not be excluded. Furthermore, (ii) Normfinder which minimizes such stability assessment biases (Andersen et al., 2004), assessed the stability of *rp49* as superior to that of *RPS3*. (iii) Although geNorm's V indicated that inclusion of a third normalizer is not necessarily required, the normalization strategy suggested here combines the overall most unaffected normalizer (*ef1a*) with endogenous controls, which were found marginally affected on the temporal scale in respective treatment groups (*tubulin*, *rp49*). Furthermore, inclusion of additional genes revealed no significant negative effect on normalization ($V_{6/7} < 0.1$). (iv) Indeed, we found temporal variability in our candidate genes upon ouabain challenge. Genes that were stable on the global scale were not automatically superior across all time points.

The primary goal of this work was the establishment of robust reference genes in *O. fasciatus*. The results on their responses to ouabain are to serve as a starting point and guide for further studies on this topic. Our sample size of $N = 3$ for this portion of the analysis was lower than needed for reliable estimates (Andersen et al., 2004; Vandesompele et al., 2002). Specifically, the time $*$ treatment interaction for the ouabain treatment proved difficult. This was due to the large variation introduced by the RT-qPCR methodology. This problem is readily apparent in Figure 4 on the beanplots where the shaped distributions halo each tick. There simply aren't enough points to reliably define a distribution.

Despite the low sample sizes for our time ∗ treatment interactions data set, our study does highlight an important hole in the literature: Relatively few studies have addressed expression stability across a temporal scale. In insects the stability of reference genes has been confined primarily to single factors like tissue, population, diet, infection, temperature, photoperiod or developmental stage (reviewed by Shi et al., 2015). Although using a common normalizer set, i.e. the same reference genes for all time points, is the convenient strategy, temporal stability should be considered to confirm that this strategy introduces minimal and passable normalization-error variations at the time points under study. Indeed, in two other arthropod studies where temporal normalization was performed, alternative normalization strategies were deemed more appropriate than internal endogenous controls (springtails: Sørensen et al., 2010; butterflies: Płachetka-Bożek and Augustyniak, 2017).

The results of this study provide suitable normalizers for use in future expression studies in the large milkweed bug. Nonetheless, it has been extensively demonstrated that ideal normalizers for every treatment do not exist, and that validation is required for each new treatment (Chapman and Waldenström, 2015; Kozera and Rapacz, 2013; Shakeel et al., 2018; Shi et al., 2015). Thus, evaluation of the suitability of the normalizers' presented here across other biologically relevant conditions will be required before use. Along similar lines, *TATA box-binding protein* and *arginine kinase*, though not suitable for the analyses presented here, may prove as suitable normalizers for other treatments and under other conditions (Bansal et al., 2012; Bansal et al., 2016; Zhai et al., 2014). To our knowledge, only two different endogenous control genes have been used so far for gene expression analysis in *O. fasciatus: Rp49* (Dean et al., 2016) and *actin* (Ginzburg et al., 2017; Lohr et al., 2017). Specifically, in the recently conducted study using *actin* as a normalizer and including a cardiac glycoside challenge, *ef1a* was evaluated as less stable than *actin* (Lohr et al., 2017), a gene found to have higher instability here. Unfortunately, as with much RT-qPCR work, differences between the experimental methods preclude direct comparison (Bustin and Nolan, 2017), which highlights again the importance of reference gene stability re-evaluation before each experiment.

Besides the validation of adequate reference genes, the efficient removal of residual genomic DNA (gDNA) from RNA samples is essential (Bustin, 2002; Bustin and Nolan, 2004; Nolan et al., 2006). Residual gDNA can lead to expression overestimation and impair quantification reliability (Bustin, 2002; Cui et al., 2007; Laurell et al., 2012). As genomic sequence information is rapidly accumulating the design of intron-spanning or exon-exon junction-binding transcript specific primers becomes more feasible for non-model insect species. Currently the genomes of 304 arthropod species have been sequenced and approximately 58 % of them are easily

accessible by genome databases, like the i5k workspace (Poelchau et al., 2015), InsectBase (Yin et al., 2016) or Lepbase (Challis et al., 2016) (http://i5k.github.io/arthropod_genomes_at_ncbi). Although this is explicitly addressed by the MIQE guidelines (Bustin et al., 2009; Bustin et al., 2010) this strategy is still rare among insect expression studies (only one of those quoted here: Cameron et al., 2013). While intron spanning primer pairs will not prevent amplification of gDNA in contrast to exon-exon junction binding ones, this priming strategy essentially spots quantification inference by gDNA contamination. Since this approach can further increase the reliability of expression results, we strongly recommend implementing it in gene expression studies in general, whenever genomic information is available.

Conclusions

In summary, this study highlights that stable reference gene selection is not necessarily a straightforward process. The comprehensive and critical evaluation by classical statistics, stability methods, data subsets and gathered gene information is indispensable to minimize method associated pitfalls and hence to identify the best normalizers. In addition, an appropriate priming strategy, i.e. designing transcript-specific primer pairs, is a further and valuable safeguard to ascertain a high degree in accuracy and reliability.

Chapter 2

Molecular basis of cardenolide sequestration in the large milkweed bug, *Oncopeltus fasciatus*

Abstract

Although sequestration is a widespread strategy among phytophagous insects to cope with the chemical defense systems of their host plants, little is known about the underlying molecular mechanisms in insects. The large milkweed bug, *Oncopeltus fasciatus* (DALLAS, 1852), is one of the best-characterized species concerning the physiological mechanisms of sequestration of ingested host plant toxins, in this case cardenolides. In this chapter I investigate the presence of ATP-binding cassette (ABC) subfamily B full transporters and their role in cardenolide sequestration of the large milkweed bug. These members of the ABC superfamily, present from bacteria to humans, were widely discussed as mediating a basic protection against cardenolides as well as their storage. Transcriptome, immunohistochemical and expression analyses showed that the large milkweed bug possesses two ABCB full transporters, OfABCB1 and OfABCB2. Furthermore, RNA interference revealed that in contrast to OfABCB2, OfABCB1 is indeed essential for efficient sequestration of the polar standard cardenolide ouabain. My data imply further that *Ofabcb2* is under complex transcriptional control, a potential mechanism diversifying its functions and enabling adaptive flexibility. This work thereby provides the first evidence that an ABCB full transporter is essential for cardenolide sequestration in *O. fasciatus* and thus provides a solid molecular basis for further research.

Introduction

The coevolution of plants and herbivorous insects resulted in an intriguing array of adaptations and counter-adaptations. The plants' chemical defense systems in particular challenged phytophagous insects to evolve sophisticated physiological mechanisms to circumvent the potent effects of induced or constitutively synthesized deterrent plant metabolites (Brattsten, 1992; Futuyma and Keese, 1992). Whilst some of these compounds act rather indirectly, e. g. by reducing digestibility and thereby energetic value, others possess a direct deterrent effect due to their high toxicity (War et al., 2020; Wink and Schimmer, 2010). For the latter, some

herbivores not only evolved mechanisms mediating toxin tolerance and resistance by target-site insensitivity or detoxification, but also enabling their sequestration (Beran and Petschenka, 2022; Duffey, 1980; Jeckel et al., 2022; Opitz and Müller, 2009). Sequestration is a striking way to incorporate the host-plant-derived defense into one's own body for predator deterrence (Beran and Petschenka, 2022; Jeckel et al., 2022; McLain and Shure, 1985). It is therefore a crucial step in the escalation of the evolutionary arms race to the third trophic level (Malcolm, 1991; Petschenka and Agrawal, 2015, 2016).

Sequestration of ingested host plant toxins is known for > 275 species belonging to Coleoptera, Diptera, Lepidoptera, Hemiptera, Hymenoptera and Orthoptera (Agrawal et al., 2024b; Beran and Petschenka, 2022; Opitz and Müller, 2009). Among the broad set of different sequestered metabolites by these species, the frequent occurrence of cardenolides is striking. Cardenolides are a class of highly toxic C23 steroids characterized by their five-membered β-lactone ring at C17 and are synthesized predominantly in members of the Apocynaceae plant family (see also Table 1) (Agrawal et al., 2012; Luckner and Wichtl, 2000; Malcolm, 1991). Their potent toxicity is mediated due to their binding to the α-subunit of the Na,K-ATPase, thereby inhibiting this essential enzyme present in animal cells (Agrawal et al., 2012; Horisberger, 2004; Lingrel et al., 1990; Steyn and van Heerden, 1998; Sticher, 2010). Tolerance to these toxins through target-site insensitivity, i.e. insensitive α1-subunits, and also cardenolide sequestration are known in at least five insect orders in which members have specialized on cardenolide-producing plants (Coleoptera, Diptera, Lepidoptera, Hemiptera, Orthoptera) (Agrawal et al., 2024b; Beran and Petschenka, 2022; Dobler et al., 2012; Dobler et al., 2015; Dobler et al., 2019; Yang et al., 2019; Zhen et al., 2012).

The large milkweed bug, *Oncopeltus fasciatus* (DALLAS, 1852; Lygaeinae: Lygaeidae: Hemiptera), which feeds on plants of the genus *Asclepias* spp. (L.; Apocynaceae: Angiosperms; see also Table 1), can efficiently accumulate ingested cardenolides in a specialized thoracic storage compartment (Bramer et al., 2017; Duffey et al., 1978; Scudder and Meredith, 1982a). While this is a basal trait of members of the Lygaeinae subfamily, *O. fasciatus* has evolved the most sophisticated type in terms of the releasing mode. In addition to storage, the species can passively release a cardenolide enriched defensive fluid at predetermined breaking points in the storage compartment cuticle, making it even unpalatable for attacking predators *prior* to consumption (Berenbaum and Miliczky, 1984; Bramer et al., 2017; Bramer et al., 2018; Hill, 2006; Scudder and Meredith, 1982a). This elaborated defense system is based on a highly complex and selective sequestration mechanism that is closely linked to the physicochemical properties of cardenolides (Agrawal et al., 2022; Bramer et al.,

2015; Detzel and Wink, 1995; Duffey et al., 1978; Duffey and Scudder, 1974; Meredith et al., 1984; Moore and Scudder, 1985; Rubiano-Buitrago et al., 2023; Rubiano-Buitrago et al., 2024; Scudder et al., 1986; Scudder and Duffey, 1972; Scudder and Meredith, 1982b; Yoder et al., 1976). In general, cardenolides exhibit a broad polarity range which varies with plant organ and species (Agrawal et al., 2012; López-Goldar and Agrawal, 2023; Rasmann and Agrawal, 2011). The seeds, which the large milkweed bug predominantly feeds on, can contain especially high amounts of cardenolides (Agrawal et al., 2012; Chaplin, 1980; Duffey, 1970; Eggermann and Bongers, 1971; Miller and Dingle, 1982; Ralph, 1976; Rasmann and Agrawal, 2011; Vaughan, 1979). Since polarity determines the passive membrane penetration potential of compounds, this causes the actual challenge to sequester cardenolides: apolar ones need to be trapped at the sequestration site, whereas polar ones need to somehow reach it (Agrawal et al., 2012; Duffey, 1980; Wink and Schneider, 1990). The LogP value (XlogP3 when predicted) can be used as a measure of the hydrophilicity (negative values) or lipophilicity (positive values) of a substance and can give a first estimate of the passive diffusibility of cardenolides, which is also important for their biological activity (Pádua et al., 2022; Rutkowska et al., 2013). In fact, uptake and sequestration differs for cardenolides of different polarities in *O. fasciatus*. The uptake of apolar cardenolides into the hemolymph is much faster than that of polar ones (Detzel and Wink, 1995; Scudder and Meredith, 1982b; Yoder et al., 1976). However, for uptake into the storage compartment this is reversed (Duffey et al., 1978). In addition, polarity range of ingested cardenolides is narrowed by biotransformation which likely occurs *prior* to storage. However, mechanisms and locations where biotransformation takes place are not well understood (Agrawal et al., 2022; Duffey and Scudder, 1974; Rubiano-Buitrago et al., 2023; Rubiano-Buitrago et al., 2024; Scudder and Meredith, 1982b). In the end, polar cardenolides and those with intermediate polarity are preferentially sequestered into the storage compartment (Duffey et al., 1978; Duffey and Scudder, 1974; Rubiano-Buitrago et al., 2024).

Despite our extensive knowledge of cardenolide adaptations in *O. fasciatus*, we have no information on the molecular components of its cardenolide transport network and their cellular mechanisms. Previous physiological studies on transport kinetics have, with one exception (Meredith et al., 1984), only pointed to passive transport mechanisms in this network in adult bugs. Yet, sequestration is selective and a steep concentration gradient at the thoracic storage compartments basal lamina can be suggested as outlined above. Mechanisms such as emulsion particles, sieving function or protein-binding at the thoracic storage compartment were discussed but were not further confirmed to date (Bramer et al., 2017; Duffey et al., 1978; Scudder et al., 1986; Scudder and Meredith, 1982a). The lack of knowledge about such

molecular components and their mechanisms applies not only to *O. fasciatus*, but to the majority of host-plant-metabolite-sequestering insects (Beran and Petschenka, 2022).

Although the possible involvement of active transporters in the sequestration of plant metabolites has been extensively discussed (e.g. see Detzel and Wink, 1995; Nickisch-Rosenegk et al., 1990b), their identification has so far been limited to three of the more than 275 host-plant-metabolite-sequestering insect species (Beran and Petschenka, 2022; Kowalski et al., 2020; Opitz and Müller, 2009; Strauss et al., 2013; Yang et al., 2021). All of these molecular key players belong to one of the following two superfamilies present from bacteria to humans: the major facilitator superfamily or the ATP-binding cassette (ABC) transporter superfamily (Dassa and Bouige, 2001; Higgins, 1992; Kowalski et al., 2020; Pao et al., 1998; Strauss et al., 2013; Yang et al., 2021). Insects possess eight different ABC subfamilies (A, B, C, D, E, F, G and H) classified by their protein architecture and homology to mammalian ortho- and paralogs (reviewed by Dermauw and van Leeuwen, 2014). While knowledge about their functional role in insects, particularly their involvement in pesticide resistance, is advancing (Amezian et al., 2024; Dermauw and van Leeuwen, 2014), transport and substrate-specificities have been almost exclusively characterized for mammals. Several members of subfamily A, B, C, G have been linked to drug resistance (Borst and Elferink, 2002; Marquez and van Bambeke, 2011; Schinkel and Jonker, 2003; Theodoulou and Kerr, 2015; Vasiliou et al., 2009). In fact, cardenolide transport by full transporters (FT) of the ABC subfamily B, namely ABCB1, has been known in mammals for some time (Mayer et al., 1996; Pauli-Magnus et al., 2001). Recently, transport was also demonstrated in vitro for insect ABCB full transporters homologous to ABCB1 (Kowalski et al., 2020). Primary active ABCB full transporters have a “typical” ABC transporter structure (TMD-NBD-TMD-NBD) consisting of two fused, duplicated functional domain associations: the nucleotide binding domain for hydrolysis of ATP (NBD) and the transmembrane domain (TMD) where substrate binding and transport takes place. Half transporters (HT) of this subfamily consist of only one functional domain association (TMD-NBD) *prior* to dimerization (Culbertson and Liao, 2025; Dassa and Bouige, 2001; Higgins, 1992; Linton and Higgins, 2007). They have been implicated in physiological roles at intracellular compartments like the mitochondria, endoplasmic reticulum and lysosomes as well as in secondary plant metabolite detoxification (Jin et al., 2020; Schaedler et al., 2015; Trowsdale et al., 1990; Zhang et al., 2000).

One of the most important physiological functions of ABCB1 is its chemoprotective role in the blood(or hemolymph)-brain barrier, which is evolutionarily conserved between mammals and insects (Mayer et al., 2009; Szeri et al., 2009). Increasing evidence suggests that this also

confers a basal resistance to cardenolides, regardless of the degree of specialization to cardenolide-containing host plants. Something similar is also suggested for its absorption-regulating role in the digestive tract (Dobler et al., 2015; Groen et al., 2017; Kowalski et al., 2020; Petschenka et al., 2013b).

ABCB1 homologs have been discussed for some time as prime candidates in the cardenolide transport network, including a role in sequestration (Agrawal et al., 2012; Dobler et al., 2015). Kowalski et al. (2020) characterized the cardenolide spectrum of three ABCB full transporters in leaf beetles and suggest that these also play a role in transport to the beetles' defensive glands and thus in sequestration. However, nothing further is known about the significance or indispensability of ABCB full transporters in this context.

In this chapter, I studied the presence and role of ABCB proteins in the large milkweed bug, *O. fasciatus*, as possible adaptations to cardenolides, focusing on their involvement in sequestration in the living organism. I focused specifically on ABCB full transporters, as they play an important role in cardenolide transport in mammals and cardenolide transport has also recently been demonstrated in insects, as outlined above. Furthermore, I investigated ABCB full transporter tissue distribution on transcript and protein level as well as the responsiveness of gene expression to cardenolides. Finally, I demonstrate that depletion of ABCB full transporter transcript levels by in vivo RNA interference resulted in severe reduction of the capacity for polar ouabain (XlogP3 = -1.7) sequestration.

Material & Methods

Experimental animals

Milkweed bugs were obtained from our laboratory culture, which consisted of two lines: one reared exclusively on sunflower seeds (SS) and one reared additionally on milkweed seeds (*Asclepias syriaca*; MS) (for details see Lohr et al., 2017). If not otherwise noted, all experiments were conducted with adult female bugs which were anesthetized by freezing (-20 °C for 4 - 5 min) *prior* to tissue preparation or injections.

Tissue dissections

In general, tissue preparations of freeze-anesthetized animals were conducted on ice in 1x PBS buffer (pH 7.4). For immunolabeling, Malpighian tubules and the nervous system (including brain, suboesophageal-, thoracic- and composite-ganglion and abdominal connectives (Johansson 1957)) were dissected, immediately embedded in Tissue-Tek®

O.C.T.™ Compound (Sakura Finetek, Germany) and stored at -80 °C until sectioning. To infer *Ofabcb* full transporter expression by RT-qPCR, five additional tissues were dissected: the digestive tract (esophagus, first to third stomach and pylorus excluding Malpighian tubules and rectum (Hood, 1937)), paired salivary glands with ducts, female ovaries, male testis and the thoracic region. The latter consisted of the pronotum, metathorax and scutellum. Major thoracic flight muscles were removed as far as possible.

Immunohistochemical staining

For immunofluorescence staining of tissues, 14 µm cryosections (Leica CM1950, chamber: T = -15 °C, block: T = -10 °C, decreased by 5 °C for Malpighian tubule sectioning) were mounted onto slides (SuperFrost™ Ultra, Thermo Scientific) and air-dried at room temperature for at least 1 h. Furthermore, insects were dorso-ventrally squeezed with forceps and the released defensive fluids were also mounted onto slides and air-dried. Subsequently, sections/ defensive fluids were post-fixed for 10 min at -20 °C with acetone, air-dried for 30 min and washed three times 10 min each with 1x PBS. After blocking for 1 h at room temperature (5 % normal goat serum (NGS), 1 % IgG-free bovine serum albumin (BSA), 0.1 % Triton-X100 in PBS), sections were incubated overnight at 4 °C with the respective primary anti-mouse monoclonal antibodies (mAb) diluted in blocking buffer. As secondary antibody control, one slide was exclusively incubated with blocking buffer, i.e., the primary antibody was omitted. Slides were washed three times 10 min each with 1x PBS and incubated with a Cy3 fluorescently labeled secondary goat anti-mouse antibody (3.75 µg/ml, Dianova, Germany) for 2 h at room temperature in the dark. After three further PBS washings, sections were mounted with IS mounting medium DAPI (Dianova, Germany). In addition, the released defensive fluid was stained with a mixture (4:1) of toluidine blue-O (Merck, Darmstadt, Germany) and pyronine-G (Serva, Heidelberg, Germany) (Bramer et al., 2017). Imaging was conducted with an Olympus BX51 microscope (X-Cite Series 120, Excelitas Technologies) equipped with an Olympus DP71 camera (Cell software (Olympus Soft Imaging Solutions)) and different filter sets (none, Cy3, DAPI). Images were merged with Photoshop CC (v 19.1.6) (Adobe Systems, San José, CA, USA). Tonal correction was applied to bright-field images. Image recording conditions and applied modifications are specified in detail in the respective figure legends.

Monoclonal antibodies

For the detection and examination of the subcellular localization of putative ABCB full transporters, tissues and defensive fluids were stained with the commercially available monoclonal antibody C219 (5 µg/ml; Thermo Fisher Scientific). The nervous system and the

defensive fluid were further stained with additional ABCB detecting monoclonal antibodies, C494 (5 µg/ml; Calbiochem, Merck) and JSB-1 (1:20 diluted; Abcam, UK).

Protein extraction and Western blot

Protein extraction was conducted according to Baum (2015). Briefly, adult males and females (n = 3 each) were homogenized in liquid nitrogen. Ground powder was incubated for 2 h with extraction buffer on ice (100 mM sodium phosphate, 0.3 M sucrose, protease inhibitor (cOmplete™, Roche), pH 7.4). Supernatants were freed from solid matter by two rounds of centrifugation at 9,000 x g (4 °C for 15 min), and ultra-centrifuged at 4 °C for 1 h (40,000 rpm; Beckman L-80 with rotor Type 80 Ti) to separate cytosolic and membrane protein fraction (100 µl resuspension). Protein concentrations were determined by Bradford assay (Bradford reagent, Sigma Aldrich) and BSA standard. After denaturation for 5 min at 55 °C in loading buffer (0.25 M Tris-HCL, 30 % glycerol, 4 % SDS, 0.05 % bromophenol blue, 5 % beta-mercaptoethanol), proteins (membrane: 200 µg; cytosolic: 165 µg) were separated by SDS-PAGE (30 min 100 V, 30 min 120 V, resolving gel: 7.5 % acrylamide, 0.1 % SDS, 0.1 % APS, 1 % TEMED, 0.25 M Tris pH 8.8; running buffer: 250 mM glycine, 25 mM Tris, 0.1 % SDS) followed by blotting on a nitrocellulose membrane at 4 °C for approximately 1.5 h at 60 V (HP42.1, Carl Roth; blotting buffer: 0.7 M glycine, 25 mM Tris, pH 8.2; Mini-PROTEAN Tetra Handcast System (Biorad)). Protein amount was checked by Ponceau S staining (0.1 % Ponceau S, 5 % acetic acid), and thereafter the solution was removed by washing with ddH_2O. Subsequently, membranes were blocked with 5 % milk powder in TBST for 1 h at room temperature followed by incubation with 2 µg/µl C219 anti-mouse monoclonal antibody overnight at 4 °C. After washing the membrane three times with TBST for 10 min, membranes were incubated with 4 µg/ml goat anti-mouse horseradish peroxidase secondary antibody (HRP, Dianova, Germany) for 2 h at 4 °C. After three more washes with TBST for 10 min, staining was performed by chemiluminescence (Roti®-Lumin ultra, Carl Roth) and detected on a Multi-Imaging-System (FUSION-FX7 Advance SUPER-BRIGHT, PEQLAB, VWR).

De novo transcriptome assembly

For identification of ABC transporters in the large milkweed bug, *Oncopeltus fasciatus*, previously published RNA-seq data (Zhen et al., 2012) was mined from http://genomics-pubs.princeton.edu/insect_genomics/data.shtml. Briefly, this data consisted of single (7,888,794 reads with 95 - 100 bp) and paired end reads (27,109,674 with 101 bp length) sampled from adult *O. fasciatus* whole body (Zhen et al., 2012). Two de novo assemblies were performed by different assembly software. One de novo assembly was conducted by Trinity

r2014-04-13p1 (Grabherr et al., 2011) as described in Chapter 1. A second de novo assembly was conducted by CLC Genomics Workbench 7.0.3 (www.qiagenbioinformatics.com) with the following trim parameters: limit of 0.01 for removal of low quality reads (is equivalent to a PHRED score of 20), maximal two ambiguous nucleotides allowed in reads, one nucleotide is removed from the 5' and 3' read end und minimum sequence length = 50 nt.

In silico identification of putative ABCB full transporters in *O. fasciatus*

Both transcript catalogues were searched for putative ABCB transporter of the multidrug-resistant-(MDR)-type using local tblastn (E-value cut-off = 1e-30) with a total of 14 MDR proteins from seven species as homology search targets (Mammals: *Homo sapiens* (n = 2); Insecta: Diptera: *Drosophila melanogaster* (n = 3), Lepidoptera: *Bombyx mori* (n = 3), Coleoptera: *Tribolium castaneum* (n = 2), Hymenoptera: *Apis mellifera* (n = 1) and Hemiptera: *Acyrthosiphon pisum* (n = 2), *Lygus hesperus* (n = 1)). Subsequently, transcripts were analyzed by blastx against the NCBI nr database. Contigs putatively encoding ABCB transporter were then analyzed by Pfam to identify the presence and architecture of characteristic domains, i. e., transmembrane domain (TMD) - conserved nucleotide-binding domain (NBD) in alternating order (TMD-NBD-TMD-NBD). Furthermore, both putative ABCB transporter transcript catalogues were compared by local blastn to identify respective contig clusters. These clusters were then aligned by MAFFT (parameters: G-INS-i, leave gappy regions) (Katoh et al., 2019), checked and where applicable manually curated in BioEdit (Hall, 1999). Sequences revealing complete or almost complete domain architectures (maximum one domain missing) were retained in further analyses. Transmembrane helices prediction by TMHMM 2.0 webserver (Krogh et al., 2001) and likelihood of subcellular localization by WoLFPSORT (Horton et al., 2007) was then explored for translated proteins. Putative ABCB full transporters were mapped to the *O. fasciatus* genome for gene structure prediction as described in Chapter 1 (i5k Workspace@NAL blast tool database: Ofas.scaffolds_new_ids.fa with 17,224 sequences, October 2018) and re-analyzed additionally with HmmScan at HMMER web application (version 2.41.2; http://hmmer.org/) and TOPCONS (Tsirigos et al., 2015). 3D structure modelling was conducted by Phyre^2 (Kelley et al., 2015). Protein features were visualized by PROTTER (https://wlab.ethz.ch/protter/start/) (Omasits et al., 2014). Gene structure prediction for genomic scaffold regions of interest (252 or 214) was also conducted by FGENESH+ (v. 2.6; http://www.softberry.com) which uses Hidden Marcov Model-based and similar protein-based gene prediction (Solovyev, 2008). The human MDR1 protein sequence (UniProtKB acc. number: P08183.3) was selected as "similar protein". Specific gene-finding parameters were based on the pea aphid (*Acyrthosiphon pisum*), the only

genome-specific parameters available for members of the Hemiptera at the time of the analysis.

Phylogenetic inference

The phylogenetic reconstruction was focused exclusively on ABCB full transporter because only these have been implicated in transport of cardenolides. ABCB full transporter sequences of a total of 91 homologs from 32 taxa were mined from NCBI, OrthoDB and Ensemble (Table S 8, Table S 9) to infer the phylogenetic relationship of identified *Ofabcb* full transporters with previously identified carriers of other metazoans. As several of these were exclusively predicted in silico, sequences were searched for characteristic ABCB full transporter architecture in ExPASY PROSITE with the profiles PS50929 and PS50893. Only sequences encompassing an unambiguous and almost intact architecture (at least NBD-TMD-NBD) were included in the subsequent analysis. The phylogenetic reconstruction involved 72 ABCB full transporters from 30 species and 998 positions after alignment with MUSCLE and exclusion of sites with coverage lower than 95 % in MEGA7 (Kumar et al., 2016). The LG+R7 substitution model was selected as optimal model according to BIC by ModelFinder (Kalyaanamoorthy et al., 2017). Phylogenetic inference was performed by maximum likelihood (ML) method with IQ-Tree (Trifinopoulos et al., 2016) using ultrafast bootstrap (Minh et al., 2013) and SH-aLRT branch test, each with 1000 replicates. The ML tree was midpoint rooted and then visualized by iTOL (Letunic and Bork, 2016).

Cardenolide injections

Cardenolide injections were conducted to (i) study the temporal expression patterns of *Ofabcb* full transporters upon exposure and (ii) to analyze the ability to store cardenolides in RNAi knockdown animals. For this, the polar cardenolide ouabain (10 µg in 0.9 % NaCl; Sigma-Aldrich, Germany) was injected laterally between the fourth and fifth abdominal segment using a 10 µl syringe with a 34 gauge needle (Hamilton®, Romania). (i) For temporal expression pattern analysis, seven day old unmated bugs were sacrificed 1 h, 6 h, 16 h and 32 h *post* injection (n = 3 - 10 each) by freezing in liquid nitrogen and stored at -80 °C. Also, for each time period additional bugs (n = 3 - 10 each) were injected with saline only (NaCl 0.9 %) as control. Injection of RNAi animals was conducted as described below.

DNA extraction, RNA extraction and cDNA synthesis

In general, DNA extraction, RNA extraction, quantification, and cDNA synthesis were conducted as described in Chapter 1. For reverse transcription of tissue-specific RNA, RNA

and primers were additionally denatured at 65 °C for 5 min and then reverse transcribed at 42 °C for 60 min, followed by incubation for 20 min at 65 °C. All cDNAs were diluted to 10 ng/µl for quantitative expression analysis. For initial tissue-specific ABCB transporter testing, tissues and complete bugs were extracted by RNAmagic (Bio-Budget) as follows: the sample was homogenized in 1 ml RNAmagic reagent. Subsequently it underwent three freeze-thaw-cycles in liquid nitrogen. After adding 200 µl chloroform (Carl Roth, Karlsruhe, Germany) it was mixed for 3 min, incubated 10 min on ice and centrifuged at full speed for 10 min at 4 °C. The aqueous phase was transferred to a new reaction tube and RNA was precipitated for 1 h at -20 °C with the same volume of isopropanol (approx. 400 µl) followed by centrifugation at full speed for 45 min at 4 °C. The supernatant was discarded and the pellet was washed with 250 µl 70 % ethanol and centrifuged twice for 10 min at full speed. The pellet was dried at 65 °C for 3 min and resuspended in 20 - 50 µl RNAse free water. Furthermore, this and RNA used for cloning was reverse transcribed with superscript reverse transcriptase III (Invitrogen, Waltham, USA) according to manufacturer instructions with random hexamers and a T17 primer. The extraction method also allowed to analyze fatty tissues like the fat body. However, these samples revealed rather poor 260/230 ratios and methods were therefore changed as described above.

Primer design and specificity

Primers were designed for sequencing, expression analysis, RNA interference and cloning by Primer3 (Untergasser et al., 2012) and manufactured by Eurofins Genomics (Ebersberg, Germany) (Table S 10, Table S 11, Table S 12). Quantitative real-time PCR primers were designed to flank or span a predicted exon-exon junction to preclude genomic DNA amplification and transcripts with intronic sequences (Figure S 22). Specificity of designed RT-qPCR primers was confirmed by testing for genomic DNA amplification (gDNA) as outlined in Chapter 1 (Figure S 12).

Standard PCR, sequencing and cloning of putative ABCB full transporter in *O. fasciatus*

Standard PCRs were conducted to analyze the in silico identified putative ABCB transporter in tissues and to amplify their coding sequence regions for sequencing and cloning. Most standard PCR reactions were performed using standard recombinant Taq polymerase (0.04 U/µl) (Thermo Fisher Scientific) in 1x Taq buffer with 0.2 mM dNTP each, 0.5 µM primer each, 2 mM $MgCl_2$ added to 25 µl with water. In some cases, bovine serum albumin (0.5 µg/µl) was added to improve amplification. PCR parameters were optimized dependent on template. In

general, the standard protocol comprised the following parameters: Initial denaturation at 94 - 95 °C for 1 - 10 min, 35 cycles of denaturation at 94 - 95 °C for 45 - 60 s, annealing at a melting temperature (Tm) determined by gradient PCR (rarely based on primer Tm) for 30 s and elongation at 72 °C for 1 min per 1kb template followed by final elongation at 72 °C for 5 - 10 min. Long fragments like those for cloning were amplified with Phusion high fidelity DNA-Polyermase (0.02 U/µl) (Thermo Fisher Scientific) in 1x Phusion HF with 200 µl dNTP each, 0.5 µM primer each, 1 mM $MgCl_2$ added to 25 µl with water. PCR cycling was as follows: 30 s initial denaturation at 98 °C followed by 35 cycles of 10 s denaturation at 98 °C, 30 s annealing at optimal melting temperature and 30 s per kb template elongation at 72 °C followed by final elongation at 72 °C for 10 min. PCR products were analyzed by gel electrophoresis with 1 to 1.5 % agarose gels stained with ethidium bromide (1× TAE buffer, 100 V, 30 - 40 min). Sequencing was conducted by GATC Biotech (Constance, Germany) and PCR products/ plasmids submitted according to their guidelines. Open reading frame (ORF) cloning is described elsewhere (Lisiecki, MSc thesis, 2018).

Sequencing of PCR fragments to verify the transcript sequence indicated mixed sequences in several amplicons, particularly those of *Ofabcb2*. For these, cloning was performed as follows: Ligations were set up with 0.5 µl pGEM®-T vector (Promega, Madison, USA), 1.5 to 3.5 µl PCR product, 0.5 µl T4 DNA Ligase (5 Weiss units/µl; Thermo Scientific), 0.5 µl T4 Ligase buffer (10x; Thermo Scientific), adjusted to 5 µl with H_2O and incubated overnight at 4 °C or for 1 h at 20 °C. 2.5 µl was added to 25 to 50 µl competent *E. coli* cells (JM109 (Promega) or XL10-GOLD (Stratagene, La Jolla, USA)), incubated for 30 min on ice, followed by heat shock at 42 °C for 45 s. After cooling for 2 minutes on ice, 250 to 350 µl of SOC medium (2 % (w/v) tryptone, 0.5 % (w/v) yeast extract, 10 mM NaCl, 2.5 mM KCl, 10 mM $MgCl_2$, 10 mM $MgSO_4$, 20 mM glucose) was added before incubation at 37 °C for 1 h with horizontal shaking at 225 rpm (Eppendorf Thermomixer comfort). Afterwards 100 µl were plated on LB agar plates (1 % (w/v) tryptone, 0.5 % (w/v) yeast extract, 1.5 % (w/v) agarose, 1 % (w/v) NaCl, 100 mg/ml ampicillin, 40 µg/ml IPTG, 100 µg/ml X-Gal) and incubated overnight at 37 °C. White colonies were picked and resuspended in 20 µl H_2O. 2.5 to 5 µl of this was used for colony PCRs with the primers T7 and Sp6. The remainder was stored in 250 to 500 µl LB medium with ampicillin (100 µg/ml) at 4 °C. Plasmids of interest were subsequently isolated by mini-preparations und sequenced.

Quantitative real-time PCR

The relative transcript levels of *Ofabcb* full transporter transcripts were quantified in whole animals and tissues of insects feeding on natural cardenolides as well as in animals injected

with the polar cardenolide ouabain by quantitative real-time PCR (RT-qPCR) with EvaGreen chemistry (for further details see Chapter 1; Table S 12). RT-qPCR was also used to confirm the RNAi-mediated mRNA knockdown of *Ofabcb1* and *2*. Primer efficiencies were determined by serial dilution of pooled treatment cDNA samples (Table S 13, Table S 14, Table S 15, Table S 16). Identified suitable reference genes of Chapter 1 were revalidated in different treatments by the reference gene stability algorithms Normfinder and geNorm (see Chapter 1 for further details). The stability of previously identified stable normalizer candidates (*Ofef1a*, *Ofrp49*, *Oftubulin*) was reassessed for whole body samples and used for normalization. For milkweed bug tissues reference gene stability was determined for *Ofef1a*, *Ofrp49* and *Ofactin5C*. All three genes were then used as reference genes for tissue-specific expression quantification.

RNA interference

To induce a knockdown in the expression of ABCB full transporters, dsRNA was synthesized by the MEGAscript®RNAi Kit (Thermo Fisher Scientific, Germany) following manufacturer instructions. PCR products were amplified with primer pairs given in Table S 12 and control sequenced before being used as templates for synthesis (Table S 17). Eluted dsRNA was quantified with a NanoDrop spectrophotometer (Thermo Fisher Scientific, Germany) and 700 ng dsRNA was injected into one to two-week-old insects (SS) (n = 28 - 33 per treatment). Single as well as double knockdowns were induced for ABCB full transporters. DsRNA of the enhanced green fluorescent protein (*egfp*) was injected as a control as well as elution buffer only. In an initial experiment, animals were sacrificed seven (n = 2) and ten days (n = 3) after injection to determine the remaining expression level at these time points. Furthermore, the effect of a higher *Ofabcb*2 dsRNA injection amount (1.17 µg) was explored. To study the effect of reduced ABCB full transporter expression on the ability to sequester ouabain, bugs were injected with ouabain as described above one week after dsRNA injection. Defensive fluids sampled from five to seven individuals injected with *egfp* or *Ofabcb* (single or both combined) dsRNA, or buffer, were analyzed by reversed-phase high-performance liquid chromatography (HPLC). RNA was extracted from three to four individuals per treatment and analyzed by RT-qPCR to determine the level of expression reduction.

Sampling and cardenolide extraction of defensive fluids for HPLC analysis

For quantification of the sequestered ouabain amount in the thoracic storage compartment in dsRNA treated insects, the stored defensive fluid was sampled 2 h *post* ouabain injection (n = 5 - 11 per treatment). Insects were squeezed as described in the section

“Immunohistochemical staining” and the released fluid was collected in 2 µl glass capillaries (Hirschmann®, Germany). The measured volume was ejected in methanol with subsequent capillary flushing (three times) and extracted as described by Petschenka and Agrawal (2015) with minor modifications: 1 ml methanol (Carl Roth, Karlsruhe, Germany) containing the defensive fluid sample was spiked with 10 µg digitoxin (Sigma-Aldrich, Darmstadt, Germany) as internal standard (ITSD). After ultra-sonication for 5 min and centrifugation for 10 min (13.4 rpm, MiniSpin; Eppendorf, Hamburg, Germany), the transferred supernatant was filtered (0.45 µm nylon filter; Carl Roth, Karlsruhe, Germany), and evaporated completely by vacuum centrifugation (Eppendorf Concentrator 5301, Eppendorf, Hamburg, Germany). Extracted cardenolides were re-dissolved in a total volume of 100 µl methanol, ultra-sonicated for 5 min, transferred to HPLC vials (Chromatographie Zubehör Trott, Kriftel, Germany), and stored at -20 °C until analysis.

Internal standard multi-level calibration for ouabain quantification

To quantify the amount of ouabain in the defensive fluid by HPLC, a multi-level calibration was conducted as follows: A five-point standard curve was prepared and measured with decreasing ouabain concentration in 1 to 2 dilution steps starting at 0.2 µg/µl, but simultaneously keeping the internal standard substance, digitoxin, constant at 0.1 µg/µl. The response and amount ratios were calculated and a calibration curve established by linear regression forced through the origin ($y = 1.0052*x$, $R^2 = 0.9975$).

High-performance liquid chromatography

The amount of ouabain in the defensive fluid of injected bugs was quantified by reversed-phase high-performance liquid chromatography (HPLC) on an Agilent 1100 system, equipped with a C18 column (5 µm, 4.6 mm, 250 mm; Nucleodur C18 HTec, Machery-Nagel, Düren, Germany). 10 µl of samples were injected and eluted with an acetonitrile (ACN):water gradient (HPLC grade, Carl Roth, Karlsruhe, Germany) at 0.7 ml/min as follows: 8 % ACN at 0 - 2 min, 70 % ACN at 28.5 min, 95 % at 33.5 min, 95 % at 38.5 min including a 15 min *post* run period. Recording and quantification was conducted as described by Rasmann et al. (2009) and Petschenka and Agrawal (2015). Each measurement included at least one blank sample containing the solvent only, i.e., methanol. Further details and optimizations are described in Chapter 3.

Data Analysis

All statistical analyses were conducted by R-3.5.1 (R Core Team, 2018) and R Studio 2024.12.1+563 including among others the packages stats, car, MASS, psych, Rcmdr, ggplot2, MESS and PMCMR. Validity of assumptions for Analysis of Variances (ANOVA) was checked by Levene's test for homogeneity of variances and Shapiro-Wilk test of residuals assisted by diagnostic model plots. In general, follow-up post hoc tests to ANOVA were conducted by Tukey's Honestly Significant Difference method to account for family-wise Type I error increase (FWR) for multiple testing. If assumptions for parametric tests were violated, Kruskal-Wallis or Scheirer-Ray-Hare tests were conducted using Dunn's all-pairs test with Benjamin-Hochberg's correction as post hoc test. Two-sample tests of small, equal sample sizes were routinely conducted by Welch's Test and adjusted like non-parametric tests for multiple comparisons. Differences in counts were analyzed by Fisher's exact test for count data. All indicated error margins are standard error of the mean (SEM).

Results

Immuno-detection and subcellular localization of putative ABCB full transporters in *O. fasciatus*

The epitope of monoclonal antibody C219 is conserved, well characterized (van den Elsen et al., 1999), and hence this monoclonal antibody has been widely used to detect ABCB full transporters of the MDR-type across species (Mayer et al., 2009; Murray et al., 1994; Petschenka et al., 2013b). In humans, for example, the epitope can be found in ABCB1 (Pgp-1/MDR1) as well as in ABCB4 (MDR3) (Georges et al., 1990; Schinkel et al., 1991).

Immunoblotting with C219 identified a protein of about 130 kDa in the crude membrane fraction of milkweed bugs (Figure 7). Furthermore, immunohistochemistry with C219 resulted in specific signals in all examined tissues with significant prevalence in cardenolide handling, (i) cells of the thoracic storage compartment, (ii) the nervous system and (iii) the Malpighian tubules. In contrast, the monoclonal antibodies C494 and JSB-1, rather used for detection in mammals (Beaulieu et al., 1995; Georges et al., 1990; Schinkel et al., 1991), revealed divergent signals as outlined below. The epitope of JSB-1 is not characterized, but it is referred to as human ABCB1 specific (Rao et al., 1995). The epitope recognized by C494 in ABCB full transporters varies within and between mammalian species (Georges et al., 1990).

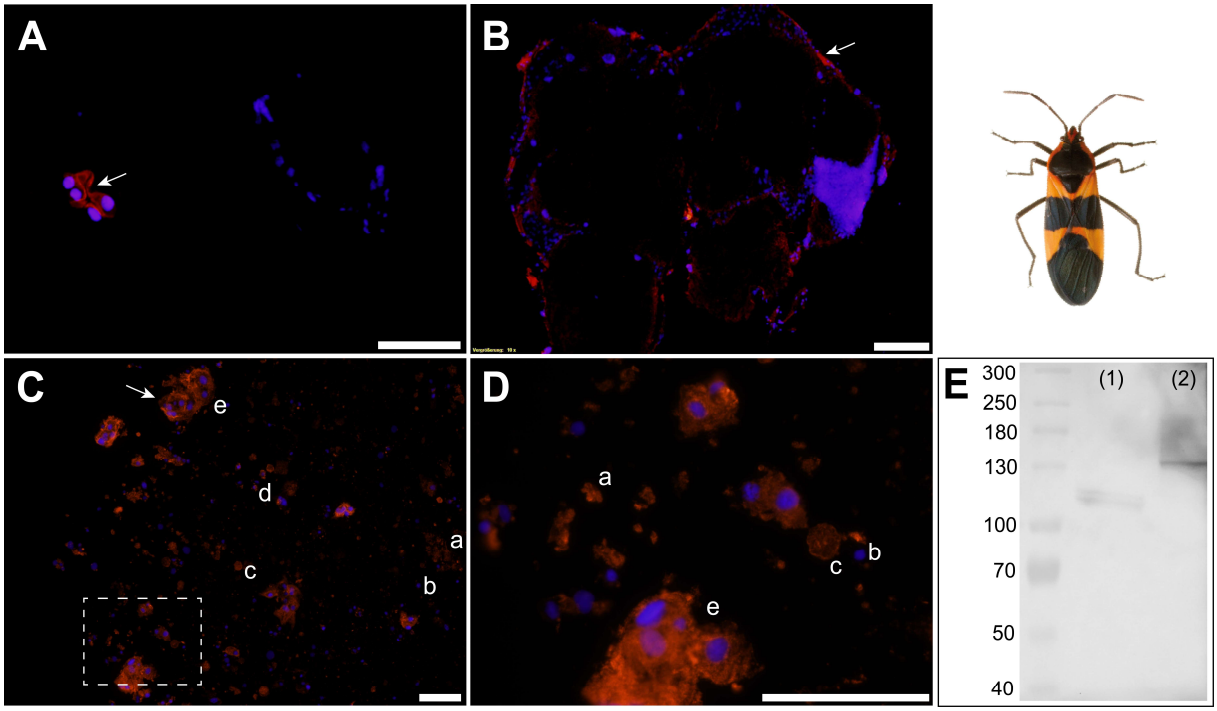


Figure 7 Immunofluorescence staining of different tissues and defensive fluids of *O. fasciatus* individuals stained with a commercially available anti-ABCB full transporter antibody (C219). ABCB full transporter positive staining is indicated by red fluorescence (Cy3 secondary antibody). Nuclei are stained by DAPI and appear blue. A: Malpighian tubules (Cy3: 500 ms, DAPI: 20 ms), B: Brain (Cy3: 500 ms, DAPI: 20 ms), C - D: Cells present in released defensive fluids. Letters in C indicate different cellular components observed: a = cell debris, b = single nuclei, c = discrete spherical cellular structures without nuclei, d = spherical cellular structures with nuclei, e = assemblies of voluminous cells (Cy3: 100 ms, DAPI: 20 ms). D: Area indicated by the dashed square in C, shown at higher magnification (Cy3: 50 ms, DAPI: 10 ms). E: Western Blot of cytosolic (1) and crude membrane extracts (2) of *O. fasciatus* stained with mAb C219. Images were scaled, cropped, and scale bars were adjusted to 100 µm for illustrative purposes. For the original images, see the appendix. Adult *Oncopeltus fasciatus* photo by Samuel Waldron.

(i) The thoracic storage compartment. Consistent with the previously described fragility of the thoracic storage compartment (Scudder and Meredith, 1982a), I was not able to retrieve sufficiently intact whole body cryosections to examine unequivocally the presence of ABCB full transporter within the storage compartment. Nonetheless, I successfully bypassed this difficulty by testing for ABCB transporter presence in the released defensive fluids as these comprise a non-negligible number of cellular components when released. These components could be roughly differentiated into cell debris, single nuclei, discrete spherical cellular structures without or with nuclei and assemblies of voluminous cells (Figure 7, Figure 8, Figure S 13). Two out of three tested monoclonal antibodies revealed signals indicative of MDR-type ABCB full transporter presence in these cells. Signal intensity was highest for C219 in assemblies of voluminous cells. In contrast, C494 intensity was lower and rather observed in the discrete spherical cellular structures. No signal was found by staining with the monoclonal antibody JSB-1 (Figure 7, Figure S 14).

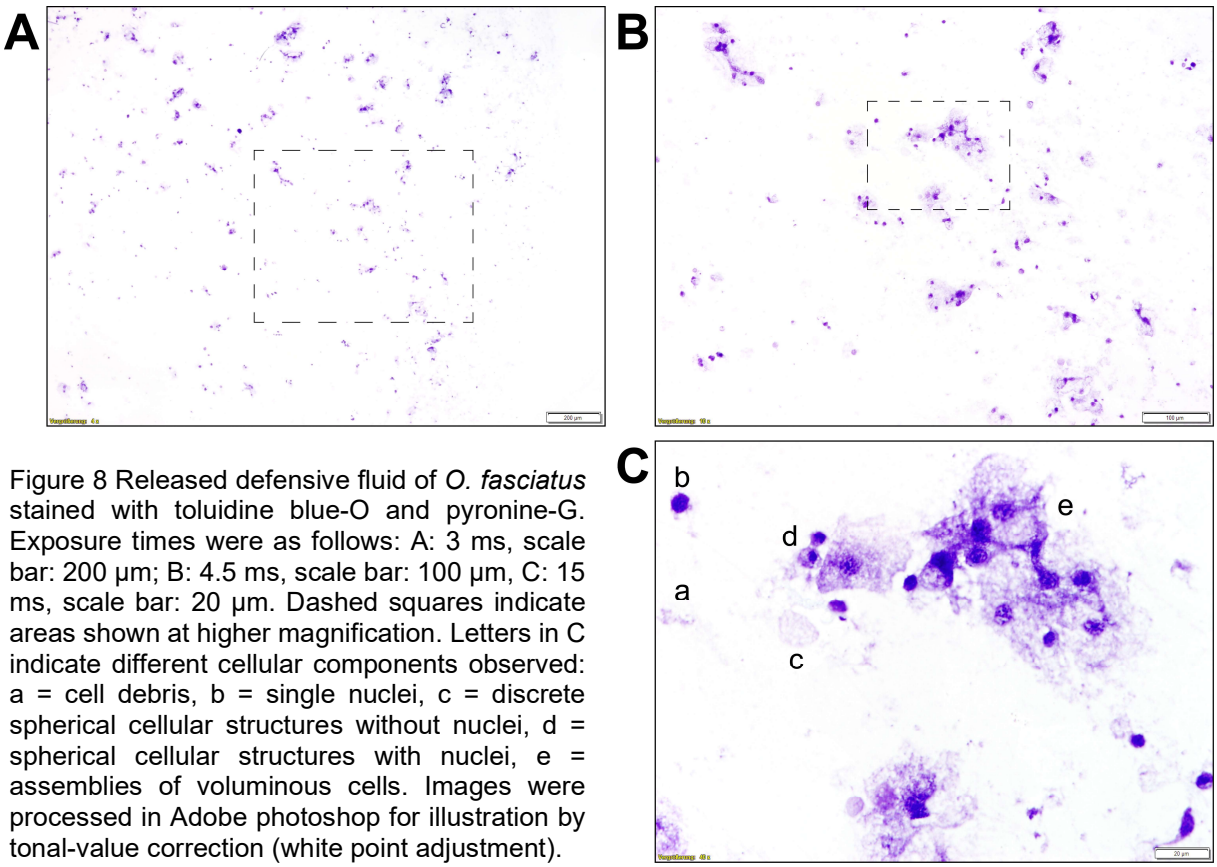


Figure 8 Released defensive fluid of *O. fasciatus* stained with toluidine blue-O and pyronine-G. Exposure times were as follows: A: 3 ms, scale bar: 200 µm; B: 4.5 ms, scale bar: 100 µm, C: 15 ms, scale bar: 20 µm. Dashed squares indicate areas shown at higher magnification. Letters in C indicate different cellular components observed: a = cell debris, b = single nuclei, c = discrete spherical cellular structures without nuclei, d = spherical cellular structures with nuclei, e = assemblies of voluminous cells. Images were processed in Adobe photoshop for illustration by tonal-value correction (white point adjustment).

(ii) The nervous system. Monoclonal antibodies C219 and C494 indicated the presence of MDR-type ABCB full transporter also in the nervous system in contrast to JSB-1. While signals by C494 were detected throughout the nervous system, those by C219 were specifically located to the nervous system's periphery (Figure 7, Figure S 15).

(iii) Malpighian tubules. The monoclonal antibody C219 revealed highest signal intensity exclusively restricted to the apical part of tubule cells of the apical Malpighian tubule region. No indication of ABCB full transporter presence by this monoclonal antibody was found in the more proximal tubule regions examined (Figure 7, Figure S 16).

Identification of putative ABCB transporters in *O. fasciatus*

The initial immunohistochemical investigations showed that ABCB transporters occur in the large milkweed bug at major sites known to be involved in adaptations to cardenolides. Thus, transcript catalogues constructed by two different assemblers (Trinity and CLC; Table S 18, Table S 19) were searched for ABCB protein homologs using previously identified ABCB carriers from seven species as queries.

ABCB-like transcript identification in different transcriptome assemblies

Homology search by tblastn in different transcript catalogues of the large milkweed bug and subsequent blastx and Pfam analyses revealed the presence of transcripts for at least two ABCB full transporter (FT; *Ofabcb1* and *Ofabcb2*) and three ABCB half transporter (HT) (*Ofabcb6*, *Ofabcb7*, *Ofabcb10*). All these transcripts were sufficiently complete to encode putatively functional proteins (Figure S 17, Table S 20). In general, full and half transporter candidates shared significant identity with ABCB proteins of other species including hemipterans (Table S 21, Table S 22). In addition to these candidates, further sequences (Trinity: n = 9; CLC: n = 7) were found to share high identity with ABCB members (including MDR-type full transporter and ABCB8 half transporter), but these were highly partial showing incomplete or disrupted domain architectures (Figure S 17, Table S 20). It is unclear if these represent incomplete or rudimentary transcripts or resulted by inaccurate assembly, as indeed some differences between assemblies were observed. However, candidate contigs from different assemblies coincided well and only showed few ambiguities in overlapping regions except for *Ofabcb10* (Figure S 17). Homology search also resulted in transcripts sharing higher identities with ABCC members, a subfamily for which close phylogenetic relationship to subfamily B has been shown (Igarashi, 2004; Xiong et al., 2015) (Table S 20, Table S 21, Table S 22).

Putative OfABCB full transporters in *O. fasciatus*

OfABCB1

The *Ofabcb1* transcript, confirmed by ORF sequencing, encodes a protein of 1282 amino acids with predicted molecular mass of 142.1 kDa (Table S 24). Hence, it coincided well in size with the protein detected in the insects' crude membrane fraction by C219, with its epitope identified in the OfABCB1 N- and C-terminal region (Figure 9). The protein itself shared 45 % sequence identity with the human ABCB1 transporter (NP_001335874) and 37 - 41 % with *D. melanogaster* MDR carriers (MDR49: NP_001163132, MDR50: NP_523740, MDR65: NP_476831). Domain architecture prediction by HmmScan, TMHMM, TOPCONS, homology based 3D structure modelling by Phyre[2] and subcellular prediction by WoLFPSORT suggest that this protein is likely indeed a functional ABCB transporter (Figure 9, Figure S 18, Table S 23). Its topology significantly matched that of human ABCB1 (MDR1, Pgp): two nucleotide-binding domains (NBD) exhibiting all motifs typical of ABC transporters (Walker A, Walker B, ABC signature) and two transmembrane domains (TMD) composed of six transmembrane helices (TMs) each, in alternating order. The first in-frame AUG codon present in the Trinity

transcript resulted in an intact TMD_6-NBD-TMD_6-NBD protein structure (1223 aa, ORF: 3672 bp) predicted by Pfam, TMHMM, and Phyre[2], but yielded a very short and hence rather atypical intracellular N-terminus (3 - 12 aa dependent on structure prediction) (Figure S 19). A further comparison of this transcript with the current annotated genome assembly of *O. fasciatus* discovered an upstream in-frame start codon resulting in a full-length transcript with coding region size comparable to the human *ABCB1* transporter (ORF *Ofabcb1*: 3849 bp, ORF human *ABCB1* transporter (CCDS5608.1): 3843 bp).

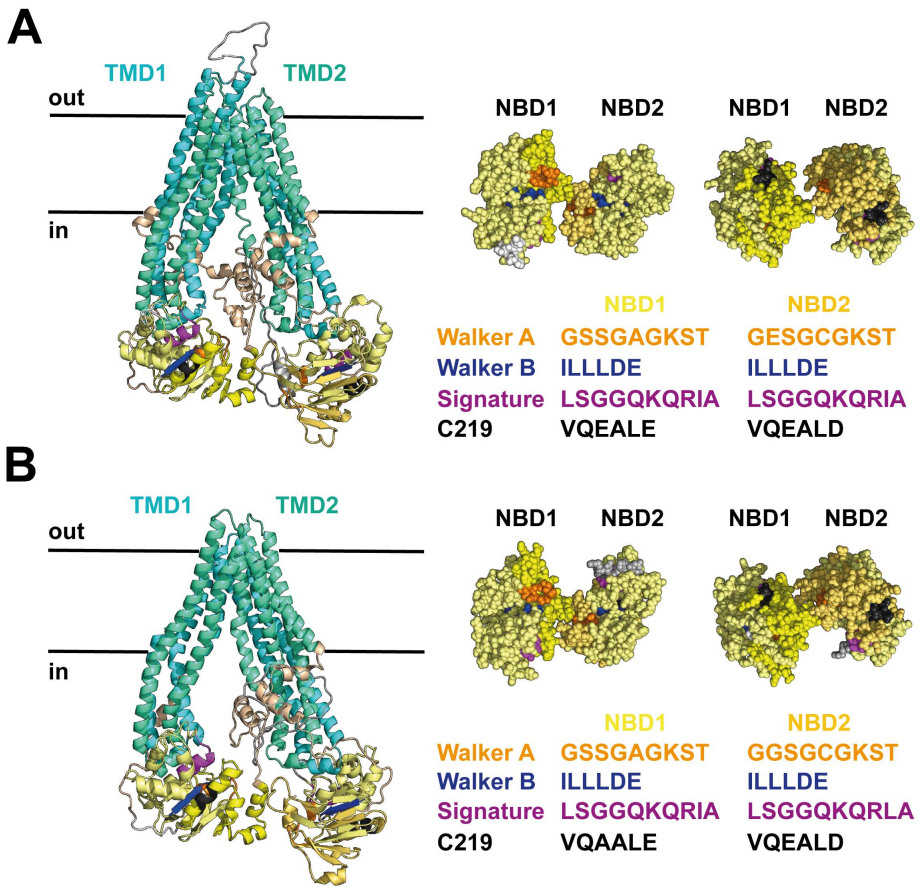


Figure 9 3D model of OfABCB1 (A; 1282 aa) and partial OfABCB2 (B; CLC contig 4439 (1148 aa)) illustrating characteristic ABCB transporter architecture with two transmembrane domains (TMD) and nucleotide-binding domains (NBD) based on Phyre[2]. 97 % of residues of both proteins were modelled with > 90 % confidence based on selected templates (c4f4cA, c3g5uB and c6c0vA). *Ab initio* modelled residues are indicated in medium grey. Approximate localization in the plasma membrane was determined by TMHMM. Out specifies the extracellular, and in the intracellular space. NBDs are further illustrated by spheres with motifs or epitopes in colors. Putative mAb C494 binding in the N-terminal region is indicated in white. There, the PNTLEGN epitope matched with a maximum of four residues. Three residues matched in the C-terminal region. Left illustrates the extracellular and right the intracellular view of the NBDs.

Ofabcb1 gene structure. Comparison with the current version of the *O. fasciatus* genome indicates that the *Ofabcb1* encoding gene consists of at least 23 coding exons which is in line with the exon number range (11 - 50) known for human ABC transporter members (Srinivasan

et al., 2009). However, the total number could not be unequivocally identified because three segments were assigned to other scaffolds (Figure 10). This also explains why FGENESH+ prediction resulted only in a 960 aa protein encoded by 19 exons. All potential identified splice junctions of consecutively mapped regions, i.e., neighboring exons aligning to the same scaffold, revealed highly conserved splice sites, GT at donor and AG at acceptor sites, supporting this preliminary gene model. This also suggests a predominantly canonical pre-mRNA processing of *Ofabcb1*.

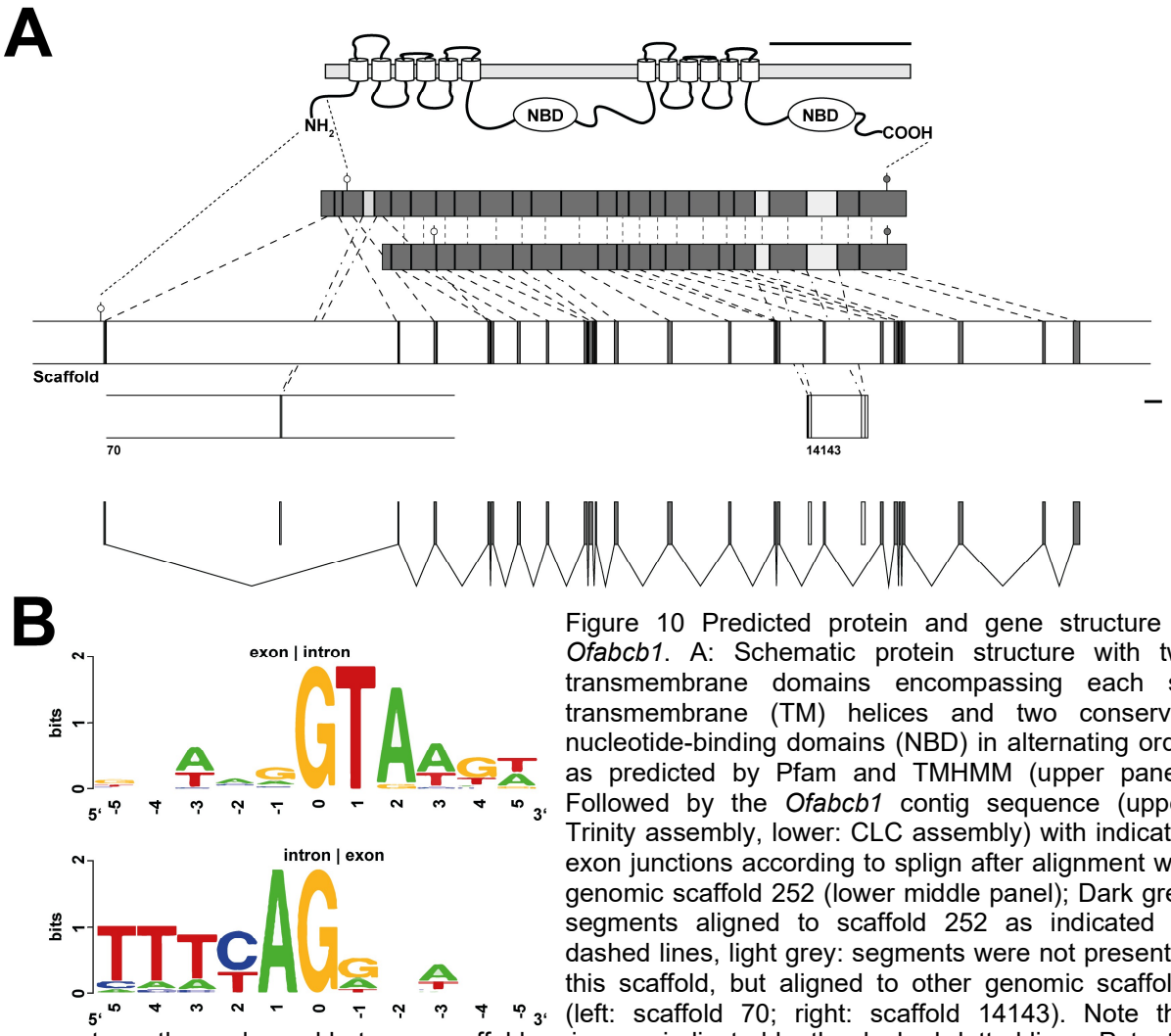


Figure 10 Predicted protein and gene structure of *Ofabcb1*. A: Schematic protein structure with two transmembrane domains encompassing each six transmembrane (TM) helices and two conserved nucleotide-binding domains (NBD) in alternating order as predicted by Pfam and TMHMM (upper panel). Followed by the *Ofabcb1* contig sequence (upper: Trinity assembly, lower: CLC assembly) with indicated exon junctions according to splign after alignment with genomic scaffold 252 (lower middle panel); Dark grey: segments aligned to scaffold 252 as indicated by dashed lines, light grey: segments were not present in this scaffold, but aligned to other genomic scaffolds (left: scaffold 70; right: scaffold 14143). Note that segments partly overlapped between scaffold regions as indicated by the dashed-dotted lines. Potential intronic regions in genomic scaffolds are indicated by white boxes or flexed lines in predicted pre-mRNA structure (lower panel). Open scaffold ends indicate existence of up- or downstream non-aligning scaffold regions. Stemmed circles within the contig sequence mark start (white) and stop codon (grey) of the longest open reading frame. Comparison with the genomic scaffold (252) further revealed an in-frame start codon (stemmed white circle in scaffold sequence) 5 bp upstream of the contig 5' prime end which led to a prolonged N-terminus (dotted lines) and slightly different TM helix position predictions according to TMHMM. Scale bars represent 1 kb. B: Sequence logos of intron-exon boundaries (upper: donor site, lower: acceptor site) according to contig alignment (Trinity) with scaffold 252. Negative numbers mark position in exon regions, positive numbers mark position in intron regions. Overall height indicates conservation while symbol height indicates relative frequency of a base at that particular position. Note that only segments which aligned without gaps were included (n = 18; donor & acceptor sites: n = 17). Logos were generated by WebLogo 3 (Crooks et al., 2004).

OfABCB2

In contrast to *Ofabcb1*, the transcriptomic data for *Ofabcb2* was more complex. In total, nine contig sequences were recovered in the two assemblies for this transporter (CLC: n = 1, Trinity: n = 8 (Table S 20)). Initial bioinformatic analyses showed that no transcript had a complete ABCB full transporter protein structure (Figure S 17, Table S 20). This analysis supported by transcripts' comparison with the annotated genome assembly of *O. fasciatus* showed that these sequences were partial (5' prime end partial: CLC: n = 1, Trinity: n = 1; 3' prime end partial: Trinity: n = 7; Figure 11; see *Ofabcb2* gene structure section). Transcript sequence overlaps identified by MAFFT and manual curation resulted in seven divergent isoforms (1, 2, 5, 6, 7, 8, 11) varying in length (5983 to 7470 bp), predicted exon number, and exon location on the genomic scaffold (see *Ofabcb2* gene structure section). Six of these isoforms were predicted by sorted six-frame translation to encode a 1088 aa protein exhibiting a TMD_3-NBD-TMD_6-NBD structure (118.6 kDa; Phyre^2: TMD_4-NBD-TMD_6-NBD). In contrast, isoform 6 revealed an extended first TMD region (TMD_5-NBD-TMD_6-NBD, 1189 aa; 130.4 kDa) (Figure S 19, Table S 23). This isoform (6) coincided thus to the greatest extent with the typical ABCB full transporter topology with predicted highest likelihood to occur in the plasma membrane by WoLFPSORT. However, Pfam analysis predicted the first TMD region to stretch out over the predicted start codon for each isoform indicating that also these transcripts potentially were partial at the 5' prime end. The direct sequencing of overlapping PCR amplicons (including the 5' prime end upstream region of isoform 6) and clones of PCR products revealed an *Ofabcb2* sequence (5905 bp, cds position 97 to 3807 bp) which did not match any isoform completely, but was predicted to encode a 1237 aa protein with almost typical ABCB full transporter structure (135.8 kDa, TMHMM: TMD_5-NBD-TMD_6-NBD, Phyre^2 = TMD_7-NBD-TMD_6-NBD; Figure S 20, Table S 25). While its sequence start matched isoform 6 from position 770 to 1030 which is upstream of this isoforms' predicted start codon (position 1487 - 1489), it lacked position 1031 to 1507. This 477 bp sequence section was also present in isoform 2, 7, and 11 and corresponds to predicted exon region six (see *Ofabcb2* gene structure section below) (Figure S 21). It further contained the predicted start codon of isoform 6 (cds 1487 to 5053 bp) which hence was missing. Further sequence ambiguities that were not apparent from the transcriptome data were determined at the sequences' 3' end by segmental PCR amplification and cloning. Two of four clones revealed a 10 bp insertion (sequence: 5'-TTTGTTTCAG-3') at position 3069 (intracellular loop between TMD2 and NBD2) of the *Ofabcb2* sequence which elongated the predicted *Ofabcb2* ORF slightly (position 97 to 3816; 1240 aa). One of these clones had an additional insertion of 97 bp at *Ofabcb2* position 3264 bp which was absent in the other clones (Figure S 22). This insertion induced a frame shift in the predicted second

NBD and resulted thereby in a truncated protein of 1064 aa (cds: 97 to 3288 bp). Both insertions could be matched to the genomic scaffold and were likely the results of alternative or mis-splicing. The full-length *Ofabcb2* sequence composition still needs further clarification, as the complete full-length could not yet be amplified in one piece.

Ofabcb2 gene structure. Subsequent comparison of all *Ofabcb2* variants with the *O. fasciatus* genome and FGENESH+ analysis supports indeed a sophisticated pre-mRNA processing of this gene as indicated by PCR amplifications. All variants highly resembled the genomic DNA sequence (scaffold 214) with only minor ambiguities and scaffold displacements (to scaffold 170, 8088 and 12657; a 113 bp fragment present in all in silico sequences and sequenced clones or PCR products was not found in the genome; Figure 11). In total 25 potential exonic regions were identified on scaffold 214 spanning a genomic region from 352169 to 399336 bp, similar to that predicted by FGENESH+ (358573 to 397068) (Table S 26). Discrepancies were expected due to the scaffold displacements, as also observed for *Ofabcb1*. Majority of aligned sequences revealed canonical splice-junctions (GT-AG) in line with extensive alternative splicing of the *Ofabcb2* gene (Figure 11, Table S 26). Some exon-intron boundaries could not be clearly determined due to a lack of sequence information (scaffold displacements, lack of 113 bp in the genome, mid-exon sequence starts). These were therefore determined to be non-canonical splice sites during the splign analysis. Yet, for most of these regions also exons were predicted by FGENESH+ (Table S 26). The experimental *Ofabcb2* sequence (without insertions detected in clones) contained in total 22 exons on scaffold 214 plus two scaffold displacements and the 113 bp sequence lacking genome support. Different in silico isoforms contained different exonic regions (in total 21 to 23 exons) and versions thereof indicating alternative splicing processes like exon skipping (exon 3 and 5), alternative 3’ site splicing and intron retention (exon region 4 and 6) (Figure 11). The latter was especially prominent in exonic region six which consists of three distinct exons (6.2a, 6.3b and 6.4g) according to the PCR and clone sequence data (Table S 26). Additional evidence for the complex splicing of the *Ofabcb2* gene was also found in the newly generated sequences as described before. The 97 bp insertion matched completely to the genomic scaffold 214 and revealed the canonical splice sites GT-AG. Hence, its likely an intron retention between *Ofabcb2* exon 22 and 23 (Figure S 22). The nature of the smaller 10 bp insertion a little further ahead at the predicted junction of exons 21 and 22, is not as clear because it revealed non-canonical splice sites (TT-AG). Yet, as it was also found in the intron retaining clone, it is most likely also a form of alternative splicing, not complete pre-mRNA processing or mis-splicing. A partial intron retention or non-canonical 3' splicing would be possible mechanisms. Another important aspect also became clear during the comparison. Interestingly, exon 1 and 2 (only present in isoform 11) were

found to be much further upstream than the start of isoform 6 (exon 5) and flanked by canonical splice sites. That suggests that the actual transcription start of the *Ofabcb2* gene may be before the start of isoform 6, which was studied here.

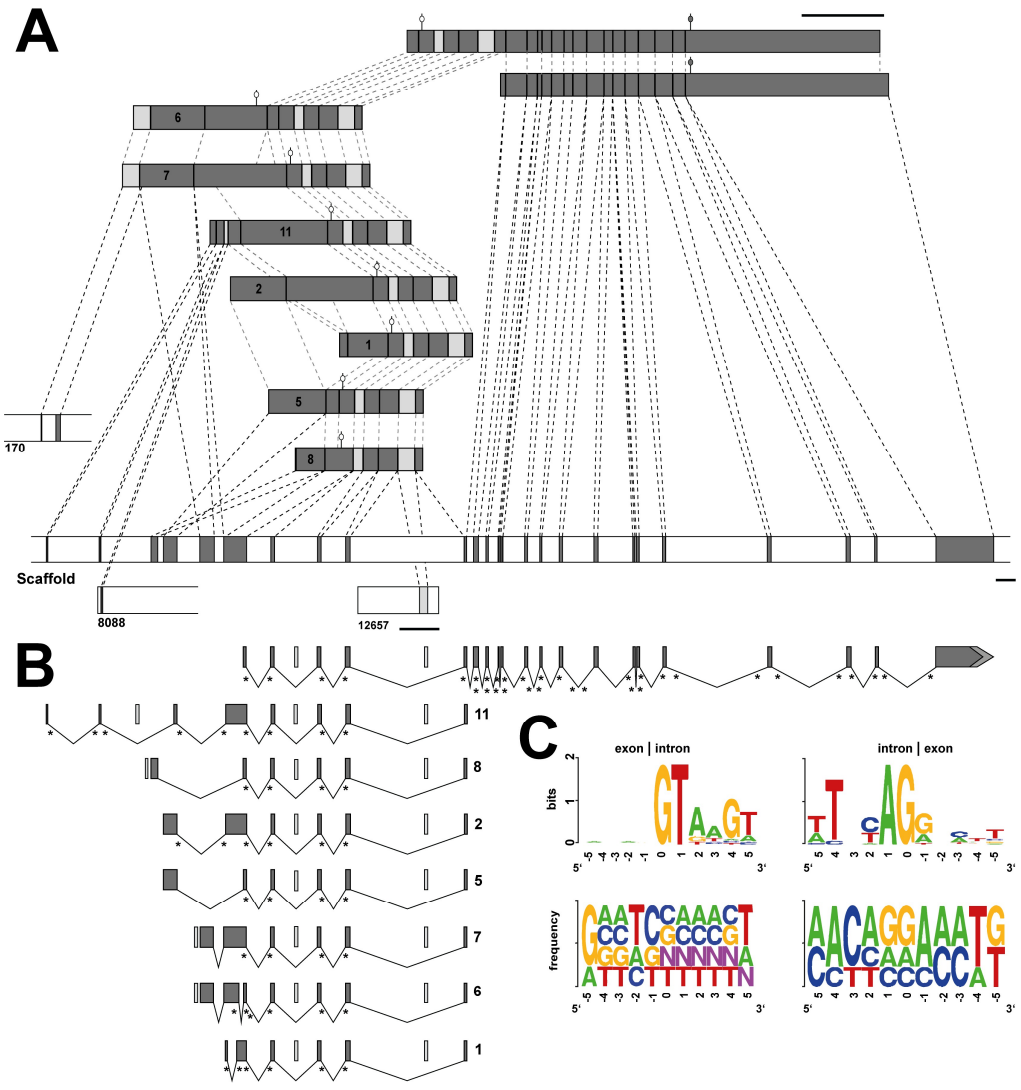


Figure 11 Predicted gene structure of *Ofabcb2* based on transcriptomic contig and genomic DNA sequence comparison. A: *Ofabcb2* contig sequences (first: CLC contig followed by eight contigs of the trinity assembly, one contig corresponding to 3' mRNA and seven isoforms corresponding to the 5' mRNA of the CLC transcript) with exon junctions according to splign after alignment with genomic scaffold 214 (lower panel); Dark grey: segments aligned to scaffold 214 as indicated by dashed lines, light grey: segments aligned to other genomic scaffolds (left: scaffold 170, middle: 8088, right: scaffold 12658). Note that one segment lacked genomic sequence support. Potential intronic regions in genomic scaffolds are indicated by white boxes or flexed lines in predicted pre-mRNA structure shown in B. Open scaffold ends indicate existence of up- or downstream non-aligning scaffold regions. Stemmed circles within the contig sequence mark start (white) and stop codon (grey) of the longest open reading frame. Scale bars represent 1 kb. C: Sequence logos of potential exon - intron junctions according to contig alignment with scaffold 214. Only unique identified boundaries and boundaries of consecutively mapped exonic regions were included. Negative numbers mark position in exon regions, positive numbers mark positions in intron regions. Upper panel represents logos of potential canonical splice junctions marked with an asterisk in predicted pre-mRNAs (left: donor site, right: acceptor site). Lower panels show base frequency at respective position of other junctions. Logos were generated by WebLogo 3 (Crooks et al., 2004).

Phylogenetic inference of ABCB proteins

Phylogenetic inference revealed no clear orthologous relationship between the 72 included ABCB full transporter from a total of 30 species which is in line with previous studies investigating the phylogenetic relationships of arthropod ABCB full transporters (Table S 8, Table S 9). Furthermore, the overall tree topology coincided well with a previous phylogenetic reconstruction by Dermauw and van Leeuwen (2014) who similar to here used complete transporter sequences. This is adequate for tree resolution as long as analysis is within an ABC subfamily and their structure organization (full or half transporters) (Dean and Annilo, 2005; Dermauw and van Leeuwen, 2014). The phylogenetic inference conducted here by maximum likelihood method assigned the full transporters to five well-supported clades: one encompassing all vertebrate full transporters, whereas arthropod full transporters were split into four clades (Figure 12). Full transporters of insect species from eight different orders (Blattodea, Coleoptera, Diptera, Hymenoptera, Isoptera, Lepidoptera, Odonata, Plecoptera) segregated into two clades containing the multiple drug resistance proteins (MDR) of *Drosophila melanogaster*, MDR50 (Clade 4) or MDR49, and MDR65 (Clade 5), respectively. In contrast, most hemipteran full transporters formed a distinct clade with transporters of the red spider mite, *Tetranychus urticae* (Clade 1). Within this clade, mites and hemipteran full transporters separated into well-supported order-specific subclades, a segregation also observed by Hull et al. (2014). While inner node support was in general weak, both OfABCB proteins revealed homology to full transporters of the brown marmorated stink bug, *Halyomorpha halys* (Figure 12). Nonetheless and rather surprisingly, two hemipteran transporters, one of *Laodelphax striatellus* and the *Nilaparvata lugens* full transporter, segregated into Clade 5 and did not cluster with Clade 1.

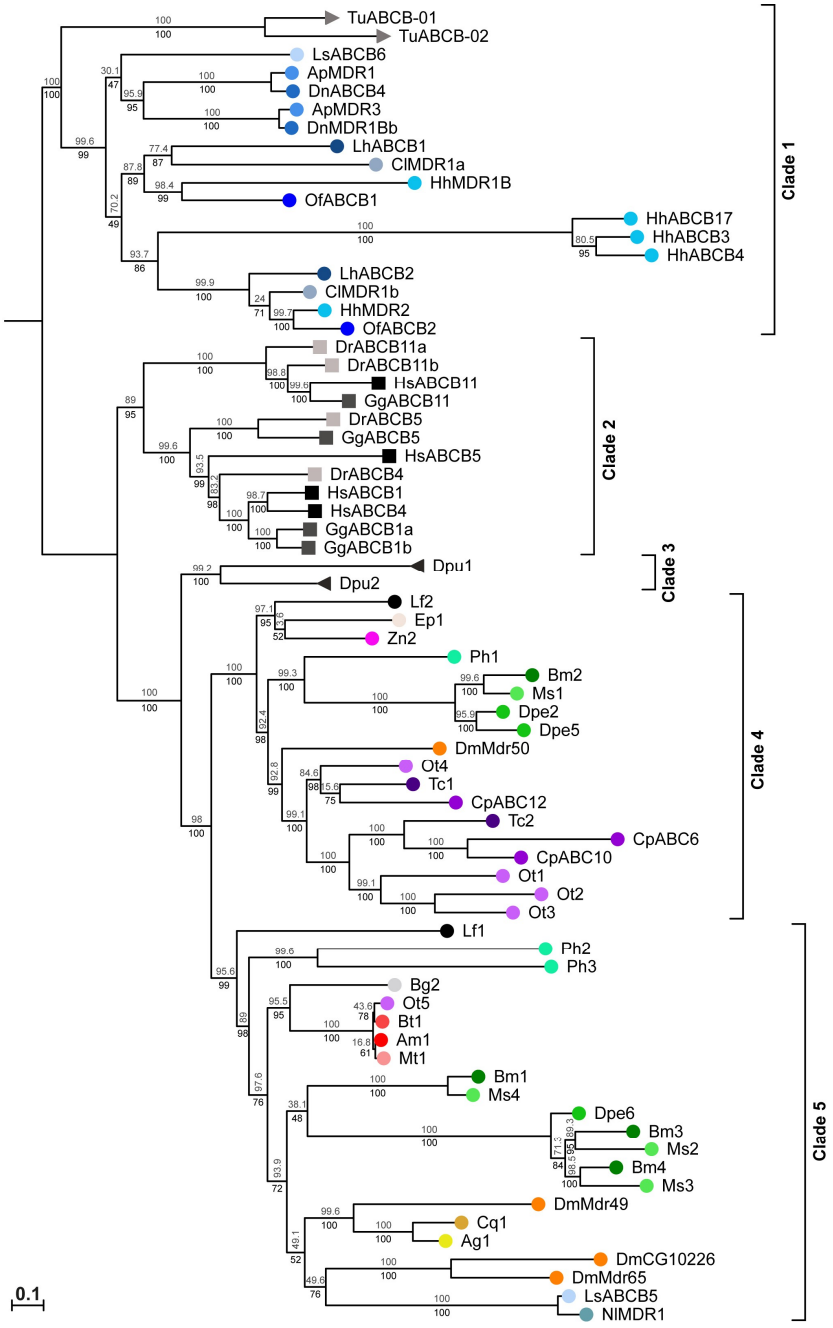


Figure 12 Phylogenetic analysis of ABCB full transporters of identified OfABCB proteins with transporters of three vertebrate and 26 arthropod species. Grey values above branches indicate SH-aLRT support and black values below branches indicate ultrafast bootstrap support (1000 replicates each). Species abbreviations are as follows: Vertebrates (square): Hs = *Homo sapiens*, Gg = *Gallus gallus*, Dr = *Danario rerio*; Arthropods: Acari (right triangle) – Tu = *Tetranychus urticae*; Crustacaea (left triangle) – Dpu: *Daphnia pulex*; Insecta (circle): Hemiptera: Ap = *Acyrthosiphon pisum*, Cl = *Cimex lectularius*, Dn = *Diuraphis noxia*, Hh = *Halyomorpha halys*, Lh = *Lygus hesperus*, Ls = *Laodelphax striatellus*, Nl = *Nilaparvata lugens*, Of = *Oncopeltus fasciatus*; Diptera: Dm = *Drosophila melanogaster*, Ag = *Anopheles gambiae*, Cq = *Culex quinquefasciatus*; Blattodea: Bg = *Blattella germanica*; Coleoptera: Cp = *Chrysomela populi*, Tc = *Tribolium castaneum*, Ot = *Onthophagus taurus*, Ephemeroptera: Ep = *Ephemera danica*; Hymenoptera: Am = *Apis mellifera*, Bt = *Bombus terrestris*, Mt = *Megachile rotundata*; Isoptera: Zn = *Zootermopsis nevadensis*; Lepidoptera: Bm = *Bombyx mori*, Dpe = *Danaus plexippus*, Ms = *Manduca sexta*; Odonata: Lf = *Libellula fulva*; Phthiraptera: Ph = *Pediculus humanus*.

Revalidation of reference gene stability

In general, all tested references genes (*Ofef1a*, *Ofrp49*, *Oftubulin* and *Ofactin5C*) had acceptable stabilities (geNorm M-value < 1.5) in all treatments (Vandesompele et al., 2002). *Ofef1a* was revalidated as single most stable gene in all treatments (tissues, diet, RNAi knockdown for seven days, RNAi knockdown for seven days plus ouabain injection) by both algorithms, Normfinder and geNorm (Table S 27). *Ofef1a* and *Oftubulin*, were the most stable gene combination recommended by both algorithms in animals with seven days RNAi duration with and without ouabain injection. In contrast, the gene combination recommended by both algorithms differed in milkweed bugs feeding on different diets (sunflower seeds with and without *A. syriaca* seeds) as well as in tissues (Table S 27). Interestingly, geNorm recommended *Ofrp49* in combination with *Ofactin5C* as most stable for expression normalization across tissues, although *Ofactin5C* was the most unstable single reference gene. In fact, *actin* was previously identified as stable normalizer in milkweed bug tissues including muscles (Lohr et al., 2017). Yet, direct comparison is not possible due to differences in experimental designs highlighting the importance of revalidation (Bustin and Nolan, 2017; Chapman and Waldenström, 2015; Kozera and Rapacz, 2013; Shakeel et al., 2018; Shi et al., 2015). *Ofactin5C* revealed a more balanced expression pattern compared to *Ofef1a* and *Ofrp49*, which were found enriched in the ovary. That points to its normalizer value across tissues. Still, besides the ovary, expressions differences between tissues were found narrower for both protein-related genes (Figure S 23). Consequently, I decided to use all three genes for normalization. This also corresponds more closely with our previously recommended three reference genes for whole body normalization (*Ofef1a*, *Ofrp49*, *Oftubulin*; see Chapter 1), resulting in more similar normalizations between treatments. Nonetheless, normalization by either two or three references genes (*Ofef1a* + *Oftubulin* vs. those + *Ofrp49*) did not significantly affect expression analysis in animals with ten days RNAi duration for which normalizer stability was not explicitly checked here (Figure S 24). Hence, if sample volumes or plate space or similar is limited, *Ofef1a* and *Oftubulin* are the normalizers of choice.

Differential systemic and tissue-specific *Ofabcb* transporter expression

Expression analysis in milkweed bugs whole bodies by RT-qPCR revealed significant abundance differences between the two transporters ($t_{(3.001)}$ = 12.5, *P* = 0.0011). *Ofabcb1* was 107.9-fold (± 37.5, n = 3) more abundant than *Ofabcb2* on the systemic level (Figure 13). This divergent abundance was in general also observed when their expression was examined in more detail, i.e., across seven different tissues (n = 3). Further, both transporters revealed divergent tissue-specific expression patterns (Welch's ANOVA; *Ofabcb1*: $F_{(6, 5.79)}$ = 35.17, *P* = 0.0003; *Ofabcb2*: $F_{(3, 4.06)}$ = 35.24, *P* = 0.002). The high abundance transporter *Ofabcb1* was differentially expressed between the reproductive organs with predominant expression in the ovarian tissue. It was furthermore enriched in the nervous system and the thoracic region (pronotum, meso- and metathorax including the thoracic storage compartment, thoracic muscles and scutellum) (Figure 13). In contrast, *Ofabcb2* was predominantly expressed in the salivary glands and thoracic region, albeit in the latter the expression was not significantly different compared to other tissues. In fact, the extraordinary low transcript levels of *Ofabcb2* observed in the digestive tract, the Malpighian tubules and the nervous system did not allow accurate expression quantifications. Consequently, these and also the ovarian tissue revealed the highest differences in abundance between both transporters (mean fold difference in transcript level of *Ofabcb1* vs. *Ofabcb2*: Malpighian tubules (~384.4 ± 179.2) > nervous system (~365.6 ± 84.3) > female gonads (225.8 ± 43.9) > digestive tract (~97.3 ± 64.0) > thoracic region (21.9 ± 7.7) > male gonads (5.4 ± 1.8) > salivary glands (0.4 ± 0.3).

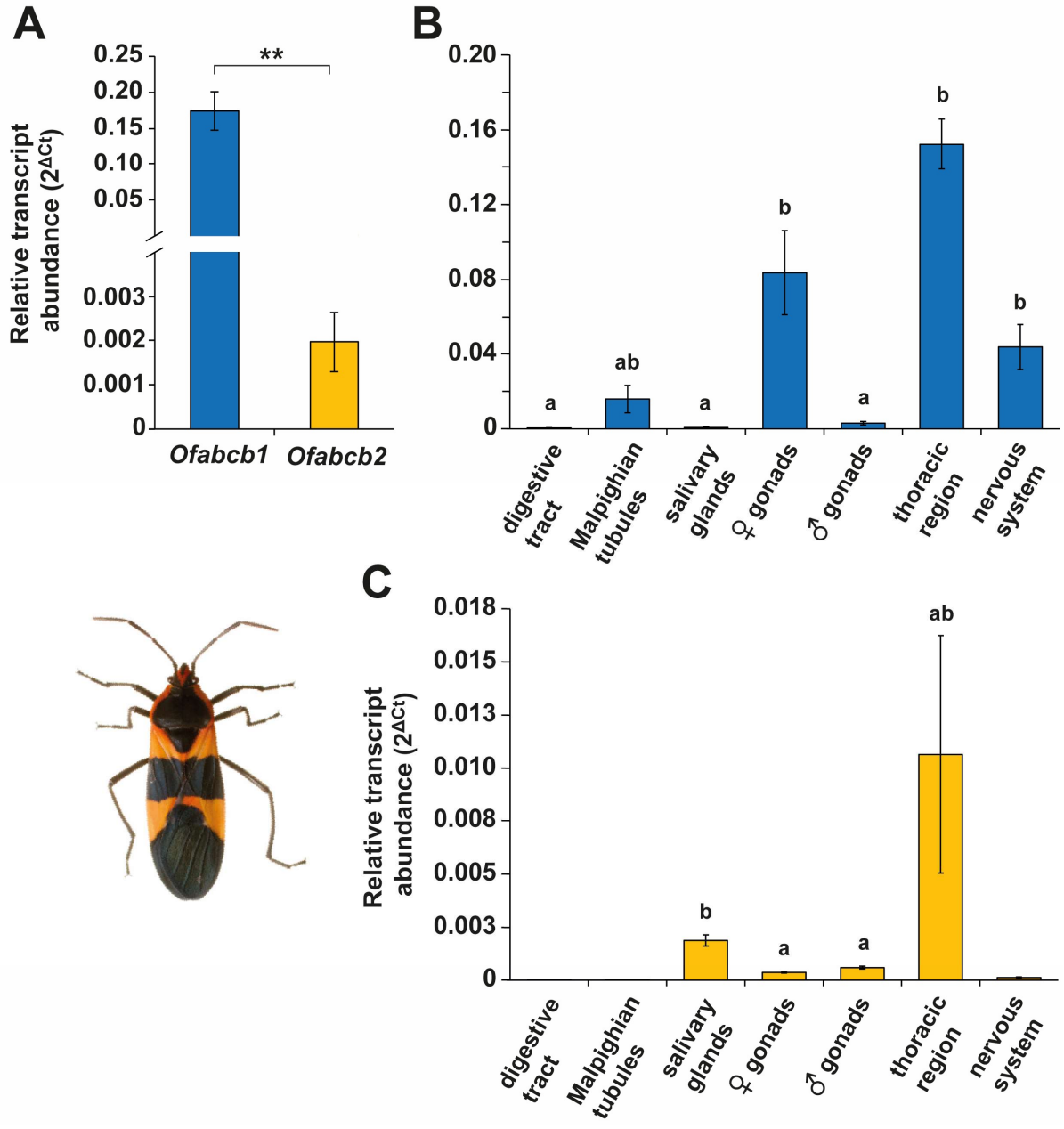


Figure 13 *Ofabcb* transporter expression in large milkweed bugs. A: Relative transcript abundance of *Ofabcb* genes in whole insect bodies (normalized to *Ofef1a, Ofrp49 and Oftubulin*; n = 3); ** = $P < 0.01$. B - C: Relative expression levels (three biological replicates) of *Ofabcb1* (blue) (B) and *Ofabcb2* (yellow) (C) in different tissues of adult milkweed bugs (normalization to *Ofef1a, Ofrp49 and Ofactin5C*). Bars with different letters indicate significant expression differences between tissues (Dunnett-T3 post hoc test, $P < 0.05$). All analyzed individuals fed on milkweed seeds in all life stages. Adult *Oncopeltus fasciatus* photo by Samuel Waldron.

Constitutive *Ofabcb* transporter gene expression in the presence of cardenolides

Examining the expression in adults reared over several generations (n > 90) on a non-cardenolide or cardenolide-containing diet (sunflower seeds only vs. mixed with milkweed seeds) showed that insects of different diet histories possessed similar expression levels of *Ofabcb1* ($t_{(2.78)}$ = -0.29, *P* = 0.792) and *Ofabcb2* ($t_{(2.82)}$ = -2.24, *P* = 0.116) (Figure 14). However, as expression profiles can change rapidly, *Ofabcb* transporter expressions were studied over 32 hours (1 h, 6 h, 16 h, and 32 h) in insects of the sunflower line which were exposed to a single dose of the polar standard cardenolide, ouabain, by injection into the hemocoel. The transcript levels of both transporters were neither significantly altered by time *post* injection (*Ofabcb1* Scheirer Ray Hare test: $H_{(3)}$ = 4.57, *P* = 0.206; *Ofabcb2* ANOVA: $F_{(3)}$ = 0.28, *P* = 0.841) nor by ouabain independent (*Ofabcb1* Scheirer Ray Hare test: $H_{(1)}$ = 0.56, *P* = 0.452; *Ofabcb2* ANOVA: $F_{(1)}$ = 0.07, *P* = 0.797) or dependent on time (time x ouabain – *Ofabcb1* Scheirer Ray Hare test: $H_{(3)}$ = 2.41, *P* = 0.491; *Ofabcb2* ANOVA: $F_{(3)}$ = 4.05, *P* = 0.026, post hoc pairwise Welch's t-tests with controls in all cases *P* > 0.146) (Figure 14). Screening a larger sample panel confirmed that the initially observed *Ofabcb2* transcript level elevation at 16 h *post* injection (3.2-fold ± 0.8; n = 3) was indeed not linked to ouabain presence (1.3-fold ± 0.2, n = 10; T-test $t_{(18)}$ = -0.83, *P* = 0.417). Hence, no evidence was found that cardenolide exposure in the short or long run alters *Ofabcb* transporter transcript levels.

Efficient knockdown of *Ofabcb* transporter gene expression by RNA interference

In vivo RNA interference (RNAi) was exploited to investigate the relevance of OfABCB transporters in transport processes which facilitate cardenolide sequestration in the large milkweed bug. Robust silencing efficacy was confirmed up to ten days *post* RNAi injection by RT-qPCR as perquisite and to ensure confidence in potential functional phenotypes (mean knockdown efficacy: single knockdown *Ofabcb1*: 95.5 ± 0.6 %; single knockdown *Ofabcb2*: 68.6 ± 10.9 %; double knockdown *Ofabcb1&2*: 94.7 ± 0.3 % (*Ofabcb1*), 80.1 ± 6.4 % (*Ofabcb2*)) (Figure 15). In addition, no severe changes in expression of the second non-silenced transporter were observed in single knockdowns (mean fold-change < 2-fold) indicating absence of long-term compensatory effects. This was also observed after shorter dsRNA exposure time (seven days). However, those animals revealed a slightly higher knockdown stability for *Ofabcb2* (*Ofabcb2* single knockdown efficacy: 91.8 ± 0.9 %) while no further enhancement by an increase of the amount of dsRNA (approx. 1.7-fold) was observed (Figure 15). Thus, for the following analyses the seven days dsRNA persistence period with injection of 700 ng dsRNA was chosen. Furthermore, no significant effects of dsRNA on

viability were observed within this period (Fishers exact test for count data: $P = 0.7629$, n = 15 per treatment; survival rate 73 - 93 %; Figure S 25).

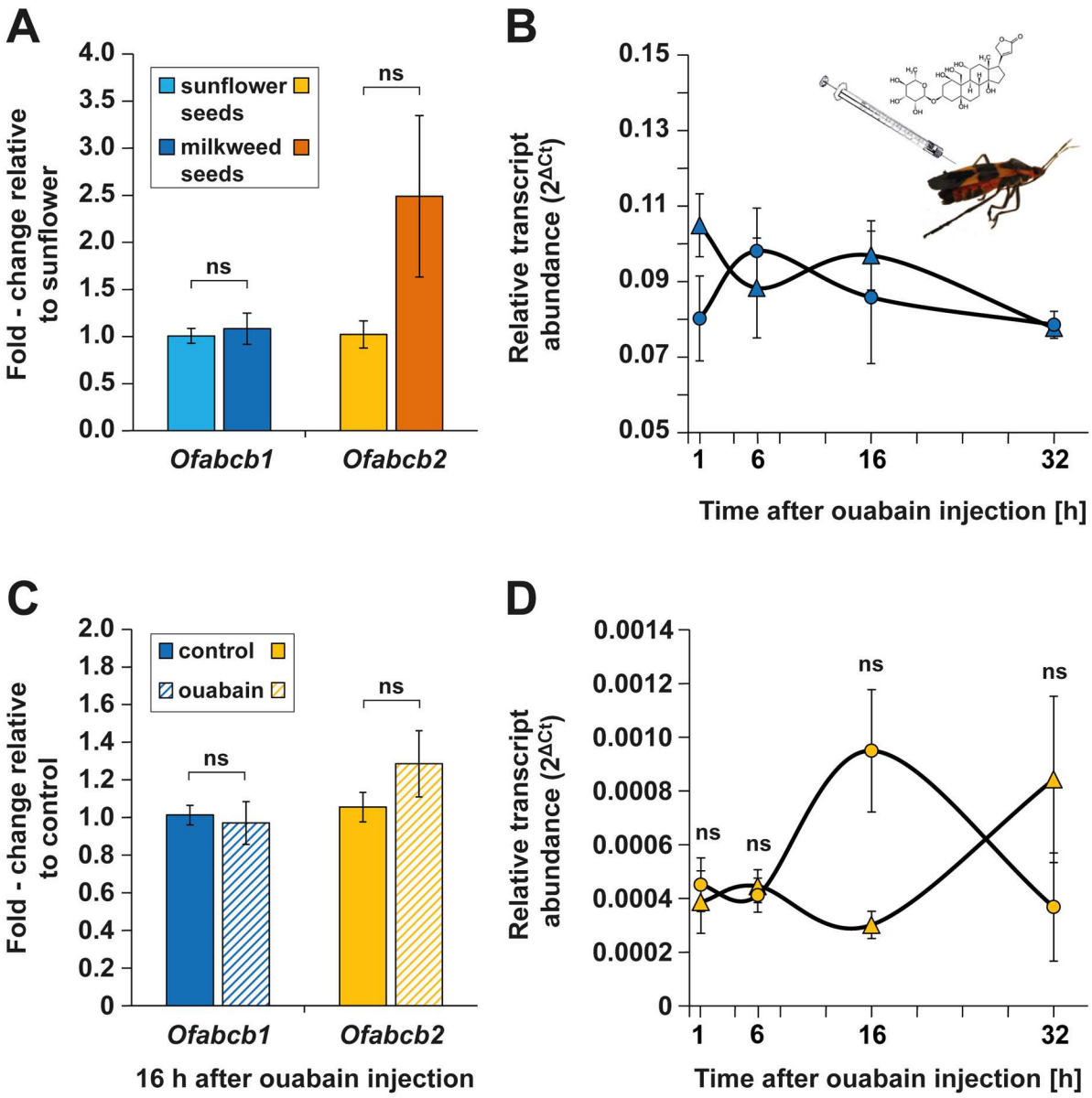


Figure 14 *Ofabcb* gene expression in adult milkweed bugs exposed to cardenolides. A: Gene expression in insects of different diet histories (sunflower seeds only vs. mixed with cardenolide containing milkweed seeds; n = 3). B & D: Temporal expression profiles of *Ofabcb1* (B) and *Ofabcb2* (D) in insects injected with either ouabain (circles) or saline (control; triangles) monitored over 1 h, 6 h, 16 h and 32 h *post* injection (n = 3); ns denotes $P > 0.05$ for post hoc pairwise comparisons between ouabain and control at different time points. C: Expression of both transporters at 16 h *post* ouabain injection compared to animals injected with saline with increased sample sizes (n = 10); *Ofabcb1* Mann-Whitney test: W = 55.5, $P = 0.705$, *Ofabcb2* T-test: $t_{(18)} = -0.831$, $P = 0.417$.

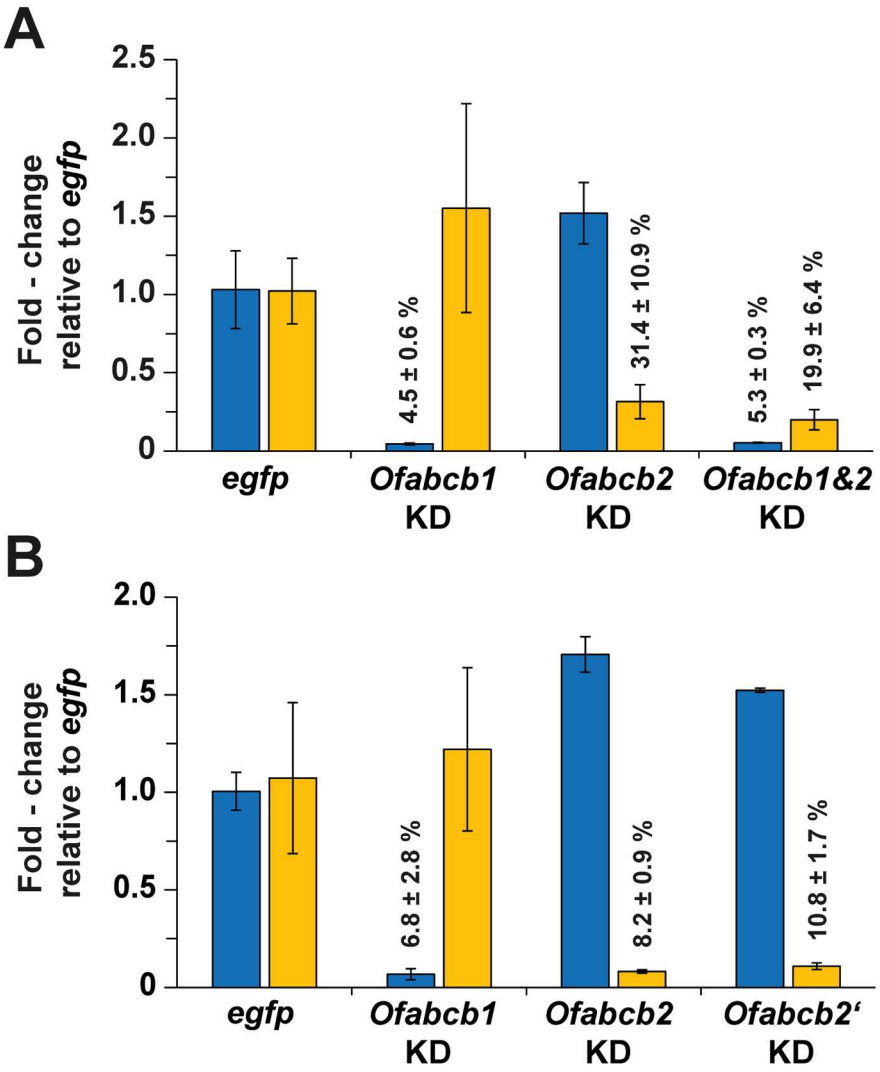


Figure 15 Verification of RNAi mediated *Ofabcb* transporter knockdown efficacy and specificity by RT-qPCR. Expression levels of *Ofabcb1* (blue) and *Ofabcb2* (yellow) in insects ten days (A) and seven days (B) after dsRNA injection (two to three biological replicates). Percentages above bars give remaining expression compared to non-targeting dsRNA controls (e*gfp* injected). KD: knockdown. *Ofabcb2'* KD: injection of 1.17 µg instead of 700 ng dsRNA.

Functional trade-off between OfABCB transporters with respect to cardenolide sequestration

RNAi treated milkweed bugs were injected with ouabain to elucidate the effect of *Ofabcb* specific knockdowns on their ability to sequester this polar cardenolide. Sampling the released defensive fluids after two hours revealed that inhibition of *Ofabcb* mRNA did not significantly affect the stored defensive fluid volume of milkweed bugs compared to controls (ANOVA: $F_{(4, 39)} = 3.69$, $P = 0.012$; Tukey HSD: comparisons with controls $P \geq 0.201$ in all cases; n = 5 - 11) (Figure 16). However, analysis of these defensive fluids by HPLC showed that the amount of sequestered ouabain of insects after *Ofabcb1* or *Ofabcb1&2* knockdown were drastically reduced (ANOVA: $F_{(4, 28)} = 15.19$, $P = 0.000001$; Tukey HSD comparisons to controls: *Ofabcb1* $P = 0.003$, *Ofabcb1&2* $P = 0.00005$; n = 7). In contrast, *Ofabcb2* animals sequestered similar ouabain amounts compared to control animals (Tukey HSD compared to controls: *Ofabcb2* $P = 0.96$). Thus, an exclusive decrease in *Ofabcb1* expression (remaining expression compared to control: 4.33 ± 0.89 %, n = 3 - 4) or in conjunction with *Ofabcb2* (*Ofabcb1*: 5.77 ± 0.67 %, *Ofabcb2*: 13.78 ± 2.09 %) impaired the insects' ability to sequester ouabain by 52.9 ± 6.5 % and 70.7 ± 1.9 %, respectively. These similar reductions in sequestration performance ($P = 0.5552$) as well as the observed unaltered sequestration abilities in *Ofabcb2* knockdown animals showed that impaired sequestration abilities were solely linked to the mRNA decrease of *Ofabcb1* (Figure 16).

Furthermore, expression analysis by RT-qPCR confirmed target-specific knockdowns also when ouabain is sequestered, without significant compensatory effects by the respective unsilenced transporter in single knockdowns as observed before (Tukey HSD; *Ofabcb1* KD: egfp - *Ofabcb2* $P = 0.840$, *Ofabcb2* KD: *egfp* - *Ofabcb1* $P = 0.843$; n = 3 - 4). Nonetheless, there was a marginal elevation of *Ofabcb1* by 1.7-fold (± 0.2) in non-dsRNA injected animals (Welch's $t_{(3.4474)} = -3.45$, $P = 0.0323$), yet this revealed no significant effect on sequestration capacity (comparison to controls: $P = 0.797$, Tukey HSD) (Figure 16).

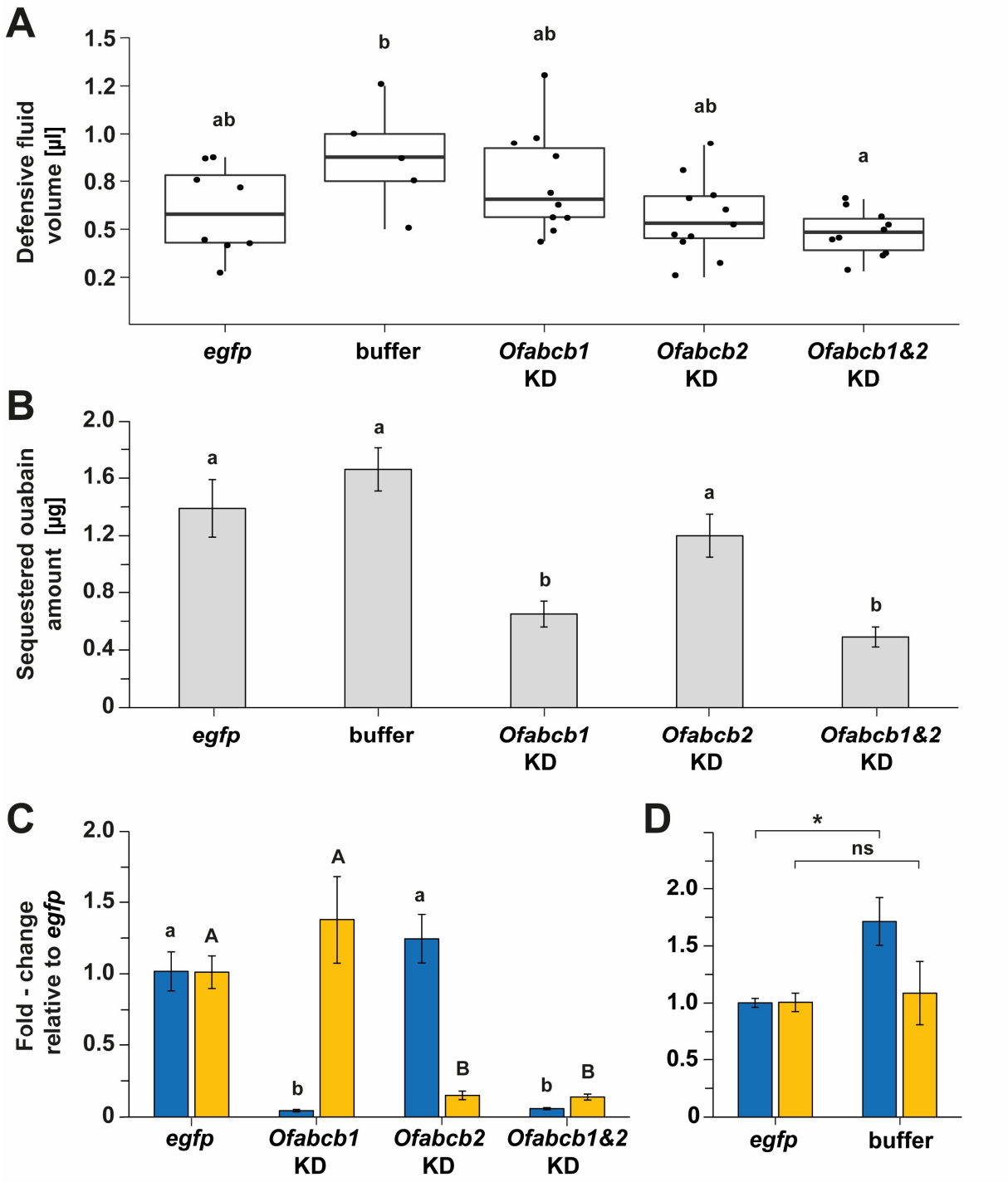


Figure 16 Cardenolide sequestration capacities and mRNA levels of *Ofabcb* knockdown animals. Insects were allowed to sequester injected ouabain for 2 h after RNAi actions for seven days to investigate the effect of reduced *Ofabcb* mRNA levels on sequestration. KD: knockdown. Buffer = injection of buffer (no dsRNA). A: Total volume of defensive fluids sampled from knockdown animals (n = 5 - 11). B: Sequestered ouabain amount in these defensive fluids as determined by HPLC (n = 5 - 7). C - D: Transcript levels of *Ofabcb1* (blue) and *Ofabcb2* (yellow) in three to four biological replicates from which defensive fluids were sampled. Different letters indicate significant differences between treatments with $P < 0.05$ as determined by Tukey HSD tests. Note that upper- and lower-case letters in C indicate post hoc tests of separate one-way ANOVAs (per gene basis). Asterisks indicate significant expression differences compared to controls ($P < 0.05$, Welch's t-test).

Discussion

In this chapter, I demonstrate that efficient ouabain sequestration relies on the ABCB full transporter protein OfABCB1 as a key player in the large milkweed bug, *O. fasciatus*. The knockdown of this gene by RNA interference resulted in a significant drop in sequestration capacity up to 70 % in vivo. This adds valuable new data to the list of plant defense compound transporters in insects, which is still short despite their significance for understanding sequestration and its evolution (Beran and Petschenka, 2022).

The molecular and histological data for OfABCB1 presented in this chapter are in line with most previous physiological data on cardenolide sequestration in *O. fasciatus* as outlined in the following sections. Combined with the knockdown by RNAi, they therefore support the conserved chemoprotective barrier function for OfABCB1, but also provide evidence for a new function in sequestration. This agrees with recent data on the leaf beetle *Chrysochus auratus*, where three ATP-consuming ABCB full transporters (CaABCB1, CaABCB2, CaABCB3) have been characterized in vitro for their cardenolide substrate spectra and are suggested to play a role in sequestration and transfer into defensive glands. Strikingly, a dual role in resistance against but tolerance for cardenolides, as described here, is also suggested for one of these leaf beetle transporters (CaABCB2) (Kowalski et al., 2020). This thus reinforces the evidence for a pleiotropic role of certain ABCB full transporters in insects that sequester cardenolides. This chapter therefore presents a critical step to disentangle the molecular basis of cardenolide transport related to sequestration in *O. fasciatus* and broadens our understanding in the functions of ABCB full transporters in cardenolide-sequestering species. The findings of this chapter will also make it possible for the first time to further dissect the association between *O. fasciatus*' target-site insensitivity and sequestration (Agrawal et al., 2024b) at the molecular level.

In vivo, a pivotal role in the accumulation of defense compounds in insects has only been shown for two other transport proteins to date. A key player for salicin sequestration in the leaf beetle, *Chrysomela populi*, was identified in the same superfamily, but in the ABC subfamily C (Strauss et al., 2013). In addition, a sugar porter of the major facilitator superfamily is required for glucosinolate transport in the flea beetle *Phyllotreta armoraciae* (Yang et al., 2021). Hence, OfABCB1 is the first in vivo characterized defense compound transporter related to cardenolide sequestration in insects.

The data presented here thereby link cardenolide sequestration in *O. fasciatus* with an active primary transport process. However, cardenolide sequestration has been attributed to energy-

independent transport, like diffusion or facilitated diffusion, in previous ex vivo and in vivo studies (Detzel and Wink, 1995; Duffey et al., 1978; Scudder and Meredith, 1982b; Yoder et al., 1976). Indeed, cardenolides are absorbed by the gut according to their polarity and ouabain clearance takes several days (Bramer et al., 2015; Detzel and Wink, 1995; Scudder and Meredith, 1982b). Hence, I bypassed this barrier by direct ouabain injection into the hemocoel. That allowed me to better focus on the well-established selective sequestration site, the thoracic storage compartment, with its cardenolide-enriched defensive fluid.

Strong ABC transporter expression levels indicate functional significance in a tissue while cellular localization links the protein to its physiological function (Amezian et al., 2024; Denecke et al., 2022; Hoffmeyer et al., 2000; Mayer et al., 1996). Combining RNAi knockdowns with tissue-expression and immuno-localization thus suggests that OfABCB1 performs its pivotal role in sequestration by ouabain transfer into the thoracic storage compartment. Ouabain transport by OfABCB1 is consistent with a recent study by Röpcke et al. (2024), in which the next steps towards further functional characterization of the two OfABCB full transporters were taken. This also sheds new light on the role of OfABCB2 in the cardenolide transport network. In contrast to the findings presented here, ouabain also proved to be a substrate for OfABCB2 in those in vitro enzyme assays.

The expression of *Ofabcb1* demonstrated here in four tissues involved in sequestration (thoracic storage compartment, ovaries), cardenolide tolerance (nervous system), homeostasis (Malpighian tubules), and likely biotransformation (salivary glands) suggests a pivotal role in the cardenolide transport network (Duffey et al., 1978; Duffey and Scudder, 1974; Meredith et al., 1984; Moore and Scudder, 1985; Moore and Scudder, 1986; Newcombe et al., 2013; Scudder et al., 1986; Scudder and Meredith, 1982b). Along similar lines, the observed expression patterns also suggest the involvement of OfABCB1 in physiological functions besides sequestration as outlined in more detail below. The role of its homolog, OfABCB2, remains an open question to be addressed. A function in ouabain sequestration cannot be ruled out, but my findings in this chapter suggest that, unlike OfABCB1, it might be dispensable in this regard.

The co-localization of *Ofabcb1* and *Ofabcb2* in the thoracic storage compartment combined with their substrate overlap for ouabain suggests a functional redundancy either for low transcript level compensation or for sequestration fine-tuning to extracellular concentrations (Levy et al., 2011; Marquez and van Bambeke, 2011; Röpcke et al., 2024). Focusing the sequestration system in *O. fasciatus* to a few selective barriers (for overview see Scudder et al., 1986), with at least partially redundant transporters might strike a balance between

protection against detrimental effects by mutations and flexibility for adaptation, so that sequestration does not become an evolutionary dead end (Boland, 2015; Guillaume and Otto, 2012; Marquez and van Bambeke, 2011; Petschenka and Agrawal, 2016; Roth et al., 2003).

We are still in the very early stages of characterizing the substrate spectra of ABCB full transporters in cardenolide-sequestering insects (Kowalski et al., 2020; Röpcke et al., 2024). A similar discrepant relationship between the transport capacity for a substrate and its associated physiological function, as observed here for OfABCB2, is known for human ABCB4. Liver-specific ABCB4 transports drugs like digoxin in addition to its metabolic substrate phosphatidylcholine, but does not confer drug resistance (Ishigami et al., 2013; Schinkel et al., 1991; Smith et al., 1994; Smith et al., 2000; van der Bliek et al., 1988). Thus, metabolic substrate transport might be the primary role of OfABCB2. For example, MDR49 transports a germ-cell attractant in *D. melanogaster* (Ricardo and Lehmann, 2009). Lipid transport by an ABCB full transporter is suggested in *C. elegans* (Kamal et al., 2023) and also described for human ABCB1 (van Helvoort et al., 1996). Another explanation that cannot be ruled out at present is that the remaining 8 to 24 % transcript levels of *Ofabcb2* are sufficient for full capacity ouabain sequestration or that the knockdown was not functional on the protein level by mechanisms such as mRNA stabilization, protein degradation protection, or protein pool recruitment (Löscher and Gericke, 2020).

In general, *Ofabcb2*'s low transcript levels parallel the low-level expression profiles reported for certain ABCB full transporters in other insects, like in the lepidopterans *Spodoptera exigua* (You et al., 2025) and *Helicoverpa armigera* (Denecke et al., 2021), or in the leaf beetles *C. populi* (Strauss et al., 2014) and *C. auratus* (Kowalski et al., 2020). Low transcript levels are a suggested special subfunctionalization type to preserve the original ancestral functions also between old gene duplicates (Qian et al., 2010). Although the internal branching patterns within the hemipteran ABCB full transporter subclade were weakly supported in my phylogenetic inference, I suggest that both OfABCB full transporters arose *prior* to cardenolide specialization of *O. fasciatus*, based on the well-supported more terminal nodes of OfABCB1 and OfABCB2 clustering with other hemipteran ABCBs rather than with each other. However, the needs behind such low ABCB full transporter baseline levels are poorly understood as studies often focus on high expressions or inductive changes (for review see Amezian et al., 2024; Dermauw and van Leeuwen, 2014). Along these lines, the recently identified full-length *Ofabcb2* sequence (Röpcke et al., 2024) resembles the here identified *Ofabcb2* sequence well. The only significant difference was at the N-terminus, a region also diverged between other mammalian and insect isoforms (Seong et al., 2016; van der Bliek et al., 1988; Wu et al., 1991).

In the half-transporter ABCB6, for example, the N-terminal region is crucial for its subcellular localization in the cell (Kiss et al., 2015). Both sequences therefore are identical in regions important for gene expression quantification and RNA interference. The now established full length sequence shows that the initiation of the *Ofabcb2* full transcript lies upstream of the 5`strand end of isoform 6, as I previously suggested.

Certain ABCB full transporters often predominate in a particular tissue, indicating a local functional division of labour between the ABCB full transporter set (for example see Denecke et al., 2021; Denecke et al., 2022; Kowalski et al., 2020; Xu et al., 2021; You et al., 2025). Both identified OfABCB full transporters showed no strong evidence for a tissue-specific division of labor between them, although the slightly increased *Ofabcb2* expression in the salivary glands might indicate a more specialized role there. Furthermore, it is possible that both ABCB full transporter roles are more differentiated between other tissues, like the fat body (Xu et al., 2021; You et al., 2025), or during development and reproduction (Hull et al., 2014; Ricardo and Lehmann, 2009) or upon other environmental changes. Also, the diet can influence ABCB full transporter gene expression in insects (Koenig et al., 2015; Krueger et al., 2022; Tapadia and Lakhotia, 2005). However, both OfABCB transporters were not responsive to ouabain and showed a similar expression between milkweed bug lines reared on different diets. They therefore do not appear to belong to the narrow ABC transporter repertoire that specifically responds in terms of the total mRNA level to host plant changes, as has been reported for other cardenolide-sequestering species (Birnbaum et al., 2017; Tan et al., 2019). Lastly, although the number of ABCB full transporters determined here is consistent with the range determined in other insect species, one to nine transporters (Denecke et al., 2021; Dermauw and van Leeuwen, 2014), it is possible that there are additional transporters that were not identified from the transcriptome data. Since the number varies between species, the completeness of an ABCB full transporter repertoire is difficult to assess. The hemipterans *Laodelphax striatellus* and *Acyrthosiphon pisum* for example have two (Sun et al., 2017), *Lygus hesperus* and *Nilaparvata lugens* have three (Hull et al., 2014; Li et al., 2025), *Halyomorpha halys* has five (Sparks et al., 2014), but *Diaphorina citri* lacks ABCB full transporters (Wang et al., 2019). Similar to other studies (e.g. Hull et al., 2014; Strauss et al., 2014; Sun et al., 2017), several short ABCB-like fragments were identified in both transcriptome assemblies. Assembly-related influences are therefore unlikely, but the challenge of the RNA-seq data used in this thesis has been addressed elsewhere (Denecke et al., 2021).

In general, most ABC transporters are rather ubiquitously expressed in mammals and insects (Langmann et al., 2003; Schmidt et al., 2019), highlighting the pivotal role of this superfamily for organisms' transport networks. Beside the thoracic storage compartment, *Ofabcb1* was significantly expressed in the nervous system. The combination with the immunolocalization of ABCB transporter at the neural sheath, consisting of neural lamina and perineurium in *O. fasciatus* (Johansson, 1957), suggests a chemoprotective role in the blood-brain barrier. This function is evolutionarily conserved and protects mammals and insects alike, among others from the neurotoxic effects of cardenolides (Groen et al., 2017; Mayer et al., 1996; Mayer et al., 2009; Petschenka et al., 2013b). It is thus one of the permeability barriers suggested to mediate a certain basal degree of cardenolide resistance independent of host plant specialization (Dobler et al., 2015; Groen et al., 2017; Petschenka et al., 2013b). At the same time, there was no significant effect on viability or visible motoric impacts in knockdown animals when challenged with ouabain. A possible explanation for this is the pronounced target-site insensitivity of their Na,K-ATPase, even for the most sensitive paralog (α1C), which predominates in neural tissue due to its primary ion-pumping function (Bramer et al., 2015; Dalla et al., 2017; Dalla and Dobler, 2016; Dobler et al., 2012; Herbertz et al., 2022; Herbertz et al., 2025; Lohr et al., 2017). Another explanation could be the impermeability of the blood-brain barrier to ouabain by its cellular tightness, as observed in *D. nerii* (Petschenka et al., 2013b). However, in previous work of our group, we showed that a knockdown of the resistant Na,K-ATPase paralogs (α1A, α1B) can be lethal but only when the insects are simultaneously challenged with the same ouabain dose as used here (Lohr et al., 2017). One possible explanation could be that the protection of the blood-brain barrier in *O. fasciatus* may not be sufficient at such doses. However, we cannot comment on the functionality of the blood-brain barrier itself in these experimental animals and the barrier is known to contain other transporters within and beyond the ABC transporter superfamily in insects and mammals (DeSalvo et al., 2014; Hagenbuch et al., 2002). The same applies to possible lethal effects outside of the nervous system. Nonetheless, a certain leakage across the blood-brain barrier would be in line with the hypothesis that a certain degree of Na,K-ATPase insensitivity is required in the evolution of cardenolide sequestration (Agrawal et al., 2024b).

Besides the thoracic storage compartment and the nervous system, *Ofabcb1* had a significant expression level in the ovary. If that is due to a barrier-function like that known for mammals (Juliano and Ling, 1976; Schinkel and Jonker, 2003; Smit et al., 1999) or cardenolide sequestration into the eggs (Duffey and Scudder, 1974; Moore and Scudder, 1985; Newcombe et al., 2013) awaits further investigations. In general, the physiological function of ABCB full transporters in the reproductive organs of insects is not well understood. ABCB and other

subfamily members have been rather associated with reproductive and developmental processes so far (Broehan et al., 2013; Liu et al., 2011; Xu et al., 2021). *C. auratus* expresses also its cymarin-transporting CaABCB2 at an appreciable level in its reproductive organs, but it is not known if the species also sequesters cardenolides in their eggs like *O. fasciatus* does or simply relies on the cardenolide content of fecal shields for egg protection (Sady, 1994).

The moderate expression level and the apical localization in Malpighian tubule cells indicates an additional role of OfABCB1 in excretion. Malpighian tubules are an important regulator for cardenolide homeostasis orchestrating excretion from and reabsorption into the hemolymph to prevent loss of sequestered cardenolides. While at the apical tubule region ouabain excretion into the tubule lumen takes place, it is reabsorbed at the proximal tubule region (Meredith et al., 1984). A participation of OfABCB1 in the reabsorption of ouabain is therefore rather unlikely based on the absence in the more proximal tubule region. Its moderate expression suggests further that other transporter within and beyond the ABC superfamily might play a more pivotal role in this context (Groen et al., 2017; Schmidt et al., 2019; Torrie et al., 2004).

Something similar can be suggested for the intestine (Detzel and Wink, 1995), the salivary glands and male gonads. In general, the negligible expression of the two *Ofabcb* transporters, *Ofabcb1* and *Ofabcb2*, in the gut is in agreement with the increased cardenolide permeability described for the gut of milkweed bugs compared to non-cardenolide-specialized insects (Scudder and Meredith, 1982b). Gut impermeability to cardenolides mediated by efflux transporters like ABCB1 homologs is similar to the blood-brain barrier, a suggested barrier mechanism that confers a certain basal resistance to these toxins independent of specialization on cardenolide-producing plants (Dobler et al., 2015; Groen et al., 2017; Li et al., 2025; Petschenka and Agrawal, 2015, 2016). It is plausible for a sequestering species to reduce this barrier for cardenolide uptake. Yet, a marginal ABCB array also in the gut of sequestering species might be beneficial for timing or indirectly affecting absorption of cardenolides with different polarities and hence homeostasis. In *C. auratus*, for example, CaABCB3 is primarily located in the gut and transports the host plant compound calotropin (XlogP-AA: 0.9) (Kowalski et al., 2020). At the same time, in *O. fasciatus* the elimination of ouabain from the gut takes several days (Bramer et al., 2015), suggesting additional mechanisms and likely transporters here.

The only tissue in which the *Ofabcb2* expression was slightly increased compared to *Ofabcb1* was the salivary glands. Unlike *Poekilocerus pictus* (Pyrgomorphidae: Orthoptera) (Pugalenthi and Livingstone, 1995), nothing is known about storage in this region in *O. fasciatus*, but highly

apolar digitoxin and probably other ingested cardenolides are metabolized already there (Moore and Scudder, 1985; Scudder and Meredith, 1982b). Both OfABCBs could therefore play a role in the provision for biotransformation or in the flux for metabolite absorption. In humans a physiological and excretory function into the salvia is suggested for ABCB1, yet not well understood (Uematsu et al., 2001; Uematsu et al., 2003). Insect and mammalian ABCB1 homologs also have metabolic substrates, as outlined before. A metabolic function of the two OfABCB transporters as previously discussed is therefore also conceivable here, in particular because the saliva emulsifies and suspends seed contents (Woodring et al., 2007).

Alternative or mis-splicing of ABC transporters has been shown to confer resistance to inorganic or bio-insecticides in insects and can be an alternative to expression changes for conveying resistance (Mathew et al., 2018; Pauchet et al., 2016; Seong et al., 2016; Tay et al., 2015; Xiao et al., 2014). In *Drosophila*, an N-terminally truncated MDR49 variant, resembling in its structure six of the predicted *Ofabcb2* variants (TMD_3 - NBD - TMD_6 - NBD), confers resistance to DTT (Seong et al., 2016). The complex alternative splicing pattern of the *Ofabcb2* gene, indicated by multiple sequence combinations in silico and in vitro, could therefore enable flexible and versatile adaptation to changing environmental conditions. However, another truncated MDR49 variant increased the fruit flies' sensitivity to colchicine (Wu et al., 1991). Since ABCB full transporters primarily ensure compartmentalization through substrate efflux from cells and tissues in animals (Schinkel and Jonker, 2003; Wessler et al., 2013), this also sheds new light on alternative splicing as a putative tool for functional tissue-specific deactivations. In general, it is becoming apparent that the ABCB transporter structure does not necessarily have to be "typically" intact in order to fulfil a function, and that downregulation, regardless of the type, could be just as functional in resistance as upregulation (Amezian et al., 2024; Gerard and Gillet, 2024; Seong et al., 2016). Further functional investigation of such splice variants is an exciting area of research, as little is generally known about this in insects and even in humans (Park et al., 2017; Srinivasan et al., 2009).

Conclusion

In this chapter I show that OfABCB1, an ABCB full transporter, is tightly connected to ouabain sequestration in the large milkweed bug. The loss of more than 50 % of ouabain storage capacity in single and double RNAi knockdowns, combined with high level tissue expression and immunohistochemistry supports OfABCB1's direct localization at the thoracic storage compartment. The combination of my data and previous physiological as well as morphological data supports the conclusion that OfABCB1 has taken on a new storage function in addition to

its conserved neuro-protection and excretion function. The enigmatic role of its homolog, OfABCB2, in the cardenolide network requires further research. Furthermore, OfABCB2 might diversify its function by alternative splicing, a rather rarely characterized mechanism in ABCB efflux pumps so far. In summary, this chapter broadens our understanding of the molecular basis of cardenolide sequestration in insects and is the first evidence that an ABCB efflux pump plays a decisive role in the cardenolide sequestration mechanism of *O. fasciatus.*

Chapter 3

Insights into sequestration dynamics and related factors in the large milkweed bug, *Oncopeltus fasciatus* (DALLAS, 1852)

Abstract

The large milkweed bug, *Oncopeltus fasciatus*, is a well-characterized model organism, especially in terms of its adaptation to toxic secondary plant metabolites, the cardenolides. However, little is known about how the common practice of rearing *O. fasciatus* in the laboratory without cardenolides affects their sequestration performance, as has previously been shown for their life history traits. In this chapter, I study the influence of diet on sequestration performance, with a focus on temporal sequestration dynamics. I show that sequestration saturates one day after an artificial cardenolide has entered the hemocoel. Additionally, I demonstrate that dietary history influences the capacity for sequestration in terms of the amount of sequestered ouabain, but not the concentration. Chemical and immunohistological analyses suggest that this is related to nutritional and molecular mechanisms involving ABCB full transporter proteins. Furthermore, I show that the volume of released defensive fluid is related to several factors including the amount of stored cardenolides as well as the animals' biomass, sex, and the age of females. Sequestration is also functionally closely linked to cardenolide tolerance through target-site insensitivity of the bugs' Na,K-ATPase enzymes. By immunohistochemistry, I could detect this enzyme in the Malpighian tubules, but barely in the defensive fluid cells of the thoracic storage compartment. In addition, one of the resistant Na,K-ATPase α1-subunit genes, α1A, responds in its expression to ouabain. In summary, this chapter broadens our understanding of the dynamics and factors related to sequestration and provides insights into its relationship with cardenolide tolerance strategies. Furthermore, it characterizes our laboratory line with regard to the stored cardenolide spectrum by an optimized HPLC protocol, which is particularly suitable for accurate quantification of polar cardenolides, such as those found in dietary seeds of *Asclepias syriaca*.

Introduction

Sequestration is a fundamental principle of life in the sense of reorganizing external to internal substances. It refers to the storage of a variety of different substances derived from food, such as nutrients, physiological potentiators like pheromone precursors, but also toxins such as cardenolides (summarized by Duffey, 1980). From an evolutionary perspective, sequestration of non-nutritive substances can facilitate the occupation of an ecological niche, chemical defense against predators, reproduction, or communication (see reviews by Beran and Petschenka, 2022; Duffey, 1980; Opitz and Müller, 2009). Toxin-adapted insects have an advantage over non-adapted animals by using poisonous plants in terms of competition avoidance and obtaining an enemy-free space (Bernays and Graham, 1988; Murphy, 2004). The chemical defense against predators, mediated by toxic cardenolides, is considered the main driver for their sequestration (Petschenka and Agrawal, 2015, 2016). Members of the leaf beetle genus *Oreina* spp. have even evolved the ability to synthesize cardenolides de novo (Dobler et al., 1996; Pasteels, 1993; Pasteels et al., 1995). While de novo synthesis makes the insects' defense system independent of toxin-producing host plants, sequestration of dietary toxins is considered a more metabolically cost-effective strategy (Beran and Petschenka, 2022; Rowell-Rahier et al., 1995).

Across the five insect orders in which dietary cardenolide sequestration has been demonstrated, the subfamily Lygaeinae (Lygaeidae: Hemiptera) represents a striking example (Agrawal et al., 2024b; Beran and Petschenka, 2022; Opitz and Müller, 2009). Both cardenolide sequestration and tolerance by insensitivity of the target-site to cardenolides in the Na,K-ATPase are basal and synapomorphic traits in this subfamily (Bramer et al., 2015). The milkweed bug, *O. fasciatus*, is the most intensively studied species in this context for several reasons: *O. fasciatus* is a well-established laboratory model species in developmental and evolutionary biology (Burdfield-Steel and Shuker, 2014; Chipman, 2017; Feir, 1974; Liu and Kaufman, 2009; Panfilio et al., 2019). A major advantage of this species, compared to other members of the subfamily Lygaeinae, such as *Spilostethus saxatilis* (SCOPOLI, 1763) (Petschenka et al., 2022), is its dietary flexibility and the ability for long-term rearing on commercially available non-host diets, such as husked *Helianthus annuus* L. seeds (Eggermann and Bongers, 1971; Feir, 1974; Gordon et al., 1971; Isman, 1977; Liu and Kaufman, 2009). Cardenolide-free rearing on sunflower seeds is common practice (see e.g. Berenbaum and Miliczky, 1984; Bramer et al., 2015; Detzel and Wink, 1995; Duffey and Scudder, 1972; Hill, 2006; Rubiano-Buitrago et al., 2023) and is a highly valuable asset for cardenolide adaptation studies such as those in this thesis in order to establish a distinct

relationship between observed effects and cardenolides. However, diet switches to natural host plants are accompanied by physiological adaptations that can change growth rates and fecundity over several generations (Feir, 1974; Gordon et al., 1971; Hill, 2006) through processes like adaptive oosorption. Once adapted, no negative or beneficial effects were found after returning to the ancestral milkweed diet for females, in contrast to males, which invest more in their germ cell development at the expense of their longevity (Attisano et al., 2012; Moore and Attisano, 2011). In summary, diet switches shape physiological changes in fitness and life-history traits in *O. fasciatus*. These changes, which need time and are not necessarily cost neutral, are linked to the diets' energetic value and cardenolide composition (Attisano et al., 2012; Feir, 1974; Gordon et al., 1971; Heyworth et al., 2023; Hill, 2006; Moore and Attisano, 2011; Pokharel et al., 2021). However, little is known about dietary effects on the sequestration performance, especially in the long term. Duffey and Scudder (1974) reported a drastic reduction in sequestration capacity in the first generation of sunflower-fed animals, while Yoder et al. (1976) found no effect on intestinal ouabain uptake ex vivo. In fact, some Lygaeinae species, such as the European *Arocatus longiceps* (STÅL, 1872), which switched to non-poisonous host plants, have completely lost the ability to sequester toxic cardenolides, presumably saving the costs associated with sequestration (Bramer et al., 2015). However, whether and which costs are associated with sequestration in *O. fasciatus* is still under debate. Most studies found no costs to development, growth, or reproduction (Agrawal et al., 2022; Isman et al., 1977; Vaughan, 1979), in contrast to a recent study with controlled individual cardenolides, such as ouabain (Pokharel et al., 2021). A recent finding indicates costs to oxidative state linked to pigmentation and aposematism (Heyworth et al., 2023) which are closely related to sexual selection and chemical defense (Berenbaum and Miliczky, 1984; Burdfield-Steel and Shuker, 2014).

The aim of this chapter is thus to evaluate the effects of long-term diet switches and the common cardenolide-free rearing practice on the sequestration performance of *O. fasciatus*. The focus here is specifically on the temporal dynamics of ouabain sequestration, while most previous studies have focused on single or few endpoint cardenolide sequestration capacities (Agrawal et al., 2022; Bramer et al., 2015; Duffey et al., 1978; Duffey and Scudder, 1974; Isman, 1977; Isman et al., 1977; Moore and Scudder, 1985; Pokharel et al., 2021; Rubiano-Buitrago et al., 2023; Rubiano-Buitrago et al., 2024; Scudder et al., 1986; Scudder and Meredith, 1982b; Vaughan, 1979). For this, ouabain was chosen because it is an established, commercially available plant-derived substitute for host plant cardenolides (Scudder et al., 1986) and because it is rapidly and specifically stored in the thoracic storage compartment (Chapter 2; Duffey et al., 1978; Duffey and Scudder, 1974; Scudder et al., 1986; Scudder and

Meredith, 1982b). In addition, ouabain storage occurs via an active transporter (ABCB full transporter) through a pathway that is not yet fully understood (Chapter 2). Therefore, I examine here, using immunohistochemistry, potential changes in defensive fluids regarding these key proteins in our two long-term laboratory lines that, although of common origin, have been maintained on different diets for more than 90 generations: one reared on cardenolide-free husked sunflower seeds, and one additionally reared on host plant milkweed seeds and seed pods of *Asclepias syriaca*.

Another peculiarity of *O. fasciatus*, along with other Lygaeinae members, is the ability to passively release stored cardenolides in defensive fluids from their specialized storage compartment, which is mainly located at the lateral thoracic margins (Bramer et al., 2017; Duffey et al., 1978; Duffey and Scudder, 1972; Duffey and Scudder, 1974; Moore and Scudder, 1985; Rubiano-Buitrago et al., 2024; Scudder et al., 1986; Scudder and Meredith, 1982a). Although comparative chemosensory studies on enhanced protection by fluid release are still pending, it can be considered a key advantage compared to other cardenolide-sequestering insect species, such as monarch butterflies, which trap dietary cardenolides within their bodies in a stationary way (for overview see Opitz and Müller, 2009). For example, while consumption of *O. fasciatus* results in emetic predator responses and predator-specific avoidances (Berenbaum and Miliczky, 1984; Bramer et al., 2018), the defensive fluid itself, when applied to flies, deters predatory spiders in contrast to pure cardenolides such as ouabain and digitoxin (Hill, 2006). The significance of the defensive fluid is underscored by the stepwise evolution of the releasing mode, reaching in *O. fasciatus* the highest complexity observed so far, in contrast to the ancestral storage compartment within the Lygaeinae (Bramer et al., 2017). Most research has focused on chemical cardenolide composition of the defensive fluid and associated uptake kinetics (Duffey et al., 1978; Duffey and Scudder, 1974; Moore and Scudder, 1985; Rubiano-Buitrago et al., 2024; Scudder and Meredith, 1982b), largely neglecting the role of the fluid itself. However, it does contain a warning odorant (2-isobutyl-3-methoxypyrazine) (Aldrich et al., 1997), uncharacterized proteins (Duffey and Scudder, 1974), and is likely involved in conveying concentrations relevant to predator perception or deterrence and hence chemical defense. Also, its physiological origin is still not fully understood (Bramer et al., 2017; Moore and Scudder, 1985; Scudder et al., 1986; Scudder and Meredith, 1982a). To better understand the nature of the released defensive fluid and its relationship to the stored cardenolides themselves, in this chapter I also examine the influence of animals' biomass, sex, age, and diet on the volume of defensive fluids. The chemical defense by cardenolides is exerted by their bitterness and toxicity via Na,K-ATPase inhibition (Brower, 1969; Euw et al., 1967; Glendinning, 1992; Groen et al., 2017; Hill, 2006; Lohr et al., 2017; Malcolm, 1991;

Moore and Scudder, 1986; Petschenka et al., 2022; Petschenka and Agrawal, 2015; Sticher, 2010). *O. fasciatus* has therefore evolved an unsurpassed target-site insensitivity that far exceeds that of most other investigated insects (Bramer et al., 2015; Moore and Scudder, 1986; Petschenka et al., 2013a; Petschenka et al., 2018), through sophisticated subunit compositions of its Na,K-ATPase. These combinations mediate distinct and specifically tuned tolerances and pumping activities to prevent autointoxication by ingested cardenolides (Herbertz et al., 2024; Lohr et al., 2017). As previously mentioned: target-site insensitivity and sequestration are interrelated basal traits of the subfamily Lygaeinae (Bramer et al., 2015). It can therefore be suggested that they are also closely linked at the tissue level. The highly cardenolide insensitive Na,K-ATPase α1-subunits, α1A and α1B (Dalla et al., 2017; Dalla and Dobler, 2016; Herbertz et al., 2024), predominate for example in tissues known to be involved in cardenolide transport and storage, like the Malpighian tubules or the ovary (Duffey and Scudder, 1974; Lohr et al., 2017; Meredith et al., 1984; Moore and Scudder, 1985; Newcombe et al., 2013). Here, for the first time, I investigate, by immunohistochemistry, the presence of this enzyme in the major storage tissue that is released with the milkweed bugs' defensive fluids. In addition to our previous study, I also reexamine the expression response of the most abundant and highly insensitive α1A paralog (Dalla et al., 2017; Dalla and Dobler, 2016; Herbertz et al., 2024; Lohr et al., 2017) to ouabain, but here on a finely tuned timescale, to detect both early and late responsiveness.

In summary, this chapter provides insights into how diet switches can shape sequestration capacities and the interplay of sequestration and tolerance strategies in *O. fasciatus*. In addition, it sets a new focus for future sequestration research and optimizes the methodological basis for chemical cardenolide analyses in this context.

Material and Methods

Laboratory animals

The origin of milkweed bugs used in this study has been previously described by Lohr et al. (2017). Briefly, the laboratory lines under study originated from *O. fasciatus* adult animals collected 2010 in Ithaca (New York, USA). Additional animals, collected near the University of Chicago (Illinois, USA), were introduced into existing lines in 2014 to counteract genetic impoverishment and inbreeding. All animals were reared at 16 h light to 8 h dark conditions at 25 °C and subjected to two different dietary conditions: either exclusively with husked *Helianthus annuus* seeds (Alnatura, Darmstadt, Germany) (individuals are not able to penetrate intact sunflower seed hulls (Eggermann and Bongers, 1971)) or paired with

milkweed seeds and pods (*Asclepias syriaca*). Mature seeds were supplied by Anurag Agrawal (Cornell University, New York, USA) and seed pods were obtained from the botanical garden of the Universität Hamburg (Hamburg, Germany).

Defensive fluid sampling and volume quantification

Animals were enclosed dorso-ventrally by forceps, periodically squeezed and the released defensive fluids were collected with 2 µl micro-glass capillaries (minicaps ®, Hirschmann Laborgeräte GmbH & Co.KG, Eberstadt, Germany). Subsequently, the fluid-filled length within each disposable micro-capillary and its total length were measured on millimeter paper. This allowed a measurement to an accuracy of 0.5 mm and thus 0.03 µl, but was at the same time less susceptible to handling errors than weighing to determine the volume. Released defensive fluid volumes were then calculated by multiplication of the determined fluid filling distance with the ratio of calibrated volume and total capillary length measured.

Ouabain sequestration assay

Adult females of both dietary lines, hereafter referred to as dietary histories, were injected into their hemocoel with 10 µg ouabain (Sigma-Aldrich, Taufkirchen, Germany) dissolved in a 0.9 % NaCl solution (Carl Roth, Karlsruhe, Germany) (for details see Chapter 2). Animals were then allowed to sequester the injected ouabain for five different periods (1 h, 4 h, 24 h, 3 and 5 days, n = 2 - 6) and were kept under rearing conditions. After these assigned sequestration periods, defensive fluids were collected as previously described and immediately subjected to cardenolide extraction, as co-released cellular components rapidly precipitated after collection. Based on the observed temporal sequestration trends, additional samples of the defensive fluid were collected two hours after ouabain injection, as described above. In contrast to the above, only the defensive fluid droplets from the metathoracic flanges were collected, where possible. This should allow for a better correlation of ouabain sequestration with the immunohistochemical data of the defensive fluid droplets from the flanges, as described in the corresponding methods section.

Cardenolide extraction

High-performance liquid chromatography (HPLC) was performed to quantify sequestered ouabain amounts as well as to verify the presence of cardenolides in milkweed bugs defensive fluids and dietary seeds. Seeds were processed as previously described by Lohr et al. (2017). Seeds were freeze-dried and thoroughly ground by a mortar and pestle. After suspension in 2 ml methanol (100 %, Carl Roth, Karlsruhe, Germany) with 20 µg digitoxin as internal standard

(Sigma-Aldrich, Taufkirchen, Germany), the samples were heated at 55 °C for 20 min in a water bath. Subsequent to ultrasonication for 20 min, methanol was evaporated for 2 h by vacuum centrifugation. Samples were resuspended in 200 µl methanol and filtered with a 0.45 µm filter (KX Nylon Syringe Filter, Kinesis Scientific Experts, St. Neots, Cambridgeshire, UK). Collected defensive fluids were ejected from glass micro-capillaries into 100 µl methanol with the capillaries being flushed three times and ejected twice after each flushing. Solutions were transferred to 900 µl methanol containing 10 µg digitoxin as internal standard. Subsequent to vortexing, samples were ultrasonicated for 5 min in a heated water bath (55 °C) followed by centrifugation for 10 min at 13.4 rpm (MiniSpin, Eppendorf, Hamburg, Germany). Supernatants were transferred to 2 ml reaction tubes and methanol was completely evaporated by vacuum centrifugation for at least two hours (Eppendorf Concentrator 5301, Eppendorf, Hamburg, Germany). Supernatants of 2 h ouabain sequestration samples were additionally filtered as described in Chapter 2. 100 µl methanol was added and after anew ultrasonication for 5 min and short centrifugation, samples were transferred to HPLC vials with 300 µl inlets (Klaus Trott, Chromatographie Zubehör, Kriftel, Germany). Samples were stored at -80 °C until HPLC measurement.

Cardenolide preparation

For isolation and purification of the cardenolides calotropin and calactin semi-preparative HPLC runs were conducted as described by Petschenka et al. (2018) and Herbertz et al. (2024). Monarch butterfly caterpillars (*Danaus plexippus* (LINNAEUS, 1758)) (about 8 g dry weight) reared on *A. curassavica* were extracted with methanol, followed by hexane and chloroform extraction. Methanol dissolved total cardenolides were then separated into six compounds by HPLC system III (see below). Compounds five (calotropin) and six (calactin) were crystallized and the cardenolide structure was analyzed by NMR spectroscopy. For further details see Gathemann (2017). A one-to-ten dilution of calotropin (sample M2_P5) and calactin (sample M2_P6) was run along several defensive fluids in HPLC system II.

High-performance liquid chromatography

Reversed-phase high-performance liquid chromatography (RP-HPLC) was conducted on an Agilent 1100 series HPLC system (Agilent, Waldbronn, Germany) with three different C18 columns hereafter referred to as system I, II and III. A *post* column diode-array (DAD) detector allowed absorbance detection of wavelengths from 200 to 400 nm and was set to record elution profiles at 218 nm for cardenolide quantification. All compounds revealing symmetrical absorbance spectra and maxima within the 216 - 222 nm range were inferred to be

cardenolides (Lohr et al., 2017). If multiple sample replicates were present, compounds had to reveal a distinct spectrum in the majority of samples to be classified as cardenolides. A maximum difference of 0.09 min in retention times (RTs) and 0.01 min in relative retention times (RRTs) was tolerated to classify cardenolides as identical. Relative retention times were calculated by dividing the retention time of the internal standard by that of the compound of interest to allow comparison between HPLC runs. Non-polar compounds therefore have relative retention times close to one. Multi-level calibration of ouabain (5-point 1:2 dilutions of 0.2 µg/µl) with a constant internal standard concentration (0.1 µg/µl) was performed to verify linear responses and used for ouabain quantification (Table S 28). In contrast, natural cardenolides were quantified assuming a one-to-one response ratio to digitoxin. Very rare cardenolides (n < 3 in defensive fluids) were excluded from quantifications. Cardenolide spectra were analyzed by calculating diversity and polarity indices as described by Rasmann and Agrawal (2011). Briefly, the diversity index is an adaptation of the Shannon-Wiener index taking also the relative amounts into account. The polarity index enables a comparison even with significantly different spectra by, among other things, weighting the peaks according to their relative quantity.

HPLC system I

HPLC system I has been previously described by Lohr et al. (2017) and was used for initial analysis of ouabain sequestration assay defensive fluid samples (n = 2 - 3 per time point and diet history). Briefly, compounds were eluted with a constant flow rate (0.7 ml/min) by an acetonitrile (ACN; HPLC grade, Carl Roth, Karlsruhe, Germany) : water (Carl Roth, Karlsruhe, Germany) gradient from a NUCLEODUR® C18 ec column (3 µm, Ø 4.6 mm ID, 150 mm; Macherey-Nagel, Düren, Germany). Two minutes after injection, the ACN percentage starting at 16 % was gradually increased by 2.35 % min^{-1}. At 25 min, this rate was further increased to 5 % min^{-1} followed by an isocratic flow (95 % ACN : 5 % H_2O) at 30 min for 5 min. Column equilibration was conducted for 10 min ahead of subsequent injections. In that system also a digoxin standard in methanol was recorded. In addition to multi-level calibration as outlined above, also single-level calibration by internal response factor was conducted and compared. For this purpose, either an internal response of 1 was arbitrarily assumed or the empirically determined internal response (IRF.e) of an equimolar concentration of ouabain and standard (0.1 µg/µl) was used. The latter was calculated as follows: $IRF.e = \frac{Area_{standard} * Amount_{ouabain}}{Amount_{standard} * Area_{ouabain}}$.

HPLC system II

HPLC system II was equipped with a NUCLEODUR® C18 HTec column (5 µm, Ø 4.6 mm ID, 250 mm; Macherey-Nagel, Düren, Germany). This system was used to identify the most reliable conditions for cardenolide quantification based on potential limitations of the quantification accuracy detected in HPLC system I. Six different elution gradients varying in their starting organic solvent percentage (2 - 16 %) (Table S 29) were run to identify adequate conditions for accurate ouabain and natural cardenolide quantifications. Based on these findings, the final run conditions were as follows: 10 µl of samples were analyzed by gradient elution beginning at 8 % ACN : 92 % H_2O for 2 min, increasing then gradually to 70 % ACN at 28.5 min followed by an increase to 95 % ACN : 5 % H_2O at 33.5 min, which was prolonged isocratically for 5 min and a subsequent *post* run of 15 min. Flow rate was held constant at 0.7 ml min^{-1} throughout each run. In this system ouabain had a median retention time of 12.1 to 12.3 min and the internal standard digitoxin of 27 min. The two standard substances are defined as polar and apolar and flanked the natural cardenolides in the HPLC chromatograms. Thus, I used this elution range to define the polarity of the natural cardenolides as follows: polar (≤ 17.0 min), intermediate-polar (> 17 and ≤ 22.0 min), apolar (> 22 min). OpenChrom® (v 1.5.0) was used for chromatogram visualization (Wenig and Odermatt, 2010).

HPLC system III

HPLC system III was equipped with a NUCLEODUR® C18 HTec column (5 µm, Ø 10 mm ID, 250 mm; Macherey-Nagel, Düren, Germany). This system was used for preparation of calotropin and calactin from monarch butterfly caterpillars fed on *A. curassavica* as previously described by Petschenka et al. (2018) and Herbertz et al. (2024). 75 µl of sample were separated by gradient elution starting at 16 % ACN : 84 % H_2O for 2 minutes, increasing then gradually to 30 % ACN at 10 min followed by an increase to 50 % ACN : 50 % H_2O at 25 min prolonged isocratically for 5 min. Flow rate was held constant at 3 ml min^{-1}.

Determination of factors related to the volume of released defensive fluid

To gain further insights into defensive fluid associated parameters, defensive fluids were sampled from female and male adult insects (n = 20, each) from both laboratory lines, i.e. diet histories (total n = 80). Insects that did not release any further fluid were transferred into previously weighed 1.5 ml reaction tubes and weighed, calculating the fresh mass of each animal. In addition to volume quantification, the identity of the release sites, and age (visually classified into three categories: young, intermediate and old) were determined for all female individuals.

Immunofluorescence staining and fluorescence quantification of defensive fluids

Defensive fluids from the metathoracic flanges were obtained by dorsoventral squeezing of female animals with forceps and applied to histological slides (SuperFrost™ Ultra, Thermo Scientific). Defensive fluids from milkweed seed line animals were stained with specific monoclonal antibodies (mAb) to study the distribution of proteins related to cardenolide adaptations, ABCB full transporters (see Chapter 2) and the Na,K-ATPase (monoclonal antibodies - ABCB full transporter: C219 (5 µg/ml, Thermo Fisher Scientific), C494 (5 µg/ml, Calbiochem, Merck), Na,K-ATPase: α-subunit a5s (5 µg/ml), β-subunit Nrv5F7s (2.5 µg/ml)). An α-tubulin monoclonal antibody (12G10; 1 µg/ml) was used as positive control (Developmental Studies Hybridoma Bank, University of Iowa, USA). To investigate whether sequestration capacities might be related to ABCB full transporter expression in the compartment, the defensive fluids of the metathoracic flanges of two biological replicates from each diet line were stained. Nuclei counting and immunofluorescence quantification of these stained defensive fluids were conducted by thresholding with Fiji (ImageJ v1.54g) (Schindelin et al., 2012; Schneider et al., 2012). Each image was split into its blue, green and red channel. Scale bars were removed from regions of interest (ROIs) *prior* to analysis. The total number of nuclei was counted by the Li thresholding algorithm and “watershed” nuclei separation in smoothed blue channel images of sampled defensive fluids (from 5 individuals (sunflower: n = 2, milkweed n = 3)). Automatic nuclei separation was reviewed and manually curated where necessary. Fluorescence area and background-corrected fluorescence intensity (four background signal measurements) were quantified by manual thresholding (set = 21) in red channel images of defensive fluids (n = 8 from two biological replicates for each diet history) stained with either monoclonal antibodies C219 or C494. Total area and total corrected fluorescence intensity (sum of calculated corrected total cell fluorescence) were then normalized to total nuclei number and compared. Exposure times for Cy3 were 160 ms and for DAPI 100 ms. Staining always included a secondary antibody control in which the primary antibody was omitted. For further details on staining procedure, fluorescence microscopy, and image processing see Chapter 2.

Na,K-ATPase gene expression analysis and immunohistochemistry

Sequestration and target-site insensitivity are two interrelated adaptations in the subfamily Lygaeinae (Bramer et al., 2015). Therefore, I also investigated the expression pattern of the highly cardenolide-insensitive Na,K-ATPase α1-subunit paralog α1A after ouabain exposure (1 h to 32 h) by RT-qPCR (for details see Chapter 2) in the previously determined time frame

of peak sequestration, using the paralog-specific primers described by Zhen et al. (2012). In addition, transverse Malpighian tubule cryosections were stained with the monoclonal antibody a5s (5 µg/ml), specific for the Na,K-ATPase α-subunit as described in Chapter 2.

Statistics

Statistical analyses were conducted using R (R Core Team, 2018) and RStudio (2024.12.1 Build 563). Graphical data examinations were conducted with standard graphics, ggplot2 (Wickham, 2016), ggridges (Wilke, 2018), ggpubr (Kassambara, 2018), and GGally (Schloerke et al., 2025). Pairwise correlations were established by Spearman rank correlations. In general, initial analyses were performed by General Linear Models (LM) with variables of main interest, including Analysis of Covariance (ANCOVA) with appropriate sums of squares, or by two-sample Welch's t-test. Normality and variance homogeneity assumptions were checked by Shapiro-Wilk test of residuals (or data of interest) and Score Test for Non-Constant Error Variance and when reasonable with Levene's test (i.e. in case of ANCOVA) (car package (Fox and Weisberg, 2011)). Generalized Linear Models (GLM) or Generalized Additive Models (GAM) or Scheirer-Ray-Hare tests were performed when assumptions were violated. Appropriate distributions for GLM modelling were selected visually and by Akaike's Information Criterion (AIC) using the fitdistrplus package (Delignette-Muller and Dutang, 2015). Linkage of responses to linear predictors was determined based on *a priori* assumption or exploratory data analyses as outlined below. All chosen models used to infer effect significance were assessed furthermore by diagnostic plots to ascertain assumption validity with selected exponential families. Effect significance was determined by Analyses of Deviance for GLM fits by Likelihood ratio (LRT) or approximate F tests of nested models differing in the respective effect of interest. Group differences were further analyzed by estimated marginal means (emmeans package (Lenth)).

Ouabain quantification accuracy by HPLC system I

In my preliminary analysis of defensive fluids to study the temporal dynamics of ouabain sequestration by HPLC I, I found that ouabain elution was partitioned into two distinct peaks. An initial main effect gamma GLM with identity link was conducted to assess the effect of animals' diet history as well as differential peak integration in conjunction with different quantification strategies (multi-level calibration *versus* empirically determined internal response factor (IRF.e) or hypothesized internal response factor (IRF.h = 1); model: total ouabain amount [µg] ~ quantification method + identity of peak used for integration + diet

history of animals). Subsequently, LRTs were performed to infer the effect of each predictor as well as their interactions.

Temporal ouabain sequestration dynamics

Statistical inferences of temporal dynamics in ouabain sequestration in relation to animals' dietary history were performed based on trends observed by exploratory graphical analyses. Sequestration time was treated as covariate to study the accumulated ouabain amounts in dependence of animals' diet history over time by Analysis of Covariance (ANCOVA (LM): stored ouabain amount ~ log(sequestration time) + dietary history). An interaction term was included to test the assumption of homogeneity of the regression slopes. A multiple linear regression was performed to additionally derive the influence of the cardenolide concentration stored in animals of the milkweed seed line on the amount of ouabain sequestered (LM: stored ouabain amount ~ log(sequestration time) + natural cardenolide concentration). For the other parameters examined as independent variables, i.e. total released defensive fluid volume and stored ouabain concentrations, analyses were conducted with sequestration time as a factor. I consider this appropriate, as initial data analyses did not reveal an explicit linear relationship with sequestration time. Nonetheless, potential covariates were included when reasonable. For example, an ANCOVA was conducted to investigate the effect of sequestration time and stored natural cardenolide amount on the released defensive fluid volume in animals of the milkweed seed line. When non-normal errors were indicated, appropriate error distributions were selected individually for GLMs.

Analysis of factors possibly related to defensive fluid volume

Analysis of defensive fluid volumes (dfv) with individuals' biomasses, sex and diet histories (cardenolide-free vs. cardenolide-containing diet) was performed after model exploration by a multiplicative main effect gamma GLM (dfv ~ biomass + sex + diet history) according to AIC of response variable, dfv (model 3, Table S 30). Log link was chosen as appropriate link function between response and linear predictor to ensure positive response values. Dfv is exclusively positive and bounded to zero. Note that based on this link function, interpretation of coefficients is multiplicative; briefly, exp(coef(x)) gives the factor by which response changes for one-unit change of x. Approximate F-tests for nested models differing in their independent variable of interest were conducted because those include dispersion estimates. Dispersion estimates were checked, residual deviance test for goodness of fit and McFadden's pseudo-R^2 calculated. In addition, the effect of age, diet history, as well as defensive fluid releasing sites (in terms of total released defensive fluid droplets sampled) was studied in female animals with

the same model type after model exploration (model 3, Table S 31). Outlier analysis was conducted by R functions influence() (package stats), cooks.distance (), and outlierTest() (both package car).

Results

Ouabain peak resolution is a function of HPLC starting acetonitrile concentration

The initial analysis of ouabain amounts sequestered in animals' defensive fluids differing in their diet history by HPLC system I revealed that ouabain elutes into two distinct peaks (retention time = RT = 2.07 min and 4.25 min). When investigating quantification reliability, I found that quantified ouabain amounts varied significantly based on the peak identity used for quantification (LRT: Deviance(1) = 4.968, $P < 0.001$), quantification method (LRT: Deviance(1) = 8.395, $P < 0.001$), and samples with respect to the animals' dietary history (LRT: Deviance (1) = 28.61, $P < 0.001$, Figure 17). As expected, single peak integrations yielded significantly lower quantities when the altered response relationship with the internal standard was not adequately adjusted, either by multi-level calibration or by empirically determined internal response factors (LRT peak x method interaction: Deviance (1) = 4.060, $P = 0.0107$; Table S 28, Table S 32). However, even when they were taken into account, the estimated individual peak amounts for milkweed seed line animals differed significantly (LRT peak x diet interaction: Deviance (1) = 6.132, $P < 0.001$, Table S 33) (Figure 17). The examination of absorbance spectra showed that the signals of peak 1 were indeed occasionally masked by co-eluting substances. Since the retention time of this peak was also exceptionally low, I suspected that a significant amount (~50 %) of ouabain eluted with the initial solvent front without interacting with the C18 column matrix. Consistent with this, I found that decreasing the initial elution strength by reducing the amount of organic solvent (acetonitrile) leads to a continuous reduction in the retention times between peaks. The sample resuspension in methanol had a decisive influence on this elution partitioning, since the elution profiles of ouabain dissolved in water resulted in a single, well-developed peak (Figure S 26, Figure S 27, Figure S 28).

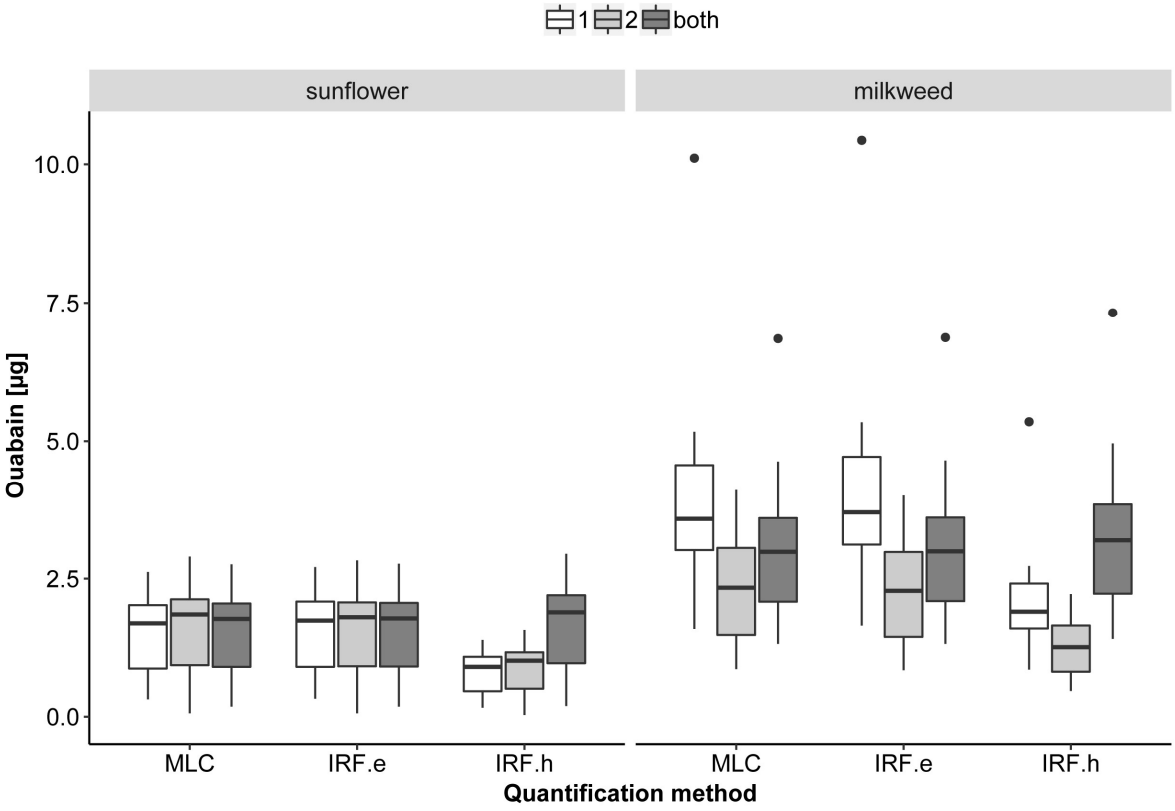


Figure 17 Ouabain amount quantified with HPLC system I in animals with different diets using different quantification methods. MLC = multi-level calibration, IRF = internal response factor. E and h indicate whether empirically determined or hypothetical IRFs (= 1) were used. Different colors indicate quantification based either on the individual peak areas of the respective ouabain peak (1 = peak (2.07 min) was used, vs. 2 = peak (4.25 min)) or on both.

Dietary cardenolides accumulated in defensive fluids

Milkweed bug defensive fluids differed from their dietary sources (mature *A. syriaca* seeds and still maturing seeds from seed pods) in cardenolide identity, richness (peak number), diversity, polarity, and individual cardenolide abundances (Table S 34). In total, 42 different cardenolides were identified based on absorbance spectra and different retention times. Several cardenolides were only present in defensive fluids (18) or in mature seeds and/or seed pods (6). Most of these showed low abundances (9 or 4 ≤ 1 % of total cardenolide amount) or were detected infrequently in defensive fluids (5 less than 3 times). While defensive fluids had a higher cardenolide richness (peak number) than seeds and seed pods (36 vs. 23 vs. 7), the average diversity and average polarity were intermediate to these dietary sources (Table S 34). In general, 20 cardenolides were at least recorded in half of analyzed defensive fluids while nine were common to all (n =15). Five of these common cardenolides were dominant (≥ 5 % of the total cardenolide content) accounting for 84 % of total cardenolide sequestered, but only four were also present in dietary milkweed seeds and/or pods. One polar cardenolide (c9,

15.14 min) in particular accounted for 47 ± 1 % of stored cardenolides (on average 6.5 ± 1.3 µg up to a concentration of 19.3 µg/µl) and was absent from seeds and seed pods (Table S 34). It, like the other unique cardenolides, likely originated from biotransformation of seed cardenolides or from their enrichment above the analytical detection limit of the system (Agrawal et al., 2022; Duffey, 1980; Duffey and Scudder, 1974; Moore and Scudder, 1985; Rubiano-Buitrago et al., 2023; Scudder and Meredith, 1982b). The other three subdominant compounds unique to defensive fluids were polar (c7) to intermediate-polar (c20, c25). One of these intermediate-polar compounds (c25, 20.67 min; 1.4 % of total cardenolide) was also the most lipophilic subdominant cardenolide stored. While not identical, this compound eluted similarly to intermediate-polar calotropin (20.79 min, retention time difference = 0.12 min), which was also absent in seeds and pods, similar to its stereoisomer calactin (21.79 min). The only apolar cardenolide of seeds (c27, 23.08 min) was therefore not sequestered. However, the cardenolides found exclusively in seeds and pods covered the entire polarity range, with the most polar (c1, 12.94 min) and the most non-polar cardenolide (c27, 23.08 min) recorded here. The most polar seed cardenolide was not found in any of the total defensive fluids, but once in a defensive fluid derived exclusively from the metathoracic flanges. In summary, it can be suggested that these seed cardenolides not detected in defensive fluids were also metabolized, stored, or excreted elsewhere in the animal, similar to phenomena described in other studies (Agrawal et al., 2022; Duffey, 1980; Duffey and Scudder, 1974; Moore and Scudder, 1985; Pokharel et al., 2021; Rubiano-Buitrago et al., 2023; Scudder and Meredith, 1982b).

A further indication of such regulatory processes was the altered dominance proportions of six cardenolides in the bugs' defensive fluids compared to the seeds of the host plant (in seeds 4 to 66 times more; in defensive fluids 2 to 5 times more) (Table S 34). For example, the abundance of the polar cardenolide c13 (16.21 min; 54.6 %) was 10 to 66-fold higher in seed pods than in the storage compartment. On the other hand, the dominant polar cardenolide c12 (15.91 min) was three to five times more abundant in the defensive fluid than in seeds and pods. However, I cannot generalize the conclusions on this point too much, since the variability of cardenolide composition in the dietary sources limits the interpretation of which substances are putatively metabolized or excreted and to what extent.

Nevertheless, the relative abundances of frequently detected cardenolides (27; n ≥ 3) in defensive fluids were extremely constant, while the total amount and concentration of cardenolides showed a high variation (29-fold for quantity (1.4 - 40.3 µg); 8-fold for concentration (5.1 - 38.7 µg/µl)) (Figure 18, Figure 19). This suggests that a particular

compound is stored at a specific rate that does not appear to be limited and is neither clearly related to the available amount of this particular cardenolide in the diet nor to its polarity.

In general, all sequestered cardenolides were predominantly polar (88 %) based on their retention times. Among these, another dominant sequestered cardenolide (c4, 13.53 min, 8.8 ± 1.3 %) showed a very high polarity, close to that of ouabain (12.12/12.28 min). Its peak shape also suggested that similar elution partitioning effects as observed with ouabain might have occurred (c3/c4 = 13.38/13.53 min). At the same time, it was also the most abundant cardenolide in mature seeds (36.6 ± 0.9 %) and was also dominant in seed pod seeds (8.16 %). A high proportion of polar cardenolides was also a commonality of mature seeds and maturing seeds in seed pods (at least 71 % of total cardenolides). Interestingly, however, the dominant cardenolides of mature seeds were more polar (average polarity: 14.1 ± 0.07) and only mature seeds had unique cardenolides (16) compared to immature seeds from seed pods (average polarity: 17.8) (Figure 18). Further differences were observed in cardenolide number, cardenolide quantity, average diversity, and individual cardenolide abundances (Table S 34), which were expected since host plant cardenolide spectra are dynamic and depend on a variety of biotic and abiotic factors (Agrawal et al., 2012; Agrawal et al., 2022; Rasmann et al., 2009; Rasmann and Agrawal, 2011).

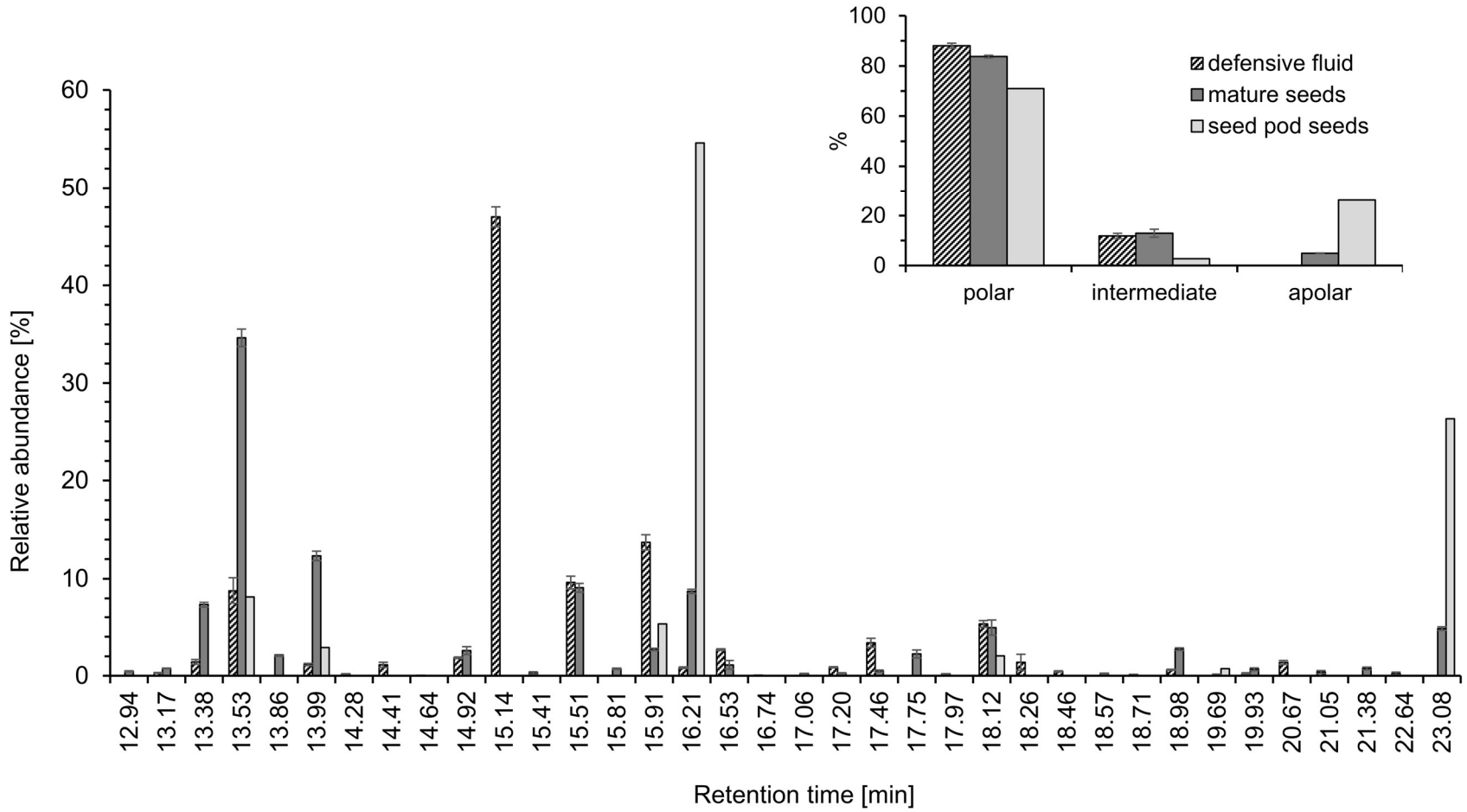


Figure 18 Relative abundance of single cardenolides with respect to polarity detected in milkweed bug defensive fluids (n = 15) and their diet (milkweed seeds of different degrees of maturation and from different geographic populations). Relative abundance of single cardenolides was calculated with regard to total cardenolide amount found in respective samples (for defensive fluid cardenolides only abundant ones, i.e., frequency n ≥ 3, were considered). Polarities were classified using the elution times of the standard cardenolide ouabain (highly polar, median retention time (12.1/ 12.3 min)) and digitoxin (highly apolar, ret: approx. 27.0 min) as reference, as follows: polar 12 to ≤ 17 min, intermediate polarity > 17 to ≤ 22 min, apolar > 22 min.

Temporal dynamics of ouabain sequestration

HPLC quantification of ouabain sequestered in defensive fluids sampled at different time periods (1 h to 5 days) showed that its accumulation in the thoracic storage compartment progressively increased with sequestration time (Figure 19; $F(1, 28) = 14.689$, $P < 0.001$, Shapiro-Wilk test of residuals: $W = 0.9578$, $P = 0.2381$; Non-constant Variance Score Test: $\chi^2 = 2.051$, $P = 0.1521$, Levene's Test for Homogeneity of Variance between groups: $F(1) = 0.012$, $P = 0.9147$). About 20 % of ouabain was already accumulated four hours after injection into the hemolymph (sunflower line animals: 19.7 % ± 4.1 (standard error), milkweed seed line animals: 24.6 ± 5.2 %). The accumulation rate decreased over time and largely reached saturation after 24 hours (sunflower line (SS): 24.4 ± 2.7 %, milkweed seed line (MS): 29.2 ± 4.4 %; 5 days: SS: 22.2 ± 7.2 %, MS: 35.4 ± 9.8 %). Furthermore, accumulated amounts significantly differed between animals of different diet histories ($F(1, 28) = 6.285$, $P = 0.0180$). Although milkweed seed fed animals had considerable amounts of natural cardenolides stored in their thoracic storage compartments (1.4 - 40.3 µg), those accumulated constantly higher ouabain amounts (Figure 19), with consistent relationships to dietary history across sequestration time intervals (time x diet: $F(1, 28) = 0.815$, $P = 0.3743$). However, since the inclusion of the interaction caused a change in significance level for dietary history (diet: $F(1, 28) = 0.3398$, $P = 0.5646$; time: ($F(1, 28) = 15.085$, $P < 0.001$), the interpretation of its relationship with sequestration time may not be as straightforward as this might indicate. The amount of sequestered ouabain by animals of the milkweed seed line was indeed significantly positively related to the stored natural cardenolide concentration (F-tests of nested models: cardenolide concentration: $F(1) = 8.142$, $P = 0.0145$; sequestration time: $F(1) = 14.810$, $P = 0.0023$, full model = model 2 see Table S 35). The concentration was used instead of its individual underlying components, the sequestered natural cardenolide amount and the released defensive fluid amount, because these correlated with each other. The released defensive fluid volume did also not show a linear relationship with the sequestered ouabain amount in contrast to sunflower line animals (Figure S 31). Surprisingly, no diet-related differences were found in terms of sequestered ouabain concentration in contrast to sequestered ouabain amount (F test of nested gamma GLMs with identity link - diet: $F(1) = 0.0119$, $P = 0.914$, diet x time: $F(4) = 1.620$, $P = 0.2047$, time: $F(4) = 4.820$, $P = 0.0048$; post hoc estimated marginal mean (emmean) for 1 h with all other periods $P < 0.05$; no difference between other periods ($P \geq 0.8932$; emmean – 1 h: 1.12 ± 0.25 µg/µl, 4 h: 3.53 ± 0.79 µg/µl, 24 h: 4.60 ± 1.04 µg/µl, 72 h: 4.83 ± 1.19 µg/µl, 120 h: 4.02 ± 0.75 µg/µl); Table S 36). Thus, no clear time-related trend was observed in contrast to accumulated ouabain amount. This

was due to the volume of released defensive fluids, which varied considerably (Figure 19). None of the exploratory models conducted could model the observed defensive fluid data to a satisfactory extent or without violating corresponding statistical methodological assumptions (Table S 37). However, the released defensive fluid volume was significantly related to the stored natural cardenolide amount in bugs of the milkweed seed line (ANCOVA: $F(1) = 14.814$, $P = 0.0039$) and also to ouabain sequestration time ($F(1) = 6.121$, $P = 0.0116$, Shapiro-Wilk test of residuals: $W = 0.955$, $P = 0.6026$; Non-constant Variance Score Test: $\chi^2 = 0.004$, $P = 0.9469$, Levene's Test for Homogeneity of Variance between groups: $F(1) = 0.416$, $P = 0.7935$). Interestingly, the released volume decreased rapidly over the ouabain sequestration period and then stabilized (post hoc emmean for 1 h with 4 h, 24 h, and 120 h $P < 0.05$; no difference between other periods ($P \geq 0.0530$; emmean – 1 h: 1.29 ± 0.11 µl, 4 h: 0.66 ± 0.11 µl, 24 h: 0.70 ± 0.12 µl, 72 h: 0.76 ± 0.11 µl, 120 h: 0.60 ± 0.13 µl). There was no statistically significant interaction between ouabain sequestration time and the amount of natural cardenolide stored, but as previously observed, the significance levels of the main effects were affected (time $F(1) = 2.228$, $P = 0.2015$; cardenolide $F(1) = 6.535$, $P = 0.0509$, time x cardenolide $F(1) = 0.728$, $P = 0.6096$).

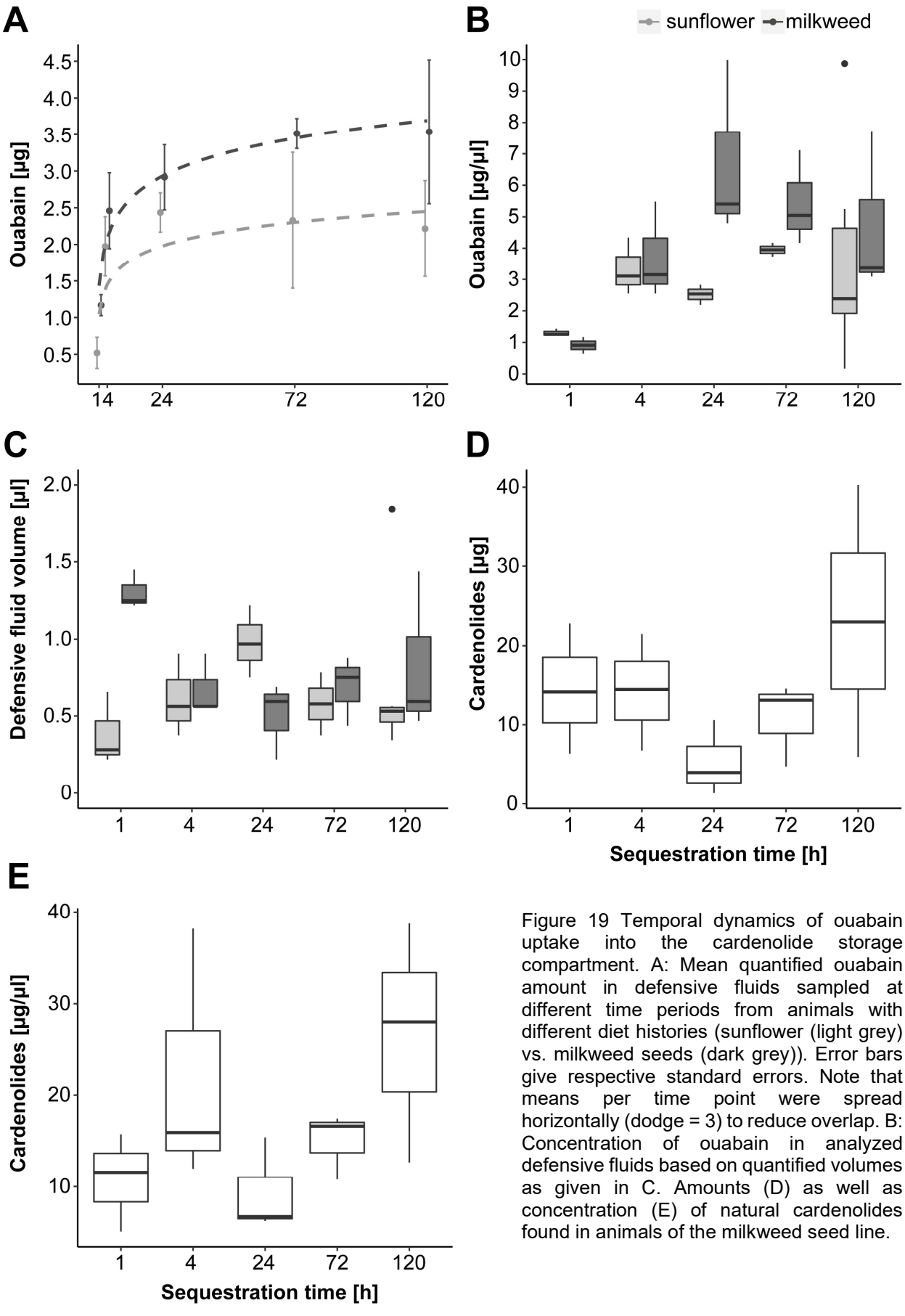


Figure 19 Temporal dynamics of ouabain uptake into the cardenolide storage compartment. A: Mean quantified ouabain amount in defensive fluids sampled at different time periods from animals with different diet histories (sunflower (light grey) vs. milkweed seeds (dark grey)). Error bars give respective standard errors. Note that means per time point were spread horizontally (dodge = 3) to reduce overlap. B: Concentration of ouabain in analyzed defensive fluids based on quantified volumes as given in C. Amounts (D) as well as concentration (E) of natural cardenolides found in animals of the milkweed seed line.

Factors related to fluid levels in the thoracic storage compartment

Based on observed variation in released defensive fluid volumes, I became interested in the factors related to fluid filling. The analysis of animals' defensive fluid volumes (dfv, n = 80) revealed that those were significantly related to individuals' sex and biomasses (bm). Reasonably, the higher the biomass, the higher was the released volume (gamma GLM with log link followed by F-test of nested models: $F(1) = 27.36$, $P < 0.001$) as increase in biomass implies in theory larger spaces for fluid storage (Figure 20). However, male adults, which had noticeably lower biomasses (male: mean(bm) = 33.42 ± 6.47 mg (standard deviation), female: mean(bm) = 47.99 ± 6.47 mg), released on average more than two-fold the volume females released (male: mean(dfv) = 1.17 ± 0.37 µl, female: mean(dfv) = 0.51 ± 0.32 µl) (sex: $F(1)= 78.70$, $P < 0.001$; biomass x sex: $F(1) = 1.08$, $P = 0.302$).

No definite evidence was found that stored fluid volumes were significantly related to previous cardenolide exposure, in terms of animals' diet history ($F(1) = 3.77$, $P = 0.056$) (Figure 20). However, it is important to note here that diet history was deemed to have a significant effect on defensive fluid fillings ($F(1) = 8.41$, $P = 0.005$) when a single extreme observation was excluded with no differential effects among sex (diet x sex: $F(1) = 0.0019$, $P = 0.9649$) or in relation to individuals' biomasses (diet x biomass: $F(1) = 0.6399$, $P = 0.4263$).

In females, fluid release most frequently occurred at the releasing sites of the thorax and more specifically at the metathorax flanges (Figure S 32). In addition, released volumes were also significantly different between female individuals of different ages (n =40) (gamma GLM with log link followed by F-tests of nested models: $F(2) = 4.987$, $P = 0.0126$). Accounting for effects related to biomass ($F(1) = 37.474$, $P < 0.001$), diet history ($F(1) = 3.636$, $P = 0.0650$), and defensive fluid droplet release number ($F(1) = 26.064$, $P < 0.001$), intermediate aged individuals were found to release significantly higher volumes on average than old ones ($P = 0.006$ (z ratio = 3.047); young - intermediate: $P = 0.1710$ (z ratio = 1.167); young - old: $P = 0.4728$ (z ratio = -1.796)). No indications of inter-dependencies with other factors affecting defensive fluid volume were found (biomass x age: $F(2) = 0.0339$, $P = 0.9667$; diet x age: $F(2) = 0.804$, $P = 0.4565$; release sites x age: $F(2) = 1.866$, $P = 0.1712$).

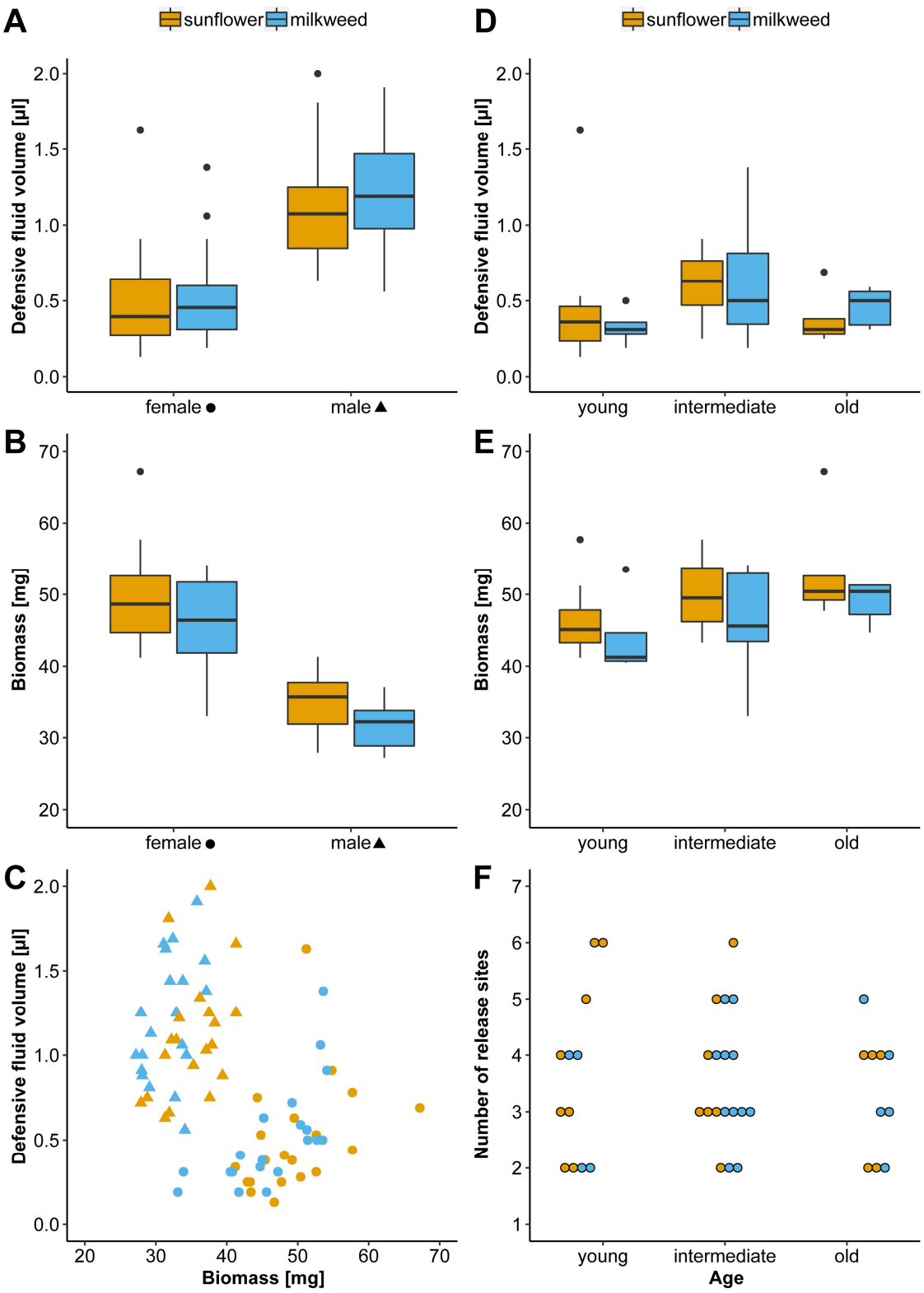


Figure 20 Defensive fluid volumes in relation to biotic factors potentially related to fluid fillings. A - C: Defensive fluid fillings and biomasses in dependence of sex and different diet histories (sunflower = cardenolide-free in yellow vs. milkweed = cardenolide containing diet in blue (n = 20, each)). D - F: Defensive fluid fillings, biomasses and total number of releasing sites from which defensive fluid droplets were sampled in dependence of visually determined and classified age of females (diet: n = 20 each; age: young: n = 12, intermediate: n = 18, old: n = 10).

Proteins related to cardenolide adaptations in milkweed bug laboratory lines with different diet histories

In Chapter 2, I showed that cells ejected with the defensive fluid possess ABCB full transporter signals, carriers indispensable for efficient cardenolide (ouabain) sequestration in *O. fasciatus*. When I observed that the sequestration capacity of milkweed bugs reared long-term without cardenolides changed, I became interested in the distribution of ABCB full transporters in these animals compared to animals continuously exposed to cardenolides via their diet. The total number of nuclei found in released fluid varied considerably, but was on average similar across diet lines. However, the fluorescence area and intensity with monoclonal antibody C219 per nucleus were significantly increased in animals reared with milkweed seeds, suggesting a more pronounced cellular ABCB full transporter composition in their thoracic storage compartment (Figure 21, Figure S 33, Figure S 34). Such a difference was not observed for the monoclonal antibody C494. In terms of sequestration performance, no difference was found in the sequestered ouabain amount (Welch t-test: $t(4.6)= -0.235$, $P = 0.824$), concentration ($t(4.6)= -0.384$, $P = 0.718$) or defensive fluid volume ($t(3.2)= 0.570$, $P = 0.606$) of metathoracic flanges samples from milkweed or sunflower seed line animals sampled two hours *post* ouabain injection. The previously determined difference in sequestration capacity therefore seems to be due to the entire sequestration system and not exclusively to these release sites.

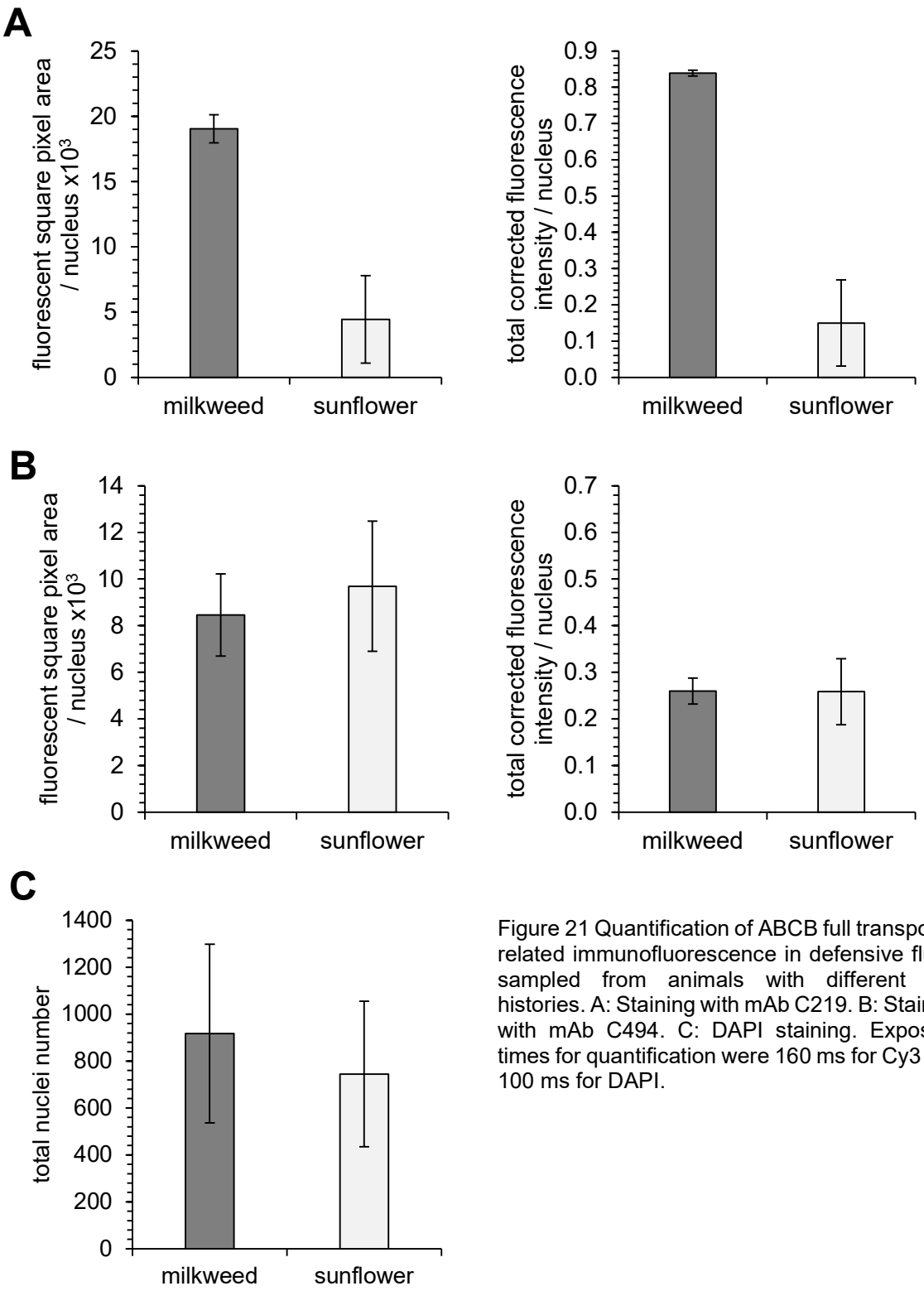


Figure 21 Quantification of ABCB full transporter related immunofluorescence in defensive fluids sampled from animals with different diet histories. A: Staining with mAb C219. B: Staining with mAb C494. C: DAPI staining. Exposure times for quantification were 160 ms for Cy3 and 100 ms for DAPI.

Na,K-ATPase tissue localization and expression response to ouabain

Animals of the sunflower line significantly elevated their Na,K-ATPase α1A paralog expression on average by 1.5-fold when challenged by ouabain (Scheirer-Ray-Hare test: $H_{ouabain}$ = 5.203, P = 0.023; H_{time} = 2.283, P = 0.516; $H_{ouabain\ x\ time}$ = 1.488, P = 0.685) (Figure 22). Upregulation was very rapid because it was observed already one hour after injection, the minimal tested time interval here. The Na,K-ATPase α1A paralog is a highly cardenolide-insensitive copy that also exhibits the highest transcript abundance of the four paralogs present in *O. fasciatus* (Herbertz et al., 2024; Lohr et al., 2017; Yang et al., 2019; Zhen et al., 2012). A strong Na,K-ATPase α-subunit protein expression was observed in the basal membrane of the Malpighian tubule cells (Figure S 35) consistent with the predominant mRNA expression of the resistant α1-subunit paralogs, α1A and α1B (Herbertz et al., 2023; Lohr et al., 2017). This also shows that the Na,K-ATPase and ABCB full transporter have a polarized cell localization in the tubule cells (see further Chapter 2). Both Na,K-ATPase subunits, α and β, were barely detected in the defensive fluid. No clear cellular assignment could be made due to the low fluorescence signal in contrast to the positive control α-tubulin and mAb C219, specific for ABCB full transporters (Figure 23, Figure S 36).

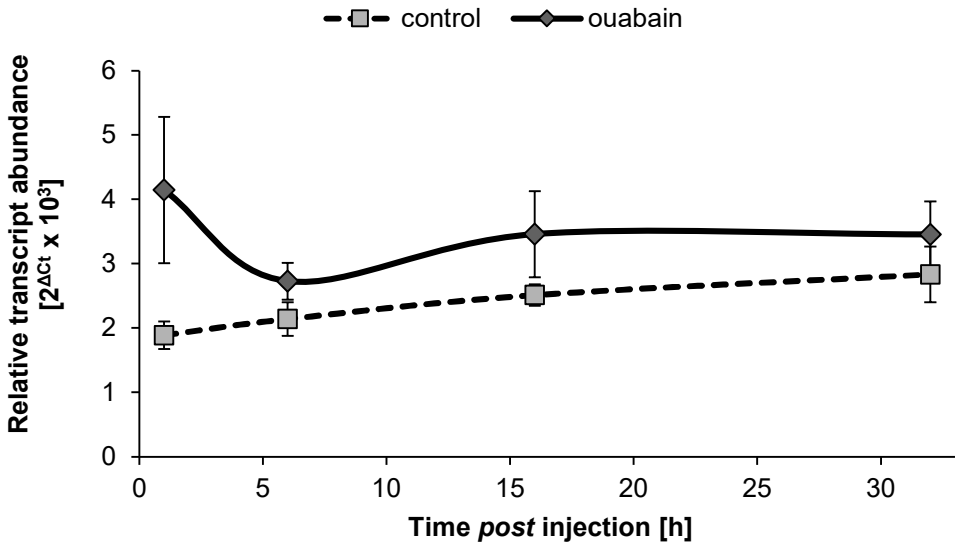


Figure 22 Relative transcript abundance of Na,K-ATPase paralog α1A in *O. fasciatus* challenged by ouabain via injection.

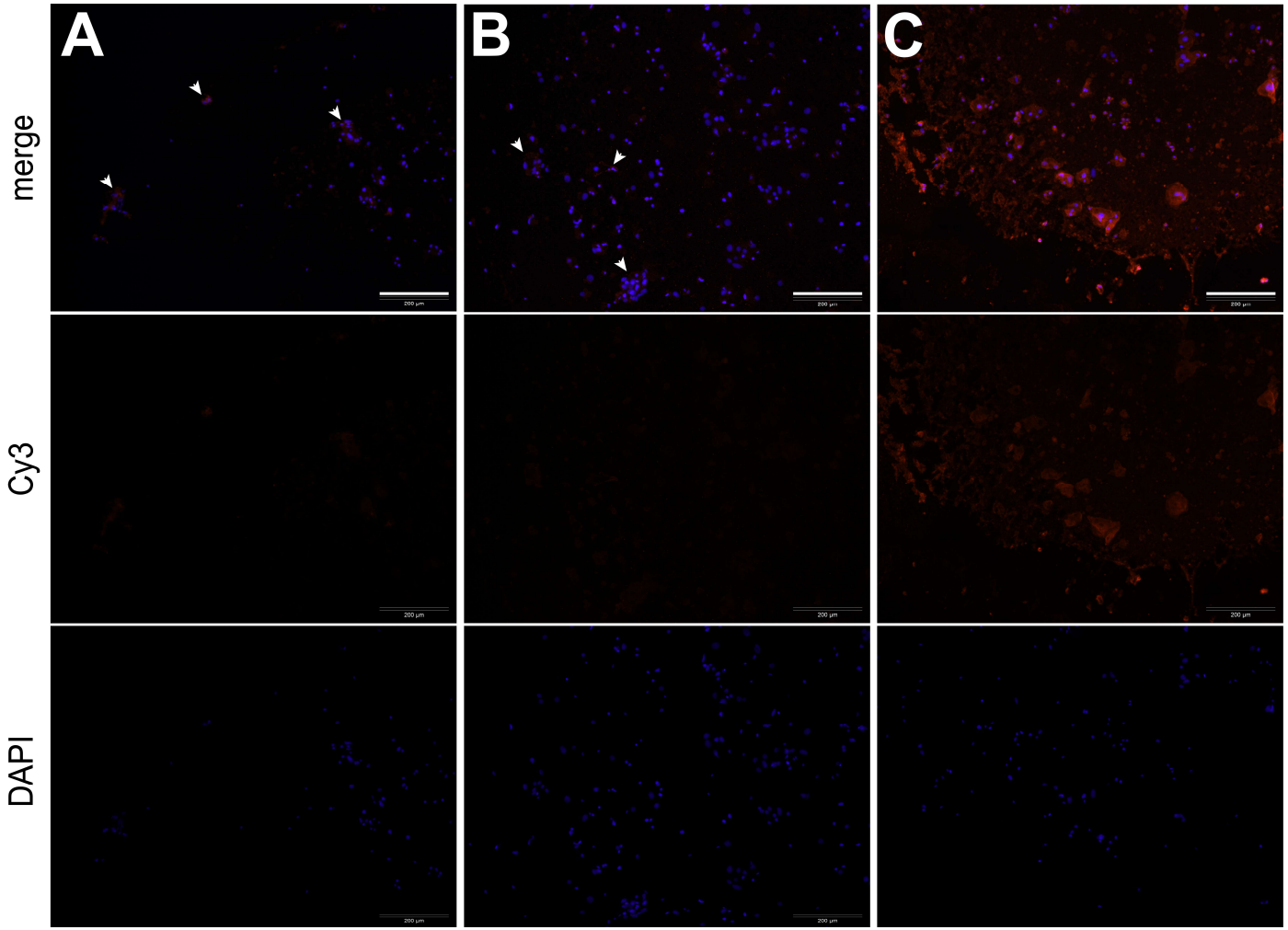


Figure 23 Na,K-ATPase subunit immunofluorescence staining of defensive fluids of *O. fasciatus* adults from the laboratory milkweed seed line. A: α-subunit (mAb 5as). B: β-subunit (mAb Nrv5F7s), C: α-tubulin (positive control). Exposure times were 100 ms for Cy3 and 20 ms for DAPI, scale bars are equivalent to 200 µm. Tonal-value correction (0-1-130) and additional scale bars were applied to merged images for illustrative purposes.

Discussion

My findings in this chapter show that sequestration capacity is shaped by the animals' dietary history, and imply that adaptive as well as directly diet-related mechanisms, as known for life-history traits (Attisano et al., 2012; Chaplin, 1980; Gordon et al., 1971; Hill, 2006; Moore and Attisano, 2011; Pokharel et al., 2021), take place after diet switches. Surprisingly, the effect of cardenolide-free rearing strategy on sequestration performance of *O. fasciatus* has been only marginally addressed by previous studies, despite being common practice (see e.g. Baerwald and Delcarpio, 1983; Bramer et al., 2015; Duffey and Scudder, 1972; Jones et al., 1983; Liu and Kaufman, 2009; Panfilio et al., 2019; Petschenka et al., 2022; Pokharel et al., 2021). Duffey and Scudder (1974) reported a much lower sequestration capacity for first generation sunflower-reared milkweed bugs than was observed here. Likely reasons for this are either the stabilization of adaptations over generations in my animals or differences in the animals' genetic backgrounds (Duffey, 1980; Feir, 1974; Gordon et al., 1971; Pokharel et al., 2021). Nonetheless, nymphs with the same genetic background accumulated also lower cardenolide concentrations from milkweed leaves until adulthood with sunflower as seed source compared to milkweed seeds in a previous study. However, due to the impact of diet composition on animals' biomasses in this study (Carlson and Agrawal, 2023), it is not possible to attribute this directly to sequestration capacity. The nutritional compositions were more balanced here by supplementation of the milkweed line with sunflower seeds, also reflected in the similar biomasses of the animals of the two lines. This, together with the focus on a single life stage, allows for a better correlation of the sequestration capacity with the diet in relation to secondary seed metabolites.

My finding that ouabain sequestration is positively and linearly related to the stored natural cardenolide concentration in defensive fluids, suggests a kind of positive feedback loop for ouabain sequestration. It reinforces the evidence for a link between available cardenolide amount or concentration and uptake for storage and provides, for the first time, insights into how this affects sequestration capacity in temporal dynamics. Previous studies showed that the more cardenolides are available, the more is stored in *O. fasciatus* (Duffey et al., 1978; Heyworth et al., 2023; Isman, 1977; Pokharel et al., 2021; Scudder and Meredith, 1982b; Vaughan, 1979). However, there is disagreement about the relationship between cardenolide amount or concentration and storage. For example, a positive linear relationship, as seen here, was observed between ingested ouabain concentration and uptake into the storage compartment when natural cardenolides were additionally present as well as with co-injected artificial cardenolides (Duffey et al., 1978), but not when it was ingested alone. In that case,

increased and hence non-constant uptake rates were found at high ouabain doses (Scudder and Meredith, 1982b). Additional chemical structural aspects in such positive feedback loops could therefore be present.

At the same time, my preliminary data show that abundance of ABCB full transporters in defensive fluid components differs between the diet lines and suggest their involvement in phenotypic plasticity. An ABCB protein is a key player for the efficient storage of ouabain in the thoracic storage compartment, as shown in Chapter 2. Initial immunohistochemical fluorescence quantifications suggest that animals of the ancestral milkweed seed line have larger ABCB-expressing cell dimensions and/or more cellular ABCB-expressing components, thus likely facilitating higher storage capacities. If this is indeed the case, it will be interesting to see to what extent general adaptive mechanisms or a potentially in the meantime differentiated genetic background of our laboratory milkweed bug lines play a role. However, this will only be clearly demonstrated by an investigation at the cellular level in the storage compartment itself, which currently represents a bottleneck in my research and requires further methodological optimization. Nevertheless, physiological changes in the storage compartment itself are plausible, since I bypassed the intestine by injection, ouabain is rapidly and mainly stored there (this chapter; Duffey et al., 1978; Scudder et al., 1986; Scudder and Meredith, 1982b), and uptake into midgut cells is similar in such diet lines (Yoder et al., 1976). Furthermore, a molecular basis for inter- and intraspecific differences in sequestration is also suggested in other cardenolide-adapted specialists (Duffey, 1980; Freedman et al., 2021). Whether this positive feedback is due to the cardenolides themselves or to other accompanying substances with absorption-modulating abilities present in the phytocomplex (Eder and Mehnert, 2000 and references therein) and which mechanisms are responsible for this will ultimately be an exciting topic for future research. ABCB transporters are also good candidates for functional mediation of such positive feedback loops, since modulators and substrates themselves can enhance their translocation rates (Phang et al., 1993; Sharom et al., 1996). Since ABC transporters have specific substrate spectra (for a summary see for example Borst and Elferink, 2002; Marquez and van Bambeke, 2011; Schinkel and Jonker, 2003), this would also be consistent with the putative structural aspects in positive feedback loops discussed above.

Saturation of sequestration capacity has never been reported for *O. fasciatus*, in contrast to the monarch butterfly, *D. plexippus* (Duffey et al., 1978; Heyworth et al., 2023; Isman, 1977; Jones et al., 2019; Malcolm, 1991; Petschenka and Agrawal, 2015; Pokharel et al., 2021; Scudder and Meredith, 1982b). Here, I show for the first time that sequestration has a temporal

limit and is rapidly and stably saturated when hemolymph and storage compartment restore their natural concentration ratio (Duffey et al., 1978). The fate of the remaining ouabain, not stored in the defensive fluid, is likely its accumulation in other body tissues, like the eggs and fat body, as well as excretion (Meredith et al., 1984; Moore and Scudder, 1985; Pokharel et al., 2021). Eggs significantly contribute to the total amount stored in bugs while the fat body accumulates a smaller fraction, but surprisingly accumulates polar cardenolides similar in polarity to those in excreta (Chaplin, 1980; Duffey and Scudder, 1974; Feir, 1974; Moore and Scudder, 1985; Newcombe et al., 2013). For ouabain, a complex mechanism involving excretion, metabolism and reabsorption by the Malpighian tubules has been described (Meredith et al., 1984). However, consistent with our previous study on storage in the whole animal and other studies, I found no evidence of such metabolites in defensive fluids (Agrawal et al., 2022; Duffey and Scudder, 1974; Lohr et al., 2017; Pokharel et al., 2021; Scudder and Meredith, 1982b). In general, the relationship between sequestration rate into the storage compartment, accumulation elsewhere and excretion rate for cardenolides is not well understood. However, the remarkable constancy in relative proportions of the individual cardenolides, despite strong inter-individual variation in total quantity, implies a well-coordinated regulation. The degree of accumulation of secondary plant metabolites can depend on their excretion rates (Kumar et al., 2014; Yang et al., 2021; Züst and Agrawal, 2016). Yet, a proportional relationship between both is unlikely for ouabain, since ouabain accumulation in the body appears to be dose-dependent, but its excretion is not (Pokharel et al., 2021).

Qualitative and quantitative regulation of sequestration is driven by excretion, selective enrichment and biotransformation. Excretion and biotransformation both narrow the sequestered cardenolide polarity range, as observed here. Biotransformation also alters cardenolide identity and abundance, enables thus selective enrichment of parental form and/or metabolites, and can diversify the cardenolide spectrum in animals. Likely, the 18 unique identified cardenolides in animals here were thus formed by biotransformation or by enrichment above methodological detection levels (Agrawal et al., 2022; Moore and Scudder, 1985; Rubiano-Buitrago et al., 2023). The cardenolide richness found here, as high as 36 common cardenolides in defensive fluids compared to 23 in seeds, is particularly impressive and surpasses that observed after feeding on *A. speciosa* and *A. curassavica* seeds (Moore and Scudder, 1985; Rubiano-Buitrago et al., 2023). This adds to the evidence that host plant chemistry elicits interaction-specific mechanisms, as is the case with the cardenolide labriformin of *A. syriaca* in *O. fasciatus* (Agrawal et al., 2022; Jones et al., 2019; Moore and Scudder, 1985; Petschenka et al., 2022; Petschenka and Agrawal, 2015; Pokharel et al., 2020;

Rubiano-Buitrago et al., 2023). The *O. fasciatus* - *A. syriaca* - interaction is thus a valuable model for physiological and molecular studies on sequestration.

The role of biotransformation for cardenolide insensitivity as well as for sequestration in *O. fasciatus* is still under debate (Agrawal et al., 2022; Rubiano-Buitrago et al., 2024). Recent findings suggest that, in addition to the sensitivity of the animals' own Na,K-ATPase to certain cardenolides, the Na,K-ATPase sensitivity of predators drives selective sequestration. For example, frugoside, a potent inhibitor of invertebrate and vertebrate Na,K-ATPases, is preferred by *O. fasciatus* for sequestration, despite its own rather unfavourable Na,K-ATPase sensitivity to that particular cardenolide (Rubiano-Buitrago et al., 2023; Rubiano-Buitrago et al., 2024). Thoracic storage compartment cells have been deemed ouabain insensitive (Scudder et al., 1986). The target-site insensitivity of the milkweed bug Na,K-ATPase is well established and is mediated by sophisticated combinations of paralog subunits resulting in different ion-pumping activities and cardenolide insensitivities (Dalla et al., 2017; Dalla and Dobler, 2016; Dobler et al., 2012; Herbertz et al., 2024; Lohr et al., 2017; Moore and Scudder, 1986; Zhen et al., 2012). Here, however, I show that the insensitivity of the storage cells is likely due to the absence of the Na,K-ATPase, based on the barely present immunohistochemical fluorescence signals in defensive fluids. Methodologically, the same restrictions apply as outlined before. With this caveat in mind, the absence of the target in the storage tissue could be an additional tolerance strategy coupled with sequestration (Jeckel et al., 2022). Nevertheless, target-site insensitivity in *O. fasciatus* is mandatory to prevent autointoxication as we recently showed (Lohr et al., 2017). The immunolocalization of the Na,K-ATPase α-subunit at the basolateral membrane of Malpighian tubule cells here indicates that the enzyme can be exposed to cardenolides in the hemolymph, where substantial cardenolide doses are expected within the first day of entry (this chapter; Duffey et al., 1978). It is not without reason that the most insensitive α1 paralogs, α1A and α1B, predominate in their mRNA expression there (Lohr et al., 2017). My finding of elevated α1A expression after injection of ouabain in the hemocoel is in line with the pivotal role of target-site insensitivity during cardenolide transport for sequestration or excretion. The narrow upregulation, within previously reported arbitrary expression cut-off ranges (Birnbaum et al., 2017; Krueger et al., 2022; Sun et al., 2017), could explain why we missed this responsiveness in our previous study (Lohr et al., 2017). At the same time, it underlines the importance of multiple stable reference genes for gene expression analyses, as carried out in this thesis (see Chapter 1; Chapter 2). The functional relevance of a 1.5-fold change in expression at the tissue level may be debatable, but in analyses of whole animals, the situation differs. Different mammalian cells, for example, show divergent expression responses to ouabain stress (Tian et al., 2009),

potentially masking net effects. A logical next step is to break the expression of Na,K-ATPase paralogs down at the tissue level, including also the other α and β Na,K-ATPase subunit paralogs (Herbertz et al., 2022; Herbertz et al., 2024; Yang et al., 2019; Zhen et al., 2012).

Determination of intra- and extracellular cardenolide concentration is standard practice to study the mode of cardenolide transport, passive, facilitated, or active (e.g. see Betz et al., 2025; Detzel and Wink, 1995; Duffey and Scudder, 1974; Meredith et al., 1984; Nickisch-Rosenegk et al., 1990a; Scudder and Meredith, 1982b; Yoder et al., 1976). My finding that the sequestered ouabain amount, but not its concentration in defensive fluids, is related to the animals' diet history raised the question of whether fluid accumulation and cardenolide storage are physiologically linked or operate independently. Both seem to be the case. I show that the volume released is linked to the amount of sequestered cardenolides, but also depends on biomass, sex, and age, some of which have also been associated with sequestration (Duffey and Scudder, 1974; Isman et al., 1977; Moore and Scudder, 1985; Pokharel et al., 2021; Rubiano-Buitrago et al., 2024).

While cardenolides are stable within the storage compartment once stored, they are not mandatory for fluid filling (this chapter; Duffey, 1980; Duffey and Scudder, 1974; Isman et al., 1977). Little is known about the physiological origin, composition and regulation of the defensive fluid. Once released, I observed rapid crystallization on surfaces, which is typical for supersaturated solutions (Ting and McCabe, 1934) or can occur as a result of a coagulation cascade. Besides cardenolides, the fluid consists of cellular components of the compartment, uncharacterized hemolymph-like proteins, unknown ninhydrin-positive components and pyrazines (Aldrich et al., 1997; Duffey and Scudder, 1974; Scudder et al., 1986). Its origin, whether intracellular from the vacuolated cell layer of the compartment, interstitial or extracellular, is still not well understood (Bramer et al., 2017; Moore and Scudder, 1985; Scudder et al., 1986; Scudder and Meredith, 1982a). An exclusively intracellular origin is actually rather unlikely considering the bugs' ability to release defensive fluid very quickly after a previous release (personal observation; Scudder and Meredith, 1982b). On the other hand, an intracellular or vesicular origin or unknown emulsification or conversion mechanisms might explain the ability to store such high cardenolide concentrations (5.1 to 38.7 µg/µl), despite low water solubility, which lies even for the highly polar ouabain only at 10.3 mg/ml (Eder and Mehnert, 2000; National Center for Biotechnology Information, 2025). Therefore, solubility constraints could drive fluid filling in the storage compartment, which is also consistent with the positive relationship between natural cardenolide amount and fluid volume observed in animals of the milkweed seed line. Along these lines, it is not evident why ouabain, unlike natural

cardenolides, did not show a clear relationship with the released fluid volume in these animals in contrast to sunflower line animals. A likely explanation is the masking of this relationship by natural cardenolide storage under *ad libitum* conditions.

Cardenolides exert their defensive effect through their bitter taste and toxicity (Brower, 1969; Euw et al., 1967; Glendinning, 1992; Groen et al., 2017; Hill, 2006; Lohr et al., 2017; Malcolm, 1991; Moore and Scudder, 1986; Petschenka et al., 2022; Petschenka and Agrawal, 2015). Mammalian bitter taste receptors each have specific and often narrow receptor ranges (Meyerhof et al., 2010). The importance of taste perception in predator-prey interactions is demonstrated by interspecific sensitivity differences and related avoidance thresholds for the same cardenolide or prey (Fink and Brower, 1981; Glendinning, 1992). Toxin effects may depend on structural properties, show non-monotonic dose response relationships, or involve specific dose thresholds (Agrawal et al., 2022; Brower, 1969; Groen et al., 2017; Herbertz et al., 2024; Pokharel et al., 2020; Rubiano-Buitrago et al., 2023; Rubiano-Buitrago et al., 2024). Volume regulation could therefore be a mechanism to meet the perceptive range of certain predators or to achieve certain effective doses when concentrations in the underlying tissue vary, as is the case between the sexes in *O. fasciatus*. Despite this difference, similar cardenolide concentrations prevail in their defensive fluids (Moore and Scudder, 1985; Rubiano-Buitrago et al., 2024). My finding of sexual dimorphism in fluid fillings, in which females have significantly less fluid than males, is consistent with this, as they were not linked to animals' biomass, another related factor in agreement with the finding of Rubiano-Buitrago et al. (2024). Interestingly, the concentration of sequestered cardenolides decreases with weight according to Pokharel et al. (2021). The female fluid retention was furthermore related to age and likely reproductive status, which in turn is linked to differences in space requirements for egg production, food intake, and excretion (personal observation; Feir, 1974; Ross, 1978; Woodring et al., 2007). These factors could also contribute to the high individual variation in sequestration levels, from 1.4 to 40.3 µg. Interestingly, insects caught in the field show even stronger intraspecific differences in sequestration performance, from 0 to 375 µg. This also shows that cardenolide-free periods occur in nature (Isman et al., 1977). In summary, it can be suggested that the observed lower fluctuations in natural cardenolide concentrations compared to quantity could represent a way to specifically design the chemical defense of *O. fasciatus*. However, mechanistic chemosensory studies are generally lacking (Mohammadi et al., 2022).

Quantification of total cardenolides and volume in the storage compartment is challenging. Stored cardenolide concentrations are robust if fluid and sequestered content is incompletely

released and, as described above, are considered crucial for the effectiveness of chemical protection against predators (Brower, 1969; Duffey and Scudder, 1974; Fink and Brower, 1981; Glendinning, 1992; Moore and Scudder, 1985; Rubiano-Buitrago et al., 2024). Yet, my findings in Chapter 2 suggest a key role for active transport in sequestration of *O. fasciatus*. Active transport decouples molecular transport from existing concentrations and gradients. This raises the fundamental question, also from a methodological perspective: What is physiologically and functionally crucial for cardenolide sequestration, the amount of cardenolide or its concentration? While the exact relationship between the intake of cardenolides for sequestration and fluid accumulation is still an open question, in this chapter I have identified valuable factors and their interrelationships that will make it possible to investigate this issue in more detail in the future. Furthermore, if these factors are not taken into account, cardenolide concentration as a parameter alone may hamper appropriate interpretations of uptake dynamics.

My optimization of the initial acetonitrile starting percentage of the HPLC analysis provides a solid foundation for accurate quantifications of polar cardenolides, such as ouabain. Two recent studies (Pokharel et al., 2021; Rubiano-Buitrago et al., 2023) already deviated from the commonly used 16 % gradient elution start of cardenolide analyses (Agrawal et al., 2021; Heyworth et al., 2023; Jones et al., 2019; Lohr et al., 2017; Newcombe et al., 2013; Pasteels et al., 1995; Petschenka et al., 2022; Petschenka and Agrawal, 2015; Pokharel et al., 2020). While ouabain is one of the most commonly used standard substances in studies on adaptations to cardenolides, this greater accuracy is especially important for the analysis of natural cardenolides from plant parts with a predominantly polar cardenolide spectrum, like *A. syriaca* seeds (this chapter; Agrawal et al., 2021; Bramer et al., 2015; Detzel and Wink, 1995; Dobler et al., 2012; Duffey et al., 1978; Duffey and Scudder, 1974; Euw et al., 1967; Groen et al., 2017; Heyworth et al., 2023; Hill, 2006; Jones et al., 1983; Moore and Scudder, 1985; Moore and Scudder, 1986; Pasteels et al., 1995; Petschenka et al., 2022; Petschenka and Agrawal, 2015; Pokharel et al., 2021; Rasmann and Agrawal, 2011; Rubiano-Buitrago et al., 2023; Scudder and Meredith, 1982a; Yoder et al., 1976). The observed similarity in retention times between a cardenolide dominant in seeds (c4) here and ouabain further indicates that ouabain represents the lower extreme of the natural polarity spectrum of *A. syriaca* cardenolides found in *O. fasciatus*.

In summary, this chapter shows that diet switches can shape sequestration capacity in the large milkweed bug, *O. fasciatus*. Our stable laboratory lines allow us to create a framework for comparative studies to further study the gene network responsible for cardenolide

sequestration. Along the same lines, my findings also highlight the great care that must be taken when working with laboratory animals. Fortunately, sequestration itself is a highly conserved process, as demonstrated by the animals' ability to sequester cardenolides even after 400 generations without exposure (Newcombe et al., 2013). This chapter also broadens the scope of future research on sequestration by introducing a new focus: the defensive fluid, which is linked to stored cardenolide quantity, biomass, sex, and age as demonstrated here. Combined with my optimized HPLC parameters, this opens new directions for studying the chemical, molecular, and physiological drivers in insect chemical defense systems and will improve our understanding about them in the future.

General Discussion and outlook

Strategies of herbivorous insects to adapt to their chemical host plant defense are classified as tolerance and resistance mechanisms. Tolerance strategies protect the animals against the harmful effects of secondary plant metabolites either by insensitivity, compartmentalization or compensation by overexpression. Resistance mechanisms against secondary plant metabolites can be carried out by secondary plant compound biotransformation and excretion and/or sequestration characterized by active transport (Jeckel et al., 2022).

All resistance mechanisms have been demonstrated in *O. fasciatus*. Nonetheless sequestration into the thoracic storage compartment has so far been exclusively linked to passive transport kinetics. Yet, this species selectively stores polar to intermediate-polar cardenolides as shown in Chapter 3 and other studies, which are difficult to move across cell membranes based on their physiochemical properties (Agrawal et al., 2022; Bramer et al., 2015; Duffey et al., 1978; Duffey, 1980; Duffey and Scudder, 1974; Moore and Scudder, 1985; Rubiano-Buitrago et al., 2023; Rubiano-Buitrago et al., 2024; Scudder et al., 1986; Scudder and Meredith, 1982a; Scudder and Meredith, 1982b; Wink and Schneider, 1990).

My dissertation can be regarded as a proof of concept that ABC transporter are prime candidates for the molecular base of plant secondary metabolite sequestration. It suggests the selection for robust genetic systems (Guillaume and Otto, 2012) for the evolution of sequestration in agreement with the few other studies on that topic (Kowalski et al., 2020; Strauss et al., 2013; Yang et al., 2021). This thesis shows that ABCB full transporter are molecular key proteins for ouabain storage capability and capacity in *O. fasciatus* (Chapter 2 and Chapter 3). The findings in Chapter 2 link sequestration of the polar ouabain by milkweed bugs for the first time to an active energy-driven primary transporter. This evidence originates

from the living, complex animal and represents the previously pending functional connection between ABCB transporters and cardenolide sequestration in vivo. RNAi knockdowns combined with immunolocalization and tissue expression support a pivotal role of OfABCB1 in ouabain sequestration in the thoracic storage compartment. The role of its homolog, OfABCB2, is likely dispensable in this regard. However, its function in the cardenolide transporter network needs to be specified by further studies as discussed in Chapter 2. Tissue localization further suggests a type II pleiotropy (Wagner and Zhang, 2011) for OfABCB1 with additional functions as chemoprotective neural barrier and to some degree excretory gatekeeper, but not as notable intestinal one. Along these lines, my validated and revalidated reference genes (Chapter 1, Chapter 2) provide high reliability of these expression and RNAi findings. In line with transfer selectivity into the thoracic storage compartment (Duffey et al., 1978; Scudder and Meredith, 1982b), Chapter 3 demonstrates that narrowly stored cardenolide spectra have proportionally constant single sequestration rates. Furthermore, it shows that polar ouabain sequestration is robust, but sequestration capacity is shaped by diet with ABCB full transporters as a possible link. That supports the significance of OfABCB transporter for cardenolide sequestration identified in Chapter 2. That chapter further provides insights for exploring the mechanistic basis of sequestration related to chemical defense in the future. The identification of the first molecular key player linked to cardenolide storage in this thesis now also allows to study the interrelation between target-site insensitivity and sequestration of *O. fasciatus* at the molecular and cellular level, as shown in the first steps in Chapter 3. Further interesting aspects of this chapter, like compartmentalization and compensation as tolerance mechanisms, will be discussed in the following.

In summary, this thesis suggests that certain OfABCB full transporters, here OfABCB1, are tightly linked to ouabain sequestration and have acquired pleiotropic roles in the tolerance for and resistance against cardenolides in *O. fasciatus*. This dissertation is therefore a critical step to disentangle the molecular basis of cardenolide transport related to sequestration in *O. fasciatus* and broadens our understanding of the functions of ABCB full transporters in cardenolide-sequestering species.

Role of ABC transporter in the sequestration of phytochemicals

The identification of secondary plant metabolite transporting proteins is of major importance to understand the evolution of sequestration (Beran and Petschenka, 2022). This thesis is the first work, which links an ABC subfamily B member to cardenolide sequestration in the living, complex organism, the hemipteran *Oncopeltus fasciatus* (Chapter 2). It adds therefore

valuable new data to the list of plant defense compound transporters in insects, which is still short despite their significance for understanding sequestration (Beran and Petschenka, 2022). Regarding the role of ABC transporters in sequestration as molecular basis of chemical defense strategies in insects, the list of functionally characterized ABC transporters has been restricted to two leaf beetle species (Kowalski et al., 2020; Strauss et al., 2013) which corresponds to a share of about 0.7 % of all known sequestering species (Beran and Petschenka, 2022).

My thesis thus provides the first evidence for a functional association of ABCB full transporters with cardenolide sequestration in vivo, which was previously pending. That agrees with earlier findings by Kowalski et al. (2020) that ABCB full transporters of the cardenolide-sequestering leaf beetle *Chrysochus auratus* (Eumolpinae: Chrysomelidae: Coleoptera) are activated by and likely transport certain cardenolides in vitro. Also, modulated gene expressions by milkweed feeding support the role of ABC transporters, including the B subfamily, in adaptations to cardenolides in sequestering generalist and specialized insects (Birnbaum et al., 2017; Krueger et al., 2022; Tan et al., 2019), as will be discussed in more detail in one of the following sections (see section “Transcriptional changes by feeding on toxic plants ”). Yet, the functional relation to sequestration and information about substrates in those species is still pending.

My data supports the evidence that ABCB full transporters are important key players in the transport networks of cardenolide-sequestering species. This is all the more remarkable when one considers that *O. fasciatus* and *C. auratus* have very different morphological sequestration structures and that their ancestors diverged around 373 million years ago (Bramer et al., 2017; Dobler et al., 1998; Misof et al., 2014; Scudder et al., 1986; Scudder and Meredith, 1982a). In this context, it should of course be remembered that sequestration developed independently within and between the six insect orders which specialized on cardiac glycoside-producing plants (see most current review by Agrawal et al., 2024b). A commonality between both species is that they have similar challenges in terms of cardenolide transport from the site of ingestion to the site of storage. Other similarities are (i) the cardenolide enrichment in defensive fluids, (ii) the low amounts of cardenolides in other body parts and (iii) narrower stored cardenolide profiles compared to host plants cardenolide spectra (Chapter 3; Dobler et al., 1998; Duffey and Scudder, 1974; Moore and Scudder, 1985). Chapter 2 of this dissertation shows that the same molecular protein type, here OfABCB1, known to protect other vertebrates and invertebrates from cardenolides (Groen et al., 2017; Hagenbuch et al., 2002; Li et al., 2025; Mayer et al., 1996; Petschenka et al., 2013b) is required in the specialized

O. fasciatus for its efficient storage of the cardenolide ouabain. That suggests that OfABCB1 is a pleiotropic gene and parallels functions suggested for CaABCB2 in *C. auratus* (Kowalski et al., 2020) as discussed in Chapter 2.

Pleiotropy can be a mechanism for evolutionary novelty or result in evolutionary constraints (Guillaume and Otto, 2012; Torday, 2015). Pleiotropic roles of ABC transporter help plants to adapt to their environment in addition to fulfill metabolic functions (Nuruzzaman et al., 2014) and are suggested to mediate multidrug resistance in cancer in an additional way other than the known substrate efflux (He et al., 2021). The key player in the sequestration system of the poplar leaf beetle has, as far as is known, exclusively a physiological function in the sequestration process of ingested salicin (Strauss et al., 2013), but is also highly expressed in the fat body (Strauss et al., 2014). Salicin is a toxic phenolic glycoside, but those rather act as feeding deterrents and affect the fitness of insects (Boeckler et al., 2011). Furthermore, it only acquires a chemical defense function in *C. populi* after metabolization to volatile salicylaldehyde (Boland, 2015; Discher et al., 2009; Strauss et al., 2013). Thus, it is far from being comparable to the toxicity of cardenolides, which inhibit the Na,K-ATPase, an essential enzyme of animal cells (Agrawal et al., 2012; Horisberger, 2004; Lingrel et al., 1990). The biological activity of secondary plant metabolites and the associated preadaptations might thus play a crucial role in the convergent evolution of sequestration (see also section “Putative substrates of OfABCB full transporters”).

The chemoprotective function by ABCB full transporter homologs in the blood-brain barrier is evolutionarily conserved (Denecke et al., 2022; Hagenbuch et al., 2002; Mayer et al., 2009; Petschenka et al., 2013b). It is therefore tempting to speculate that this is the ancestral role that gave rise to the molecular strategy for cardenolide sequestration and escalation of the evolutionary arms race to the third trophic level (Malcolm, 1991; Petschenka and Agrawal, 2015, 2016). However, not all specialists that rely on this protection, like the oleander hawk moth (*Daphnis nerii*), also store cardenolides (Petschenka et al., 2013b; Petschenka and Dobler, 2009).

We are just beginning to understand the role of ABC transporters in insects and particularly for sequestration in specialized insects. There is still a long way to go before we can say what allows some species to store cardenolides or other phytochemicals while others do or cannot. The findings in Chapter 2 of this thesis, in agreement with the few other studies on this topic, suggest that a minimum requirement for this is an active primary transporter with appropriate substrate spectrum in the specialized storage structure (Kowalski et al., 2020; Röpcke et al., 2024; Strauss et al., 2013). Extending this to other superfamilies, such as the major facilitator

superfamily (MFS), we also find secondary and likely also facilitative transporters in tissues involved in the selective handling of secondary metabolites (Schmidt et al., 2019; Yang et al., 2021). Tissue-specific transcript and protein profiling (Strauss et al., 2013; Strauss et al., 2014; Yang et al., 2021) is thus one of the promising approaches to identify further key elements in the cardenolide transport network of *O. fasciatus* and other specialized insects.

Lysosomal gossypol accumulation observed *in vitro* by HaABCB6, likely a human ABCB6 ortholog, is suggested to be part of the cotton bollworms' detoxification metabolism rather than aimed at chemical defense against predators (Jin et al., 2020; Kiss et al., 2015). However, it may represent a way how an efflux transporter could mediate influx for sequestration as discussed in one of the following sections (see section "Synthesis on possible sequestration mechanisms mediated by OfABCB full transporters").

In general, specialized storage structures are not necessarily required for cardenolide accumulation in the body. Members of the orders Diptera, Lepidoptera, and also within Hemiptera accumulate cardenolides without such known sophisticated structural specializations in the integument or hemolymph (see current review by Agrawal et al., 2024b). ABCB1 homologs are expressed in the skin or cuticle of vertebrates and invertebrates and are involved in dermal drug absorption in mammals and in resistance to pesticides in insects (Hashimoto et al., 2013; Ito et al., 2008; Lanning et al., 1996; Skazik et al., 2011; You et al., 2025). The milkweed bugs' specialized thoracic storage compartment, which contains ABCB full transporter expressing cells and vesicles (Chapter 2), is also suggested to be formed from its double-layered integument (Scudder et al., 1986; Scudder and Meredith, 1982a). Thus, ABCB full transporter are good candidates for preadaptations allowing also nymphs (Scudder and Meredith, 1982a) and other species like *Syntomeida epilais* (Ctenuchidae: Lepidoptera) (Nickisch-Rosenegk et al., 1990a; Wink and Schneider, 1990), *Danaus plexippus* (Danaidae: Lepidoptera) (Dreisbach et al., 2023), *Poekilocerus bufonius* or *P. pictus* (Pyrgomorphidae: Orthoptera) cardenolide sequestration into the integument (Euw et al., 1967; Pugalenthi and Livingstone, 1995). However, aphids, like *Aphis nerii* or the more specialized *Myzocallis asclepiadis* (both Aphididae: Hemiptera), accumulate favorably apolar cardenolides likely through passive mechanisms in the hemolymph and the integument. Nonetheless, sequestration capacity and selectivity are tightly associated with aphids' diet specialization. While the underlying regulatory mechanisms are not fully understood, excretory capacities for polar cardenolides seem to be involved (Züst and Agrawal, 2016). There are therefore diverse physiological strategies for sequestration that are closely related to the degree of specialization and cardenolide polarity. Whether ABCB full transporters as preadaptation represent the basis

for all these strategies or are related to the degree of specialization or to lineage-specific adaptations is a comprehensive research field that is now ready for study. In the case of the Lygaeinae, a preadaptive role of ABCB full transporters can certainly be suggested, since cardenolide sequestration is a basal trait of this subfamily (Bramer et al., 2015).

OfABCB full transporter functions in *O. fasciatus*

The function of both OfABCB full transporters in *O. fasciatus* can be suggested to result from the interplay of their tissue expression, cellular localization, substrate spectrum and interaction with other components of the cardenolide transport network in *O. fasciatus*. In mammals, for example, the presence and expression level of ABCB1 homologs determines the excretory route of digoxin and its intestinal permeability (Hoffmeyer et al., 2000; Mayer et al., 1996). In *Drosophila*, ABCB1 homolog distribution, localization and substrate spectrum are crucial for tolerance or susceptibility to a pesticide (Denecke et al., 2022). Expression levels are thus an indicator for significance in a tissue while cellular localization and substrate spectra link the transporter to its roles and functions in the tissue (Amezian et al., 2024; Denecke et al., 2022). The data of Chapter 2 of this thesis thus provide a first picture of how the OfABCB full transporter, 1 and 2, might participate in the physiological transport of ouabain in the large milkweed bug (Figure 24).

Function of OfABCB full transporter in the cardenolide transport network of *O. fasciatus*

The tissue distribution of OfABCB1 in combination with RNAi phenotypes with reduced ouabain sequestration capacities up to 70 % suggests that this transporter exerts its indispensable role in ouabain sequestration directly by ouabain transfer into the thoracic storage compartment as already discussed in Chapter 2. This agrees with recent in silico and in vitro data on ouabain as substrate of OfABCB1 (Röpcke et al., 2024). OfABCB1's localizations in four tissues important for cardenolide tolerance (nervous system), homeostasis (Malpighian tubules), and sequestration (ovaries, thoracic storage compartment), and one tissue suggested to be involved in biotransformation (salivary glands) support its tight connection to the cardenolide network. Its tissue enrichments also suggest further functions, including chemoprotection and to some degree excretion (for detailed discussion see Chapter 2) (Duffey et al., 1978; Duffey and Scudder, 1974; Meredith et al., 1984; Moore and Scudder, 1985; Moore and Scudder, 1986; Newcombe et al., 2013; Scudder et al., 1986; Scudder and Meredith, 1982b).

The exact role that OfABCB2 plays in this network remains an open question to be addressed. Its role in ouabain sequestration cannot be ruled out, but the findings of this thesis suggest it is likely dispensable in this context in contrast to OfABCB1. Co-localization of both transporters in the thoracic storage compartment and substrate overlap for ouabain suggest a functional redundancy of both transporters either for low transcript level compensation or for sequestration fine-tuning to extracellular concentrations (Levy et al., 2011; Marquez and van Bambeke, 2011; Röpcke et al., 2024). Low expression levels of individual ABCB full transporters are more widespread in insects (e.g. see Denecke et al., 2021; Kowalski et al., 2020; Strauss et al., 2014; You et al., 2025), but causes or mechanistic significance are unexplored. In accordance with the ouabain uptake dynamics described in Chapter 3, high extracellular concentrations were likely present. One hypothesis is therefore that OfABCB1 became the primary transporter not mirrored by its transcript level, thereby compensating for the RNAi induced transcript loss of OfABCB2. On the other hand, a similar paradox regarding substrate transport and function, as found here for OfABCB2, has been described for human ABCB4. The liver-specific ABCB4 protein transports drugs such as digoxin in addition to its metabolic substrate phosphatidylcholine, but confers no resistance to these drugs (Ishigami et al., 2013; Schinkel et al., 1991; Smith et al., 1994; Smith et al., 2000; van der Bliek et al., 1988). Thus, OfABCB2 might have a different primary physiological role than cardenolide transport in *O. fasciatus*. At present, other explanations are also possible as outlined in more detail in the discussion of Chapter 2 and OfABCB2s enigmatic role requires further investigations.

My thesis suggests a tight connection between OfABCB full transporters and the cardenolide transport network in *O. fasciatus* adults. Nonetheless many questions about their roles in cardenolide transport and beyond are still open as discussed already in Chapter 2. That includes for example more specialized functions between other tissues than those examined here, like for example in the fat body (Xu et al., 2021; You et al., 2025), or by other unknown transport proteins, also within subfamily ABCB. That is in particular possible in the Malpighian tubules and in the gut, in which ABCBs are often enriched in insects, including species adapted to other secondary plant metabolites (Groen et al., 2017; Koenig et al., 2015; Labbé et al., 2011a; Strauss et al., 2014; Xu et al., 2021; You et al., 2025). Nonetheless, the overall low expression levels in these tissues parallel findings in *C. auratus* (Kowalski et al., 2020) and might allow adaptation to the requirements for cardenolide sequestration, while maintaining conserved barrier and secretory functions. At the same time, sequestration capacities and spectra change during development in *O. fasciatus* (Duffey and Scudder, 1974; Rubiano-Buitrago et al., 2023), as is also the case, for example in *D. plexippus* (Jones et al., 2019). Many ABC transporters change dynamically their expression during insect development

(Broehan et al., 2013; Denecke et al., 2022; Groen et al., 2017; Hull et al., 2014; Liu et al., 2011). It will therefore be interesting to examine how differences in cardenolide profiles and capacities are mirrored by tissue distribution and expression of both identified OfABCB transporters in *O. fasciatus* nymphs in future studies. This may also broaden our knowledge of how such changes are related to molecular-physiological constraints or adaptations to stage-related predation pressures as suggested for monarch caterpillars (Jones et al., 2019).

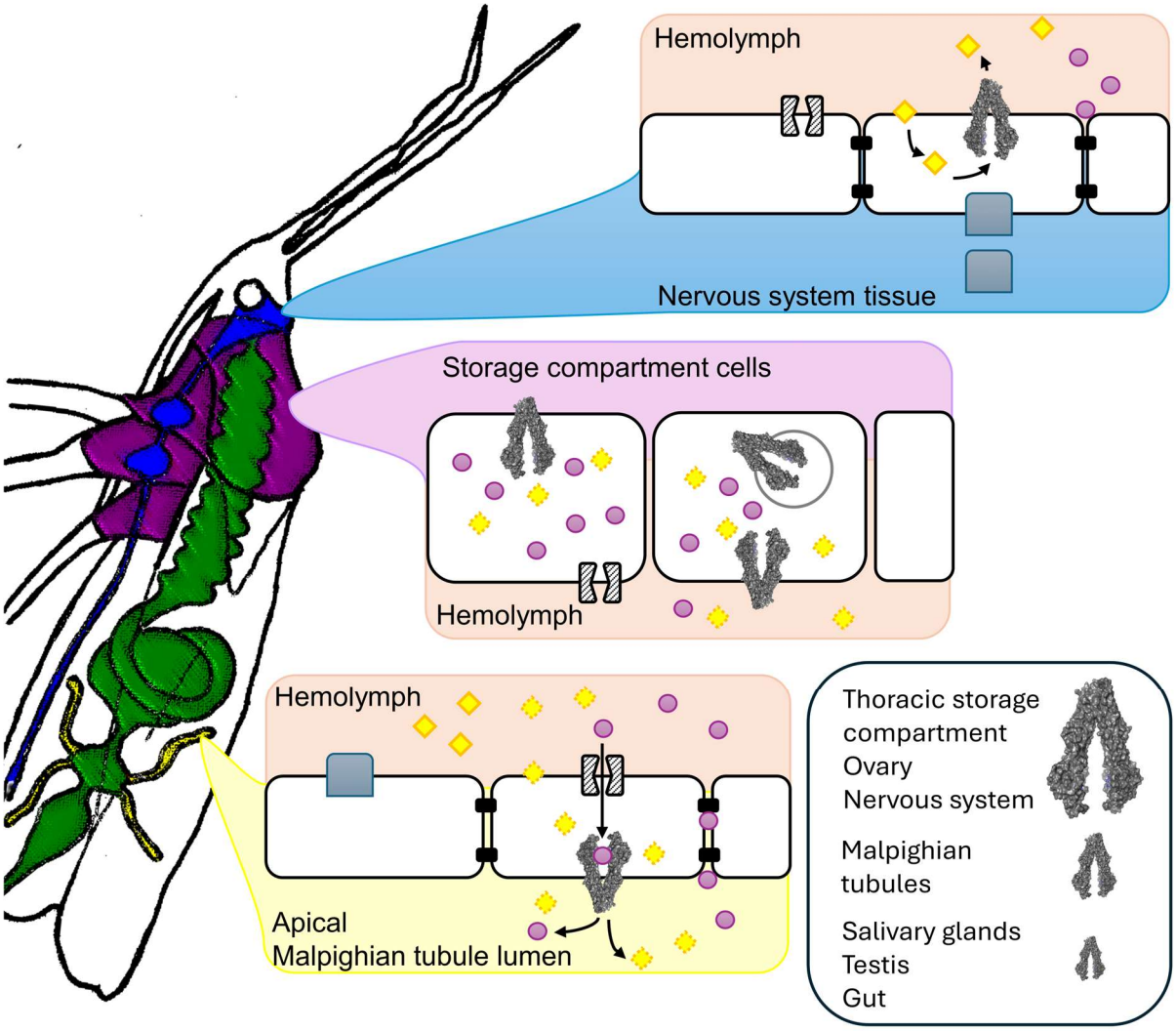


Figure 24 Summary of OfABCB full transporter distribution in adult *O. fasciatus* with possible role for cardenolides transport in different tissues. For synthesis of possible cardenolide transport mechanism in the thoracic storage compartment see Figure 26. Grey: OfABCB full transporter. Hatched: Putative important unknown transporters. Blue: Na,K-ATPase, distribution in the nervous system is according to Herbertz et al. (2022) who suggest the presence of insensitive paralogs in the perineurium of *O. fasciatus*. Yellow diamonds = apolar cardenolides, yellow diamonds with dashed lines = more hydrophilic metabolites of apolar cardenolides, purple circles = polar cardenolides. Tissue expression strength is schematically represented by different sized grey ABCB transporters in the box bottom right.

Alternative splicing of *Ofabcb2*

In silico, PCR and sequence data of cloned PCR products suggest a complex alternative splicing pattern for the *Ofabcb2* gene, which may be associated with functional changes or diversifications (see detailed discussion in Chapter 2). While this makes also expression analyses challenging, *Ofabcb2* transcript levels are in good agreement with those found in other insects as outlined before. Nonetheless, further research is needed to characterize which isoforms exist besides full-length *Ofabcb2* and how they are reflected in expression. In *Trichoplusia ni* (Noctuidae: Lepidoptera), for example, the predominant isoform is not the full-length isoform of TrnMRP1 (ABCC subfamily) (Labbé et al., 2011a). Alternative splicing and atypical protein structures of ABCB full transporters, as predicted for some *Ofabcb2* variants, mediate resistance mechanisms in human cancer and pesticide resistance in insects (Gerard and Gillet, 2024; Pauchet et al., 2016; Seong et al., 2016; Skinner et al., 2023). Alternative splicing might therefore be a further mechanistic basis for adaptation to cardenolides, reported also for other putative key proteins in this context, like UDP-glucuronosyltransferases and cytochrome P450 proteins (Birnbaum et al., 2017). However, functional characterizations of identified ABC transporter splice variants in insects besides their involvement in pesticide resistance (see discussion Chapter 2) are pending to my knowledge (e. g. see Birnbaum et al., 2017; Labbé et al., 2011a; Roth et al., 2003). Now that the full-length *Ofabcb2* transcript version is known (Röpcke et al., 2024), transcript profiling using gene expression, *in situ* hybridization and OfABCB 1 & 2 specific monoclonal antibodies can be carried out to provide further insights into this still functionally under-characterized mechanism of ABC transporter protein diversification (for review see Park et al., 2017).

Putative substrates of OfABCB full transporters

ABC transporter have an outstanding diverse substrate repertoire found at no other transporter family (Hwang et al., 2016). According to molecular docking simulations by Röpcke et al. (2024), both OfABCB full transporter are suggested to transport cardenolides of a broad polarity range from polar ouabain (*Strophantus* sp., *Acokanthera* sp., XlogP3: -1.7) to apolar oleandrin (*Nerium oleander*; XlogP3: 2.4). Among those, ouabain, frugoside (*Asclepias* species; XLogP3: 0.9) and digoxin (foxglove; XLogP3: 1.3) are known to be sequestered by *O. fasciatus* (Bramer et al., 2015; Duffey et al., 1978; Rubiano-Buitrago et al., 2023) suggesting that both transporters might play also a role in the sequestration of these cardenolides. This broad spectrum is not strictly necessary for sequestration when animals forage on *Asclepias syriaca* seeds and seed pods as shown in Chapter 3 (all sequestered seed cardenolides more polar than calotropin (XlogP3-AA: 0.9)). At the same time, it is a plausible reason how

O. fasciatus can utilize an expanded host plant range, including for example also *Nerium oleander* (Klausner et al., 1980; Miller and Dingle, 1982), without sacrificing its chemical defense (Duffey and Scudder, 1972; Isman, 1977; Isman et al., 1977). However, detailed chemical studies on stored cardenolide profiles from host plants other than *Asclepias* species (Agrawal et al., 2022; Moore and Scudder, 1985; Rubiano-Buitrago et al., 2023; Rubiano-Buitrago et al., 2024) have yet to be carried out. Furthermore, such promiscuity is one of the mechanisms suggested to prevent sequestration from being an evolutionary dead end (Petschenka and Agrawal, 2016). Efflux transporters indeed are suggested to be as important as detoxification enzymes in herbivore diet selection (Sorensen and Dearing, 2006). Homologs to OfABCBs could therefore be candidates for the preadaptation suggested in some lygaeids that have adapted to other host plant chemistries, such as alkaloids or bufadienolides (Petschenka et al., 2022). This would then be accompanied by further molecular adaptations, as *O. fasciatus* is unable to sequester bufadienolides and is sensitive to certain toxic alkaloids (Jones et al., 1983; Petschenka et al., 2022).

In line with my in vivo findings pointing to ouabain transport by OfABCB1 in Chapter 2, recent in vivo evidence suggests that this transport ability may be more widespread in insects (Groen et al., 2017; Li et al., 2025). Ouabain can be considered a rather unusual substrate also with regard to mammalian ABCB full transporters. It is neither a substrate of human ABCB1 (Gozalpour et al., 2013; Pauli-Magnus et al., 2001), nor are many of its suggested substrates similarly polar (Figure 25). The notoriety of these efflux pumps stems precisely from the fact that they keep hydrophobic substrates in check through their involvement in compartmentalization as demonstrated by numerous studies (Marquez and van Bambeke, 2011; Schinkel and Jonker, 2003). Yet, the substrate transport mechanism is complex and in addition to polarity, other factors such as residue interactions and membrane compositions also play an important role (Alam et al., 2019; Culbertson and Liao, 2025; Gozalpour et al., 2013).

We are just at the very beginning of the substrate characterization of OfABCB full transporters, as is the case with other insect species (Kowalski et al., 2020). In this context, the ability of some mammalian and arthropod ABCB full transporters to transport both xenobiotic and metabolic substrates (Ishigami et al., 2013; Ricardo and Lehmann, 2009; van Helvoort et al., 1996; Wu et al., 1991) is an interesting area for further research. Lipid transport in particular could be relevant for selective barrier formation (Kamal et al., 2023), emulsification (Stapelbroek et al., 2010) or membrane and cell regeneration in the thoracic storage compartment. In any case, cardenolides are the obvious substrates for OfABCB full

transporters, given the conservation of substrate specificity for this chemical class in ABCB full transporter proteins from distantly related taxa (Gozalpour et al., 2013; Kowalski et al., 2020; Röpcke et al., 2024).

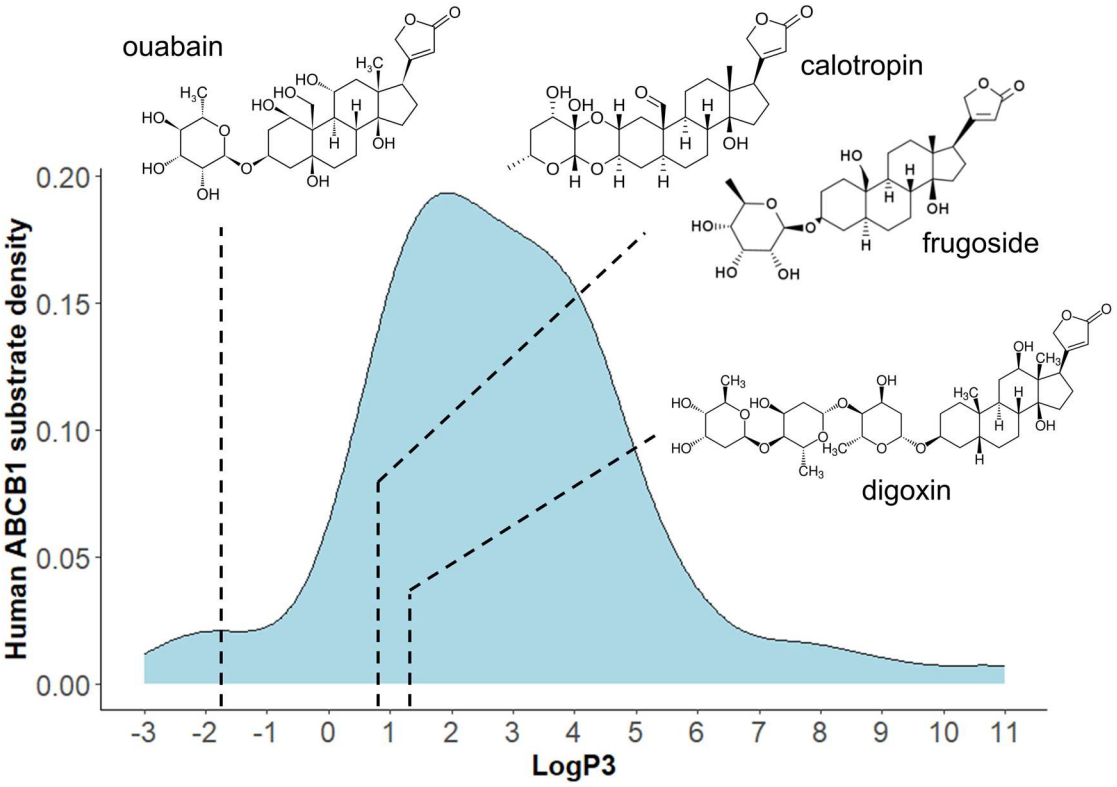


Figure 25 LogP3 distribution of human ABCB1 substrates. LogP3 values for 72 substrates (Dean et al., 2001; Hughes and Crowe, 2010; Marquez and van Bambeke, 2011; Schinkel and Jonker, 2003) were mined from PubChem. LogP3 values of different cardenolides are indicated by dotted lines. Note that only digoxin has so far been identified as a human ABCB1 substrate.

Synthesis on possible sequestration mechanisms mediated by OfABCB full transporters

As described above, my findings in Chapter 2 suggest that OfABCB1 and possibly also OfABCB2 have a key role directly in cardenolide transport into the thoracic storage compartment. However, immunohistology of sclerotized insects is challenging (Barbosa, 2014). In agreement with a previous study (Bramer et al., 2017), the exact histological structure in the compartment was therefore a bottleneck in this thesis. The presence of OfABCB transporter there could nevertheless be further clarified indirectly by immunohistochemistry of the released defensive fluids. Combining my immunohistochemical data and the previously described compartment histology (Scudder and Meredith, 1982a), I suggest that ABCB transporters are part of the membrane and of intracellular components of the inner vacuolated voluminous cell layer in the thoracic storage compartment (Figure S 36). However, how an efflux pump exactly facilitates an uptake into the compartment, is unclear at present. Several

mechanisms could be conceivable as illustrated in Figure 26, including: (A) an import function similar to few plant ABCB full transporters (Kamimoto et al., 2012; Lee et al., 2008) or efflux into intracellular vesicles coupled with (B) a yet unknown upstream carrier or transporter similar to the sequestration system suggested for *C. populi* (Strauss et al., 2013) or (C) coupled to passive diffusion driven by ongoing substrate depletion from the cytosol. Vesicles might fuse to or with intracellular vacuoles (E) described by Scudder and Meredith (1982a) which likely disintegrated upon release, as vacuole-like structures were never observed here in the defensive fluids. A way how ABCB efflux pumps can be part of the voluminous cell plasma membrane without exporting cardenolides back into the hemolymph might be an inactive state (D) abolished just upon vesicle formation similar to lysosomal drug accumulation in the blood-brain barrier (Löscher and Gericke, 2020).

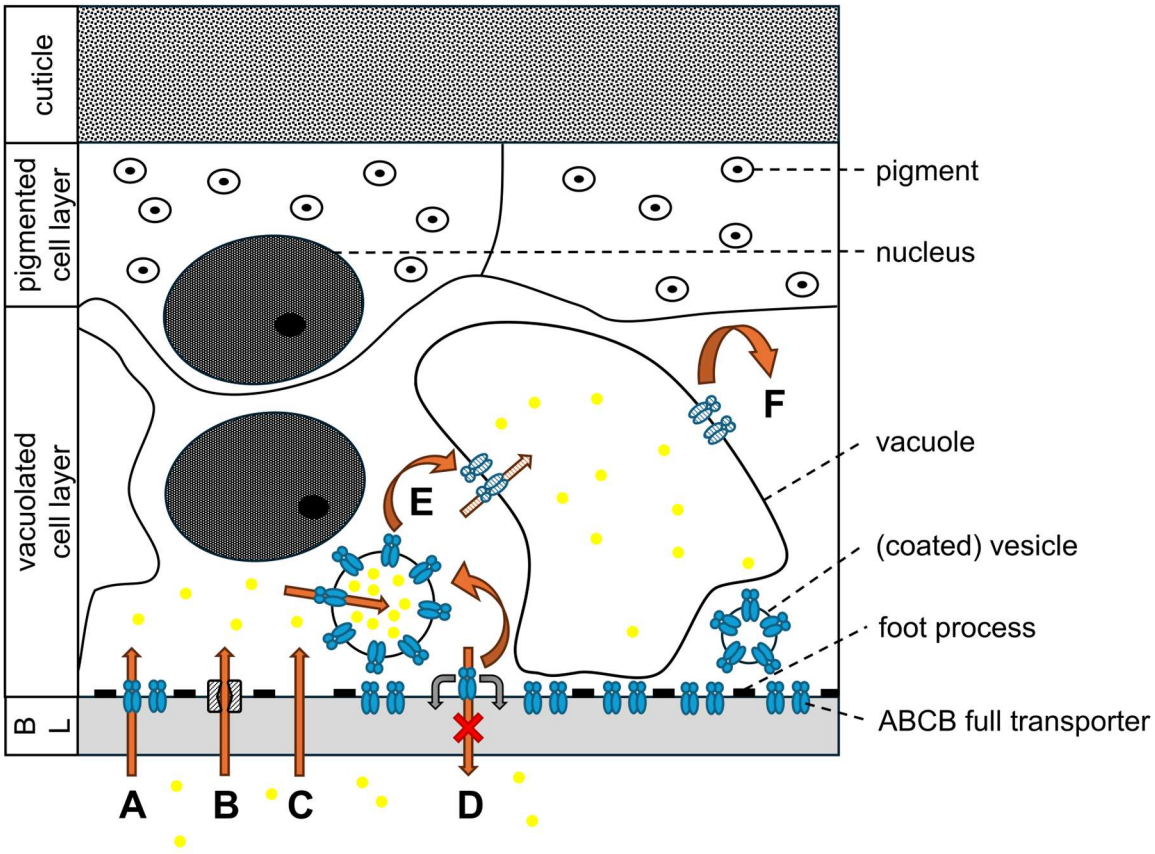


Figure 26 Putative mechanisms for cardenolide transport into the thoracic storage compartment involving ABCB full transporter in the double-layered integument according to the histology of Scudder et al. (1986). ABCB full transporter location suggested by immunohistochemistry is indicated in blue. Hatched proteins: putative location in vacuoles which were not observed here, but were described by Scudder and Meredith (1982a). BL = basal lamina. Yellow circles: cardenolides. A: Import function; intracellular vesicular transport coupled with B: a yet unknown upstream carrier or transporter, or C: passive diffusion. D: traffic from lipid to non-lipid raft regions from plasma membrane pools to or during vesicle formation (Löscher and Gericke, 2020). Final storage in vesicles or in vacuoles by vesicular fusion (E) and recycling (F). For details see text.

Some of these suggested mechanisms are in principle compatible with previously proposed "passive" sequestration mechanisms. To summarize again, these hypothesis postulated: (i) a physical emulsion-particle-based mechanism, (ii) protein-binding in the inner vacuolated epidermal cells, (iii) protein encapsulation and (iv) sieving function of the basal lamina of the thoracic storage compartment (Duffey et al., 1978; Scudder et al., 1986; Scudder and Meredith, 1982a). Despite the rapid uptake even against a cardenolide concentration gradient, as can also be suggested in Chapter 3 for ouabain in agreement with other studies, sequestration mechanisms were suggested to be passive, because of first order uptake kinetics and histological characteristics (Duffey et al., 1978; Scudder et al., 1986; Scudder and Meredith, 1982a; Scudder and Meredith, 1982b). However, due to specific cell localizations, it might be difficult to distinguish between the involvement of active transporters and passive mechanisms using physiological kinetics. Such a case can be suggested for the apical Malpighian tubules, where passive ouabain transport was previously suggested (Meredith et al., 1984), but OfABCB transporters are expressed along the electrochemical gradient at the luminal membrane (Chapter 2). Localization in intracellular vesicles in thoracic storage compartment cells and the resulting decoupling of intra- and extracellular concentrations might also be such a case, as long as vesicle formation is not exhausted. Furthermore, it is unknown how permeable the compartment is for cardenolides in the para- and transcellular pathways and to what extent other transporters are involved, which jointly might determine and mask certain net transports (Graaf et al., 1996; Taskar et al., 2017). Yet, the findings in Chapter 2 and Chapter 3 suggest that the proportion of transport pathways independent of OfABCB1 is manageable, at least in the case of ouabain sequestration into the thoracic storage compartment. However, Duffey et al. (1978) observed no effect of 2,4-dinitrophenol on ouabain sequestration and thus concluded that energy-independent mechanisms are involved. One possible explanation could be that this mitochondrial uncoupler in *O. fasciatus* did not reach its targets in vivo at effective doses. 2,4-dinitrophenol conjugates are yeast and mammalian ABC transporter substrates (Vaidya et al., 2009; Wawrzycka et al., 2010), and no information on the inhibitory efficacy of this substance was provided by the authors. Finally, the different ouabain sequestration capacities in our milkweed bug lines and proportionally constant storage rates of individual cardenolides, as shown in Chapter 3, can hardly be explained by passive diffusion-related mechanisms alone. In summary, active energy-dependent transport processes by OfABCB transporter are certainly not the only, but nevertheless important components of the cardenolide sequestration network in *O. fasciatus*.

Transcriptional changes by feeding on toxic plants

Herbivorous insects respond to changes in their diet through transcriptional changes in gene families, which are particularly important in canonical detoxification of phases I to III. While the extent and directional change per gene family is highly context-dependent, well-known gene families like cytochrome P450, glutathione-S-transferases, UDP-glucuronosyltransferases and ABC transporters are usually involved. That helps specialists as well as generalists to adapt to plants within or outside of their host plant range. Those adjustments, for example, allow the solanaceous plant specialist *Manduca sexta* (Sphingidae: Lepidoptera) to adapt to non-hosts with other chemical secondary metabolite classes without significant costs in development. That also includes an intestinal upregulation of ABCB full transporters when fed on plant diets (Koenig et al., 2015) suggesting a canonical stress response to plant material ingestion. The highly polyphagous two-spotted spider mite (*Tetranychus urticae*: Tetranychidae: Acari) establishes distinct transcriptomic alterations for long-term acclimatization to different plants allowing a finely tuned plastic response to different nutrient and plant defense chemistries. Those involve in addition also gene families like the MFS (Snoeck et al., 2018), which has been previously linked to sequestration, like ABC transporters, as outlined before (Kowalski et al., 2020; Schmidt et al., 2019; Strauss et al., 2013; Yang et al., 2021). However, it is challenging to distinguish between general stress responses and specific adaptations to host plants or chemical compounds on the transcript level alone (Koenig et al., 2015; Rösner et al., 2021a). Physiological studies combined with functional molecular experiments as conducted in this dissertation thus strengthen adaptation-related conclusions.

The few large-scale transcriptomic profiles of cardenolide-sequestering species feeding on different milkweed plants show a similar picture in the modulation of gene families involved in detoxification, transport, and hydrolysis. For ABC transporters there is a very narrow, likely herbivore-plant-interaction-specific dynamic, which is also suggested to be associated with sequestration (Birnbaum et al., 2017; Krueger et al., 2022; Tan et al., 2019). The observation of elevated OfABCB protein levels in storage compartments (Chapter 3), in contrast to similar total *Ofabcb1* and *2* mRNA levels in both diet lines (Chapter 2), may indicate that the total gene product amount in the body is in balance, even if expression in tissue changes. However, at present it is not known how well OfABCB protein levels correlate with the corresponding mRNA level (Herbertz et al., 2023; Labbé et al., 2011b; Lynch and Marinov, 2015; Schmidt et al., 2019). Furthermore, I cannot heavily rely on my conclusions on this point at present, since the number of biological replicates for immunofluorescence was small in this pilot experiment. Nonetheless, this finding lines up well with the sequestration plasticity among milkweed bug

diet lines demonstrated in Chapter 3 and discussed in more detail in the following section. Similarly, oleander aphids establish no long-term adjustments in their total ABCB full transporter mRNA expression upon feeding on different milkweed species. But they do so by downregulation of an ABCG member and upregulation of ABCC members when feeding on high cardenolide content and likely more toxic host plants (Birnbaum et al., 2017). Monarchs downregulate eight out of their 60 ABC transporters, including an ABCB full transporter, when feeding on higher-cardenolide-content milkweeds within a generation. None are upregulated (Krueger et al., 2022; Tan et al., 2019). Tan et al. (2019) suggests that high mRNA levels on low-level cardenolide plants may be a sequestration-associated compensatory mechanism. However, cellular and functional characterizations are pending in this regard (Birnbaum et al., 2017; Krueger et al., 2022; Tan et al., 2019) which, as explained before, makes it difficult to draw conclusions regarding biological functions and adaptations.

Interestingly, chronic substance exposure can result in constitutive overexpression in systems where ABC transporter exercise their famous protective function, as is for example well established in cancer cells (for review see Theile and Wizgall, 2021) or documented in pesticide resistant insect populations (Xu et al., 2021). My preliminary findings in Chapter 2 and Chapter 3 in this regard that gene products are in balance in the body, but might be exposure-dependent adjusted in tissues highlight the opposite perspective in a chemical specialist with a long evolutionary history of cardenolide feeding (Bramer et al., 2015). Further studies characterizing the functional roles of diet-modulated genes, such as ABC transporters, are needed to understand their contributions, benefits or constraints, to sequestration and its plasticity. That may include sequestration capacity and tissue distribution experiments within milkweed bug lines where cardenolide feeding is controlled in terms of exposure duration and physiochemical properties of individual cardenolides or their mixtures, including host plant phytocomplexes. Combined with transcriptional and protein profiling on a larger scale this can also help us to identify additional prime candidates for cardenolide transport within and outside the suspected gene families.

Cardenolide sequestration dynamics in *O. fasciatus*

My findings in Chapter 3 demonstrate that diet can shape sequestration capacity in *O. fasciatus* suggesting plasticity of the sequestration system in this regard. Cardenolide sequestration plasticity has also been observed among worldwide monarch butterfly populations, with the history of host plant association suggested as one possible driver (Freedman et al., 2021). Monarch caterpillars in particular possess a diet history related sequestration plasticity which

allows them to compensate for low dietary cardenolide amounts (Jones et al., 2019). While the underlying regulation is not yet well understood, ABC transporter are likely involved (Krueger et al., 2022; Tan et al., 2019) and this parallels my preliminary finding in this regard in *O. fasciatus*. Dietary specialization is also associated with sequestration capacity in aphids (Züst and Agrawal, 2016). Furthermore, it is suggested that switches to cardenolide-free host plants led to the complete loss of cardenolide storage capacity in some Lygaeinae species, like *Arocatus longiceps* (Bramer et al., 2015). Nutritional composition and diet choices therefore appear to be a modulator of cardenolide sequestration capacity in and across species. However, underlying mechanisms in these species are still poorly understood due to limited knowledge in general about the genetic basis of cardenolide sequestration. This thesis therefore gains new insights into what will help us in the future to understand how this plasticity manifests itself at the molecular level.

My findings in Chapter 3 imply that adaptive as well as directly diet-related mechanisms, as known for life-history traits (Attisano et al., 2012; Chaplin, 1980; Gordon et al., 1971; Hill, 2006; Moore and Attisano, 2011; Pokharel et al., 2021), take place after diet switches. The association of ouabain sequestration with natural cardenolide sequestration in *O. fasciatus* suggests positive feedbacks between accumulation capacity and cardenolide uptake. It therefore reinforces the evidence for a link between available cardenolide amount or concentration and uptake for storage (Duffey et al., 1978; Heyworth et al., 2023; Isman, 1977; Pokharel et al., 2021; Scudder and Meredith, 1982b; Vaughan, 1979). Furthermore, Chapter 3 extends the knowledge in this regard by providing insights into the temporal uptake dynamics for sequestration. These dynamics suggest that physiological transport mechanisms for ouabain change quantitatively rather than qualitatively in connection with long-term dietary changes in *O. fasciatus*, at least for ouabain uptake from the hemocoel into the thoracic storage compartment. Whether this is also the case with intestinal absorption remains to be seen. Nevertheless, it is likely, because according to a previous ex vivo study, there are no differences in abdominal absorption between such lines (Yoder et al., 1976).

An open question to be addressed is to what extent and how exactly dietary compounds and adaptive mechanisms modulate sequestration plasticity. OfABCB full transporters are good candidates for providing both (see also discussion of Chapter 3). My pilot immunofluorescence experiment of the defensive fluids suggests that cellular composition and associated ABCB full transporter protein levels in the thoracic storage compartment might be involved.

The here observed sequestration plasticity among lines is also in agreement with previous studies on first generation sunflower animals (Carlson and Agrawal, 2023; Duffey and

Scudder, 1974) suggesting that sequestration capacity in general adapts rapidly. However, the more closely matched nutritional composition, the focus on a single life stage and the likely buffered impact of diet on other life-history traits by long-term acclimatization (Feir, 1974; Gordon et al., 1971) realized here allows for a better correlation of sequestration capacity to diet in terms of secondary seed metabolites.

Diet specialization likely led to the loss or to the acquisition of new sequestration abilities during speciation of some Lygaeinae members (Bramer et al., 2015; Petschenka et al., 2022). While plasticity may save costs of sequestration, especially when molecular mechanisms like protein translation are involved (Lynch and Marinov, 2015), my findings suggest also the robustness of the entire sequestration system in *O. fasciatus*. Even several hundred generations without cardenolide exposition do not alter the milkweed bugs' basic ability to sequester cardenolides (Newcombe et al., 2013). Monarch butterflies living on islands also retain their ability to store cardenolides even after 40 years without selection pressure by avian predators (Freedman et al., 2021). The absence of significant changes in uptake dynamics between milkweed bugs lines also suggests that plasticity controls the utilization of sequestration pathways, but not their use per se. This, together with the immunochemical pilot characterization in Chapter 3, suggests that the key function of ABCB full transporters in ouabain sequestration identified in Chapter 2 is valid and transferable to other lines and populations. Our two laboratory lines, will help to confirm that and to identify which switches are being flipped to fine-tune sequestration plasticity in *O. fasciatus*.

Chemical defense by defensive fluid release in *O. fasciatus*

The main advantage of cardenolide sequestration is that their toxicity can be used for the organisms' own chemical defense against predators (Beran and Petschenka, 2022; Duffey, 1980; Malcolm, 1991). For example, birds reject monarch butterflies (Brower, 1969) and mantids do so for *O. fasciatus* (Berenbaum and Miliczky, 1984). The release of defensive fluids into the environment offers additionally the benefit to deter predators before the harm is fatal (Eisner and Meinwald, 1966).

Despite its significance for predator deterrence (Hill, 2006), the physiological origin and formation of released defensive fluids is poorly understood in *O. fasciatus* (Bramer et al., 2017; Moore and Scudder, 1985; Scudder et al., 1986; Scudder and Meredith, 1982a). To my knowledge, this is also the case for many other species that release cardenolide-containing defensive fluids, such as the grasshopper *P. bufonis* (Euw et al., 1967), leaf beetles like *C. cobaltinus* and *C. auratus* (Dobler et al., 1998) or other Lygaeinae species (Bramer et al., 2017;

Duffey and Scudder, 1974; Scudder and Duffey, 1972). My findings in Chapter 3 narrow this gap by showing that fluid filling in the thoracic storage compartment of *O. fasciatus* is complex and associated with a variety of factors, such as biomass, sex, adult female age and also to some degree with the stored cardenolide amount (see detailed discussion in Chapter 3). Similar applies to the defensive froth produced by Lubber grasshoppers (*Romalea guttata* and *Taeniopoda eques* (Romaleidae: Orthoptera)), which have a different defensive chemistry and release system. The volume released is related to the same factors depending on the species: biomass, sex, age and diet (Whitman et al., 1992). Biomass association and sexual dimorphism in deterrent secretion volumes were also observed in the pill milliped (*Glomeris marginata*: Glomeridae: Glomerida) (Carrel, 1984), suggesting that these are more common factors associated with the release capacity of deterrent fluids in arthropods.

In agreement with findings by Duffey and Scudder (1974) neither dietary cardenolides nor both OfABCB full transporters as shown in Chapter 2 are mandatory for fluid release by *O. fasciatus*. Some factors, like biomass or gender, are also associated with cardenolide sequestration (Isman, 1977; Moore and Scudder, 1985; Pokharel et al., 2021). However, Chapter 3 shows that gender and in line with a previous study also biomass (Rubiano-Buitrago et al., 2024) do not relate to fluid filling in the same way as described for cardenolide sequestration (see also the discussion in this chapter).

The differential effect of diet on the amounts and concentrations of stored ouabain in Chapter 3 points to underlying effects in molecular transport for non-glandular sequestration in *O. fasciatus* that are rather detached from defensive fluid accumulation. This is in agreement with my findings in Chapter 2 that animals with reduced ouabain storage capacity (*Ofabcb1* knockdowns) released similar amounts of defensive fluids. It also represents a crucial difference to the glandular sequestration mechanism in *C. populi*, where the failure of its storage-related key proteins leads to the loss of secretion ability (Schmidt et al., 2019; Strauss et al., 2013). Whether there is a general difference or even an advantage in terms of evolutionary constraints between non-glandular or glandular sequestration is an interesting question that we may be able to answer in the long term. However, to achieve this, we still need to gain a much better understanding of the molecular cellular sequestration mechanisms.

In summary, my findings in Chapter 3 suggest that several factors influence the released defensive fluid volume and hence likely defensive efficacy of *O. fasciatus*. At the same time, there are probably not yet understood mechanisms that counteract this in order to maintain a certain chemical defense effectiveness, as the lower variability in cardenolide concentration compared to stored amounts suggests. However, mechanistic chemosensory studies are

generally lacking in this regard (Mohammadi et al., 2022). As outlined in the discussion of Chapter 3, considerations regarding cardenolide solubility constraints, chemosensory predator deterrence and physiological transport kinetics, highlight that fluid formation and composition are issues beyond cardenolides to be considered and studied in the future.

From gene expression to physiological function: Methodological aspects

Gene expression studies have always played a key role in the research on ABC transporters in the context of multidrug and pesticide resistance (Amezian et al., 2024; Dermauw and van Leeuwen, 2014; Theodoulou and Kerr, 2015). On larger scales, they allow comprehensive analyses between genes and their putative functions. Nonetheless, quantitative real-time PCR is the method of choice for RNA-seq data confirmation in particular for rare transcripts (Lv et al., 2025), as observed here for *Ofabcb2*. A great effort in Chapter 1 of this thesis was therefore undertaken to identify a set of reference genes for accurate gene expression quantification in this thesis and future studies, which was of general need in *O. fasciatus* as outlined in more detail in the chapter. The expression stability evaluation of seven out of ten identified reference gene candidates in O. *fasciatus* in Chapter 1 and their partial revalidation in Chapter 2 demonstrate their validity and broad applicability for gene expression studies in *O. fasciatus*. These revalidations underline that there are no universal stable reference genes (Chapman and Waldenström, 2015; Kozera and Rapacz, 2013; Shakeel et al., 2018; Shi et al., 2015), although *Ofef1a* comes very close to this state under all conditions tested in this thesis (ouabain injection, tissue, diet, RNAi knockdown for seven days with and without ouabain injection). *Ef1a* has recently been used as normalizer to study the genetic basis of pigmentation in *O. fasciatus* (Francescutti et al., 2022). Also other genes identified and analyzed here, like *tubulin*, *GAPDH*, *RPS3* or *Actin*, have meanwhile been used for expression quantification in tissues and RNAi knockdowns in *O. fasciatus* (Amukamara et al., 2020; Herbertz et al., 2023; Lohr et al., 2017). The genes identified and selected here are therefore now an accepted set of robust normalizer genes in *O. fasciatus*, which can be fine-tuned depending on the application and research question under study.

While expression levels are a crucial indicator of the functional significance of ABC transporters in tissues, cellular localization provides information about the physiological function within the tissue as outlined in more detail before (Amezian et al., 2024; Denecke et al., 2022; Hoffmeyer et al., 2000; Mayer et al., 1996). The use of three different commercially available monoclonal antibodies (mAb C219, C494 and JSB-1) against mammalian ABCB full transporters (ABCB1 and/or ABCB4) (Georges et al., 1990; Liu et al., 1997) ensured a reliable

detection of ABCB full transporters in *O. fasciatus* in particular by the monoclonal antibody C219. That is in good agreement with its widespread use in insects (e. g. see Denecke et al., 2022; Dobler et al., 2015; Mayer et al., 2009; Petschenka et al., 2013b). Its epitope identification in silico in both OfABCB full transporter proteins and the agreement of fluorescence signals with transcript expressions suggests its specific detection of OfABCB full transporters in *O. fasciatus*, but does not allow for differentiation between transport proteins. MAb C494, specific for human ABCB1 and certain mammalian homologs (Georges et al., 1990), revealed distinct fluorescence signals that were more or less well localized at cellular plasma membranes, but its epitope barley matched in silico in both OfABCB full transporters (maximum four out of seven amino acids). Along with C219, the C494 mAb has been previously used for ABCB full transporter detection associated with pesticide resistance in the tobacco budworm (*Heliothis virescens*: Noctuidae: Lepidoptera) (Lanning et al., 1996). In addition to cross-reactivity (Rao et al., 1994), detection of other ABCB-like transporters in *O. fasciatus* is another possible explanation for the C494 fluorescence signals since both generated transcriptome assemblies revealed several short ABCB-like fragments leaving the option that there might be further so far unidentified transporters. New transcriptome data (Röpcke et al., 2024) are currently being used to reassess subfamily completeness in this regard.

Transport proteins work in cross-regulated networks (Erb and Robert, 2016). RNA interference makes it possible to study the effect of a gene of interest on the realization of a phenotype in its natural gene environment with all regulatory feedback loops, interaction partners and signaling pathways. Such a functional characterization is important for distinguishing specific gene functions from canonical functions such as in stress or metabolic reactions (Rösner et al., 2021a). Many physiological functions of insect ABC transporters and other proteins involved in phytochemical-related aspects have now been discovered by RNAi in this way (e. g. see Broehan et al., 2013; Groen et al., 2017; Herbertz et al., 2023; Torrie et al., 2004), in particular those involved in phytochemical-transport in specialized herbivorous insects (Kumar et al., 2014; Strauss et al., 2013; Yang et al., 2021). Along these lines, unraveling the effect of a single gene on a phenotype is challenging. Downregulation of different genes can result in almost identical phenotypes, no phenotypes at all or can obscure substrate associations (Chahine et al., 2012b; Denecke et al., 2021; Ewen-Campen et al., 2013). The loss of ABCB1 and other ABC transporters is for example compensated by upregulation of homologs in *Aedes aegypti* (Culicidae: Diptera), a mechanism suggested to offset the fitness costs of gene loss (Pacheco et al., 2025). Also, off-target effects of systemic RNAi by long dsRNA are difficult to predict because siRNAs are not standardized (Mehlhorn et al., 2021; Scott et al., 2013; Vogel

et al., 2018). Those were monitored in Chapter 2 on the expression of both OfABCB transporters, but I cannot comment on other proteins. A second dsRNA targeting a different, non-overlapping gene region can be used, for example, to further confirm gene knockdown-specific phenotypes (Bewick et al., 2019; Mehlhorn et al., 2021). In conclusion, the agreement of the *Ofabcb1* knockdown phenotype with substrate spectrum (Röpcke et al., 2024), its tissue expression and immunohistochemistry (Chapter 2) strongly support the tight connection of OfABCB1 to ouabain sequestration. Similarly, *C. populi* larvae were not able to compensate for the loss of their sequestration key player (CpMRP/Cpabc35), even though an intestine-specific ABCG transporter was induced in the defensive glands upon its loss (Strauss et al., 2014).

Adaptation strategies to cope with toxic cardenolides: Who needs whom?

Adaptation to poisonous plants give herbivorous insects an advantage in obtaining an enemy free space and avoiding competition (Bernays and Graham, 1988; Murphy, 2004). Insects specialized at least 28 times on cardenolide host plant feeding. Yet, four different syndromes classified on the basis of target-site insensitivity, sequestration, and aposematism repeatedly evolved according to recent comprehensive research in the cardenolide-feeder complex (Agrawal et al., 2024b). Syndrome I encompasses species with susceptible target-sites that do not sequester cardenolides, although the sequestering beetle *Diabrotica nummularis* is the exception of this rule. *Lilioceris merdigera* (Chrysomelidae: Coleoptera), for example, excretes ingested cardenolides almost completely, but larvae rely on chemical defensive faecal shields (Baum and Dobler, 2024). Similarly to *L. merdigera*, sensitive and specialized *Euchaetes egle* prevents cardenolide accumulation (Agrawal et al., 2024b). However, also polyphagous *Amata mogadorensis* and pyrrolizidine alkaloid specialized *Creatonotos transiens* (all three: Erebidae: Lepidoptera) mainly excrete ingested cardenolides (Wink and Schneider, 1990). That shows, as already stated in the introduction, that protective permeability barriers are preadaptations not tied to cardenolide specialization. At the same time, it does not mean that the degree of selective compartmentalization is insignificant, as will become clear below. Syndrome II also encompasses non-sequestering species, but those are characterized by modest to even high target-site insensitivities (Agrawal et al., 2024b). The modestly insensitive target-site of the oleander hawk moth (*Daphnis nerii*: Sphingidae: Lepidoptera) is protected by mechanic and biochemical compartmentalization through the blood-(hemolymph-) brain barrier (Petschenka et al., 2013b). *D. nerii* is thereby able to withstand cardenolide injections into the hemocoel (Petschenka and Dobler, 2009), but the modestly insensitive common crow (*Euploea core:* Nymphalidae: Lepidoptera), in contrast, is not (Petschenka and Agrawal, 2015). Similar to *O.*

fasciatus (Scudder and Meredith, 1982b) and to other adapted or non-cardenolide-adapted Lepidoptera (Agrawal et al., 2024b; Wink and Schneider, 1990), the gut of *E. core* is permeable to cardenolides. However, this species degrades cardenolides in its midgut, preventing their absorption into the hemocoel (Dreisbach et al., 2023). Preadaptations can therefore protect, but do not have to. Additional tolerance or resistance mechanisms may be essential depending on Na,K-ATPase sensitivity, blood-brain barrier and gut leakage to cardenolides. However, more research is needed to better understand that interplay. Most relevant studies have focused on lepidopterans. These exhibit a cardenolide-unrelated restriction of their single Na,K-ATPase to the nervous system (Petschenka et al., 2012) in contrast to other species, like *O. fasciatus* or *P. pictus* (syndrome IV), which duplicated and subfunctionalized the targeted enzymes (Dobler et al., 2019; Lohr et al., 2017; Yang et al., 2019; Zhen et al., 2012). In general, a certain intestinal cardenolide permeability is mandatory for sequestering species, which belong to the highly convergent syndromes III and IV. However, high target-site insensitivity is only found for species of the so-called “sequestering specialist syndrome” (IV), which also includes *D. plexippus* and *O. fasciatus* (Agrawal et al., 2024b). Arctiid moths (III), like *Empyreuma pugione* or *Cycnia tenera* (both Erebidae: Lepidoptera), for example, accumulate high cardenolide amounts reaching even sequestration levels of the monarch butterfly, but only have modest insensitivities (Agrawal et al., 2024b; Petschenka et al., 2012). A modest Na,K-ATPase insensitivity is therefore suggested to be a common prerequisite for cardenolide sequestration in insects (Agrawal et al., 2024b). This mechanistic link is supported by recent reverse genetics in *D. melanogaster*. Ouabain is particularly toxic to fruit flies in concentrations found in milkweed plants (Groen et al., 2017). However, larvae that have acquired ouabain resistance through monarch-butterfly-like Na,K-ATPase α-subunit gene editing accumulate small amounts of ouabain, which are even transferred to the adult stage (Karageorgi et al., 2019). Thus, as soon as animals survive, a non-specialized, likely passive accumulation also of polar cardenolides seems to be possible. Nonetheless, in chemical and dietary specialists like *O. fasciatus* or *D. plexippus* sequestration is an extremely fine-tuned process. My dissertation provides the first evidence for a key protein involved in genetic adaptation in *O. fasciatus* in this regard.

Interrelation of cardenolide sequestration and Na,K-ATPase insensitivity

Cardenolide sequestration is suggested to involve a trade-off between cardenolide toxicity to the organism itself and toxicity to predators for an effective chemical defense (Agrawal et al., 2024a; Jones et al., 2019; Rubiano-Buitrago et al., 2024). Monarch butterflies, for example, preferentially sequester those cardenolides that are less inhibitory to themselves, but still

potent to Na,K-ATPases of vertebrates (Agrawal et al., 2024a; Jones et al., 2019). In aphids, however, it is rather the opposite, as they accumulate more toxic cardenolides (Züst et al., 2018) by their likely passive cardenolide accumulation (Züst and Agrawal, 2016). Thus, Na,K-ATPase-related cardenolide toxicity can act as a driver of selective sequestration. However, tritrophic effects are difficult to predict and to generalize, as they depend on the interaction between host plant chemistries and interspecies Na,K-ATPase sensitivities (Agrawal et al., 2022; Agrawal et al., 2024a; Jones et al., 2019; Rubiano-Buitrago et al., 2024). In *O. fasciatus,* predator pressure is suggested an additional driver shaping sequestration selectivity by favoring sequestration of even self-harmful cardenolides, like frugoside, when these provide an advantage in chemical predator defense (Rubiano-Buitrago et al., 2024). The near absence of Na,K-ATPases demonstrated in defensive fluids of *O. fasciatus* suggests with certain caveats in mind (see discussion Chapter 3) that no adverse costs likely arise as soon as cardenolides have reached storage sites. Thus, accumulation in compartmentalized defensive fluids removes toxins from the metabolism what can be considered as safe storage. As outlined before, intracellular lysosomal gossypol accumulation is a suggested detoxification mechanism in the cotton bollworm (Jin et al., 2020). Targeted accumulation is also a mechanism suggested in adaptation to pesticides in order to mitigate their harmful effects on insects (Chen et al., 2024; Deng et al., 2025; Karunaratne et al., 1993). My finding thus sheds new light on compartmentalized storage as a means of shielding *O. fasciatus* from detrimental effects. Along these lines, Na,K-ATPase target-site insensitivity is certainly mandatory in *O. fasciatus* to prevent autointoxication (Lohr et al., 2017) as discussed in Chapter 2 and Chapter 3. Nonetheless, the well-managed pathways to storage sites without target enzymes as a tolerance strategy (Jeckel et al., 2022) probably free the sequestration in *O. fasciatus* from certain toxicity constraints, as is the case with the cardenolide frugoside (see further the discussion of Chapter 3). Since preferentially sequestered frugoside largely originates from its less inhibitory glycosylated form by endogenous biotransformation (Rubiano-Buitrago et al., 2023; Rubiano-Buitrago et al., 2024), this opens up a new perspective on the costs of cardenolide metabolite sequestration, which have previously been considered more costly (Jones et al., 2019).

The overexpression of the strongly cardenolide insensitive Na,K-ATPase α1A paralog (Dalla et al., 2013; Dalla and Dobler, 2016; Herbertz et al., 2024) shown in Chapter 3 suggests fast adaptive and possibly compensatory changes upon ouabain accumulation in milkweed bugs. Similarly, a rapid bufadienolide-induced expression upregulation of the resistance-mediating Na,K-ATPase α-subunit gene paralog *ATP1a3* has been described in toxin-adapted garter snakes (Mohammadi et al., 2017). Genes suggested to be related to dietary cardenolide

toxicity in the aphid *A. nerii*, like glutathione-transferases and other ABC transporters, respond to a similar extent as observed here for α1A (Birnbaum et al., 2017). Overexpression can be a tolerance mechanism to stochastically compensate harmful target effects by secondary plant metabolites (Jeckel et al., 2022). For example, proteases are overexpressed in cowpea weevils (*Callosobruchus maculatus*: Chrysomelidae: Coleoptera) after soybean protease inhibitor ingestion (Moon et al., 2004). Furthermore, constitutive overexpression of a cytochrome P450 gene leads to the acquisition of resistance to nicotine in the generalist aphid *M. persicae* (Bass et al., 2013) which occasionally also feeds on milkweed plants (Züst and Agrawal, 2016). At the same time, the Na,K-ATPase has other cellular functions besides cardenolide-targeted ion-pumping, such as in cellular signaling and in epithelial physiology (see current review by Blaustein and Hamlyn, 2024). Furthermore, there are likely regulatory feedback loops between subunit paralog expressions in *O. fasciatus* (Herbertz et al., 2023) that could have overall dose-regulating effects (Correll et al., 2014) in order to maintain the physiological balance, given the enzymes' important biological functions. In general, Na,K-ATPase expression responses specifically to cardenolides have been rarely studied in insects. We previously did not detect a significant response of Na,K-ATPase α1-subunit paralogs to ouabain or milkweed seeds (Lohr et al., 2017), likely related to the challenge of quantifying subtle expression changes as outlined in the discussion of Chapter 3. At the same time, Na,K-ATPases show no expression adjustments related to host plant associated cardenolide toxicity in cardenolide-sequestering and insensitive *D. plexippus* or *A. nerii* (Birnbaum et al., 2017; Tan et al., 2019). Also neural Na,K-ATPase enzyme activity of oleander hawk moths, is not influenced by previous dietary cardenolide exposure (Petschenka and Dobler, 2009). However, unlike *O. fasciatus* these species have no duplicated Na,K-ATPase α1-subunits (Zhen et al., 2012), which makes a housekeeping function likely. Fine-tuning the expression of subfunctionalized Na,K-ATPase paralogs in *O. fasciatus* (Herbertz et al., 2024; Lohr et al., 2017), on the other hand, would be a coherent mechanism for coping with dynamic demands during the sequestration process.

Outlook

Aside from biotransformation (Agrawal et al., 2022; Rubiano-Buitrago et al., 2023; Rubiano-Buitrago et al., 2024), selective transport mechanisms have to be crucial for sequestration selectivity in *O. fasciatus*. Such are to be expected at three tissue barriers at the minimum: at the thoracic storage compartment in particular (Duffey et al., 1978; Duffey and Scudder, 1974; Scudder and Meredith, 1982a; Scudder and Meredith, 1982b), the Malpighian tubules (Meredith et al., 1984) and to a certain extent in the gut (Detzel and Wink, 1995). An open

question in this context that needs to be addressed by future research is: How many transporters sets with more or less selective substrate spectra are enough at which sites for coordinated and adaptable tissue selectivity in cardenolide transport?

Specialized storage structures in particular have a rather specific transporter set (Schmidt et al., 2019), in which one transporter within its ABC subfamily seems to occupy a rather unique functional position (Kowalski et al., 2020; Strauss et al., 2013; Strauss et al., 2014). Although this is consistent with the findings on OfABCB1 in this thesis, such an exceptional role within its subfamily, as discussed before, is not yet entirely clear. The Malpighian tubules and the gut are among the tissues richest in transporter systems in insects due to their significance for regulatory compound absorption and excretion (Hixson et al., 2022; Schmidt et al., 2019). In *O. fasciatus* they provide different degrees of selective cardenolide transport as outlined in more detail already in the introduction (Detzel and Wink, 1995; Meredith et al., 1984; Scudder and Meredith, 1982b; Yoder et al., 1976). Insect ABC transporters are numerous in these tissues in particular (Schmidt et al., 2019; Xu et al., 2021), but the striking observation for both OfABCB transporters investigated here is rather their absence there, as discussed above. There are likely a number of other transporters within the two largest transporter families, the ABC transporter superfamily and the major facilitator superfamily (Dassa and Bouige, 2001; Pao et al., 1998), that complement or extend cardenolide mediated transport by OfABCB1 and OfABCB2 in some tissues, like the thoracic compartment, and take on the major cardenolide transport role for sequestration in others, like the Malpighian tubules or the gut.

Half transporters of the ABCB subfamily and members of the subfamily C, G and H are eligible to take on such a role within the ABC transporter superfamily just like eventually still undiscovered ABCB full transporters. As outlined before, ABCB half transporters have been previously linked to lysosomal accumulation for detoxification of secondary plant metabolites (Jin et al., 2020). Furthermore, half transporters have been reported to be inducible or constitutively modulated by pesticides (Pignatelli et al., 2018; Xu et al., 2021). While subfamily B, C and G are considered most relevant for secondary plant metabolite sequestration, subfamily H is expressed along with ABCCs and ABCGs in glandular sequestration tissue (Schmidt et al., 2019; Strauss et al., 2014). Subfamily H is diversified within the Hemiptera (Denecke et al., 2021) and its role in the formation and regeneration of the thoracic storage compartment, about which we do also not know much yet, is worth investigating. Members of this subfamily are suggested to transport cuticular hydrocarbons and lipids for cuticle formation and recent findings suggest an additional role in lipid and pesticide transport (Chen et al., 2025; Yu et al., 2017; Zuber et al., 2018). A role of ABC transporters, including ABCB, ABCC, and

ABCG members, has been suggested by diet-related transcriptional changes in cardenolide sequestering species, as outlined before (Birnbaum et al., 2017; Krueger et al., 2022; Tan et al., 2019). Subfamily C is involved in Malpighian tubule mediated xenobiotic excretion (Chahine et al., 2012a; Chahine et al., 2012b) and its members can be expressed at apical and basolateral tubule cell surfaces (Labbé et al., 2011b). ABCCs are furthermore frequently enriched in the Malpighian tubules and in insect guts (Labbé et al., 2011a; Pignatelli et al., 2018) and have been associated with pesticide resistance (Pignatelli et al., 2018; Xu et al., 2021). They are an important part of phase III detoxification by transport of GSH-S-transferase and UDP-glucuronosyltransferase conjugates (Kitamura et al., 2010; Toyoda et al., 2008; Vaidya et al., 2009). The enzymes involved in conjugation are also suggested to be important in adaptations to cardenolides of milkweed plant-feeding insects (Birnbaum et al., 2017; Krueger et al., 2022; Tan et al., 2019). Thus, they might also play a role in *O. fasciatus* for sequestration or excretion of cardenolides and their metabolites. In general, which barriers are to what extent involved in cardenolide metabolite transport is not well understood. While it is not known where natural cardenolides are metabolized, digitoxin biotransformation occurs already in the digestive system (Scudder and Meredith, 1982b) suggesting that metabolite sequestration also depends on selective transport systems. Also, the subfamily G is of interest in this regard. ABCGs play a role in insect metabolism, like in pigmentation of eyes and in Malpighian tubules, in renal excretion, in cuticular lipid transport, and in reproduction (Broehan et al., 2013; Rösner et al., 2021a; Wang et al., 2023). Furthermore, they are enriched exclusively or in addition to the digestive/excretory organs in the fat body, are stress responsive in the red flour beetle (Rösner et al., 2021a) and mediate pesticide resistance in other insects, like *Bactrocera dorsalis* (Tephritidae: Diptera) (Wang et al., 2023) or *Spodoptera litura* (Noctuidae: Lepidoptera) (Liang et al., 2025). SlABCG3 of *S. litura* also mediates resistance to dietary secondary plant metabolites, like nicotine or gossypol. ABCG members are like ABCCs also expressed in neural tissue (DeSalvo et al., 2014; Pignatelli et al., 2018; Rösner et al., 2021a) and gene disruptions in *D. melanogaster* affect neural biochemistries (Borycz et al., 2008). Thus, these subfamilies are prime candidates for selectivity gatekeepers in permeability barriers like the gut or blood-(hemolymph-) brain barrier, in the Malpighian tubules as well as in the fat body, where a cardenolide spectrum most similar to that found in excreta (feces + urine), accumulates in *O. fasciatus* (Moore and Scudder, 1985).

The major facilitator superfamily (MFS) is a part of the solute carrier superfamily (SLC, #2.A in the transporter classification database (TCDB)) and contains a plethora of protein families consisting of facilitative and secondary active transporters. This superfamily contains candidates for carriers that particularly mediate the influx into cells, whereby this depends in

the individual case on the cellular arrangement, the transport mode, and electrochemical gradient (Pao et al., 1998; Pizzagalli et al., 2021; Wang et al., 2020).

Organic Anion Transporting Polypeptides (OATP) (SLCO formerly SLC21) belong to the Organo Anion Transporter (OAT) family (#2.A.60 TCDB), a distant family within the MFS (Wang et al., 2020). These likely sodium- and ATP-independent antiporters (Roth et al., 2012) are counterparts to ABCB full transporters in the protective compartmentalization and elimination function against cardenolides in mammals and insects (Groen et al., 2017; Kullak-Ublick et al., 2001; Li et al., 2025; Mikkaichi et al., 2004; Taskar et al., 2017). They might therefore equally be involved in cardenolide transport for sequestration. This is particularly likely for the second selective barrier, the Malpighian tubules (Meredith et al., 1984), where other transporters might have a more crucial role than both OfABCB transporters (see discussion Chapter 2). In other insects, OATPs are strongly expressed basolateral in the Malpighian tubules and involved in the elimination of cardenolides and other xenobiotics (Chahine et al., 2012a; Chahine et al., 2012b; Rösner et al., 2021b; Torrie et al., 2004). This makes them good candidates for cellular cardenolide uptake into the tubules (Figure 24), which is probably also necessary there as a counterpart to OfABCB transporters (see Chapter 2).

Another family of the MFS, the sugar porter family (SP, #2.A.1.1 TCDB) (Pao et al., 1998), provides key proteins for the Malpighian reabsorption mechanism for glucosinolate sequestration in the flea beetle *Phyllotreta armoraciae* (Chrysomelidae: Coleoptera) (Yang et al., 2021). A similar physiological mechanism is also known for ouabain in the Malpighian tubules of *O. fasciatus* and suggested to be linked to sodium ion transport (Meredith et al., 1984). Reduction in excretion is a driver for secondary plant metabolite sequestration also in other insects (Discher et al., 2009; Kumar et al., 2014). Sugar transporters are also suggested to be important components in the specialized glandular sequestration of *C. populi* (Schmidt et al., 2019) and are therefore interesting as additional components for sequestration into the thoracic storage compartment (B, Figure 26). They are also prime candidates for intestinal uptake of cardenolides, as shown by ex vivo studies with the sugar porter inhibitor phloridzin in *O. fasciatus* nymphs (Detzel and Wink, 1995). In summary, many more network players are yet to be discovered. In any case, the present dissertation shows that ABCB full transporters play an important role in the cardenolide transport network of *O. fasciatus*, thus providing an important starting point for understanding the molecular basis of cardenolide sequestration.

References

Agrawal, A.A., Hastings, A.P., Duplais, C., 2024a. Testing the selective sequestration hypothesis: Monarch butterflies preferentially sequester plant defences that are less toxic to themselves while maintaining potency to others. Ecology Letters 27, e14340. https://doi.org/10.1111/ele.14340.

Agrawal, A.A., Hastings, A.P., Lenhart, P.A., Blecher, M., Duplais, C., Petschenka, G., Hawlena, D., Wagschal, V., Dobler, S., 2024b. Convergence and Divergence among Herbivorous Insects Specialized on Toxic Plants: Revealing Syndromes among the Cardenolide Feeders across the Insect Tree of Life. The American Naturalist 204, 201–220. https://doi.org/10.1086/731277.

Agrawal, A.A., Del Espinosa Alba, L., López-Goldar, X., Hastings, A.P., White, R.A., Halitschke, R., Dobler, S., Petschenka, G., Duplais, C., 2022. Functional evidence supports adaptive plant chemical defense along a geographical cline. Proceedings of the National Academy of Sciences of the United States of America 119, e2205073119. https://doi.org/10.1073/pnas.2205073119.

Agrawal, A.A., Böröczky, K., Haribal, M., Hastings, A.P., White, R.A., Jiang, R.-W., Duplais, C., 2021. Cardenolides, toxicity, and the costs of sequestration in the coevolutionary interaction between monarchs and milkweeds. Proceedings of the National Academy of Sciences of the United States of America 118. https://doi.org/10.1073/pnas.2024463118.

Agrawal, A.A., Petschenka, G., Bingham, R.A., Weber, M.G., Rasmann, S., 2012. Toxic cardenolides: chemical ecology and coevolution of specialized plant-herbivore interactions. New Phytologist 194, 28–45. https://doi.org/10.1111/j.1469-8137.2011.04049.x.

Alam, A., Kowal, J., Broude, E., Roninson, I., Locher, K.P., 2019. Structural insight into substrate and inhibitor discrimination by human P-glycoprotein. Science 363, 753–756. https://doi.org/10.1126/science.aav7102.

Aldrich, J.R., Leal, W.S., Nishida, R., Khrimian, A.P., Lee, C.-J., Sakuratani, Y., 1997. Semiochemistry of aposematic seed bugs. Entomologia Experimentalis et Applicata 84, 127–135. https://doi.org/10.1046/j.1570-7458.1997.00207.x.

Amezian, D., Nauen, R., van Leeuwen, T., 2024. The role of ATP-binding cassette transporters in arthropod pesticide toxicity and resistance. Current Opinion in Insect Science 63, 101200. https://doi.org/10.1016/j.cois.2024.101200.

Amukamara, A.U., Washington, J.T., Sanchez, Z., McKinney, E.C., Moore, A.J., Schmitz, R.J., Moore, P.J., 2020. More Than DNA Methylation: Does Pleiotropy Drive the Complex Pattern of Evolution of Dnmt1? Frontiers in Ecology and Evolution 8, 4. https://doi.org/10.3389/fevo.2020.00004.

Andersen, C.L., Jensen, J.L., Ørntoft, T.F., 2004. Normalization of real-time quantitative reverse transcription-PCR data: A model-based variance estimation approach to identify genes suited for normalization, applied to bladder and colon cancer data sets. Cancer Research 64, 5245–5250. https://doi.org/10.1158/0008-5472.CAN-04-0496.

Aspiras, A.C., Smith, F.W., Angelini, D.R., 2011. Sex-specific gene interactions in the patterning of insect genitalia. Developmental Biology 360, 369–380. https://doi.org/10.1016/j.ydbio.2011.09.026.

Attisano, A., Moore, A.J., Moore, P.J., 2012. Reproduction-longevity trade-offs reflect diet, not adaptation. Journal of Evolutionary Biology 25, 873–880. https://doi.org/10.1111/j.1420-9101.2012.02476.x.

Baerwald, R.J., Delcarpio, J.B., 1983. Double membrane-bounded intestinal microvilli in *Oncopeltus fasciatus*. Cell and Tissue Research 232, 593–600.

Bansal, R., Mittapelly, P., Chen, Y., Mamidala, P., Zhao, C., Michel, A., 2016. Quantitative RT-PCR Gene Evaluation and RNA Interference in the Brown Marmorated Stink Bug. PLOS One 11. https://doi.org/10.1371/journal.pone.0152730.

Bansal, R., Mamidala, P., Mian, M.A.R., Mittapalli, O., Michel, A.P., 2012. Validation of Reference Genes for Gene Expression Studies in *Aphis glycines* (Hemiptera: Aphididae). Journal of Economic Entomology 105, 1432–1438. https://doi.org/10.1603/EC12095.

Barbosa, P., 2014. Insect histology: Practical laboratory techniques. Wiley/Blackwell, Chichester, West Sussex, Hoboken, NJ.

Bass, C., Zimmer, C.T., Riveron, J.M., Wilding, C.S., Wondji, C.S., Kaussmann, M., Field, L.M., Williamson, M.S., Nauen, R., 2013. Gene amplification and microsatellite polymorphism underlie a recent insect host shift. Proceedings of the National Academy of Sciences of the United States of America 110, 19460–19465. https://doi.org/10.1073/pnas.1314122110.

Baum, M., 2015. Transmembrane carriers of cardenolide-adapted leaf beetles (Coleoptera, CHRYSOMELIDAE). Dissertation. Hamburg.

Baum, M., Dobler, S., 2024. Fecal Deployment: An Alternative Way of Defensive Host Plant Cardenolide Use by *Lilioceris merdigera* Larvae. Journal of Chemical Ecology 50, 63–70. https://doi.org/10.1007/s10886-023-01465-8.

Beaulieu, E., Demeule, M., Pouliot, J.-F., Averill-Bates, D.A., Murphy, G.F., Béliveau, R., 1995. P-glycoprotein of blood brain barrier: cross-reactivity of MAb C219 with a 190 kDa protein in bovine and rat isolated brain capillaries. Biochimica et Biophysica Acta (BBA) - Biomembranes 1233, 27–32. https://doi.org/10.1016/0005-2736(94)00239-L.

Beran, F., Heckel, D.G., 2024. Escalation by duplication: Milkweed bug trumps Monarch butterfly. Molecular Ecology 33, e17443. https://doi.org/10.1111/mec.17443.

Beran, F., Petschenka, G., 2022. Sequestration of Plant Defense Compounds by Insects: From Mechanisms to Insect-Plant Coevolution. Annual Review of Entomology 67, 163–180. https://doi.org/10.1146/annurev-ento-062821-062319.

Berenbaum, M.R., Miliczky, E., 1984. Mantids and Milkweed Bugs: Efficacy of Aposematic Coloration Against Invertebrate Predators. American Midland Naturalist 111, 64. https://doi.org/10.2307/2425543.

Berman, H.M., Westbrook, J., Feng, Z., Gilliland, G., Bhat, T.N., Weissig, H., Shindyalov, I.N., Bourne, P.E., 2000. The Protein Data Bank. Nucleic Acids Research 28, 235–242. https://doi.org/10.1093/nar/28.1.235.

Bernays, E., Graham, M., 1988. On the Evolution of Host Specificity in Phytophagous Arthropods. Ecology 69, 886–892. https://doi.org/10.2307/1941237.

Betz, A., Höglinger, B., Walker, F., Petschenka, G., 2025. Regionality and Temporal Dynamics of Sequestration and Relocation of Cardenolides in the Monarch Butterfly, *Danaus plexippus*. Journal of Chemical Ecology 51, 19. https://doi.org/10.1007/s10886-025-01572-8.

Bewick, A.J., Sanchez, Z., McKinney, E.C., Moore, A.J., Moore, P.J., Schmitz, R.J., 2019. Dnmt1 is essential for egg production and embryo viability in the large milkweed bug, *Oncopeltus fasciatus*. Epigenetics & chromatin 12, 6. https://doi.org/10.1186/s13072-018-0246-5.

Birnbaum, S., Abbot, P., 2018. Insect adaptations toward plant toxins in milkweed-herbivores systems - a review. Entomologia Experimentalis et Applicata 166, 357–366. https://doi.org/10.1111/eea.12659.

Birnbaum, S.S.L., Rinker, D.C., Gerardo, N.M., Abbot, P., 2017. Transcriptional profile and differential fitness in a specialist milkweed insect across host plants varying in toxicity. Molecular Ecology 26, 6742–6761. https://doi.org/10.1111/mec.14401.

Blaustein, M.P., Hamlyn, J.M., 2024. Sensational site: the sodium pump ouabain-binding site and its ligands. American Journal of Physiology. Cell physiology 326, C1120-C1177. https://doi.org/10.1152/ajpcell.00273.2023.

Boeckler, G.A., Gershenzon, J., Unsicker, S.B., 2011. Phenolic glycosides of the Salicaceae and their role as anti-herbivore defenses. Phytochemistry 72, 1497–1509. https://doi.org/10.1016/j.phytochem.2011.01.038.

Boland, W., 2015. Sequestration of plant-derived glycosides by leaf beetles: A model system for evolution and adaptation. Perspectives in Science 6, 38–48. https://doi.org/10.1016/j.pisc.2015.06.001.

Borst, P., Elferink, R.O., 2002. Mammalian ABC transporters in health and disease. Annual Review of Biochemistry 71, 537–592. https://doi.org/10.1146/annurev.biochem.71.102301.093055.

Borycz, J., Borycz, J.A., Kubów, A., Lloyd, V., Meinertzhagen, I.A., 2008. Drosophila ABC transporter mutants white, brown and scarlet have altered contents and distribution of biogenic amines in the brain. Journal of Experimental Biology 211, 3454–3466. https://doi.org/10.1242/jeb.021162.

Bramer, C., Schweizer, C., Dobler, S., 2018. Cardenolide-defended milkweed bugs do not evoke learning in *Nephila senegalensis* spiders. Ethology 124, 504–513. https://doi.org/10.1111/eth.12757.

Bramer, C., Friedrich, F., Dobler, S., 2017. Defence by plant toxins in milkweed bugs (Heteroptera: Lygaeinae) through the evolution of a sophisticated storage compartment. Systematic Entomology 42, 15–30. https://doi.org/10.1111/syen.12189.

Bramer, C., Dobler, S., Deckert, J., Stemmer, M., Petschenka, G., 2015. Na+/K+-ATPase resistance and cardenolide sequestration: basal adaptations to host plant toxins in the milkweed bugs (Hemiptera: Lygaeidae: Lygaeinae). Proceedings of the Royal Society B: Biological Sciences 282. https://doi.org/10.1098/rspb.2014.2346.

Brattsten, L.B., 1992. Metabolic defenses against plant allelochemicals, in: Rosenthal, G.A., Berenbaum, M.R. (Eds.), Herbivores: Their interactions with secondary plant metabolites. Academic Press, San Diego, USA, pp. 175–242.

Broehan, G., Kroeger, T., Lorenzen, M., Merzendorfer, H., 2013. Functional analysis of the ATP-binding cassette (ABC) transporter gene family of *Tribolium castaneum*. BMC Genomics 14, 6. https://doi.org/10.1186/1471-2164-14-6.

Brower, L.P., 1969. Ecological chemistry. Scientific American 220, 22–29.

Burdfield-Steel, E.R., Shuker, D.M., 2014. The evolutionary ecology of the Lygaeidae. Ecology and Evolution 4, 2278–2301. https://doi.org/10.1002/ece3.1093.

Bustin, S., 2002. Quantification of mRNA using real-time reverse transcription PCR (RT-PCR): Trends and problems. Journal of Molecular Endocrinology 29, 23–39. https://doi.org/10.1677/jme.0.0290023.

Bustin, S., 2000. Absolute quantification of mRNA using real-time reverse transcription polymerase chain reaction assays. Journal of Molecular Endocrinology 25, 169–193. https://doi.org/10.1677/jme.0.0250169.

Bustin, S., Nolan, T., 2017. Talking the talk, but not walking the walk: RT-qPCR as a paradigm for the lack of reproducibility in molecular research. European Journal of Clinical Investigation 47, 756–774. https://doi.org/10.1111/eci.12801.

Bustin, S.A., Nolan, T., 2004. Pitfalls of Quantitative Real-Time Reverse-Transcription Polymerase Chain Reaction. Journal of Biomolecular Techniques: JBT 15, 155–166.

Bustin, S.A., Beaulieu, J.-F., Huggett, J., Jaggi, R., Kibenge, F.S.B., Olsvik, P.A., Penning, L.C., Toegel, S., 2010. MIQE précis: Practical implementation of minimum standard guidelines for fluorescence-based quantitative real-time PCR experiments. BMC Molecular Biology 11, 74. https://doi.org/10.1186/1471-2199-11-74.

Bustin, S.A., Benes, V., Garson, J.A., Hellemans, J., Huggett, J., Kubista, M., Mueller, R., Nolan, T., Pfaffl, M.W., Shipley, G.L., Vandesompele, J., Wittwer, C.T., 2009. The MIQE guidelines: Minimum information for publication of quantitative real-time PCR experiments. Clinical Chemistry 55, 611–622. https://doi.org/10.1373/clinchem.2008.112797.

Cameron, R.C., Duncan, E.J., Dearden, P.K., 2013. Stable reference genes for the measurement of transcript abundance during larval caste development in the honeybee. Apidologie 44, 357–366. https://doi.org/10.1007/s13592-012-0187-0.

Carlson, N.J., Agrawal, A.A., 2023. A nutrition-defence trade-off drives diet choice in a toxic plant generalist. Proceedings of the Royal Society B: Biological Sciences 290, 20230987. https://doi.org/10.1098/rspb.2023.0987.

Carrel, J.E., 1984. Defensive secretion of the pill millipede *Glomeric marginata*: I. Fluid production and storage. Journal of Chemical Ecology 10, 41–51. https://doi.org/10.1007/BF00987642.

Cassels, B.K., 1985. Analysis of a Maasai arrow poison. Journal of Ethnopharmacology 14, 273–281. https://doi.org/10.1016/0378-8741(85)90094-7.

Chahine, S., Seabrooke, S., O'Donnell, M.J., 2012a. Effects of genetic knock-down of organic anion transporter genes on secretion of fluorescent organic ions by Malpighian tubules of *Drosophila melanogaster*. Archives of Insect Biochemistry and Physiology 81, 228–240. https://doi.org/10.1002/arch.21066.

Chahine, S., Campos, A., O'Donnell, M.J., 2012b. Genetic knockdown of a single organic anion transporter alters the expression of functionally related genes in Malpighian tubules of *Drosophila melanogaster*. Journal of Experimental Biology 215, 2601–2610. https://doi.org/10.1242/jeb.071100.

Challis, R.J., Kumar, S., Dasmahapatra, K.K.K., Jiggins, C.D., Blaxter, M., 2016. Lepbase: the Lepidopteran genome database. bioRxiv (preprint). https://doi.org/10.1101/056994.

Chaplin, S.J., 1980. An energetic analysis of host plant selection by the large milkweed bug, *Oncopeltus fasciatus*. Oecologia 46, 254–261. https://doi.org/10.1007/BF00540134.

Chapman, A., 2009. Numbers of living species in Australia and the world: Report for the Australian Biological Resources Study, 2nd ed. Australian Government Department of the Environment, Water, Heritage and the Arts, Canberra.

Chapman, J.R., Waldenström, J., 2015. With Reference to Reference Genes: A Systematic Review of Endogenous Controls in Gene Expression Studies. PLOS One 10, e0141853. https://doi.org/10.1371/journal.pone.0141853.

Chen, J., Duan, Y., Zhou, Y., Yang, Q., 2025. Squeeze pumping of lipids and insecticides by ABCH transporter. Cell 188, 944-957.e19. https://doi.org/10.1016/j.cell.2024.11.033.

Chen, X., Lei, Y., Liang, C., Lei, Q., Wang, J., Jiang, H., 2024. Odorant Binding Protein Expressed in Legs Enhances Malathion Tolerance in *Bactrocera dorsalis* (Hendel). Journal of Agricultural and Food Chemistry 72, 4376–4383. https://doi.org/10.1021/acs.jafc.3c08458.

Chen, X.-Y., Wang, J.-Q., Yang, Y., Li, J., Chen, Z.-S., 2021. Natural Product as Substrates of ABC Transporters: A Review. Recent Patents on Anti-Cancer Drug Discovery 16, 222–238. https://doi.org/10.2174/1574892816666210218220943.

Chipman, A.D., 2017. *Oncopeltus fasciatus* as an evo-devo research organism. Genesis 55. https://doi.org/10.1002/dvg.23020.

Cordon-Cardo, C., O'Brien, J.P., Casals, D., Rittman-Grauer, L., Biedler, J.L., Melamed, M.R., Bertino, J.R., 1989. Multidrug-resistance gene (P-glycoprotein) is expressed by endothelial cells at blood-brain barrier sites. Proceedings of the National Academy of Sciences 86, 695–698. https://doi.org/10.1073/pnas.86.2.695.

Correll, R.N., Eder, P., Burr, A.R., Despa, S., Davis, J., Bers, D.M., Molkentin, J.D., 2014. Overexpression of the Na+/K+ ATPase α2 but not α1 isoform attenuates pathological cardiac hypertrophy and remodeling. Circulation Research 114, 249–256. https://doi.org/10.1161/CIRCRESAHA.114.302293.

Crooks, G.E., Hon, G., Chandonia, J.-M., Brenner, S.E., 2004. WebLogo: a sequence logo generator. Genome Research 14, 1188–1190. https://doi.org/10.1101/gr.849004.

Cui, W., Taub, D.D., Gardner, K., 2007. qPrimerDepot: A primer database for quantitative real time PCR. Nucleic Acids Research 35, D805-9. https://doi.org/10.1093/nar/gkl767.

Culbertson, A.T., Liao, M., 2025. Cryo-EM of human P-glycoprotein reveals an intermediate occluded conformation during active drug transport. Nature Communications 16, 3619. https://doi.org/10.1038/s41467-025-58561-4.

Dalla, S., Dobler, S., 2016. Gene duplications circumvent trade-offs in enzyme function: Insect adaptation to toxic host plants. Evolution 70, 2767–2777. https://doi.org/10.1111/evo.13077.

Dalla, S., Baum, M., Dobler, S., 2017. Substitutions in the cardenolide binding site and interaction of subunits affect kinetics besides cardenolide sensitivity of insect Na,K-ATPase. Insect Biochemistry and Molecular Biology 89, 43–50. https://doi.org/10.1016/j.ibmb.2017.08.005.

Dalla, S., Swarts, H.G.P., Koenderink, J.B., Dobler, S., 2013. Amino acid substitutions of Na,K-ATPase conferring decreased sensitivity to cardenolides in insects compared to mammals. Insect Biochemistry and Molecular Biology 43, 1109–1115. https://doi.org/10.1016/j.ibmb.2013.09.006.

Dassa, E., Bouige, P., 2001. The ABC of ABCS: a phylogenetic and functional classification of ABC systems in living organisms. Research in Microbiology 152, 211–229. https://doi.org/10.1016/s0923-2508(01)01194-9.

Dean, C.A.E., Teets, N.M., Koštál, V., Šimek, P., Denlinger, D.L., 2016. Enhanced stress responses and metabolic adjustments linked to diapause and onset of migration in the large milkweed bug *Oncopeltus fasciatus*. Physiological Entomology 41, 152–161. https://doi.org/10.1111/phen.12140.

Dean, M., Rzhetsky, A., Allikmets, R., 2001. The human ATP-binding cassette (ABC) transporter superfamily. Genome Research 11, 1156–1166. https://doi.org/10.1101/gr.184901.

Dean, M., Annilo, T., 2005. Evolution of the ATP-binding cassette (ABC) transporter superfamily in vertebrates. Annual Review of Genomics and Human Genetics 6, 123–142. https://doi.org/10.1146/annurev.genom.6.080604.162122.

Delignette-Muller, M.L., Dutang, C., 2015. fitdistrplus: An R Package for Fitting Distributions. Journal of Statistical Software 64, 1–34.

Denecke, S., Bảo Lương, H.N., Koidou, V., Kalogeridi, M., Socratous, R., Howe, S., Vogelsang, K., Nauen, R., Batterham, P., Geibel, S., Vontas, J., 2022. Characterization of a novel pesticide transporter and P-glycoprotein orthologues in *Drosophila melanogaster*. Proceedings of the Royal Society B: Biological Sciences 289, 20220625. https://doi.org/10.1098/rspb.2022.0625.

Denecke, S., Rankić, I., Driva, O., Kalsi, M., Luong, N.B.H., Buer, B., Nauen, R., Geibel, S., Vontas, J., 2021. Comparative and functional genomics of the ABC transporter superfamily across arthropods. BMC Genomics 22, 553. https://doi.org/10.1186/s12864-021-07861-2.

Denecke, S., Fusetto, R., Batterham, P., 2017. Describing the role of *Drosophila melanogaster* ABC transporters in insecticide biology using CRISPR-Cas9 knockouts. Insect Biochemistry and Molecular Biology 91, 1–9. https://doi.org/10.1016/j.ibmb.2017.09.017.

Deng, M., Xu, X., Huang, X., Xiao, T., Wang, W., Li, J., Zhao, X., Pan, B., Jiang, Y., He, Z., Yang, Z., Lu, K., 2025. Mechanistic exploration of odorant binding protein-mediated chlorpyrifos resistance in *Nilaparvata lugens*: Insights from insecticide sequestration and transcriptional regulation. International Journal of Biological Macromolecules 284, 138108. https://doi.org/10.1016/j.ijbiomac.2024.138108.

Dermauw, W., van Leeuwen, T., 2014. The ABC gene family in arthropods: comparative genomics and role in insecticide transport and resistance. Insect Biochemistry and Molecular Biology 45, 89–110. https://doi.org/10.1016/j.ibmb.2013.11.001.

DeSalvo, M.K., Hindle, S.J., Rusan, Z.M., Orng, S., Eddison, M., Halliwill, K., Bainton, R.J., 2014. The *Drosophila* surface glia transcriptome: evolutionary conserved blood-brain barrier processes. Frontiers in Neuroscience 8, 346. https://doi.org/10.3389/fnins.2014.00346.

Després, L., David, J.-P., Gallet, C., 2007. The evolutionary ecology of insect resistance to plant chemicals. Trends in Ecology & Evolution 22, 298–307. https://doi.org/10.1016/j.tree.2007.02.010.

Detzel, A., Wink, M., 1995. Evidence for a Cardenolide Carrier in *Oncopeltus fasciatus* (Dallas) (Insecta: Hemiptera). Zeitschrift für Naturforschung C-A Journal of Bioscience 50, 127–134.

Dheda, K., Huggett, J.F., Chang, J.S., Kim, L.U., Bustin, S.A., Johnson, M.A., Rook, G.A.W., Zumla, A., 2005. The implications of using an inappropriate reference gene for real-time reverse transcription PCR data normalization. Analytical Biochemistry 344, 141–143. https://doi.org/10.1016/j.ab.2005.05.022.

Discher, S., Burse, A., Tolzin-Banasch, K., Heinemann, S.H., Pasteels, J.M., Boland, W., 2009. A Versatile Transport Network for Sequestering and Excreting Plant Glycosides in Leaf Beetles Provides an Evolutionary Flexible Defense Strategy. ChemBioChem 10, 2131. https://doi.org/10.1002/cbic.200990059.

Dobler, S., Wagschal, V., Pick, N., Dahdouli, N., Meinzer, F., Romey-Glüsing, R., Petschenka, G., Schuette, K., 2019. New ways to acquire resistance to cardiac glycosides: pyrgomorphid grasshoppers do it differently. Proceedings of the Royal Society B: Biological Sciences. https://doi.org/10.1098/rspb.2019.0883.

Dobler, S., Petschenka, G., Wagschal, V., Flacht, L., 2015. Convergent adaptive evolution - how insects master the challenge of cardiac glycoside-containing host plants. Entomologia Experimentalis et Applicata 157, 30–39. https://doi.org/10.1111/eea.12340.

Dobler, S., Dalla, S., Wagschal, V., Agrawal, A.A., 2012. Community-wide convergent evolution in insect adaptation to toxic cardenolides by substitutions in the Na,K-ATPase. Proceedings of the National Academy of Sciences of the United States of America 109, 13040–13045. https://doi.org/10.1073/pnas.1202111109.

Dobler, S., Petschenka, G., Pankoke, H., 2011. Coping with toxic plant compounds--the insect's perspective on iridoid glycosides and cardenolides. Phytochemistry 72, 1593–1604. https://doi.org/10.1016/j.phytochem.2011.04.015.

Dobler, S., Daloze, D., Pasteels, J.M., 1998. Sequestration of plant compounds in a leaf beetle's defensive secretion: cardenolides in *Chrysochus*. Chemoecology 8, 111–118. https://doi.org/10.1007/s000490050015.

Dobler, S., Mardulyn, P., Pasteels, J.M., Rowell-Rahier, M., 1996. Host-plant switches and the evolution of chemical defense and life history in the leaf beetle genus *Oreina*. Evolution 50, 2373–2386. https://doi.org/10.1111/j.1558-5646.1996.tb03625.x.

2026. Dokumentation UHHGPT. version 5.1.

Dreisbach, D., Bhandari, D.R., Betz, A., Tenbusch, L., Vilcinskas, A., Spengler, B., Petschenka, G., 2023. Spatial metabolomics reveal divergent cardenolide processing in the monarch (*Danaus plexippus*) and the common crow butterfly (*Euploea core*). Molecular Ecology Resources 23, 1195–1210. https://doi.org/10.1111/1755-0998.13786.

Duffey, S.S., 1980. Sequestration of Plant Natural Products by Insects. Annual Review of Entomology 25, 447–477. https://doi.org/10.1146/annurev.en.25.010180.002311.

Duffey, S.S., 1970. Cardiac Glycosides and Distastefulness: Some Observations on the Palatability Spectrum of Butterflies. Science 169, 78–79. https://doi.org/10.1126/science.169.3940.78.

Duffey, S.S., Scudder, G.G.E., 1974. Cardiac glycosides in *Oncopeltus fasciatus* (Dallas) (Hemiptera: Lygaeidae). I. The uptake and distribution of natural cardenolides in the body. Canadian Journal of Zoology 52, 283–290. https://doi.org/10.1139/z74-035.

Duffey, S.S., Scudder, G., 1972. Cardiac glycosides in North American Asclepiadaceae, a basis for unpalatability in brightly coloured Hemiptera and Coleoptera. Journal of Insect Physiology 18, 63–78. https://doi.org/10.1016/0022-1910(72)90065-0.

Duffey, S.S., Blum, M.S., Isman, M.B., Scudder, G., 1978. Cardiac glycosides: A physical system for their sequestration by the milkweed bug. Journal of Insect Physiology 24, 639–645. https://doi.org/10.1016/0022-1910(78)90127-0.

Dunton, A.D., Göpel, T., Ho, D.H., Burggren, W., 2021. Form and Function of the Vertebrate and Invertebrate Blood-Brain Barriers. International Journal of Molecular Sciences 22. https://doi.org/10.3390/ijms222212111.

Eder, M., Mehnert, W., 2000. Pflanzliche Begleitstoffe — wertvolle Hilfsstoffe oder überflüssiger Ballast? Pharmazie in unserer Zeit 29, 377–384.

Eggermann, W., Bongers, J., 1971. Wasser- und Nahrungsaufnahme and Pflanzen unter besonderer Berücksichtigung der Wirtsspezifität von *Oncopeltus fasciatus* Dallas. Oecologia 6, 303–317. https://doi.org/10.1007/BF00389105.

Ehrlich, P.R., Raven, P.H., 1964. Butterflies and Plants: A Study in Coevolution. Evolution 18, 586–608. https://doi.org/10.1111/j.1558-5646.1964.tb01674.x.

Eisner, T., Meinwald, J., 1966. Defensive secretions of arthropods. Science 153, 1341–1350. https://doi.org/10.1126/science.153.3742.1341.

Erb, M., Robert, C.A.M., 2016. Sequestration of plant secondary metabolites by insect herbivores: molecular mechanisms and ecological consequences. Current Opinion in Insect Science 14, 8–11. https://doi.org/10.1016/j.cois.2015.11.005.

Euw, J. von, Fishelson, L., Parsons, J.A., Reichstein, T., Rothschild, M., 1967. Cardenolides (heart poisons) in a grasshopper feeding on milkweeds. Nature 214, 35–39.

Everaert, C., Luypaert, M., Maag, J.L.V., Cheng, Q.X., Dinger, M.E., Hellemans, J., Mestdagh, P., 2017. Benchmarking of RNA-sequencing analysis workflows using whole-transcriptome RT-qPCR expression data. Scientific Reports 7, 1559. https://doi.org/10.1038/s41598-017-01617-3.

Ewen-Campen, B., Jones, T.E.M., Extavour, C.G., 2013. Evidence against a germ plasm in the milkweed bug Oncopeltus fasciatus, a hemimetabolous insect. Biology Open 2, 556–568. https://doi.org/10.1242/bio.20134390.

Farrell, B.D., 1998. "Inordinate Fondness" Explained: Why Are There So Many Beetles? Science 281, 555–559. https://doi.org/10.1126/science.281.5376.555.

Feir, D., 1974. *Oncopeltus Fasciatus*: A Research Animal. Annual Review of Entomology 19, 81–96. https://doi.org/10.1146/annurev.en.19.010174.000501.

Fink, L.S., Brower, L.P., 1981. Birds can overcome the cardenolide defence of monarch butterflies in Mexico. Nature 291, 67–70. https://doi.org/10.1038/291067a0.

Fox, J., Weisberg, S., 2011. An {R} Companion to Applied Regression, 2nd ed. Sage, Thousand Oaks, USA.

Francescutti, C.M., Martin, A., Hanly, J.J., 2022. Knockdowns of red Malphigian tubules reveal pigmentation roles in the milkweed bug. Journal of Experimental Zoology. Part B, Molecular and Developmental Evolution 338, 382–387. https://doi.org/10.1002/jez.b.23123.

Freedman, M.G., Choquette, S.-L., Ramírez, S.R., Strauss, S.Y., Hunter, M.D., Vannette, R.L., 2021. Population-specific patterns of toxin sequestration in monarch butterflies from around the world. bioRxiv. https://doi.org/10.1101/2021.10.15.464593.

Futuyma, D.J., Keese, M.C., 1992. Evolution and coevolution of plants and phytophagous arthropods, in: Rosenthal, G.A., Berenbaum, M.R. (Eds.), Herbivores: Their interactions with secondary plant metabolites. Academic Press, San Diego, USA, pp. 440–475.

Gathemann, S., 2017. Aufreinigung sequestrierter Cardenolide von *Danaus plexippus* und Charakterisierung über NMR Spektroskopie. Thesis, Bachelor of Science. Hamburg.

Georges, E., Bradley, G., Gariepy, J., Ling, V., 1990. Detection of P-glycoprotein isoforms by gene-specific monoclonal antibodies. Proceedings of the National Academy of Sciences 87, 152–156. https://doi.org/10.1073/pnas.87.1.152.

Gerard, L., Gillet, J.-P., 2024. The uniqueness of ABCB5 as a full transporter ABCB5FL and a half-transporter-like ABCB5β. Cancer Drug Resistance 7, 29. https://doi.org/10.20517/cdr.2024.56.

Gerrard, B., Stewart, C., Dean, M., 1993. Analysis of Mdr50: a *Drosophila* P-glycoprotein/multidrug resistance gene homolog. Genomics 17, 83–88. https://doi.org/10.1006/geno.1993.1286.

Ginzburg, N., Cohen, M., Chipman, A.D., 2017. Factors involved in early polarization of the anterior-posterior axis in the milkweed bug *Oncopeltus fasciatus*. Genesis 55. https://doi.org/10.1002/dvg.23027.

Glendinning, J.I., 1992. Effectiveness of cardenolides as feeding deterrents to Peromyscus mice. Journal of Chemical Ecology 18, 1559–1575. https://doi.org/10.1007/BF00993229.

Gordon, H.T., Gordon, B.R., (Keine Angabe), 1971. Milkweed bug mutants on sunflower seed: viability and eye-color interactions. Journal of Heredity 62, 315–316. https://doi.org/10.1093/oxfordjournals.jhered.a108181.

Götz, S., García-Gómez, J.M., Terol, J., Williams, T.D., Nagaraj, S.H., Nueda, M.J., Robles, M., Talón, M., Dopazo, J., Conesa, A., 2008. High-throughput functional annotation and data mining with the Blast2GO suite. Nucleic Acids Research 36, 3420–3435. https://doi.org/10.1093/nar/gkn176.

Gozalpour, E., Wittgen, H.G.M., van den Heuvel, J.J.M.W., Greupink, R., Russel, F.G.M., Koenderink, J.B., 2013. Interaction of digitalis-like compounds with p-glycoprotein. Toxicological Sciences 131, 502–511. https://doi.org/10.1093/toxsci/kfs307.

Graaf, D. de, Sharma, R.C., Mechetner, E.B., Schimke, R.T., Roninson, I.B., 1996. P-glycoprotein confers methotrexate resistance in 3T6 cells with deficient carrier-mediated methotrexate uptake. Proceedings of the National Academy of Sciences 93, 1238–1242. https://doi.org/10.1073/pnas.93.3.1238.

Grabherr, M.G., Haas, B.J., Yassour, M., Levin, J.Z., Thompson, D.A., Amit, I., Adiconis, X., Fan, L., Raychowdhury, R., Zeng, Q., Chen, Z., Mauceli, E., Hacohen, N., Gnirke, A., Rhind, N., Di Palma, F., Birren, B.W., Nusbaum, C., Lindblad-Toh, K.,…Regev, A., 2011. Full-length transcriptome assembly from RNA-Seq data without a reference genome. Nature Biotechnology 29, 644–652. https://doi.org/10.1038/nbt.1883.

Groen, S.C., LaPlante, E.R., Alexandre, N.M., Agrawal, A.A., Dobler, S., Whiteman, N.K., 2017. Multidrug transporters and organic anion transporting polypeptides protect insects against the toxic effects of cardenolides. Insect Biochemistry and Molecular Biology 81, 51–61. https://doi.org/10.1016/j.ibmb.2016.12.008.

Guillaume, F., Otto, S.P., 2012. Gene functional trade-offs and the evolution of pleiotropy. Genetics 192, 1389–1409. https://doi.org/10.1534/genetics.112.143214.

Haas, B.J., Papanicolaou, A., Yassour, M., Grabherr, M., Blood, P.D., Bowden, J., Couger, M.B., Eccles, D., Li, B., Lieber, M., MacManes, M.D., Ott, M., Orvis, J., Pochet, N., Strozzi, F., Weeks, N., Westerman, R., William, T., Dewey, C.N.,…Regev, A., 2013. De novo transcript sequence reconstruction from RNA-seq using the Trinity platform for reference generation and analysis. Nature Protocols 8, 1494–1512. https://doi.org/10.1038/nprot.2013.084.

Hagenbuch, B., Gao, B., Meier, P.J., 2002. Transport of xenobiotics across the blood-brain barrier. Physiology 17, 231–234. https://doi.org/10.1152/nips.01402.2002.

Hall, T.A., 1999. BioEdit: A User-Friendly Biological Sequence Alignment Editor and Analysis Program for Windows 95/98/NT. Nucleic Acids Symposium Series 41, 95–98.

Hashimoto, N., Nakamichi, N., Uwafuji, S., Yoshida, K., Sugiura, T., Tsuji, A., Kato, Y., 2013. ATP binding cassette transporters in two distinct compartments of the skin contribute to transdermal absorption of a typical substrate. Journal of Controlled Release 165, 54–61. https://doi.org/10.1016/j.jconrel.2012.10.011.

He, J., Fortunati, E., Liu, D.-X., Li, Y., 2021. Pleiotropic Roles of ABC Transporters in Breast Cancer. International Journal of Molecular Sciences 22. https://doi.org/10.3390/ijms22063199.

Hellemans, J., Mortier, G., Paepe, A. de, Speleman, F., Vandesompele, J., 2007. qBase relative quantification framework and software for management and automated analysis of real-time quantitative PCR data. Genome Biology 8, R19. https://doi.org/10.1186/gb-2007-8-2-r19.

Herbertz, M., Lohr, C., Dobler, S., 2025. The large milkweed bugs' Na,K-ATPase β-subunits colocalize with septate junction proteins in a tissue-specific manner. Cell and Tissue Research 400, 347–363. https://doi.org/10.1007/s00441-025-03965-3.

Herbertz, M., Dalla, S., Wagschal, V., Turjalei, R., Heiser, M., Dobler, S., 2024. Coevolutionary escalation led to differentially adapted paralogs of an insect's Na,K-ATPase optimizing resistance to host plant toxins. Molecular Ecology 33, e17041. https://doi.org/10.1111/mec.17041.

Herbertz, M., Lohr, J., Lohr, C., Dobler, S., 2023. Knockdown of Na,K-ATPase β-subunits in *Oncopeltus fasciatus* induces molting problems and alterations in tracheal morphology. Insect Science 30, 375–397. https://doi.org/10.1111/1744-7917.13117.

Herbertz, M., Harder, S., Schlüter, H., Lohr, C., Dobler, S., 2022. Na,K-ATPase α1 and β-subunits show distinct localizations in the nervous tissue of the large milkweed bug. Cell and Tissue Research 388, 503–519. https://doi.org/10.1007/s00441-022-03580-6.

Heyworth, H.C., Pokharel, P., Blount, J.D., Mitchell, C., Petschenka, G., Rowland, H.M., 2023. Antioxidant availability trades off with warning signals and toxin sequestration in the large milkweed bug (*Oncopeltus fasciatus*). Ecology and Evolution 13, e9971. https://doi.org/10.1002/ece3.9971.

Higgins, C.F., 1992. ABC transporters: from microorganisms to man. Annual Review of Cell Biology 8, 67–113. https://doi.org/10.1146/annurev.cb.08.110192.000435.

Hill, D.E., 2006. Learned avoidance of the large milkweed bug (Hemiptera, Lygaeidae, *Oncopeltus fasciatus*) by jumping spiders (Araneae, Salticidae, *Phidippus*). Peckhamia 1, 1–21.

Hixson, B., Bing, X.-L., Yang, X., Bonfini, A., Nagy, P., Buchon, N., 2022. A transcriptomic atlas of *Aedes aegypti* reveals detailed functional organization of major body parts and gut regional specializations in sugar-fed and blood-fed adult females. eLife 11. https://doi.org/10.7554/eLife.76132.

Hoffmeyer, S., Burk, O., Richter, O. von, Arnold, H.P., Brockmöller, J., Johne, A., Cascorbi, I., Gerloff, T., Roots, I., Eichelbaum, M., Brinkmann, U., 2000. Functional polymorphisms of the human multidrug-resistance gene: multiple sequence variations and correlation of one allele with P-glycoprotein expression and activity in vivo. Proceedings of the National Academy of Sciences 97, 3473–3478. https://doi.org/10.1073/pnas.97.7.3473.

Hood, C.W., 1937. The anatomy of the digestive system of *Oncopeltus fasciatus* Dall.(Heteroptera: Lygaeidae). Ohio Journal of Science 37, 151–160.

Horisberger, J.-D., 2004. Recent insights into the structure and mechanism of the sodium pump. Physiology 19, 377–387. https://doi.org/10.1152/physiol.00013.2004.

Horton, P., Park, K.-J., Obayashi, T., Fujita, N., Harada, H., Adams-Collier, C.J., Nakai, K., 2007. WoLF PSORT: protein localization predictor. Nucleic Acids Research 35, W585-7. https://doi.org/10.1093/nar/gkm259.

Huggett, J., Dheda, K., Bustin, S., Zumla, A., 2005. Real-time RT-PCR normalisation; strategies and considerations. Genes and Immunity 6, 279–284. https://doi.org/10.1038/sj.gene.6364190.

Hughes, J., Crowe, A., 2010. Inhibition of P-glycoprotein-mediated efflux of digoxin and its metabolites by macrolide antibiotics. Journal of Pharmacological Sciences 113, 315–324. https://doi.org/10.1254/jphs.10109fp.

Hull, J.J., Chaney, K., Geib, S.M., Fabrick, J.A., Brent, C.S., Walsh, D., Lavine, L.C., 2014. Transcriptome-based identification of ABC transporters in the western tarnished plant bug *Lygus hesperus*. PLOS One 9, e113046. https://doi.org/10.1371/journal.pone.0113046.

Hwang, J.-U., Song, W.-Y., Hong, D., Ko, D., Yamaoka, Y., Jang, S., Yim, S., Lee, E., Khare, D., Kim, K., Palmgren, M., Yoon, H.S., Martinoia, E., Lee, Y., 2016. Plant ABC Transporters Enable Many Unique Aspects of a Terrestrial Plant's Lifestyle. Molecular Plant 9, 338–355. https://doi.org/10.1016/j.molp.2016.02.003.

Igarashi, Y., 2004. The Evolutionary Repertoires of the Eukaryotic-Type ABC Transporters in Terms of the Phylogeny of ATP-binding Domains in Eukaryotes and Prokaryotes. Molecular Biology and Evolution 21, 2149–2160. https://doi.org/10.1093/molbev/msh226.

Ishigami, M., Tominaga, Y., Nagao, K., Kimura, Y., Matsuo, M., Kioka, N., Ueda, K., 2013. ATPase activity of nucleotide binding domains of human MDR3 in the context of MDR1. Biochimica et

Biophysica Acta (BBA) - Molecular and Cell Biology of Lipids 1831, 683–690. https://doi.org/10.1016/j.bbalip.2012.12.016.

Isman, M.B., Duffey, S.S., Scudder, G.E., 1977. Variation in cardenolide content of the lygaeid bugs, *Oncopeltus fasciatus* and *Lygaeus kalmii kalmii* and of their milkweed hosts (*Asclepias* spp.) in central California. Journal of Chemical Ecology 3, 613–624.

Isman, M.B., 1977. Dietary influence of cardenolides on larval growth and development of the milkweed bug *Oncopeltus fasciatus*. Journal of Insect Physiology 23, 1183–1187. https://doi.org/10.1016/0022-1910(77)90151-2.

Ito, K., Nguyen, H.T., Kato, Y., Wakayama, T., Kubo, Y., Iseki, S., Tsuji, A., 2008. P-glycoprotein (Abcb1) is involved in absorptive drug transport in skin. Journal of Controlled Release 131, 198–204. https://doi.org/10.1016/j.jconrel.2008.08.004.

Jeckel, A.M., Beran, F., Züst, T., Younkin, G., Petschenka, G., Pokharel, P., Dreisbach, D., Ganal-Vonarburg, S.C., Robert, C.A.M., 2022. Metabolization and sequestration of plant specialized metabolites in insect herbivores: Current and emerging approaches. Frontiers in Physiology 13, 1001032. https://doi.org/10.3389/fphys.2022.1001032.

Jin, M., Cheng, Y., Guo, X., Li, M., Chakrabarty, S., Liu, K., Wu, K., Xiao, Y., 2020. Down-regulation of lysosomal protein ABCB6 increases gossypol susceptibility in *Helicoverpa armigera*. Insect Biochemistry and Molecular Biology 122, 103387. https://doi.org/10.1016/j.ibmb.2020.103387.

Johansson, A.S., 1957. The nervous system of the milkweed bug, *Oncopeltus fasciatus* (Dallas) (Heteroptera, Lygaeidae). Transactions of the American Entomological Society (1890-) 83, 119–183.

Jones, C.G., Hoggard, M.P., Blum, M.S., 1983. Is sequestration structure-specific in the milkweed bug, *Oncopeltus fasciatus*? Comparative Biochemistry and Physiology. C, Comparative Pharmacology 76, 283–284. https://doi.org/10.1016/0742-8413(83)90079-8.

Jones, P.L., Petschenka, G., Flacht, L., Agrawal, A.A., 2019. Cardenolide Intake, Sequestration, and Excretion by the Monarch Butterfly along Gradients of Plant Toxicity and Larval Ontogeny. Journal of Chemical Ecology 45, 264–277. https://doi.org/10.1007/s10886-019-01055-7.

Joshi, N.A., Fass, J.N., 2011. Sickle: A sliding-window, adaptive, quality-based trimming tool for FastQ files.

Juliano, R.L., Ling, V., 1976. A surface glycoprotein modulating drug permeability in Chinese hamster ovary cell mutants. Biochimica et Biophysica Acta (BBA) 455, 152–162. https://doi.org/10.1016/0005-2736(76)90160-7.

Kalyaanamoorthy, S., Minh, B.Q., Wong, T.K.F., Haeseler, A. von, Jermiin, L.S., 2017. ModelFinder: fast model selection for accurate phylogenetic estimates. Nature Methods 14, 587–589. https://doi.org/10.1038/nmeth.4285.

Kamal, M., Tokmakjian, L., Knox, J., Han, D., Moshiri, H., Magomedova, L., Nguyen, K.C., Zheng, H., Burns, A.R., Cooke, B., Lacoste, J., Yeo, M., Hall, D.H., Cummins, C.L., Roy, P.J., 2023. PGP-14 establishes a polar lipid permeability barrier within the C. elegans pharyngeal cuticle. PLOS Genetics 19, e1011008. https://doi.org/10.1371/journal.pgen.1011008.

Kamimoto, Y., Terasaka, K., Hamamoto, M., Takanashi, K., Fukuda, S., Shitan, N., Sugiyama, A., Suzuki, H., Shibata, D., Wang, B., Pollmann, S., Geisler, M., Yazaki, K., 2012. *Arabidopsis* ABCB21 is a Facultative Auxin Importer/Exporter Regulated by Cytoplasmic Auxin Concentration. Plant and Cell Physiology 53, 2090–2100. https://doi.org/10.1093/pcp/pcs149.

Kanai, R., Cornelius, F., Vilsen, B., Toyoshima, C., 2022. Cryoelectron microscopy of Na+,K+-ATPase in the two E2P states with and without cardiotonic steroids. Proceedings of the National Academy of Sciences of the United States of America 119, e2123226119. https://doi.org/10.1073/pnas.2123226119.

Kapustin, Y., Souvorov, A., Tatusova, T., Lipman, D., 2008. Splign: algorithms for computing spliced alignments with identification of paralogs. Biology direct 3, 20. https://doi.org/10.1186/1745-6150-3-20.

Karageorgi, M., Groen, S.C., Sumbul, F., Pelaez, J.N., Verster, K.I., Aguilar, J.M., Hastings, A.P., Bernstein, S.L., Matsunaga, T., Astourian, M., Guerra, G., Rico, F., Dobler, S., Agrawal, A.A., Whiteman, N.K., 2019. Genome editing retraces the evolution of toxin resistance in the monarch butterfly. Nature 574, 409–412. https://doi.org/10.1038/s41586-019-1610-8.

Karunaratne, S.H., Jayawardena, K.G., Hemingway, J., Ketterman, A.J., 1993. Characterization of a B-type esterase involved in insecticide resistance from the mosquito *Culex quinquefasciatus*. Biochemical Journal 294 (Pt 2), 575–579. https://doi.org/10.1042/bj2940575.

Kassambara, A., 2018. ggpubr: 'ggplot2' Based Publication Ready Plots.

Katoh, K., Rozewicki, J., Yamada, K.D., 2019. MAFFT online service: multiple sequence alignment, interactive sequence choice and visualization. Briefings in Bioinformatics 20, 1160–1166. https://doi.org/10.1093/bib/bbx108.

Katti, R., Kozarich, A.M., Mensah, G.A.K., Bartlett, M.G., 2025. Elucidating the Complex Structural and Molecular Mechanisms Driving P-Glycoprotein-Mediated Transport of Cardiac Glycosides. International Journal of Molecular Sciences 26. https://doi.org/10.3390/ijms26167813.

Kelley, L.A., Mezulis, S., Yates, C.M., Wass, M.N., Sternberg, M.J.E., 2015. The Phyre2 web portal for protein modeling, prediction and analysis. Nature Protocols 10, 845–858. https://doi.org/10.1038/nprot.2015.053.

Kim, S., Chen, J., Cheng, T., Gindulyte, A., He, J., He, S., Li, Q., Shoemaker, B.A., Thiessen, P.A., Yu, B., Zaslavsky, L., Zhang, J., Bolton, E.E., 2025. PubChem 2025 update. Nucleic Acids Research 53, D1516-D1525. https://doi.org/10.1093/nar/gkae1059.

Kiss, K., Kucsma, N., Brozik, A., Tusnady, G.E., Bergam, P., van Niel, G., Szakacs, G., 2015. Role of the N-terminal transmembrane domain in the endo-lysosomal targeting and function of the human ABCB6 protein. Biochemical Journal 467, 127–139. https://doi.org/10.1042/BJ20141085.

Kitamura, Y., Kusuhara, H., Sugiyama, Y., 2010. Functional Characterization of Multidrug Resistance-Associated Protein 3 (Mrp3/Abcc3) in the Basolateral Efflux of Glucuronide Conjugates in the Mouse Small Intestine. The Journal of Pharmacology and Experimental Therapeutics 332, 659–666. https://doi.org/10.1124/jpet.109.156943.

Klausner, E., Miller, E.R., Dingle, H., 1980. *Nerium oleander* as an alternative host plant for south Florida milkweed bugs, *Oncopeltus fasciatus*. Ecological Entomology 5, 137–142. https://doi.org/10.1111/j.1365-2311.1980.tb01134.x.

Klimanova, E.A., Tverskoi, A.M., Koltsova, S.V., Sidorenko, S.V., Lopina, O.D., Tremblay, J., Hamet, P., Kapilevich, L.V., Orlov, S.N., 2017. Time- and dose dependent actions of cardiotonic steroids on transcriptome and intracellular content of Na+ and K+: A comparative analysis. Scientific Reports 7, 45403. https://doi.org/10.1038/srep45403.

Koenig, C., Bretschneider, A., Heckel, D.G., Grosse-Wilde, E., Hansson, B.S., Vogel, H., 2015. The plastic response of *Manduca sexta* to host and non-host plants. Insect Biochemistry and Molecular Biology 63, 72–85. https://doi.org/10.1016/j.ibmb.2015.06.001.

Koltsova, S.V., Trushina, Y., Haloui, M., Akimova, O.A., Tremblay, J., Hamet, P., Orlov, S.N., 2012. Ubiquitous Na+i/K+i-sensitive transcriptome in mammalian cells: evidence for Ca(2+)i-independent excitation-transcription coupling. PLOS One 7, e38032. https://doi.org/10.1371/journal.pone.0038032.

Koressaar, T., Remm, M., 2007. Enhancements and modifications of primer design program Primer3. Bioinformatics 23, 1289–1291. https://doi.org/10.1093/bioinformatics/btm091.

Kowalski, P., Baum, M., Körten, M., Donath, A., Dobler, S., 2020. ABCB transporters in a leaf beetle respond to sequestered plant toxins. Proceedings of the Royal Society B: Biological Sciences 287, 20201311. https://doi.org/10.1098/rspb.2020.1311.

Kozera, B., Rapacz, M., 2013. Reference genes in real-time PCR. Journal of Applied Genetics 54, 391–406. https://doi.org/10.1007/s13353-013-0173-x.

Krenn, L., Kopp, B., 1998. Bufadienolides from animal and plant sources. Phytochemistry 48, 1–29. https://doi.org/10.1016/S0031-9422(97)00426-3.

Krogh, A., Larsson, B., Heijne, G. von, Sonnhammer, E.L., 2001. Predicting transmembrane protein topology with a hidden Markov model: application to complete genomes. Journal of Molecular Biology 305, 567–580. https://doi.org/10.1006/jmbi.2000.4315.

Krueger, A.J., Rault, L.C., Robinson, E.A., Weissling, T.J., Vélez, A.M., Anderson, T.D., 2022. Pyrethroid insecticide and milkweed cardenolide interactions on detoxification enzyme activity and expression in monarch caterpillars. Pesticide Biochemistry and Physiology 187, 105173. https://doi.org/10.1016/j.pestbp.2022.105173.

Kubista, M., Sindelka, R., Tichopad, A., Bergkvist, A., Lindh, D., Forootan, A., 2007. The Prime Technique: Real-time PCR Data Analysis. G.I.T. Laboratory Journal 11, 33–35.

Kullak-Ublick, G.A., Ismair, M.G., Stieger, B., Landmann, L., Huber, R., Pizzagalli, F., Fattinger, K., Meier, P.J., Hagenbuch, B., 2001. Organic anion-transporting polypeptide B (OATP-B) and its functional comparison with three other OATPs of human liver. Gastroenterology 120, 525–533. https://doi.org/10.1053/gast.2001.21176.

Kumar, P., Pandit, S.S., Steppuhn, A., Baldwin, I.T., 2014. Natural history-driven, plant-mediated RNAi-based study reveals CYP6B46's role in a nicotine-mediated antipredator herbivore defense. Proceedings of the National Academy of Sciences of the United States of America 111, 1245–1252. https://doi.org/10.1073/pnas.1314848111.

Kumar, S., Stecher, G., Tamura, K., 2016. MEGA7: Molecular Evolutionary Genetics Analysis Version 7.0 for Bigger Datasets. Molecular Biology and Evolution 33, 1870–1874. https://doi.org/10.1093/molbev/msw054.

Labbé, R., Caveney, S., Donly, C., 2011a. Genetic analysis of the xenobiotic resistance-associated ABC gene subfamilies of the Lepidoptera. Insect Molecular Biology 20, 243–256. https://doi.org/10.1111/j.1365-2583.2010.01064.x.

Labbé, R., Caveney, S., Donly, C., 2011b. Expression of multidrug resistance proteins is localized principally to the Malpighian tubules in larvae of the cabbage looper moth, *Trichoplusia ni*. Journal of Experimental Biology 214, 937–944. https://doi.org/10.1242/jeb.051060.

Langmann, T., Mauerer, R., Zahn, A., Moehle, C., Probst, M., Stremmel, W., Schmitz, G., 2003. Real-time reverse transcription-PCR expression profiling of the complete human ATP-binding cassette transporter superfamily in various tissues. Clinical Chemistry 49, 230–238. https://doi.org/10.1373/49.2.230.

Lanning, C.L., Fine, R.L., Corcoran, J.J., Ayad, H.M., Rose, R.L., Abou-Donia, M.B., 1996. Tobacco budworm P-glycoprotein: biochemical characterization and its involvement in pesticide resistance. Biochimica et Biophysica Acta (BBA) - General Subjects 1291, 155–162. https://doi.org/10.1016/0304-4165(96)00060-8.

Laurell, H., Iacovoni, J.S., Abot, A., Svec, D., Maoret, J.-J., Arnal, J.-F., Kubista, M., 2012. Correction of RT–qPCR data for genomic DNA-derived signals with ValidPrime. Nucleic Acids Research 40, e51-e51. https://doi.org/10.1093/nar/gkr1259.

Laursen, M., Gregersen, J.L., Yatime, L., Nissen, P., Fedosova, N.U., 2015. Structures and characterization of digoxin- and bufalin-bound Na+,K+-ATPase compared with the ouabain-bound complex. Proceedings of the National Academy of Sciences of the United States of America 112, 1755–1760. https://doi.org/10.1073/pnas.1422997112.

Lee, M., Choi, Y., Burla, B., Kim, Y.-Y., Jeon, B., Maeshima, M., Yoo, J.-Y., Martinoia, E., Lee, Y., 2008. The ABC transporter AtABCB14 is a malate importer and modulates stomatal response to CO2. Nature Cell Biology 10, 1217–1223. https://doi.org/10.1038/ncb1782.

Lenth, R. emmeans: Estimated Marginal Means, aka Least-Squares Means: R package version 1.10.7-100001.

Letunic, I., Bork, P., 2016. Interactive tree of life (iTOL) v3: an online tool for the display and annotation of phylogenetic and other trees. Nucleic Acids Research 44, W242-5. https://doi.org/10.1093/nar/gkw290.

Levy, S., Kafri, M., Carmi, M., Barkai, N., 2011. The competitive advantage of a dual-transporter system. Science 334, 1408–1412. https://doi.org/10.1126/science.1207154.

Li, Z., Zhang, M., Qiao, L., Du, Z., Gbeinbo, F.L., Yao, Z., Zhu, G., He, Y., 2025. Knockdown of Oatp and Mdr Transporter Genes Enhances Cardenolide Toxicity to the Noncardenolide Feeder, *Nilaparvata lugens*. Journal of Agricultural and Food Chemistry 73, 8833–8841. https://doi.org/10.1021/acs.jafc.4c13080.

Liang, L., Jin, L., Mao, F., Fan, C., Kong, H., Zhang, Z., Pan, Y., Shang, Q., 2025. Fat body specific ABCG3 accounts for xenobiotic tolerance and is regulated by the homeobox transcription factor Bcd in *Spodoptera litura*. Pesticide Biochemistry and Physiology 215, 106650. https://doi.org/10.1016/j.pestbp.2025.106650.

Lingrel, J.B., Orlowski, J., Shull, M.M., Price, E.M., 1990. Molecular Genetics of Na,K-ATPase. Progress in Nucleic Acid Research and Molecular Biology 38, 37–89. https://doi.org/10.1016/S0079-6603(08)60708-4.

Linton, K.J., Higgins, C.F., 2007. Structure and function of ABC transporters: the ATP switch provides flexible control. Pflügers Archiv: European Journal of Physiology 453, 555–567. https://doi.org/10.1007/s00424-006-0126-x.

Lisiecki, A., 2018. Untersuchung von ABCB-Volltransportern in der Milchkrautwanze *Oncopeltus fasciatus* und rekombinante Expression von OfABCB1. Thesis, Master of Science. Hamburg.

Liu, B., Sun, D., Xia, W., Hung, M.C., Yu, D., 1997. Cross-reactivity of C219 anti-p170(mdr-1) antibody with p185(c-erbB2) in breast cancer cells: cautions on evaluating p170(mdr-1). Journal of the National Cancer Institute 89, 1524–1529.

Liu, P., Kaufman, T.C., 2009. Morphology and husbandry of the large milkweed bug, *Oncopeltus fasciatus*. Cold Spring Harbor protocols 2009, pdb.emo127. https://doi.org/10.1101/pdb.emo127.

Liu, S., Zhou, S., Tian, L., Guo, E., Luan, Y., Zhang, J., Li, S., 2011. Genome-wide identification and characterization of ATP-binding cassette transporters in the silkworm, *Bombyx mori*. BMC Genomics 12, 491. https://doi.org/10.1186/1471-2164-12-491.

Livak, K.J., Schmittgen, T.D., 2001. Analysis of relative gene expression data using real-time quantitative PCR and the 2-ΔΔCT Method. Methods 25, 402–408. https://doi.org/10.1006/meth.2001.1262.

Lohr, J.N., Meinzer, F., Dalla, S., Romey-Glüsing, R., Dobler, S., 2017. The function and evolutionary significance of a triplicated Na,K-ATPase gene in a toxin-specialized insect. BMC Evolutionary Biology 17, 256. https://doi.org/10.1186/s12862-017-1097-6.

López-Goldar, X., Agrawal, A.A., 2023. Tissue and toxin-specific divergent evolution in plant defense Evolución divergente específica de tejido y toxina en defensa de plantas. Evolution 77, 2431–2441. https://doi.org/10.1093/evolut/qpad155.

Löscher, W., Gericke, B., 2020. Novel Intrinsic Mechanisms of Active Drug Extrusion at the Blood-Brain Barrier: Potential Targets for Enhancing Drug Delivery to the Brain? Pharmaceutics 12. https://doi.org/10.3390/pharmaceutics12100966.

Luckner, M., Wichtl, M., 2000. Digitalis: Geschichte, Biologie, Biochemie, Chemie, Physiologie, Molekularbiologie, Pharmakologie, medizinische Anwendung. Handbuch für Ärzte, Apotheker und andere Naturwissenschaftler. Wissenschaftliche Verlagsgesellschaft, Stuttgart, Germany.

Lv, Y., Wang, P., Wei, Z., Yang, X., 2025. Molecular mechanism of ATP-binding cassette transporter-mediated insecticide resistance. New Plant Protection, e70018. https://doi.org/10.1002/npp2.70018.

Lynch, M., Marinov, G.K., 2015. The bioenergetic costs of a gene. Proceedings of the National Academy of Sciences of the United States of America 112, 15690–15695. https://doi.org/10.1073/pnas.1514974112.

Malcolm, S.B., 1991. Cardenolide-Mediated Interactions between Plants and Herbivores, in: Rosenthal, G.A., Berenbaum, M.R. (Eds.), Herbivores: Their Interactions with Secondary Plant Metabolites, 2nd ed. Elsevier Science, Oxford, pp. 251–296.

Marquez, B., van Bambeke, F., 2011. ABC multidrug transporters: target for modulation of drug pharmacokinetics and drug-drug interactions. Current Drug Targets 12, 600–620. https://doi.org/10.2174/138945011795378504.

Mathew, L.G., Ponnuraj, J., Mallappa, B., Chowdary, L.R., Zhang, J., Tay, W.T., Walsh, T.K., Gordon, K.H.J., Heckel, D.G., Downes, S., Carrière, Y., Li, X., Tabashnik, B.E., Fabrick, J.A., 2018. ABC transporter mis-splicing associated with resistance to Bt toxin Cry2Ab in laboratory- and field-selected pink bollworm. Scientific Reports 8, 13531. https://doi.org/10.1038/s41598-018-31840-5.

Mayer, F., Mayer, N., Chinn, L., Pinsonneault, R.L., Kroetz, D., Bainton, R.J., 2009. Evolutionary conservation of vertebrate blood-brain barrier chemoprotective mechanisms in *Drosophila*. The Journal of Neuroscience 29, 3538–3550. https://doi.org/10.1523/JNEUROSCI.5564-08.2009.

Mayer, U., Wagenaar, E., Beijnen, J.H., Smit, J.W., Meijer, D.K., van Asperen, J., Borst, P., Schinkel, A.H., 1996. Substantial excretion of digoxin via the intestinal mucosa and prevention of long-term digoxin accumulation in the brain by the mdr 1a P-glycoprotein. British Journal of Pharmacology 119, 1038–1044. https://doi.org/10.1111/j.1476-5381.1996.tb15775.x.

McLain, D.K., Shure, D.J., 1985. Host plant toxins and unpalatability of *Neacoryphus bicrucis* (Hemiptera: Lygaeidae). Ecological Entomology 10, 291–298. https://doi.org/10.1111/j.1365-2311.1985.tb00726.x.

Mehlhorn, S., Hunnekuhl, V.S., Geibel, S., Nauen, R., Bucher, G., 2021. Establishing RNAi for basic research and pest control and identification of the most efficient target genes for pest control: a brief guide. Frontiers in zoology 18, 60. https://doi.org/10.1186/s12983-021-00444-7.

Meredith, J., Moore, L., Scudder, G.G., 1984. Excretion of ouabain by Malpighian tubules of *Oncopeltus fasciatus*. The American Journal of Physiology, Integrative and Comparative Physiology 246, R705-15. https://doi.org/10.1152/ajpregu.1984.246.5.R705.

Merzendorfer, H., 2014. Chapter One - ABC Transporters and Their Role in Protecting Insects from Pesticides and Their Metabolites, in: Cohen, E. (Ed.), Advances in Insect Physiology : Target Receptors in the Control of Insect Pests: Part II, vol. 46. Academic Press, pp. 1–72.

Meyerhof, W., Batram, C., Kuhn, C., Brockhoff, A., Chudoba, E., Bufe, B., Appendino, G., Behrens, M., 2010. The molecular receptive ranges of human TAS2R bitter taste receptors. Chemical senses 35, 157–170. https://doi.org/10.1093/chemse/bjp092.

Mikkaichi, T., Suzuki, T., Onogawa, T., Tanemoto, M., Mizutamari, H., Okada, M., Chaki, T., Masuda, S., Tokui, T., Eto, N., Abe, M., Satoh, F., Unno, M., Hishinuma, T., Inui, K.-I., Ito, S., Goto, J., Abe, T., 2004. Isolation and characterization of a digoxin transporter and its rat homologue expressed in the kidney. Proceedings of the National Academy of Sciences 101, 3569–3574. https://doi.org/10.1073/pnas.0304987101.

Miller, E.R., Dingle, H., 1982. The effect of host plant phenology on reproduction of the milkweed bug, *Oncopeltus fasciatus*, in tropical Florida. Oecologia 52, 97–103. https://doi.org/10.1007/BF00349016.

Minh, B.Q., Nguyen, M.A.T., Haeseler, A. von, 2013. Ultrafast approximation for phylogenetic bootstrap. Molecular Biology and Evolution 30, 1188–1195. https://doi.org/10.1093/molbev/mst024.

Misof, B., Liu, S., Meusemann, K., Peters, R.S., Donath, A., Mayer, C., Frandsen, P.B., Ware, J., Flouri, T., Beutel, R.G., Niehuis, O., Petersen, M., Izquierdo-Carrasco, F., Wappler, T., Rust, J., Aberer, A.J., Aspöck, U., Aspöck, H., Bartel, D.,…Zhou, X., 2014. Phylogenomics resolves the timing and pattern of insect evolution. Science 346, 763–767. https://doi.org/10.1126/science.1257570.

Mithöfer, A., Boland, W., 2012. Plant defense against herbivores: chemical aspects. Annual Review of Plant Biology 63, 431–450. https://doi.org/10.1146/annurev-arplant-042110-103854.

Mitter, C., Farrell, B., Futuyma, D.J., 1991. Phylogenetic studies of insect-plant interactions: Insights into the genesis of diversity. Trends in Ecology & Evolution 6, 290–293. https://doi.org/10.1016/0169-5347(91)90007-K.

Mohammadi, S., Yang, L., Bulbert, M., Rowland, H.M., 2022. Defence mitigation by predators of chemically defended prey integrated over the predation sequence and across biological levels with a focus on cardiotonic steroids. Royal Society Open Science 9, 220363. https://doi.org/10.1098/rsos.220363.

Mohammadi, S., Savitzky, A.H., Lohr, J., Dobler, S., 2017. Toad toxin-resistant snake (Thamnophis elegans) expresses high levels of mutant Na+/K+-ATPase mRNA in cardiac muscle. Gene 614, 21–25. https://doi.org/10.1016/j.gene.2017.02.028.

Moon, J., Salzman, R.A., Ahn, J.-E., Koiwa, H., Zhu-Salzman, K., 2004. Transcriptional regulation in cowpea bruchid guts during adaptation to a plant defence protease inhibitor. Insect Molecular Biology 13, 283–291. https://doi.org/10.1111/j.0962-1075.2004.00485.x.

Moore, L.V., Scudder, G.G., 1985. Selective sequestration of milkweed (*Asclepias* sp.) cardenolides in *Oncopeltus fasciatus* (Dallas) (Hemiptera: Lygaeidae). Journal of Chemical Ecology 11, 667–687. https://doi.org/10.1007/BF00988575.

Moore, L.V., Scudder, G., 1986. Ouabain-resistant Na,K-ATPases and cardenolide tolerance in the large milkweed bug, *Oncopeltus fasciatus*. Journal of Insect Physiology 32, 27–33. https://doi.org/10.1016/0022-1910(86)90154-X.

Moore, P.J., Attisano, A., 2011. Oosorption in response to poor food: complexity in the trade-off between reproduction and survival. Ecology and Evolution 1, 37–45. https://doi.org/10.1002/ece3.4.

Mora, C., Tittensor, D.P., Adl, S., Simpson, A.G.B., Worm, B., 2011. How many species are there on Earth and in the ocean? PLOS Biology 9, e1001127. https://doi.org/10.1371/journal.pbio.1001127.

Mori, A., Burghardt, G.M., Savitzky, A.H., Roberts, K.A., Hutchinson, D.A., Goris, R.C., 2012. Nuchal glands: a novel defensive system in snakes. Chemoecology 22, 187–198. https://doi.org/10.1007/s00049-011-0086-2.

Murali, S., Bandaranaike, D., Bellair, M., Blankenburg, K., Chao, H., Dinh, H., Doddapaneni, H., Downs, B., Dugan-Rocha, S., Elkadiri, S., Gnanaolivu, R., Hernandez, B., Javaid, M., Jayaseelan, J.C., Lee, S., Li, M., Ming, W., Munidasa, M., Muniz, J., Nguyen, L., Ongeri, F., Osuji, N., Pu, L.-L., Puazo, M., Qu, C., Quiroz, J., Raj, R., Weissenberger, G., Xin, Y., Zou, X., Han, Y., Richards, S., Worley, K.C., Muzny, D.M., Gibbs, R.A., Koelzer, S., Panfilio, K.A., 2015. *Oncopeltus fasciatus* genome assembly 1.0. Ag Data Commons. Ag Data Commons (dataset). https://doi.org/10.15482/USDA.ADC/1173238.

Murphy, S.M., 2004. Enemy-free space maintains swallowtail butterfly host shift. Proceedings of the National Academy of Sciences 101, 18048–18052. https://doi.org/10.1073/pnas.0406490102.

Murray, C.L., Quaglia, M., Arnason, J.T., Morris, C.E., 1994. A putative nicotine pump at the metabolic blood–brain barrier of the tobacco hornworm. Journal of Neurobiology 25, 23–34. https://doi.org/10.1002/neu.480250103.

Narberhaus, I., Theuring, C., Hartmann, T., Dobler, S., 2003. Uptake and metabolism of pyrrolizidine alkaloids in *Longitarsus* flea beetles (Coleoptera: Chrysomelidae) adapted and non-adapted to alkaloid-containing host plants. Journal of Comparative Physiology. B, Biochemical, systemic, and environmental physiology 173, 483–491. https://doi.org/10.1007/s00360-003-0356-6.

National Center for Biotechnology Information, 2025. PubChem Compound Summary for CID 439501: Ouabain. https://pubchem.ncbi.nlm.nih.gov/compound/Ouabain (accessed 19 July 2025).

Newcombe, D., Blount, J.D., Mitchell, C., Moore, A.J., 2013. Chemical egg defence in the large milkweed bug, *Oncopeltus fasciatus*, derives from maternal but not paternal diet. Entomologia Experimentalis et Applicata 149, 197–205. https://doi.org/10.1111/eea.12128.

Nickisch-Rosenegk, E. von, Detzel, A., Wink, M., Schneider, D., 1990a. Carrier-mediated uptake of digoxin by larvae of the cardenolide sequestering moth, *Syntomeida epilais*. Naturwissenschaften 77, 336–338. https://doi.org/10.1007/BF01138391.

Nickisch-Rosenegk, E.v., Schneider, D., Wink, M., 1990b. Time-Course of Pyrrolizidine Alkaloid Processing in the Alkaloid Exploiting Arctiid Moth, *Creatonotos transiens*. Zeitschrift für Naturforschung C 45, 881–894. https://doi.org/10.1515/znc-1990-7-822.

Nolan, T., Hands, R.E., Bustin, S.A., 2006. Quantification of mRNA using real-time RT-PCR. Nature Protocols 1, 1559–1582. https://doi.org/10.1038/nprot.2006.236.

Nonis, A., Nardi, B. de, Nonis, A., 2014. Choosing between RT-qPCR and RNA-seq: A back-of-the-envelope estimate towards the definition of the break-even-point. Analytical and Bioanalytical Chemistry 406, 3533–3536. https://doi.org/10.1007/s00216-014-7687-x.

Nuruzzaman, M., Zhang, R., Cao, H.-Z., Luo, Z.-Y., 2014. Plant pleiotropic drug resistance transporters: transport mechanism, gene expression, and function. Journal of Integrative Plant Biology 56, 729–740. https://doi.org/10.1111/jipb.12196.

Olias, P., Adam, I., Meyer, A., Scharff, C., Gruber, A.D., 2014. Reference genes for quantitative gene expression studies in multiple avian species. PLOS One 9, e99678. https://doi.org/10.1371/journal.pone.0099678.

Omasits, U., Ahrens, C.H., Müller, S., Wollscheid, B., 2014. Protter: interactive protein feature visualization and integration with experimental proteomic data. Bioinformatics (Oxford, England) 30, 884–886. https://doi.org/10.1093/bioinformatics/btt607.

Opitz, S.E.W., Müller, C., 2009. Plant chemistry and insect sequestration. Chemoecology 19, 117–154. https://doi.org/10.1007/s00049-009-0018-6.

Pacheco, S., Chiñas, M., Gómez, J.U., Peláez-Aguilar, Á.E., do Nascimento, N.A., Cantón, P.E., Sánchez, J., López-Molina, S., Gómez, I., Soberón, M., Bravo, A., 2025. ABC transporters knockout in *Aedes aegypti* induces upregulation of paralogous genes, avoiding resistance development to Bacillus thuringiensis Cry toxins. PLOS One 20, e0327221. https://doi.org/10.1371/journal.pone.0327221.

Pádua, R.M. de, Kratz, J.M., Munkert, J., Bertol, J.W., Rigotto, C., Schuster, D., Maltarollo, V.G., Kreis, W., Simões, C.M.O., Braga, F.C., 2022. Effects of Lipophilicity and Structural Features on the Antiherpes Activity of Digitalis Cardenolides and Derivatives. Chemistry & Biodiversity 19, e202200411. https://doi.org/10.1002/cbdv.202200411.

Pan, H., Yang, X., Bidne, K., Hellmich, R.L., Siegfried, B.D., Zhou, X., 2015. Selection of Reference Genes for RT-qPCR Analysis in the Monarch Butterfly, *Danaus plexippus* (L.), a Migrating Bio-Indicator. PLOS One 10, e0129482. https://doi.org/10.1371/journal.pone.0129482.

Panfilio, K.A., Vargas Jentzsch, I.M., Benoit, J.B., Erezyilmaz, D., Suzuki, Y., Colella, S., Robertson, H.M., Poelchau, M.F., Waterhouse, R.M., Ioannidis, P., Weirauch, M.T., Hughes, D.S.T., Murali, S.C., Werren, J.H., Jacobs, C.G.C., Duncan, E.J., Armisén, D., Vreede, B.M.I., Baa-Puyoulet, P.,…Richards, S., 2019. Molecular evolutionary trends and feeding ecology diversification in the Hemiptera, anchored by the milkweed bug genome. Genome Biology 20, 64. https://doi.org/10.1186/s13059-019-1660-0.

Panfilio, K.A., Vargas Jentzsch, I.M., Benoit, J.B., Erezyilmaz, D., Suzuki, Y., Colella, S., Robertson, H.M., Poelchau, M.F., Waterhouse, R.M., Ioannidis, P., Weirauch, M.T., Hughes, D.S., Murali, S.C., Werren, J.H., Jacobs, C.G., Duncan, E.J., Armisén, D., Vreede, B.M., Baa-Puyoulet, P.,…Doddapaneni, H., 2017. Molecular evolutionary trends and feeding ecology diversification in the Hemiptera, anchored by the milkweed bug genome. bioRxiv (preprint). https://doi.org/10.1101/201731.

Pao, S.S., Paulsen, I.T., Saier, M.H., 1998. Major facilitator superfamily. Microbiology and Molecular Biology Reviews: MMBR 62, 1–34. https://doi.org/10.1128/MMBR.62.1.1-34.1998.

Park, J.E., Ryoo, G., Lee, W., 2017. Alternative Splicing: Expanding Diversity in Major ABC and SLC Drug Transporters. The AAPS journal 19, 1643–1655. https://doi.org/10.1208/s12248-017-0150-0.

Pasteels, J.M., 1993. The value of defensive compounds as taxonomic characters in the classification of leaf beetles. Biochemical Systematics and Ecology 21, 135–142. https://doi.org/10.1016/0305-1978(93)90019-N.

Pasteels, J.M., Dobler, S., Rowell-Rahier, M., Ehmke, A., Hartmann, T., 1995. Distribution of autogenous and host-derived chemical defenses in *Oreina* leaf beetles (Coleoptera: Chrysomelidae). Journal of Chemical Ecology 21, 1163–1179. https://doi.org/10.1007/BF02228318.

Pauchet, Y., Bretschneider, A., Augustin, S., Heckel, D.G., 2016. A P-Glycoprotein Is Linked to Resistance to the *Bacillus thuringiensis* Cry3Aa Toxin in a Leaf Beetle. Toxins 8. https://doi.org/10.3390/toxins8120362.

Pauli-Magnus, C., Mürdter, T., Godel, A., Mettang, T., Eichelbaum, M., Klotz, U., Fromm, M.F., 2001. P-glycoprotein-mediated transport of digitoxin, alpha-methyldigoxin and beta-acetyldigoxin. Naunyn-Schmiedeberg's Archives of Pharmacology 363, 337–343. https://doi.org/10.1007/s002100000354.

Perne, A., Muellner, M.K., Steinrueck, M., Craig-Mueller, N., Mayerhofer, J., Schwarzinger, I., Sloane, M., Uras, I.Z., Hoermann, G., Nijman, S.M.B., Mayerhofer, M., 2009. Cardiac glycosides induce cell death in human cells by inhibiting general protein synthesis. PLOS One 4, e8292. https://doi.org/10.1371/journal.pone.0008292.

Petschenka, G., Agrawal, A.A., 2016. How herbivores coopt plant defenses: natural selection, specialization, and sequestration. Current Opinion in Insect Science 14, 17–24. https://doi.org/10.1016/j.cois.2015.12.004.

Petschenka, G., Agrawal, A.A., 2015. Milkweed butterfly resistance to plant toxins is linked to sequestration, not coping with a toxic diet. Proceedings of the Royal Society B: Biological Sciences 282, 20151865. https://doi.org/10.1098/rspb.2015.1865.

Petschenka, G., Dobler, S., 2009. Target-site sensitivity in a specialized herbivore towards major toxic compounds of its host plant: the Na+K+-ATPase of the oleander hawk moth (*Daphnis nerii*) is highly susceptible to cardenolides. Chemoecology 19, 235–239. https://doi.org/10.1007/s00049-009-0025-7.

Petschenka, G., Halitschke, R., Züst, T., Roth, A., Stiehler, S., Tenbusch, L., Hartwig, C., Moreno Gámez, J.F., Trusch, R., Deckert, J., Chalušová, K., Vilcinskas, A., Exnerová, A., 2022. Sequestration of Defenses against Predators Drives Specialized Host Plant Associations in Preadapted Milkweed Bugs (Heteroptera: Lygaeinae). The American Naturalist 199, E211-E228. https://doi.org/10.1086/719196.

Petschenka, G., Fei, C.S., Araya, J.J., Schröder, S., Timmermann, B.N., Agrawal, A.A., 2018. Relative Selectivity of Plant Cardenolides for Na+/K+-ATPases From the Monarch Butterfly and Non-resistant Insects. Frontiers in Plant Science 9, 1424. https://doi.org/10.3389/fpls.2018.01424.

Petschenka, G., Wagschal, V., Tschirnhaus, M. von, Donath, A., Dobler, S., 2017. Convergently Evolved Toxic Secondary Metabolites in Plants Drive the Parallel Molecular Evolution of Insect Resistance. The American Naturalist 190, S29-S43. https://doi.org/10.1086/691711.

Petschenka, G., Fandrich, S., Sander, N., Wagschal, V., Boppré, M., Dobler, S., 2013a. Stepwise evolution of resistance to toxic cardenolides via genetic substitutions in the Na+/K+ -ATPase of milkweed butterflies (lepidoptera: Danaini). Evolution 67, 2753–2761. https://doi.org/10.1111/evo.12152.

Petschenka, G., Pick, C., Wagschal, V., Dobler, S., 2013b. Functional evidence for physiological mechanisms to circumvent neurotoxicity of cardenolides in an adapted and a non-adapted hawk-moth species. Proceedings of the Royal Society B: Biological Sciences 280, 20123089. https://doi.org/10.1098/rspb.2012.3089.

Petschenka, G., Offe, J.K., Dobler, S., 2012. Physiological screening for target site insensitivity and localization of Na(+)/K(+)-ATPase in cardenolide-adapted Lepidoptera. Journal of Insect Physiology 58, 607–612. https://doi.org/10.1016/j.jinsphys.2011.12.012.

Pfaffl, M.W., 2004. Quantification Strategies in Real-time Polymerase Chain Reaction, in: Bustin, S.A. (Ed.), A - Z of quantitative PCR. Internat. Univ. Line, La Jolla, Calif., pp. 87–112.

Pfaffl, M.W., 2001. A new mathematical model for relative quantification in real-time RT–PCR. Nucleic Acids Research 29, e45.

Pfaffl, M.W., Tichopad, A., Prgomet, C., Neuvians, T.P., 2004. Determination of stable housekeeping genes, differentially regulated target genes and sample integrity: BestKeeper–Excel-based tool using pair-wise correlations. Biotechnology Letters 26, 509–515.

Phang, J.M., Poore, C.M., Lopaczynska, J., Yeh, G.C., 1993. Flavonol-stimulated efflux of 7,12-dimethylbenz(a)anthracene in multidrug-resistant breast cancer cells. Cancer Research 53, 5977–5981.

Pignatelli, P., Ingham, V.A., Balabanidou, V., Vontas, J., Lycett, G., Ranson, H., 2018. The *Anopheles gambiae* ATP-binding cassette transporter family: phylogenetic analysis and tissue localization provide clues on function and role in insecticide resistance. Insect Molecular Biology 27, 110–122. https://doi.org/10.1111/imb.12351.

Pizzagalli, M.D., Bensimon, A., Superti-Furga, G., 2021. A guide to plasma membrane solute carrier proteins. The FEBS journal 288, 2784–2835. https://doi.org/10.1111/febs.15531.

Płachetka-Bożek, A., Augustyniak, M., 2017. Evaluation of Candidate Reference Genes for Quantitative Gene Expression Analysis in *Spodoptera exigu* a after Long-time Exposure to Cadmium. Scientific Reports 7, 8338. https://doi.org/10.1038/s41598-017-08630-6.

Poelchau, M., Childers, C., Moore, G., Tsavatapalli, V., Evans, J., Lee, C.-Y., Lin, H., Lin, J.-W., Hackett, K., 2015. The i5k Workspace@NAL--enabling genomic data access, visualization and curation of arthropod genomes. Nucleic Acids Research 43, D714-9. https://doi.org/10.1093/nar/gku983.

Pokharel, P., Steppuhn, A., Petschenka, G., 2021. Dietary cardenolides enhance growth and change the direction of the fecundity-longevity trade-off in milkweed bugs (Heteroptera: Lygaeinae). Ecology and Evolution 11, 18042–18054. https://doi.org/10.1002/ece3.8402.

Pokharel, P., Sippel, M., Vilcinskas, A., Petschenka, G., 2020. Defense of Milkweed Bugs (Heteroptera: Lygaeinae) against Predatory Lacewing Larvae Depends on Structural Differences of Sequestered Cardenolides. Insects 11, 485. https://doi.org/10.3390/insects11080485.

Pugalenthi, P., Livingstone, D., 1995. Cardenolides (heart poisons) in the painted grasshopper *Poecilocerus pictus* F. (Orthoptera: Pyrgomorphidae) feeding on the milkweed Calotropis gigantea L. Journal of the New York Entomological Society, 191–196.

Qian, W., Liao, B.-Y., Chang, A.Y.-F., Zhang, J., 2010. Maintenance of duplicate genes and their functional redundancy by reduced expression. Trends in Genetics: TIG 26, 425–430. https://doi.org/10.1016/j.tig.2010.07.002.

Qiu, L.Y., Krieger, E., Schaftenaar, G., Swarts, H.G.P., Willems, P.H.G.M., Pont, J.J.H.H.M. de, Koenderink, J.B., 2005. Reconstruction of the complete ouabain-binding pocket of Na,K-ATPase in gastric H,K-ATPase by substitution of only seven amino acids. The Journal of Biological Chemistry 280, 32349–32355. https://doi.org/10.1074/jbc.M505168200.

R Core Team, 2018. R: A language and environment for statistical computing: R Foundation for Statistical Computing. Vienna, Austria, Vienna, Austria.

R Core Team, 2017. R: A language and environment for statistical computing: R Foundation for Statistical Computing. Vienna, Austria, Vienna, Austria.

Ralph, C.P., 1976. Natural food requirements of the large milkweed bug, *Oncopeltus fasciatus* (Hemiptera: Lygaeidae), and their relation to gregariousness and host plant morphology. Oecologia 26, 157–175. https://doi.org/10.1007/BF00582894.

Rao, V.V., Anthony, D.C., Piwnica-Worms, D., 1995. Multidrug resistance P-glycoprotein monoclonal antibody JSB-1 crossreacts with pyruvate carboxylase. journal of Histochemistry and Cytochemistry 43, 1187–1192. https://doi.org/10.1177/43.12.8537634.

Rao, V.V., Anthony, D.C., Piwnica-Worms, D., 1994. MDR1 Gene-specific Monoclonal Antibody C494 Cross-Reacts with Pyruvate Carboxylase. Cancer Research 54, 1536–1541.

Rasmann, S., Agrawal, A.A., 2011. Latitudinal patterns in plant defense: evolution of cardenolides, their toxicity and induction following herbivory. Ecology Letters 14, 476–483. https://doi.org/10.1111/j.1461-0248.2011.01609.x.

Rasmann, S., Agrawal, A.A., Cook, S.C., Erwin, A.C., 2009. Cardenolides, induced responses, and interactions between above- and belowground herbivores of milkweed (*Asclepias* spp.). Ecology 90, 2393–2404. https://doi.org/10.1890/08-1895.1.

Ricardo, S., Lehmann, R., 2009. An ABC transporter controls export of a *Drosophila* germ cell attractant. Science 323, 943–946. https://doi.org/10.1126/science.1166239.

Röpcke, M., Lu, S., Plate, C., Meinzer, F., Lisiecki, A., Dobler, S., 2024. Substrate Specificity of ABCB Transporters Predicted by Docking Simulations Can Be Confirmed by Experimental Tests. Molecules 29. https://doi.org/10.3390/molecules29225272.

Rösner, J., Tietmeyer, J., Merzendorfer, H., 2021a. Functional analysis of ABCG and ABCH transporters from the red flour beetle, *Tribolium castaneum*. Pest management science 77, 2955–2963. https://doi.org/10.1002/ps.6332.

Rösner, J., Tietmeyer, J., Merzendorfer, H., 2021b. Organic anion-transporting polypeptides are involved in the elimination of insecticides from the red flour beetle, *Tribolium castaneum*. Journal of Pest Science 94, 1427–1437. https://doi.org/10.1007/s10340-020-01317-4.

Ross, S., 1978. The relationship of age, sex, and reproductive state to assimilation efficiency in the adult milkweed bug, *Oncopeltus fasciatus*. Journal of Insect Physiology 24, 305–308. https://doi.org/10.1016/0022-1910(78)90027-6.

Rossi, M., Battisti, D. de, Niven, J.E., 2019. Transepithelial transport of P-glycoprotein substrate by the Malpighian tubules of the desert locust. PLOS One 14, e0223569. https://doi.org/10.1371/journal.pone.0223569.

Roth, C.W., Holm, I., Graille, M., Dehoux, P., Rzhetsky, A., Wincker, P., Weissenbach, J., Brey, P.T., 2003. Identification of the *Anopheles gambiae* ATP-binding cassette transporter superfamily genes. Molecules and Cells 15, 150–158.

Roth, M., Obaidat, A., Hagenbuch, B., 2012. OATPs, OATs and OCTs: the organic anion and cation transporters of the SLCO and SLC22A gene superfamilies. British Journal of Pharmacology 165, 1260–1287. https://doi.org/10.1111/j.1476-5381.2011.01724.x.

Rowell-Rahier, M., Pasteels, J.M., Alonso-Media, A., Brower, L.P., 1995. Relative unpalatability of leaf beetles with either biosynthesized or sequestered chemical defence. Animal Behaviour 49, 709–714. https://doi.org/10.1016/0003-3472(95)80203-7.

Rubiano-Buitrago, P., Pradhan, S., Aceves, A.A., Mohammadi, S., Paetz, C., Rowland, H.M., 2024. Cardenolides in the defensive fluid of adult large milkweed bugs have differential potency on vertebrate and invertebrate predator Na+/K+-ATPases. Royal Society Open Science 11, 231735. https://doi.org/10.1098/rsos.231735.

Rubiano-Buitrago, P., Pradhan, S., Grabe, V., Aceves-Aparicio, A., Paetz, C., Rowland, H.M., 2023. Differential accumulation of cardenolides from *Asclepias curassavica* by large milkweed bugs does not correspond to availability in seeds or biological activity on the bug Na+/K+-ATPase. Frontiers in Ecology and Evolution 11, 1175205. https://doi.org/10.3389/fevo.2023.1175205.

Rutkowska, E., Pajak, K., Jóźwiak, K., 2013. Lipophilicity--methods of determination and its role in medicinal chemistry. Acta poloniae pharmaceutica 70, 3–18.

Sady, M.B., 1994. Survey of the Blue Milkweed Beetle, *Chrysochus colbaltinus* LeConte (Coleoptera: Chrysomelidae), in Western Nevada. The Coleopterists Bulletin 48, 299.

Schaedler, T.A., Faust, B., Shintre, C.A., Carpenter, E.P., Srinivasan, V., van Veen, H.W., Balk, J., 2015. Structures and functions of mitochondrial ABC transporters. Biochemical Society transactions 43, 943–951. https://doi.org/10.1042/BST20150118.

Schindelin, J., Arganda-Carreras, I., Frise, E., Kaynig, V., Longair, M., Pietzsch, T., Preibisch, S., Rueden, C., Saalfeld, S., Schmid, B., Tinevez, J.-Y., White, D.J., Hartenstein, V., Eliceiri, K., Tomancak, P., Cardona, A., 2012. Fiji: an open-source platform for biological-image analysis. Nature Methods 9, 676–682. https://doi.org/10.1038/nmeth.2019.

Schinkel, A.H., Jonker, J.W., 2003. Mammalian drug efflux transporters of the ATP binding cassette (ABC) family: an overview. Advanced Drug Delivery Reviews 55, 3–29. https://doi.org/10.1016/s0169-409x(02)00169-2.

Schinkel, A.H., Roelofs, M.E.M., Borst, P., 1991. Characterization of the Human MDR3 P-Glycoprotein and Its Recognition by P-Glycoprotein-specific Monoclonal Antibodies. Cancer Research 51, 2628–2635.

Schloerke, B., Cook, D., Larmarange, J., Briatte, F., Marbach, M., Thoen, E., Elberg, A., Crowley, J., 2025. GGally: Extension to 'ggplot2': R package version 2.4.0.

Schmidt, L., Wielsch, N., Wang, D., Boland, W., Burse, A., 2019. Tissue-specific profiling of membrane proteins in the salicin sequestering juveniles of the herbivorous leaf beetle, *Chrysomela populi*. Insect Biochemistry and Molecular Biology 109, 81–91. https://doi.org/10.1016/j.ibmb.2019.03.009.

Schneider, C.A., Rasband, W.S., Eliceiri, K.W., 2012. NIH Image to ImageJ: 25 years of image analysis. Nature Methods 9, 671–675. https://doi.org/10.1038/nmeth.2089.

Schrödinger, L.L. The PyMOL Molecular Graphics System, Version 3.0.

Scott, J.G., Michel, K., Bartholomay, L.C., Siegfried, B.D., Hunter, W.B., Smagghe, G., Zhu, K.Y., Douglas, A.E., 2013. Towards the elements of successful insect RNAi. Journal of Insect Physiology 59, 1212–1221. https://doi.org/10.1016/j.jinsphys.2013.08.014.

Scotto, K.W., 2003. Transcriptional regulation of ABC drug transporters. Oncogene 22, 7496–7511. https://doi.org/10.1038/sj.onc.1206950.

Scudder, G.G., Moore, L.V., Isman, M.B., 1986. Sequestration of cardenolides in *Oncopeltus fasciatus*: Morphological and physiological adaptations. Journal of Chemical Ecology 12, 1171–1187. https://doi.org/10.1007/BF01639003.

Scudder, G.G.E., Meredith, J., 1982a. Morphological basis of cardiac glycoside sequestration by *Oncopeltus fasciatus* (Dallas) (Hemiptera: Lygaeidae). Zoomorphology 99, 87–101. https://doi.org/10.1007/BF00310302.

Scudder, G.G.E., Duffey, S.S., 1972. Cardiac glycosides in the Lygaeinae (Hemiptera: Lygaeidae). Canadian Journal of Zoology 50, 35–42. https://doi.org/10.1139/z72-007.

Scudder, G., Meredith, J., 1982b. The permeability of the midgut of three insects to cardiac glycosides. Journal of Insect Physiology 28, 689–694. https://doi.org/10.1016/0022-1910(82)90147-0.

Seong, K.M., Sun, W., Clark, J.M., Pittendrigh, B.R., 2016. Splice form variant and amino acid changes in MDR49 confers DDT resistance in transgenic *Drosophila*. Scientific Reports 6, 23355. https://doi.org/10.1038/srep23355.

Shakeel, M., Rodriguez, A., Tahir, U.B., Jin, F., 2018. Gene expression studies of reference genes for quantitative real-time PCR: an overview in insects. Biotechnology Letters 40, 227–236. https://doi.org/10.1007/s10529-017-2465-4.

Sharom, F.J., Yu, X., DiDiodato, G., Chu, J.W., 1996. Synthetic hydrophobic peptides are substrates for P-glycoprotein and stimulate drug transport. Biochemical Journal 320 (Pt 2), 421–428. https://doi.org/10.1042/bj3200421.

Shi, C., Hu, J., Zhang, Y., 2015. Research Progress on Reference Genes of Insect for Quantitative Real-time Reverse Transcription PCR (RT-qPCR). Universal Journal of Agricultural Research 3, 211–219. https://doi.org/10.13189/ujar.2015.030605.

Silver, N., Best, S., Jiang, J., Thein, S.L., 2006. Selection of housekeeping genes for gene expression studies in human reticulocytes using real-time PCR. BMC Molecular Biology 7, 33. https://doi.org/10.1186/1471-2199-7-33.

Skazik, C., Wenzel, J., Marquardt, Y., Kim, A., Merk, H.F., Bickers, D.R., Baron, J.M., 2011. P-glycoprotein (ABCB1) expression in human skin is mainly restricted to dermal components. Experimental Dermatology 20, 450–452. https://doi.org/10.1111/j.1600-0625.2010.01237.x.

Skinner, K.T., Palkar, A.M., Hong, A.L., 2023. Genetics of ABCB1 in Cancer. Cancers 15. https://doi.org/10.3390/cancers15174236.

Smit, J.W., Huisman, M.T., van Tellingen, O., Wiltshire, H.R., Schinkel, A.H., 1999. Absence or pharmacological blocking of placental P-glycoprotein profoundly increases fetal drug exposure. The Journal of clinical investigation 104, 1441–1447. https://doi.org/10.1172/JCI7963.

Smith, A.J., van Helvoort, A., van Meer, G., Szabo, K., Welker, E., Szakacs, G., Varadi, A., Sarkadi, B., Borst, P., 2000. MDR3 P-glycoprotein, a phosphatidylcholine translocase, transports several cytotoxic drugs and directly interacts with drugs as judged by interference with nucleotide trapping. The Journal of Biological Chemistry 275, 23530–23539. https://doi.org/10.1074/jbc.M909002199.

Smith, A.J., Timmermans-Hereijgers, J.L., Roelofsen, B., Wirtz, K.W., van Blitterswijk, W.J., Smit, J.J., Schinkel, A.H., Borst, P., 1994. The human MDR3 P-glycoprotein promotes translocation of phosphatidylcholine through the plasma membrane of fibroblasts from transgenic mice. FEBS Letters 354, 263–266. https://doi.org/10.1016/0014-5793(94)01135-4.

Snoeck, S., Wybouw, N., van Leeuwen, T., Dermauw, W., 2018. Transcriptomic Plasticity in the Arthropod Generalist *Tetranychus urticae* Upon Long-Term Acclimation to Different Host Plants. G3 (Bethesda, Md.) 8, 3865–3879. https://doi.org/10.1534/g3.118.200585.

Soldin, S.J., 1986. Digoxin--issues and controversies. Clinical Chemistry 32, 5–12. https://doi.org/10.1093/clinchem/32.1.5.

Solovyev, V., 2008. Statistical Approaches in Eukaryotic Gene Prediction, in: Balding, D.J., Bishop, M., Cannings, C. (Eds.), Handbook of Statistical Genetics, 3rd ed. Wiley-Interscience, s.l., pp. 97–159.

Sorensen, J.S., Dearing, M.D., 2006. Efflux transporters as a novel herbivore countermechanism to plant chemical defenses. Journal of Chemical Ecology 32, 1181–1196. https://doi.org/10.1007/s10886-006-9079-y.

Sørensen, J.G., Heckmann, L.-H., Holmstrup, M., 2010. Temporal gene expression profiles in a palaearctic springtail as induced by desiccation, cold exposure and during recovery. Functional Ecology 24, 838–846. https://doi.org/10.1111/j.1365-2435.2010.01687.x.

Sparks, M.E., Shelby, K.S., Kuhar, D., Gundersen-Rindal, D.E., 2014. Transcriptome of the invasive brown marmorated stink bug, *Halyomorpha halys* (Stål) (Heteroptera: Pentatomidae). PLOS One 9, e111646. https://doi.org/10.1371/journal.pone.0111646.

Spiegelaere, W. de, Dern-Wieloch, J., Weigel, R., Schumacher, V., Schorle, H., Nettersheim, D., Bergmann, M., Brehm, R., Kliesch, S., Vandekerckhove, L., Fink, C., 2015. Reference gene validation for RT-qPCR, a note on different available software packages. PLOS One 10, e0122515. https://doi.org/10.1371/journal.pone.0122515.

Srinivasan, S., Bingham, J.L., Johnson, D., 2009. The ABCs of human alternative splicing: a review of ATP-binding cassette transporter splicing. Current Opinion in Drug Discovery & Development 12, 149–158.

Stapelbroek, J.M., van Erpecum, K.J., Klomp, L.W., Houwen, R.H., 2010. Liver disease associated with canalicular transport defects: Current and future therapies. Journal of Hepatology 52, 258–271. https://doi.org/10.1016/j.jhep.2009.11.012.

Steyn, P.S., van Heerden, F.R., 1998. Bufadienolides of plant and animal origin. Natural Product Reports 15, 397. https://doi.org/10.1039/a815397y.

Sticher, O., 2010. Triterpene einschließlich Steroide, in: Hänsel, R., Sticher, O., Steinegger, E. (Eds.), Pharmakognosie - Phytopharmazie, 9th ed. Springer-Verlag Berlin Heidelberg, Berlin, Heidelberg, pp. 833–938.

Strauss, A.S., Wang, D., Stock, M., Gretscher, R.R., Groth, M., Boland, W., Burse, A., 2014. Tissue-specific transcript profiling for ABC transporters in the sequestering larvae of the phytophagous leaf beetle *Chrysomela populi*. PLOS One 9, e98637. https://doi.org/10.1371/journal.pone.0098637.

Strauss, A.S., Peters, S., Boland, W., Burse, A., 2013. ABC transporter functions as a pacemaker for sequestration of plant glucosides in leaf beetles. eLife 2, e01096. https://doi.org/10.7554/eLife.01096.

Sun, H., Pu, J., Chen, F., Wang, J., Han, Z., 2017. Multiple ATP-binding cassette transporters are involved in insecticide resistance in the small brown planthopper, *Laodelphax striatellus*. Insect Molecular Biology 26, 343–355. https://doi.org/10.1111/imb.12299.

Szeri, F., Iliás, A., Pomozi, V., Robinow, S., Bakos, E., Váradi, A., 2009. The high turnover *Drosophila* multidrug resistance-associated protein shares the biochemical features of its human orthologues. Biochimica et Biophysica Acta (BBA) - Biomembranes 1788, 402–409. https://doi.org/10.1016/j.bbamem.2008.11.007.

Tan, W.-H., Acevedo, T., Harris, E.V., Alcaide, T.Y., Walters, J.R., Hunter, M.D., Gerardo, N.M., Roode, J.C. de, 2019. Transcriptomics of monarch butterflies (*Danaus plexippus*) reveals that toxic host plants alter expression of detoxification genes and down-regulate a small number of immune genes. Molecular Ecology 28, 4845–4863. https://doi.org/10.1111/mec.15219.

Tapadia, M.G., Lakhotia, S.C., 2005. Expression of mdr49 and mdr65 multidrug resistance genes in larval tissues of *Drosophila melanogaster* under normal and stress conditions. Cell stress & chaperones 10, 7–11. https://doi.org/10.1379/csc-67r.1.

Taskar, K.S., Mariappan, T.T., Kurawattimath, V., Singh Gautam, S., Radhakrishna Mullapudi, T.V., Sridhar, S.K., Kallem, R.R., Marathe, P., Mandlekar, S., 2017. Unmasking the Role of Uptake Transporters for Digoxin Uptake Across the Barriers of the Central Nervous System in Rat. Journal of Central Nervous System Disease 9, 1179573517693596. https://doi.org/10.1177/1179573517693596.

Tay, W.T., Mahon, R.J., Heckel, D.G., Walsh, T.K., Downes, S., James, W.J., Lee, S.-F., Reineke, A., Williams, A.K., Gordon, K.H.J., 2015. Insect Resistance to *Bacillus thuringiensis* Toxin Cry2Ab Is Conferred by Mutations in an ABC Transporter Subfamily A Protein. PLOS Genetics 11, e1005534. https://doi.org/10.1371/journal.pgen.1005534.

Theile, D., Wizgall, P., 2021. Acquired ABC-transporter overexpression in cancer cells: transcriptional induction or Darwinian selection? Naunyn-Schmiedeberg's Archives of Pharmacology 394, 1621–1632. https://doi.org/10.1007/s00210-021-02112-3.

Theodoulou, F.L., Kerr, I.D., 2015. ABC transporter research: going strong 40 years on. Biochemical Society transactions 43, 1033–1040. https://doi.org/10.1042/BST20150139.

Thiebaut, F., Tsuruo, T., Hamada, H., Gottesman, M.M., Pastan, I., Willingham, M.C., 1987. Cellular localization of the multidrug-resistance gene product P-glycoprotein in normal human tissues. Proceedings of the National Academy of Sciences 84, 7735–7738. https://doi.org/10.1073/pnas.84.21.7735.

Thornton, B., Basu, C., 2011. Real-time PCR (qPCR) primer design using free online software. Biochemistry and Molecular Biology Education 39, 145–154. https://doi.org/10.1002/bmb.20461.

Tian, J., Li, X., Liang, M., Liu, L., Xie, J.X., Ye, Q., Kometiani, P., Tillekeratne, M., Jin, R., Xie, Z., 2009. Changes in sodium pump expression dictate the effects of ouabain on cell growth. The Journal of Biological Chemistry 284, 14921–14929. https://doi.org/10.1074/jbc.M808355200.

Ting, H.H., McCabe, W.L., 1934. Supersaturation and Crystal Formation in Seeded Solutions. Industrial & Engineering Chemistry 26, 1201–1207. https://doi.org/10.1021/ie50299a017.

Torday, J.S., 2015. Pleiotropy as the Mechanism for Evolving Novelty: Same Signal, Different Result. Biology 4, 443–459. https://doi.org/10.3390/biology4020443.

Torrie, L.S., Radford, J.C., Southall, T.D., Kean, L., Dinsmore, A.J., Davies, S.A., Dow, J.A.T., 2004. Resolution of the insect ouabain paradox. Proceedings of the National Academy of Sciences 101, 13689–13693. https://doi.org/10.1073/pnas.0403087101.

Toyoda, Y., Hagiya, Y., Adachi, T., Hoshijima, K., Kuo, M.T., Ishikawa, T., 2008. MRP class of human ATP binding cassette (ABC) transporters: historical background and new research directions.

Xenobiotica; the fate of foreign compounds in biological systems 38, 833–862. https://doi.org/10.1080/00498250701883514.

Trifinopoulos, J., Nguyen, L.-T., Haeseler, A. von, Minh, B.Q., 2016. W-IQ-TREE: a fast online phylogenetic tool for maximum likelihood analysis. Nucleic Acids Research 44, W232-5. https://doi.org/10.1093/nar/gkw256.

Trowsdale, J., Hanson, I., Mockridge, I., Beck, S., Townsend, A., Kelly, A., 1990. Sequences encoded in the class II region of the MHC related to the 'ABC' superfamily of transporters. Nature 348, 741–744. https://doi.org/10.1038/348741a0.

Tsirigos, K.D., Peters, C., Shu, N., Käll, L., Elofsson, A., 2015. The TOPCONS web server for consensus prediction of membrane protein topology and signal peptides. Nucleic Acids Research 43, W401-7. https://doi.org/10.1093/nar/gkv485.

Uematsu, T., Yamaoka, M., Matsuura, T., Doto, R., Hotomi, H., Yamada, A., Hasumi-Nakayama, Y., Kayamoto, D., 2001. P-glycoprotein expression in human major and minor salivary glands. Archives of Oral Biology 46, 521–527. https://doi.org/10.1016/S0003-9969(01)00012-7.

Uematsu, T., Yamaoka, M., Doto, R., Tanaka, H., Matsuura, T., Furusawa, K., 2003. Expression of ATP-binding cassette transporter in human salivary ducts. Archives of Oral Biology 48, 87–90. https://doi.org/10.1016/s0003-9969(02)00159-0.

Untergasser, A., Cutcutache, I., Koressaar, T., Ye, J., Faircloth, B.C., Remm, M., Rozen, S.G., 2012. Primer3—new capabilities and interfaces. Nucleic Acids Research 40, e115. https://doi.org/10.1093/nar/gks596.

Vaidya, S.S., Walsh, S.W., Gerk, P.M., 2009. Formation and efflux of ATP-binding cassette transporter substrate 2,4-dinitrophenyl-S-glutathione from cultured human term placental villous tissue fragments. Molecular Pharmaceutics 6, 1689–1702. https://doi.org/10.1021/mp900019z.

van den Elsen, J.M.H., Kuntz, D.A., Hoedemaeker, F.J., Rose, D.R., 1999. Antibody C219 recognizes an alpha -helical epitope on P-glycoprotein. Proceedings of the National Academy of Sciences 96, 13679–13684. https://doi.org/10.1073/pnas.96.24.13679.

van der Bliek, A.M., Kooiman, P.M., Schneider, C., Borst, P., 1988. Sequence of mdr3 cDNA encoding a human P-glycoprotein. Gene 71, 401–411. https://doi.org/10.1016/0378-1119(88)90057-1.

van Heetvelde, M., van Loocke, W., Trypsteen, W., Baert, A., Vanderheyden, K., Crombez, B., Vandesompele, J., Leeneer, K. de, Claes, K.B., 2017. Evaluation of relative quantification of alternatively spliced transcripts using droplet digital PCR. Biomolecular Detection and Quantification 13, 40–48. https://doi.org/10.1016/j.bdq.2017.09.001.

van Helvoort, A., Smith, A.J., Sprong, H., Fritzsche, I., Schinkel, A.H., Borst, P., van Meer, G., 1996. MDR1 P-Glycoprotein Is a Lipid Translocase of Broad Specificity, While MDR3 P-Glycoprotein Specifically Translocates Phosphatidylcholine. Cell 87, 507–517. https://doi.org/10.1016/S0092-8674(00)81370-7.

Vandesompele, J., Preter, K. de, Pattyn, F., Poppe, B., van Roy, N., Paepe, A. de, Speleman, F., 2002. Accurate normalization of real-time quantitative RT-PCR data by geometric averaging of multiple internal control genes. Genome Biology 3, 1-12.

Vasiliou, V., Vasiliou, K., Nebert, D.W., 2009. Human ATP-binding cassette (ABC) transporter family. Human Genomics 3, 281–290. https://doi.org/10.1186/1479-7364-3-3-281.

Vaughan, F.A., 1979. Effect of gross cardiac glycoside content of seeds of common milkweed, *Asclepias syriaca*, on cardiac glycoside uptake by the milkweed bug *Oncopeltus fasciatus*. Journal of Chemical Ecology 5, 89–100. https://doi.org/10.1007/BF00987690.

Vaughan, G.L., Jungreis, A.M., 1977. Insensitivity of lepidopteran tissues to ouabain: Physiological mechanisms for protection from cardiac glycosides. Journal of Insect Physiology 23, 585–589. https://doi.org/10.1016/0022-1910(77)90052-X.

Vogel, E., Santos, D., Mingels, L., Verdonckt, T.-W., Broeck, J.V., 2018. RNA Interference in Insects: Protecting Beneficials and Controlling Pests. Frontiers in Physiology 9, 1912. https://doi.org/10.3389/fphys.2018.01912.

Wagner, G.P., Zhang, J., 2011. The pleiotropic structure of the genotype-phenotype map: the evolvability of complex organisms. Nature Reviews Genetics 12, 204–213. https://doi.org/10.1038/nrg2949.

Wang, L., He, W., Lu, J.-M., Sun, J., Jiang, S.-D., Wang, J.-J., Wei, D.-D., 2023. Characterization and transcriptional expression of ABCG genes in *Bactrocera dorsalis*: Insights into their roles in fecundity and insecticidal stress response. International Journal of Biological Macromolecules 253, 126836. https://doi.org/10.1016/j.ijbiomac.2023.126836.

Wang, S.C., Davejan, P., Hendargo, K.J., Javadi-Razaz, I., Chou, A., Yee, D.C., Ghazi, F., Lam, K.J.K., Conn, A.M., Madrigal, A., Medrano-Soto, A., Saier, M.H., 2020. Expansion of the Major Facilitator Superfamily (MFS) to include novel transporters as well as transmembrane-acting enzymes. Biochimica et Biophysica Acta (BBA) - Biomembranes 1862, 183277. https://doi.org/10.1016/j.bbamem.2020.183277.

Wang, Z., Tian, F., Cai, L., Zhang, J., Liu, J., Zeng, X., 2019. Identification of candidate ATP-binding cassette transporter gene family members in *Diaphorina citri* (Hemiptera: Psyllidae) via adult tissues transcriptome analysis. Scientific Reports 9, 15842. https://doi.org/10.1038/s41598-019-52402-3.

War, A.R., Buhroo, A.A., Hussain, B., Ahmad, T., Nair, R.M., Sharma, H.C., 2020. Plant Defense and Insect Adaptation with Reference to Secondary Metabolites, in: Mérillon, J.-M., Ramawat, K.G. (Eds.), Co-Evolution of Secondary Metabolites, 1st ed. Springer International Publishing; Imprint: Springer, Cham, pp. 795–822.

War, A.R., Paulraj, M.G., Ahmad, T., Buhroo, A.A., Hussain, B., Ignacimuthu, S., Sharma, H.C., 2012. Mechanisms of plant defense against insect herbivores. Plant Signaling & Behavior 7, 1306–1320. https://doi.org/10.4161/psb.21663.

Wawrzycka, D., Sobczak, I., Bartosz, G., Bocer, T., Ułaszewski, S., Goffeau, A., 2010. Vmr 1p is a novel vacuolar multidrug resistance ABC transporter in *Saccharomyces cerevisiae*. FEMS yeast research 10, 828–838. https://doi.org/10.1111/j.1567-1364.2010.00673.x.

Wenig, P., Odermatt, J., 2010. OpenChrom: a cross-platform open source software for the mass spectrometric analysis of chromatographic data. BMC Bioinformatics 11. https://doi.org/10.1186/1471-2105-11-405.

Wessler, J.D., Grip, L.T., Mendell, J., Giugliano, R.P., 2013. The P-glycoprotein transport system and cardiovascular drugs. Journal of the American College of Cardiology 61, 2495–2502. https://doi.org/10.1016/j.jacc.2013.02.058.

Wheeler, B., Torchiano, M., 2016. Package 'lmPerm'. R package version, 1-24.

Whitman, D.W., Jones, C.G., Blum, M.S., 1992. Defensive Secretion Production in Lubber Grasshoppers (Orthoptera: Romaleidae): Influence of Age, Sex, Diet, and Discharge Frequency. Annals of the Entomological Society of America 85, 96–102. https://doi.org/10.1093/aesa/85.1.96.

Wickham, H., 2016. ggplot2: Elegant Graphics for Data Analysis. Springer, New York, New York.

Wiens, J.J., Lapoint, R.T., Whiteman, N.K., 2015. Herbivory increases diversification across insect clades. Nature Communications 6, 8370. https://doi.org/10.1038/ncomms9370.

Wilke, C.O., 2018. ggridges: Ridgeline Plots in 'ggplot2'.

Wink, M., Schimmer, O., 2010. Molecular Modes of Action of Defensive Secondary Metabolites, in: Functions and biotechnology of plant secondary metabolites, 2nd ed. Wiley-Blackwell, Ames, IA, pp. 21–161.

Wink, M., Schneider, D., 1990. Fate of plant-derived secondary metabolites in three moth species (Syntomis mogadorensis, *Syntomeida epilais*, and *Creatonotos transiens*). Journal of Comparative Physiology B 160, 389–400. https://doi.org/10.1007/BF01075670.

Woodring, J., Hoffmann, K.H., Lorenz, M.W., 2007. Feeding, nutrient flow, and digestive enzyme release in the giant milkweed bug, *Oncopeltus fasciatus*. Physiological Entomology 32, 328–335. https://doi.org/10.1111/j.1365-3032.2007.00582.x.

Wu, C.T., Budding, M., Griffin, M.S., Croop, J.M., 1991. Isolation and characterization of *Drosophila* multidrug resistance gene homologs. Molecular and cellular biology 11, 3940–3948. https://doi.org/10.1128/mcb.11.8.3940-3948.1991.

Xiao, Y., Zhang, T., Liu, C., Heckel, D.G., Li, X., Tabashnik, B.E., Wu, K., 2014. Mis-splicing of the ABCC2 gene linked with Bt toxin resistance in *Helicoverpa armigera*. Scientific Reports 4, 6184. https://doi.org/10.1038/srep06184.

Xiong, J., Feng, J., Yuan, D., Zhou, J., Miao, W., 2015. Tracing the structural evolution of eukaryotic ATP binding cassette transporter superfamily. Scientific Reports 5, 16724. https://doi.org/10.1038/srep16724.

Xu, H.-Q., Ma, M., Ma, Y.-P., Zhang, S.-Y., Li, W.-J., Wei, D., Wang, J.-J., 2021. Identification and Expression Characterization of ATP-Binding Cassette (ABC) Transporter Genes in Melon Fly. Insects 12, 270. https://doi.org/10.3390/insects12030270.

Yang, L., Ravikanthachari, N., Mariño-Pérez, R., Deshmukh, R., Wu, M., Rosenstein, A., Kunte, K., Song, H., Andolfatto, P., 2019. Predictability in the evolution of Orthopteran cardenolide insensitivity. Philosophical transactions of the Royal Society of London. Series B, Biological sciences 374, 20180246. https://doi.org/10.1098/rstb.2018.0246.

Yang, Z.-L., Nour-Eldin, H.H., Hänniger, S., Reichelt, M., Crocoll, C., Seitz, F., Vogel, H., Beran, F., 2021. Sugar transporters enable a leaf beetle to accumulate plant defense compounds. Nature Communications 12, 2658. https://doi.org/10.1038/s41467-021-22982-8.

Yatime, L., Laursen, M., Morth, J.P., Esmann, M., Nissen, P., Fedosova, N.U., 2011. Structural insights into the high affinity binding of cardiotonic steroids to the Na+,K+-ATPase. Journal of structural biology 174, 296–306. https://doi.org/10.1016/j.jsb.2010.12.004.

Yin, C., Shen, G., Guo, D., Wang, S., Ma, X., Xiao, H., Liu, J., Zhang, Z., Liu, Y., Zhang, Y., Yu, K., Huang, S., Li, F., 2016. InsectBase: a resource for insect genomes and transcriptomes. Nucleic Acids Research 44, D801-D807. https://doi.org/10.1093/nar/gkv1204.

Yoder, C.A., Leonard, D.E., Lerner, J., 1976. Intestinal uptake of ouabain and digitoxin in the milkweed bug, *Oncopeltus fasciatus*. Experientia 32, 1549–1550. https://doi.org/10.1007/BF01924445.

You, C., Duan, R., Chen, Y., Liu, Y., Ji, X., 2025. Identification and validation of ABCB transporter genes involved in chlorantraniliprole and emamectin benzoate tolerance in *Spodoptera exigua*. Pesticide Biochemistry and Physiology 215, 106686. https://doi.org/10.1016/j.pestbp.2025.106686.

Yu, Z., Wang, Y., Zhao, X., Liu, X., Ma, E., Moussian, B., Zhang, J., 2017. The ABC transporter ABCH-9C is needed for cuticle barrier construction in *Locusta migratoria*. Insect Biochemistry and Molecular Biology 87, 90–99. https://doi.org/10.1016/j.ibmb.2017.06.005.

Yuan, M., Lu, Y., Zhu, X., Wan, H., Shakeel, M., Zhan, S., Jin, B.-R., Li, J., 2014. Selection and Evaluation of Potential Reference Genes for Gene Expression Analysis in the Brown Planthopper, *Nilaparvata lugens* (Hemiptera: Delphacidae) Using Reverse-Transcription Quantitative PCR. PLOS One 9, e86503. https://doi.org/10.1371/journal.pone.0086503.

Zhai, Y., Lin, Q., Zhou, X., Zhang, X., Liu, T., Yu, Y., 2014. Identification and validation of reference genes for quantitative real-time PCR in *Drosophila suzukii* (Diptera: Drosophilidae). PLOS One 9, e106800. https://doi.org/10.1371/journal.pone.0106800.

Zhang, F., Zhang, W., Liu, L., Fisher, C.L., Hui, D., Childs, S., Dorovini-Zis, K., Ling, V., 2000. Characterization of ABCB9, an ATP Binding Cassette Protein Associated with Lysosomes. The Journal of Biological Chemistry 275, 23287–23294. https://doi.org/10.1074/jbc.M001819200.

Zhen, Y., Aardema, M.L., Medina, E.M., Schumer, M., Andolfatto, P., 2012. Parallel molecular evolution in an herbivore community. Science 337, 1634–1637. https://doi.org/10.1126/science.1226630.

Zuber, R., Norum, M., Wang, Y., Oehl, K., Gehring, N., Accardi, D., Bartozsewski, S., Berger, J., Flötenmeyer, M., Moussian, B., 2018. The ABC transporter Snu and the extracellular protein Snsl cooperate in the formation of the lipid-based inward and outward barrier in the skin of *Drosophila*. European journal of cell biology 97, 90–101. https://doi.org/10.1016/j.ejcb.2017.12.003.

Züst, T., Agrawal, A.A., 2016. Population growth and sequestration of plant toxins along a gradient of specialization in four aphid species on the common milkweed *Asclepias syriaca*. Functional Ecology 30, 547–556. https://doi.org/10.1111/1365-2435.12523.

Züst, T., Mou, S., Agrawal, A.A., 2018. What doesn't kill you makes you stronger: The burdens and benefits of toxin sequestration in a milkweed aphid. Functional Ecology 32, 1972–1981. https://doi.org/10.1111/1365-2435.13144.

List of abbreviations

18S ..... *ribosomal RNA 18S*

aa ..... *amino acid*

ABC ..... *ATP-binding cassette*

ABCB ..... *ATP-binding cassette subfamily B*

acc ..... *accession*

ACN ..... *acetonitrile*

AIC ..... *Akaike's Information Criterion*

AK ..... *arginine kinase*

ANCOVA ..... *Analysis of Covariance*

APS ..... *ammonium persulfate*

ATP ..... *adenosine triphosphate*

BIC ..... *Bayesian information criterion*

bm ..... *biomass*

BSA ..... *bovine serum albumin*

cDNA ..... *DNA complementary to RNA*

cds ..... *coding DNA sequence*

coef ..... *coefficient*

Cp ..... *threshold cycle value*

Cp_c ..... *inter-run calibrated threshold cycle value*

d ..... *deoxyribo*

ddH_2O ..... *double-distilled water/ deionized water*

dfv ..... *defensive fluid volume*

dNTP ..... *deoxyribonucleoside triphosphate*

dsRNA ..... *double stranded RNA*

DTT ..... *dithiothreitol*

ef1a ..... *elongation factor 1 alpha*

egfp ..... *enhanced fluorescent protein*
FT ..... *full transporter*
FWR ..... *family-wise Type I error rate*
GAM ..... Generalized Additive Model
GAPDH ..... *glyceraldehyde 3-phosphate dehydrogenase*
gDNA ..... *genomic DNA*
GLM ..... *Generalized Linear Model*
GSH ..... *glutathione*
h ..... *hour*
HPLC ..... *high performance liquid chromatography*
HT ..... *half transporter*
IgG ..... *immunoglobulin G*
IPC ..... *inter-plate calibrator*
IPTG *Isopropyl-β-d-1-thiogalactopyranoside*
IRF ..... *internal response factor*
IRF.e ..... *empirically determined internal response*
IRF.h ..... *hypothetical internal response factor*
ITSD ..... *internal standard*
kb ..... *kilobase(s) or 1000 bp*
LD_{50} ..... *median lethal dose: the dose required to be lethal to 50 % of the tested population*
LM ..... *General Linear Model*
LRT ..... *Likelihood Ratio Test*
mAb ..... *monoclonal antibody*
MDR ..... *multidrug resistant*
M_e ..... *geNorm M value after step-wise most unstable gene exclusions*
MFS ..... *major facilitator superfamily*
M_i ..... *geNorm M value before step-wise most unstable gene exclusions*
min ..... *minute*
ML ..... *maximum likelihood*
MS ..... *milkweed-seed-fed bug line*
NaCl ..... *sodium chloride*
NBD ..... *nucleotide-binding domain*
NCBI nr ..... *National Library of Medicine Nucleotide collection*
NGS ..... *normal goat serum*
NTC ..... *no template control*

ORF ..... *Open reading frame*
PBS ..... *phosphate-buffered saline*
PCR ..... *polymerase chain reaction*
r ..... *pearson's correlation coefficient with the Bestkeeper Index*
rank(BK) ..... *geometric average of stability Bestkeeper ranks (r and sd)*
$rank_{geo}$ ..... *geometric average of stability ranks*
RNAi ..... *RNA interference*
ROI ..... *region of interest*
rp49 ..... *ribosomal protein 49*
RP-HPLC ..... *reversed phase high performance liquid chromatography*
RPL11 ..... *ribosomal protein L11*
RPS3 ..... *ribosomal protein S3*
rRNA ..... *ribosomal RNA*
RRT ..... *relative retention time*
RT ..... *retention time*
RT-qPCR ..... *real-time quantitative PCR*
saline ..... *0.9 % NaCl*
sd ..... *standard deviation*
SDS ..... *sodium dodecyl sulfate*
SEM ..... *standard error of the mean*
SS ..... *sunflower-seed-fed bug line*
TBP ..... *TATA box-binding protein*
TBST ..... Tris-buffered saline with 0.05 % Tween20
TCDB ..... *transporter classification database*
TEMED ..... *tetramethylethylenediamine*
Tm ..... *melt temperature*
TM ..... *transmembrane helix*
TMD ..... *transmembrane domain*
tubulin *tubulin56D*
X-Gal *5-bromo-4-chloro-3-indolyl-β-D-galactopyranoside*

List of tables

Tables

Table 1 Overview of cardiac glycoside occurrence in different plant and animal families. 8

Table 2 Designed primer pairs for ten reference genes identified in the assembled transcriptome of *Oncopeltus fasciatus* by homology search. 30

Table 3 Overview of the methods and ranking strategies used to evaluate candidate reference gene expression comprehensively. 32

Supplementary tables

Table S 1 177

Table S 2 177

Table S 3 177

Table S 4 177

Table S 5 177

Table S 6, ... 177

Table S 7 177

Table S 8 Accession numbers of queries used for homology search in the de novo assembled transcriptomes of *Oncopeltus fasciatus.* 177

Table S 9 Sequences used for inference of ABCB full transporter phylogenetic relationships. 178

Table S 10 Primer sequences for identified *Ofabcb* half transporter transcripts. 180

Table S 11 Sequencing and standard PCR primers. 181

Table S 12 RNAi and RT-qPCR primer for both predicted OfABCB full transporters. 182

Table S 13 Determined RT-qPCR primer pair efficiencies with pooled samples of seven milkweed bug tissues 183

Table S 14 Determined RT-qPCR primer pair efficiencies with pooled samples of animals exposed to ouabain by injection for different time periods 183

Table S 15 Determined RT-qPCR primer pair efficiencies with pooled samples of dsRNA- and buffer-injected animals. 183

Table S 16 Determined RT-qPCR primer pair efficiencies with pooled samples from animals of both laboratory milkweed bug lines with different diet histories. 184

Table S 17 PCR template sequences used for RNA interference. 184

Table S 18 Trimming results of RNA-seq data by CLC Genomics workbench. 185

Table S 19 Report of the de novo assembly by CLC Genomics workbench. 185

Table S 20 Putative ABCB transporter candidate contig list found by homology search (tblastn) in two transcriptome assemblies 186

Table S 21 Results of the blastx search against the NCBI nr database for putative ABCB contigs found by homology search in the transcriptome of the large milkweed bug assembled by Trinity. 188

Table S 22 Results of the blastx search against the NCBI nr database for putative ABCB contigs found by homology search in the transcriptome of the large milkweed bug assembled by CLC. 198

Table S 23 Pfam (HmmScan), TMHMM and WoLFPSORT analysis of OfABCB proteins and merged isoforms of *Ofabcb2*. 205

Table S 24 Sequence of *Ofabcb1* after sequencing. 206

Table S 25 Sequence of *Ofabcb2* after sequencing. 207

Table S 26 Summary of gene structure analysis and prediction for *Ofabcb2* by different approaches. 209

Table S 27 Expression stabilities of the tested reference gene candidates across different treatments. 211

Table S 28 Results of multi-level calibration with two different HPLC systems. 212

Table S 29 Run conditions used for ouabain quantification optimization in HPLC system II. 212

Table S 30 Exploratory general and generalized linear model summary for modelling released defensive fluid volume as a function of diet history, biomass, sex, and sequestration time 213

Table S 31 Exploratory general and generalized linear model summary for modelling released defensive fluid volume as a function of diet history, biomass, female age, and the total number of releasing sites 215

Table S 32 Post hoc analysis results for the interaction between HPLC quantification method and peak integration using emmeans. 217

Table S 33 Post hoc analysis results for the interaction between sample origin in terms of diet history and peak integration using emmeans 218

Table S 34 Results of HPLC analysis of milkweed bug defensive fluids, mature and maturing seeds from seed pods of *A. syriaca*. 219

Table S 35 Summary of multiple regression models explored to study the effect of sequestered cardenolide concentration and sequestration time on sequestered ouabain amount. 221

Table S 36 Summary of exploratory generalized linear models for modelling sequestered ouabain concentration as a function of diet history and sequestration time 222

Table S 37 Summary of exploratory general and generalized linear models for modelling the released defensive fluid volume as a function of sequestration time, diet history, and sequestered ouabain amount.....223

List of figures

Figures

Figure 1 Chemical structure of cardiac glycosides. 6

Figure 2 Ouabain binding in pig Na,K-ATPase (left) and characteristics of Na,K-ATPase paralogs in *O. fasciatus* (right).....13

Figure 3 3D structure of human ABCB1 (left) and its localization for protective compartment function in tissues (right). 21

Figure 4 Cp_c values (interplate calibrated Cp values) of the seven tested reference genes upon control (black) or cardiac glycoside (ouabain, grey) treatment at different exposure periods (1 – 32 h) represented as beanplots. 34

Figure 5 Expression stabilities of the seven candidate reference genes as determined by Normfinder (A – without experimental group assignment), geNorm (B – *prior* to step-wise exclusion of the least stable genes), the comparative ∆Ct method (C), Bestkeeper (D) and the comprehensive stability by all four methods (E).....36

Figure 6 Expression stabilities of the seven candidate reference genes as determined by Normfinder (A) when experimental group information was included into analysis and by geNorm (B) when most unstable genes were successively excluded from M value calculation (M_e). 37

Figure 7 Immunofluorescence staining of different tissues and defensive fluids of *O. fasciatus* individuals stained with a commercially available anti-ABCB full transporter antibody (C219). 57

Figure 8 Released defensive fluid of *O. fasciatus* stained with toluidine blue-O and pyronine-G.....58

Figure 9 3D model of OfABCB1 (A; 1282 aa) and partial OfABCB2 (B; CLC contig 4439 (1148 aa)) illustrating characteristic ABCB transporter architecture with two transmembrane domains (TMD) and nucleotide-binding domains (NBD) based on Phyre[2].....60

Figure 10 Predicted protein and gene structure of *Ofabcb1*.....61

Figure 11 Predicted gene structure of *Ofabcb2* based on transcriptomic contig and genomic DNA sequence comparison. 64

Figure 12 Phylogenetic analysis of ABCB full transporters of identified OfABCB proteins with transporters of three vertebrate and 26 arthropod species. 66

Figure 13 *Ofabcb* transporter expression in large milkweed bugs. 69

Figure 14 *Ofabcb* gene expression in adult milkweed bugs exposed to cardenolides. 71

Figure 15 Verification of RNAi mediated *Ofabcb* transporter knockdown efficacy and specificity by RT-qPCR. 72

Figure 16 Cardenolide sequestration capacities and mRNA levels of *Ofabcb* knockdown animals. 74

Figure 17 Ouabain amount quantified with HPLC system I in animals with different diets 96

Figure 18 Relative abundance of single cardenolides with respect to polarity detected in milkweed bug defensive fluids (n = 15) and their diet 99

Figure 19 Temporal dynamics of ouabain uptake into the cardenolide storage compartment 102

Figure 20 Defensive fluid volumes in relation to biotic factors potentially related to fluid fillings. 104

Figure 21 Quantification of ABCB full transporter related immunofluorescence in defensive fluids sampled from animals with different diet histories 106

Figure 22 Relative transcript abundance of Na,K-ATPase paralog α1A in *O. fasciatus* challenged by ouabain via injection. 107

Figure 23 Na,K-ATPase subunit immunofluorescence staining of defensive fluids of *O. fasciatus* adults from the laboratory milkweed seed line. 108

Figure 24 Summary of OfABCB full transporter distribution in adult *O. fasciatus* with possible role for cardenolides transport in different tissues. 123

Figure 25 LogP3 distribution of human ABCB1 substrates. 126

Figure 26 Putative mechanisms for cardenolide transport into the thoracic storage compartment involving ABCB full transporter in the double-layered integument according to the histology of Scudder et al. (1986). 127

Supplementary figures

Figure S 1 223

Figure S 2 223

Figure S 3 223

Figure S 4 223

Figure S 5.....223
Figure S 6.....223
Figure S 7.....223
Figure S 8.....223
Figure S 9.....223
Figure S 10.....223
Figure S 11.....223
Figure S 12 Melt curve analysis of *Ofabcb* primer specificity testing.....224
Figure S 13 Unmerged immunofluorescence stainings of defensive fluids with mAb C219 related to Figure 7.....224
Figure S 14 Sampled defensive fluids of *O. fasciatus* individuals stained with two different commercially available anti-ABCB transporter monoclonal antibodies.....225
Figure S 15 Transverse sections of the large milkweed bug's nervous system stained with anti-ABCB transporter monoclonal antibodies.....226
Figure S 16 Transverse sections of the large milkweed bug's Malpighian tubules stained with an anti-ABCB transporter monoclonal antibody.....227
Figure S 17 Identification of potential protein domains in putative ABCB-like transcript sequences identified in two different transcriptome assemblies (Trinity and CLC) by Pfam.....228
Figure S 18 Structure prediction of OfABCB1 (1282 aa) by different software.....229
Figure S 19 3D structure modelling by Phyre^2 for different OfABCB2 isoforms and partial OfABCB1.....230
Figure S 20 Structure prediction of OfABCB2 (1237 aa) by different software.....231
Figure S 21 Section of the alignment of *Ofabcb2* contigs with sequenced PCR fragments of the *Ofabcb2* five prime end.....232
Figure S 22 Nucleotide and predicted protein sequence of *Ofabcb2*.....233
Figure S 23 Raw expression values of *Ofabcb* and reference genes in different tissues.....235
Figure S 24 Gene expression of *Ofabcb1* and *Ofabcb2* in RNAi knockdowns ten days *post* injection compared to control (*egfp*).....235
Figure S 25 Survival rate of adult milkweed bugs seven days after injection with dsRNA or buffer.....236
Figure S 26 HPLC chromatograms of ouabain standards in HPLC system II with different acetonitrile starting concentrations.....237
Figure S 27 HPLC chromatograms of ouabain standards in HPLC system II with different acetonitrile starting concentrations.....238

Figure S 28 HPLC chromatogram of ouabain standard (0.1 µg/µl) in HPLC system II with 2 % acetonitrile (ACN) as starting percentage. 239

Figure S 29 HPLC chromatograms of defensive fluids sampled from adult animals fed on milkweed seeds. 239

Figure S 30 HPLC chromatograms of defensive fluids, isolated calotropin and calactin (A), and mature and maturing milkweed seeds (B). 240

Figure S 31 Graphical exploratory analysis and pairwise Spearman correlations of parameters determined in animals of different diet lines. 241

Figure S 32 Number of released fluid droplets from different cardenolide storage compartment regions. 242

Figure S 33 Immunofluorescence staining of defensive fluids from animals of different diet histories used for ABCB full transporter fluores-cence quantifications. 243

Figure S 34 Secondary antibody control staining of defensive fluid from a metathoracic flange of a milkweed seed line animal. 244

Figure S 35 Immunofluorescence staining of the Na,K-ATPase α-subunit in transverse sections of the Malpighian tubules of *O. fasciatus.* 244

Figure S 36 ABCB transporter immunofluorescence staining of defensive fluids of *O. fasciatus* adults from the laboratory milkweed seed line. 245

Appendix

Supplementary tables

The supplementary tables Table S 1, Table S 2, Table S 3, Table S 4, Table S 5, Table S 6, and Table S 7 have been published and are accessible online at the following link: https://doi.org/10.1016/j.gene.2019.05.032.

Table S 8 Accession numbers of queries used for homology search in the de novo assembled transcriptomes of *Oncopeltus fasciatus*. [1] Flybase, [2] KEGG.

Species	Protein Name	Synonyms	Length [aa]	Type	Genbank accession number	UniProtKB accession number	Other database accessions[1,2]
Homo sapiens	multidrug resistance protein 1	Pgp-1, PGY-1, ABCB1	1280	full	NP_000918.2	P08183.3	
Homo sapiens	multidrug resistance protein 3	Pgp-3, PGY-3, ABCB4	1286	full	NP_061337.1	P21439.2	
Drosophila melanogaster	Multidrug resistance protein 49	CG3879	1302	full	NP_523724.2	Q00449.2	FBgn00045121
Drosophila melanogaster	multidrug resistance protein 50	CG8523	1313	full	NP_523740.3		FBgn00102411
Drosophila melanogaster	multidrug resistance protein 65	CG10181	1302	full	NP_476831.1	Q00748.2	FBgn00045131
Tribolium castaneum	multidrug resistance protein 1B-like	ABCB3A/ ABCB1	1261	full	XP_967244.3		
Tribolium castaneum	multidrug resistance protein 1	ABCB3B/ ABCB1	1263	full	XP_008191266.1		659847 2
Bombyx mori	multidrug resistance protein 1A-like		1268	full	XP_004924686.1		101735691
Bombyx mori	multidrug resistance protein homolog 49-like		1307	full	XP_004929922.1		101735430
Bombyx mori	multidrug resistance protein homolog 49-like		1309	full	XP_004929924.1		101735703
Apis mellifera	multidrug resistance protein homolog 49-like isoform X4		1343	full	XP_623564.3		551167 2
Acyrthosiphon pisum	multidrug resistance protein 1-like		1489	full	XP_008178171.1		100164127 2
Acyrthosiphon pisum	ATP-binding cassette sub-family B member 5-like isoform X1		1334	full	XP_001947434.2		100168150 2
Lygus hesperus	Multidrug resistance protein 1		1176	partial	JAG29193		

Table S 9 Sequences used for inference of ABCB full transporter phylogenetic relationships. Proteins marked with an asterisk were not included in phylogenetic inference because of incompleteness or unusual domain architecture. The latter is indicated further by square brackets. Invert = invertebrate. Vert = vertebrate. Abbr. = abbreviation. TMD = transmembrane domain number. NBD = nucleotide-binding domain number. Both predicted by ExPASy PROSITE. [1] Strauss et al. (2014), [2] Sun et al. (2017), [3] Hull et al. (2014), [4] Sparks et al. (2014).

Taxon	Order	Species	Common name	Abbr.	TMD	NBD		Genbank /Uniprot acc./OrthoDBID/ Genome Database ID/ENSEMBL
Invert	Blattodea	*Blattella germanica*	german cockroach	Bg1	[2]	[2]	*	*BGER026276*
Invert	Blattodea	*Blattella germanica*	german cockroach	Bg2	2	2		*BGER024586*
Invert	Blattodea	*Blattella germanica*	german cockroach				*	*BGER017945*
Invert	Coleoptera	*Chrysomela populi*	poplar leaf beetle[1]	CpABC12	2	2		JAC88902.1
Invert	Coleoptera	*Chrysomela populi*	poplar leaf beetle[1]	CpABC6	2	2		JAC88911.1
Invert	Coleoptera	*Chrysomela populi*	poplar leaf beetle[1]	CpABC10	2	2		GARF01000018.1
Invert	Coleoptera	*Dendroctonus ponderosae*	mountain pine beetle				*	*YQE_09994*
Invert	Coleoptera	*Dendroctonus ponderosae*	mountain pine beetle	Dpo1	[2]	2	*	*YQE_09993*
Invert	Coleoptera	*Dendroctonus ponderosae*	mountain pine beetle	Dpo2	[2]	1	*	*YQE_01739*
Invert	Coleoptera	*Tribolium castaneum*	red flour beetle	Tc1	2	2		*TC003797*
Invert	Coleoptera	*Tribolium castaneum*	red flour beetle	Tc2	2	2		*TC003402*
Invert	Coleoptera	*Ontophagus taurus*	taurus scarab	Ot1	2	2		*OTAU010237*
Invert	Coleoptera	*Ontophagus taurus*	taurus scarab	Ot2	2	2		*OTAU009091*
Invert	Coleoptera	*Ontophagus taurus*	taurus scarab	Ot3	2	2		*OTAU009090*
Invert	Coleoptera	*Ontophagus taurus*	taurus scarab	Ot4	2	2		*OTAU003040*
Invert	Coleoptera	*Ontophagus taurus*	taurus scarab	Ot5	1	2		*MQUAD:000cbb*
Invert	Diptera	*Anopheles gambiae*	mosquito	Ag1	2	2		*AGAP005639*
Invert	Diptera	*Culex quinquefasciatus*	southern house mosquito	Cq1	2	2		*CPIJ016887*
Invert	Diptera	*Drosophila melanogaster*	fruitfly	DmCG10226	2	2		*FBgn0035695*
Invert	Diptera	*Drosophila melanogaster*	fruitfly	DmMDR50	2	2		*Mdr50*
Invert	Diptera	*Drosophila melanogaster*	fruitfly	DmMDR65	2	2		*Mdr65*
Invert	Diptera	*Drosophila melanogaster*	fruitfly	DmMDR49	2	2		*Mdr49*
Invert	Ephemeroptera	*Ephemera danica*	mayfly	Ep1	2	2		*EDAN011836*
Invert	Ephemeroptera	*Ephemera danica*	mayfly	Ep2	[2]	2	*	*EDAN006401*
Invert	Hemiptera	*Acyrthosiphon pisum*	pea aphid	ApMDR1	2	2		XP_001943495.2
Invert	Hemiptera	*Acyrthosiphon pisum*	pea aphid	ApMDR3	2	2		XP_001947434.2
Invert	Hemiptera	*Cimex lectularius*	bed bug	ClMDR1a	2	2		XP_14242293.1
Invert	Hemiptera	*Cimex lectularius*	bed bug	ClMDR1b	2	2		XP_014242217.1
Invert	Hemiptera	*Diuraphis noxia*	Russian wheat aphid	DnMDR1A	2	2	*	XP_015373069.1
Invert	Hemiptera	*Diuraphis noxia*	Russian wheat aphid	DnMDR1Ba	2	2	*	XP_015373066.1
Invert	Hemiptera	*Diuraphis noxia*	Russian wheat aphid	DnMDR1Bb	2	2		XP_015366795.1

Taxon	Order	Species	Common name	Abbr.	TMD	NBD		Genbank /Uniprot acc./OrthoDBID/ Genome Database ID/ENSEMBL
Invert	Hemiptera	*Diuraphis noxia*	Russian wheat aphid	DnABCB4	2	2		XP_015373064.1
Invert	Hemiptera	*Halyomorpha halys*	brown marmoted stink bug[4]	HhMDR1B	2	2		XP_014273829.1
Invert	Hemiptera	*Halyomorpha halys*	brown marmoted stink bug[4]	HhMDR2	2	2		XP_014294685.1
Invert	Hemiptera	*Halyomorpha halys*	brown marmoted stink bug[4]	HhABCB17	2	2		XP_014287103.1
Invert	Hemiptera	*Halyomorpha halys*	brown marmoted stink bug[4]	HhABCB3	2	2		XP_014281320.1
Invert	Hemiptera	*Halyomorpha halys*	brown marmoted stink bug[4]	HhABCB4	2	2		XP_014281317.1
Invert	Hemiptera	*Homalodisca vitripennis*	glassy-winged sharpshooter	Hv1	1	2	*	HVIT014549
Invert	Hemiptera	*Laodelphax striatellus*	small brown planthopper[2]	LsABCB5	2	2		KF828784.1
Invert	Hemiptera	*Laodelphax striatellus*	small brown planthopper[2]	LsABCB6	2	2		KF669399.1
Invert	Hemiptera	*Lygus hesperus*	western tarnished plant bug[3]	LhABCB1	2	2		
Invert	Hemiptera	*Lygus hesperus*	western tarnished plant bug[3]	LhABCB2	1	2		
Invert	Hemiptera	*Lygus hesperus*	western tarnished plant bug[3]	LhABCB6	1	0	*	
Invert	Hemiptera	*Nilaparvata lugens*	brown planthopper	NlMDR1	2	2		XP_022184997.1
Invert	Hemiptera	*Nilaparvata lugens*	brown planthopper	NlMDR49	1	1	*	XP_022205734.1
Invert	Hymenoptera	*Apis mellifera*	western honey bee	Am1	2	2		*GB55378*
Invert	Hymenoptera	*Bombus terrestris*	buff-tailed bumblebee	Bt1	2	2		*15214933*
Invert	Hymenoptera	*Megachile rotundata*	alfalfa leafcutter bee	Mt1	2	2		*MROTU:000b30*
Invert	Isoptera	*Zootermopsis nevadensis*	termite	Zn1	2	2	*	*Znev_08525*
Invert	Isoptera	*Zootermopsis nevadensis*	termite	Zn2	2	2		*Znev_04434*
Invert	Lepidoptera	*Bombyx mori*	silk moth	Bm1	2	2		*BGIBMGA009452*
Invert	Lepidoptera	*Bombyx mori*	silk moth	Bm2	2	2		*BGIBMGA007494*
Invert	Lepidoptera	*Bombyx mori*	silk moth	Bm3	2	2		*BGIBMGA000725*
Invert	Lepidoptera	*Bombyx mori*	silk moth	Bm4	2	2		*BGIBMGA000724*
Invert	Lepidoptera	*Danaus plexippus*	monarch butterfly				*	*DPOGS213261-PA*
Invert	Lepidoptera	*Danaus plexippus*	monarch butterfly	Dpe1	2	2	*	*DPOGS207818-PA*
Invert	Lepidoptera	*Danaus plexippus*	monarch butterfly	Dpe2	2	2		*DPOGS207749-PA*
Invert	Lepidoptera	*Danaus plexippus*	monarch butterfly	Dpe3	[2]	3	*	*DPOGS207748-PA*
Invert	Lepidoptera	*Danaus plexippus*	monarch butterfly	Dpe4	[2]	2	*	*DPOGS207747-PA*
Invert	Lepidoptera	*Danaus plexippus*	monarch butterfly	Dpe5	1	2		*DPOGS207746-PA*
Invert	Lepidoptera	*Danaus plexippus*	monarch butterfly	Dpe6	2	2		*DPOGS206135-PA*
Invert	Lepidoptera	*Manduca sexta*	tobacco hornworm				*	*Msex2.14988*
Invert	Lepidoptera	*Manduca sexta*	tobacco hornworm	Ms1	2	2		*Msex2.09773*
Invert	Lepidoptera	*Manduca sexta*	tobacco hornworm	Ms2	2	2		*Msex2.09107*
Invert	Lepidoptera	*Manduca sexta*	tobacco hornworm	Ms3	2	2		*Msex2.09106*
Invert	Lepidoptera	*Manduca sexta*	tobacco hornworm	Ms4	2	2		*Msex2.07270*
Invert	Odonata	*Calopteryx splendens*	banded demoiselle	Cs1	1	1	*	*size90227-snap-gene-0.8-mRNA-1*

Taxon	Order	Species	Common name	Abbr.	TMD	NBD		Genbank /Uniprot acc./OrthoDBID/ Genome Database ID/ENSEMBL
Invert	Odonata	*Calopteryx splendens*	banded demoiselle				*	*size90227-augustus-gene-0.6-mRNA-1*
Invert	Odonata	*Calopteryx splendens*	banded demoiselle				*	*size644791-processed-gene-2.14-mRNA-1*
Invert	Odonata	*Ladona fulva*		Lf1	1	2		*LFUL010046*
Invert	Odonata	*Ladona fulva*		Lf2	2	2		*LFUL001427*
Invert	Odonata	*Ladona fulva*		Lf3			*	*LFUL001421*
Invert	Onychura	*Daphnia pulex*	water flea	Dpu1	2	2		DAPPUDRAFT347265
Invert	Onychura	*Daphnia pulex*	water flea	Dpu2	2	2		DAPPUDRAFT347264
Invert	Phthiraptera	*Pediculus humanus*	louse	Ph1	2	2		*PHUM578820*
Invert	Phthiraptera	*Pediculus humanus*	louse	Ph2	2	2		*PHUM261630*
Invert	Phthiraptera	*Pediculus humanus*	louse	Ph3	2	2		*PHUM177140*
Invert	Trombidiformes	*Tetranychus urticae*	red spide mite	TuABCB-01	2	2		tetur11g04030
Invert	Trombidiformes	*Tetranychus urticae*	red spide mite	TuABCB-02	2	2		*tetur11g04040*
Vert	Cypriniformes	*Danio rerio*	zebrafish	DrABCB4	2	2		ENSDART00000148456.3
Vert	Cypriniformes	*Danio rerio*	zebrafish	DrABCB5	2	2		ENSDART00000141616.2
Vert	Cypriniformes	*Danio rerio*	zebrafish	DrABCB11a	2	2		ENSDART00000139631.3
Vert	Cypriniformes	*Danio rerio*	zebrafish	DrABCB11b	2	2		ENSDART00000102557.5
Vert	Galliformes	*Gallus gallus*	chicken	GgABCB1a	2	2		ENSGALT00000070008.1
Vert	Galliformes	*Gallus gallus*	chicken	GgABCB1b	2	2		ENSGALT00000014493.5
Vert	Galliformes	*Gallus gallus*	chicken	GgABCB5	2	2		ENSGALT00000017732.5
Vert	Galliformes	*Gallus gallus*	chicken	GgABCB11	2	2		ENSGALT00000017711.5
Vert	Primates	*Homo sapiens*	human	HsABCB1	2	2		P08183
Vert	Primates	*Homo sapiens*	human	HsABCB4	2	2		P21439
Vert	Primates	*Homo sapiens*	human	HsABCB5	2	2		Q2M3G0
Vert	Primates	*Homo sapiens*	human	HsABCB11	2	2		O95342

Previous table continued.

Table S 10 Primer sequences for identified *Ofabcb* half transporter transcripts.

Transcript	Size [bp]	Type	Sequence (5' → 3')
Ofabcb6	462	fwd	GTTCAACAGTACACCACACG
		rev	CGACTTCCATTCTTCGATTTGA
Ofabcb7	516	fwd	CTTCCATCTCTCCAGGCAAA
		rev	ACAAGGTCTCCAACAGTCAG
Ofabcb8	518	fwd	CCCGCTGCAAAATTGGTTAT
		rev	TGGCATGTTTTCTCAAGTTCC
Ofabcb10	512	fwd	TGTGTTTCTTGTAGGTGGCT
		rev	CGGTCATGGCTAATCTGAGT

Table S 11 Sequencing and standard PCR primers. Consensus sequence refers to the transcript sequence prolonged with genomic scaffold sequences (*Ofabcb1*: 4479 bp, *Ofabcb2*: 9022 bp). CDS = protein-coding sequence (*Ofabcb1*: 3846 bp, Ofabcb2: 3711 bp). pFastBac™Dual, pGEM®-T = cloning vectors. Details of *Ofabcb1* cloning are described in the Master's thesis of Lisiecki (2018). Seq. = sequence. Fwd = forward primer, rev = reverse primer. Start position refers to matching position of the primer 5' strand end. Numbers in brackets refer to positions in cloning vectors.

Target	Primer	Type	Sequence (5' → 3')	Start position	
				Consensus sequence	CDS
Ofabcb1	OfABCB1_PW5'-1fw	fwd	GAGGAGCGACTGTTATTAGG	383	-
Ofabcb1	23955_5'UTR/2ss	fwd	GAAGCGGCGAAGGGTG	502	6
Ofabcb1	Onfa_5'UTR/1ss	fwd	CAAAAGTCAGGAATAATCGGCTTATTC	620	124
Ofabcb1	Onfa 23955-10ss	fwd	TACTCTCTATTCCACTTATGGTCTGG	1483	987
Ofabcb1	qOnfa_23955-3ss	fwd	TTCTTCAGCTATCCTACCCGAC	1763	1267
Ofabcb1	Onfa 23955/4ss	fwd	GGACTCTCAGAGTGAAGGC	2254	1758
Ofabcb1	qOnfa_23955ss	fwd	CAGGAGGCCCTGGAGAAC	2279	1783
Ofabcb1	qOnfa_23955-2ss	fwd	CTCCACCATAAGGAACGCCA	2338	1842
Ofabcb1	Onfa 23955-11ss	fwd	AGAGATGTCTATGTTGAATATTTAAAGC	3260	2764
Ofabcb1	Of_23955-12ss	fwd	TGTCAGGCGATTGTCTACTT	3344	2848
Ofabcb1	Of_23955-14ss	fwd	TGGTTGTGGAAAGTCAAC	3724	3228
Ofabcb1	Onfa 23955/2ss	fwd	GACATGAACATAGAAACATTCAATGTGAGC	3800	3304
Ofabcb1	Onfa 23955/1ss	fwd	ACATAGAAACATTCAATGTGAGC	3807	3311
Ofabcb1	Onfa 23955/3ss	fwd	GCATTGTTACCCAAGAGCCAGTGTT	3849	3353
Ofabcb1	OfABCB1_PW5'-1rv	rev	AGCTGCTGTTCTGATCAAAT	839	343
Ofabcb1	Onfa23955-6as	rev	ATCGATATCTGGGATTCGATCT	1699	1203
Ofabcb1	Onfa 23955-10as	rev	AAAGAATATTATCCGTGCGGAAGT	3541	3045
Ofabcb1	Of_23955-12as	rev	CCTCATCGAGAAGAAGGATT	4118	3622
Ofabcb1	Onfa 23955/1as	rev	CCAAGTTCAGCAACCCTC	4278	3782
Ofabcb1	Onfa 23955/2as	rev	ATGAGTTCCAAGTTCAGCAACCCTC	4285	3789
Ofabcb1	Onfa 23955/3as	rev	GCTGCTGCCTCTTGACTAACTGG	4340	3844
Ofabcb1	Onfa_3'UTR/1	rev	GGTTTTCTGTACAAATAAATAGCTTTTCTCAG	4397	-
Ofabcb1	Of_23955-14as	rev	TTTGGTTCAAAACTACCAAAA	4471	-
Ofabcb1	23955_3'UTR/2as	rev	CTTTTATTTTTGGTTCAAAACTACCAA	4479	-
Ofabcb2	OfABCB2-PW5'-2fw	fwd	TCCAAGGATAAGGATTTACGACG	2148	-
Ofabcb2	3184_5'UTR/1ss	fwd	GGCTTCAAGGAGTTCAGAAA	2296	70
Ofabcb2	Of_3184-8ss	fwd	CTTCAGCGCTAGCTACAAGA	3462	495
Ofabcb2	Onfa_3184-4ss	fwd	CCTCGAGAAATTAAGAGATATGGC	3652	685
Ofabcb2	Onfa_3184/2ss	fwd	GACGCCCACAGTGAGAA	4598	1558
Ofabcb2	Onfa_3184/1 ss	fwd	AGATGATAGTAGTTATGCGATTAAAGG	5277	2237
Ofabcb2	Of_3184-9ss	fwd	AAAAGGGATGCCAAATACAT	5579	2539
Ofabcb2	Onfa_3184-5ss	fwd	GGATGCCAAATACATGGATGAT	5584	2544
Ofabcb2	Of_3184-10ss	fwd	TCTCATTGGTCTTCTGGAAA	6160	3120
Ofabcb2	Onfa_3184-6ss	fwd	CAAGCGACTTGGAGGATTATAC	6709	3669
Ofabcb2	Of_3184-11ss	fwd	GCGAAAGAAGACTTTTACAGCA	6806	-
Ofabcb2	Of_3184-12ss	fwd	CTTCATGTGACCCTGTTGAT	7308	-
Ofabcb2	Of_3184-7ss	fwd	CGATATACACTGATTTACTAACAGCATT	7597	-
Ofabcb2	OfABCB2-PW5'-2rv	rev	TTCACATGCCGTCTCCCAG	3240	297
Ofabcb2	Of_3184-7as	rev	CCTCGCCATATCTCTTAAT	3705	712
Ofabcb2	Onfa_3184-3as	rev	TGCATTGCCCACTGTGAAG	3935	918

Target	Primer	Type	Sequence (5' → 3')	Start position	
				Consensus sequence	CDS
Ofabcb2	Of_3184-8as	rev	ACTGCAGGTTGTAGTCCTC	4284	1267
Ofabcb2	Onfa_3184-4as	rev	CCTTCTCCATCAGCTCTTCA	4769	1729
Ofabcb2	Onfa_3184/2as	rev	GAACAGAGGCATGCTGGT	5119	2079
Ofabcb2	Onfa_3184/1 as	rev	CTTGTGAAATAGCAAATACTAAGGC	5768	2728
Ofabcb2	Of_3184-9as	rev	TTTCCTTTATGGAGCAATCA	6314	3274
Ofabcb2	Of_3184-10as	rev	CGCCAATATTTTCATTTTGA	6928	-
Ofabcb2	Of_3184UTR3'-1as	rev	TCTTATACACTTTCCACGCC	6944	-
Ofabcb2	Of_3184-11as	rev	AAGTAGCTCGGTCACCTCA	7516	-
Ofabcb2	Onfa_3184-6as	rev	TTACTTAGACTGAGAATCTTGGAGAA	7886	-
Ofabcb2	Of_3184-12as	rev	TCTATGCAACATGCCCTAGT	7976	-
Ofabcb2	3184_3'UTR/1as	rev	CCCAATTGATTATGGATTGAATCA	8921	-
pFastBac ™Dual	PHD_pfastBac_fw	fwd	TTCATACCGTCCCACCAT	[4581]	
	PHD_pfastBac_rev	rev	GATCCTCTAGTACTTCTCG	[4725]	
pGEM®-T	T7	fwd	TAATACGACTCACTATAGGG	[2984]	
	Sp6	rev	TATTTAGGTGACACTATAG	[144]	

Previous table continued.

Table S 12 RNAi and RT-qPCR primer for both predicted OfABCB full transporters. Start refers to first matching position of the primer 5' strand end in the CDS of either *Ofabcb1* or *Ofabcb2*. gDNA refers to amplicon with DNA as template. The reverse RT-qPCR primer of *Ofabcb2* is designed to an in silico predicted exon-exon junction, which should not allow gDNA amplification. Underlined sequence corresponds to the T7 promoter primer sequence.

	Gene	Size [bp]	gDNA size [bp]	Type	Start	Sequence (5' → 3')
RNAi	*Ofabcb1*	475		fwd	1983	GATTAATACGACTCACTATAGGGACAATG GCTTACCAGTGGTAGTG
				rev	2409	GATTAATACGACTCACTATAGGGAACGCA GAATGTTCGCCATAGC
	Ofabcb2	572		fwd	1558	GATTAATACGACTCACTATAGG GAGACGCCCACAGTGAGAAAG
				rev	2081	GATTAATACGACTCACTATAGGGAGAGAA CAGAGGCATGCTGGT
	egfp	470		fwd	66	GATTAATACGACTCACTATAGGGACGTAA ACGGCCACAAGTTCAG
				rev	499	GATTAATACGACTCACTATAGGGATGAAG TTCACCTTGATGCCG
RT-qPCR	*Ofabcb1*	114	3369	fwd	1842	CTCCACCATAAGGAACGCCA
				rev	1995	GTGACCAGGCTGAAGTAAGC
	Ofabcb2	113	-	fwd	2877	GGACTTTGCGAAGGCCAAG
				rev	2989	CTCTGCCTTTGATCGTTGGC

Table S 13 Determined RT-qPCR primer pair efficiencies with pooled samples of seven milkweed bug tissues. Tissues: male and female gonads, salivary glands, thoracic region, Malpighian tubule, nervous system and gut. CI = 95 % confidence interval.

Gene	Type	Efficiency value	SE efficiency value	CI efficiency		Efficiency [%]	R^2
				lower	upper		
Ofactin5C	Reference	2.01	0.01	1.98	2.03	100.844	0.999
Ofef1a	Reference	1.97	0.01	1.96	1.99	97.091	0.999
Ofrp49	Reference	2.00	0.01	1.97	2.03	99.739	0.999
Oftubulin	Reference	2.03	0.01	2.01	2.05	102.835	0.999
Ofabcb1	Target	2.00	0.01	1.98	2.02	100.406	0.999
Ofabcb2	Target	2.06	0.04	1.98	2.14	105.923	0.994

Table S 14 Determined RT-qPCR primer pair efficiencies with pooled samples of animals exposed to ouabain by injection for different time periods.

Gene	Type	Efficiency value	SE efficiency value	CI efficiency		Efficiency [%]	R^2
				lower	upper		
Ofef1a	Reference	2.02	0.03	1.96	2.09	102.42	0.9937
Ofrp49	Reference	2.04	0.01	2.01	2.07	104.02	0.9992
Oftubulin	Reference	2.07	0.02	2.04	2.10	107.13	0.9987
Ofabcb1	Target	2.16	0.05	2.06	2.26	116.12	0.9901
Ofabcb2	Target	2.15	0.05	2.05	2.25	115.03	0.9912

Table S 15 Determined RT-qPCR primer pair efficiencies with pooled samples of dsRNA- and buffer-injected animals.

Gene	Type	Efficiency value	SE efficiency value	CI efficiency		Efficiency [%]	R^2
				lower	upper		
Ofef1a	Reference	1.98	0.01	1.95	2.00	97.7	0.999
Ofrp49	Reference	2.03	0.01	2.02	2.05	103.5	0.999
Oftubulin	Reference	2.12	0.01	2.09	2.14	111.6	0.999
Ofabcb1	Target	2.06	0.02	2.02	2.10	106.2	0.997
Ofabcb2	Target	2.08	0.03	2.01	2.15	108.2	0.986

Table S 16 Determined RT-qPCR primer pair efficiencies with pooled samples from animals of both laboratory milkweed bug lines with different diet histories.

Gene	Type	Efficiency value	SE efficiency value	CI efficiency lower	CI efficiency upper	Efficiency [%]	R^2
Ofactin5C	Reference	2.01	0.01	1.98	2.03	100.8	0.999
Ofef1a	Reference	1.97	0.01	1.96	1.99	97.1	0.999
Ofrp49	Reference	2.00	0.01	1.97	2.03	99.7	0.999
Oftubulin	Reference	2.03	0.01	2.01	2.05	102.8	0.999
Ofabcb1	Target	2.00	0.01	1.98	2.02	100.4	0.999
Ofabcb2	Target	2.06	0.04	1.98	2.14	105.9	0.994

Table S 17 PCR template sequences used for RNA interference. Underlined sequence corresponds to the T7 promoter primer sequence.

Ofabcb1 (475 bp)

GATTAATACGACTCACTATAGGGACAATGGCTTACCAGTGGTAGTGACACGAGAGAGAC
CAAAGTCATTGTCTGAATCAAGCTACTCTCTAGTTGAATCAGAGAAGGATGAAGATGAAG
ACGTATGCTACGAAGAGGATAAAAGCTTGGTTTTGTGGAGACTGTTAAAGTTAAATGCGA
AAGAATGGCATCTCTTGCTTTTTGGATTCCTTGCCTCTGCTGTAACTGGAGCGATTCAGC
CAATTTTTGCTTTCTTTTACGGCGAAATATTTTCGACATTTTCTATGACTGGTGATGCTCT
GGAGCAGCAACGGACACTCTGGACTTGTATGTTTGTTCTTCTTGGCGTTGTCTCTGGTTT
AGCTTATTGGTTATGGGTTGTTACTATGGCAACATCAGCTGAGTACTTGATCGCCCGCCT
GAGGTCAATGGCTATGGCGAACATTCTGCGTTCCCTATAGTGAGTCGTATTAATC

Ofabcb2 (572bp)

GATTAATACGACTCACTATAGGGAGACGCCCACAGTGAGAAAGTGGTACAGGCCGCCCT
GGAGAATGCAGCTCAAGGAAGGACAACCATCACTATAGCGCACAGGCTCTCCACCGTC
AAGAACGTAGACAGGATTTATGCCCTGAAGGATGGCAAGGTGTACGAATCGGGTAAACA
TGAAGAGCTGATGGAGAAGGAAGGTCTGTATTACAGCCTTGTAATGGCACAGAAAGGGC
GAGACCAGAAGAAGCAACTCTCGGACGATGAATCGCCAGAAGAAGATGCTCAAGTTAAT
CAGCAACCTAATGTCGTGGAAACGAAAAAACCAGGTTTCTTTTCAAGAATTTCATTAAGG
AGGCGAAAGTCTTCAGCATTGTCATTACGCAATGTTTTTGTGGGAGCTCCTAAAGACGAA
GATTCATCCAAAGAGGAACTTGCTAAGAATGTAAGCTTTTACAAAATCATCAAAATGAATT
TGTCTCTATGGCCTTTCATGCTCCTAACTCTGATTGGTTGTGCCACAGTTGGAACCAGCA
TGCCTCTGTTCTCTCCCTATAGTGAGTCGTATTAATC

egfp (482bp)

GATTAATACGACTCACTATAGGGACGTAAACGGCCACAAGTTCAGCGTGTCCGGCGAGG
GCGAGGGCGATGCCACCTACGGCAAGCTGACCCTGAAGTTCATCTGCACCACCGGCAA
GCTGCCCGTGCCCTGGCCCACCCTCGTGACCACCCTGACCTACGGCGTGCAGTGCTTC
AGCCGCTACCCCGACCACATGAAGCAGCACGACTTCTTCAAGTCCGCCATGCCCGAAG
GCTACGTCCAGGAGCGCACCATCTTCTTCAAGGACGACGGCAACTACAAGACCCGCGC
CGAGGTGAAGTTCGAGGGCGACACCCTGGTGAACCGCATCGAGCTGAAGGGCATCGAC
TTCAAGGAGGACGGCAACATCCTGGGGCACAAGCTGGAGTACAACTACAACAGCCACA
ACGTCTATATCATGGCCGACAAGCAGAAGAACGGCATCAAGGTGAACTTCATCCCTATA
GTGAGTCGTATTAATC

Table S 18 Trimming results of RNA-seq data by CLC Genomics workbench.

				low quality (limit = 0.01)	ambiguous nucleotides (max = 2 nt)	terminal nucleotides (1 at 5' and 3')	Sequences on length (< 50bp)	Length [bp]
RNA-seq reads	single end	indiv1_GGGT	input	4426748	4413703	4413699	4413008	100.0
			not trimmed	3143188	4413382	0	4172936	
			trimmed	1270515	317	4413008	0	94.5
			discarded	13045	4	691	240072	
		indiv1_TGGG T	input	3462046	3461029	3460879	3460801	95.0
			not trimmed	2323444	3458280	0	3292863	
			trimmed	1137585	2599	3460801	0	89.9
			discarded	1017	150	78	167938	
	paired end	YZ07-4	input	54219348	54191066		54183210	101.0
			not trimmed	42350512	54166552		51657373	
			trimmed	11840554	16658		0	95.27
			discarded	28282	7856		2525837	

Table S 19 Report of the de novo assembly by CLC Genomics workbench.

		Scaffold regions	
		included	not included
contig measurements	N75	370	359
	N50	654	621
	N25	1494	1394
	Minimum	137	65
	Maximum	17540	17540
	Average	569	544
	Count	84408	88185
	Total	48013032	47967217

		Count	Avg. Length [bp]	Total bases
summary statistics	Reads	59123172	97.11	5741333447
	Matched	50482378	97.08	4900940559
	Not matched	8640794	97.26	840392888
	Contigs	84408	568	48013032
	Reads in pairs	38476294	162.71	
	Broken paired reads	4995461	97.59	

Table S 20 Putative ABCB transporter candidate contig list found by homology search (tblastn) in two transcriptome assemblies (conducted with Trinity or CLC). ABCB family affiliation and clusters were determined by blastx analysis against the NCBI nr database and blastn of candidate lists against each other. The frame and position of functional protein regions on the nucleotide sequence predicted by Pfam is given as follows: TMD = ABC_membrane: transmembrane (TM) domain PF00664, Clan CL0241; NBD = ABC_tran: nucleotide-binding domain PF00005, CL0023; MTABC_N: mitochondrial ABCB-transporter N-terminal five TM region PF16185. Asterisk indicate presence of frame shifts within a contig sequence.

Blastx	Cluster	Assembly	Contig ID	Length [bp]	Frame	TMD		NBD		TMD		NBD		MTABC_N	
						from	to	from	to	from	to	from	to	from	to
ABCB	*Ofabcb1*	Trinity	c23955_g1_i2	3978	+2	176	1099	1298	1747	2147	2968	3164	3625		
ABCB	*Ofabcb1*	CLC	3211	3565	+3	3	686	885	1334	1734	2555	2751	3212		
ABCB	*Ofabcb1*	Trinity	c23955_g1_i1	597	+2							122	244		
ABCB	*Ofabcb2*	CLC	4439	5622	+1	1	636	835	1284	1756	2580	2776	3234		
ABCB	*Ofabcb2*	Trinity	c22616_g1_i1	4610	+1			13	180	652	1476	1672	2130		
ABCB	*Ofabcb2*	Trinity	c25605_g2_i7	2966	-4	1130	483	284	6						
ABCB	*Ofabcb2*	Trinity	c25605_g2_i6	2727	-5	1292	483	284	6						
ABCB	*Ofabcb2*	Trinity	c25605_g2_i2	2705	-4	1130	483	284	6						
ABCB	*Ofabcb2*	Trinity	c25605_g2_i11	2382	-5	1130	483	284	6						
ABCB	*Ofabcb2*	Trinity	c25605_g2_i5	1822	-6	1133	483	284	6						
ABCB	*Ofabcb2*	Trinity	c25605_g2_i1	1554	-5	1130	483	284	6						
ABCB	*Ofabcb2*	Trinity	c25605_g2_i8	1479	-5	1211	483	284	6						
ABCB	*Ofabcb6*	CLC	22653	2614	+1					583	1416	1600	2049	1	555
ABCB	*Ofabcb6*	Trinity	c24244_g1_i2	2093	+1					61	894	1078	1527		
ABCB	*Ofabcb6*	Trinity	c24244_g1_i1	1218	+2							203	652		
ABCB	*Ofabcb7*	Trinity	c25277_g2_i3	3098	+2					488	1339	1529	1978		
ABCB	*Ofabcb7*	Trinity	c25277_g2_i1	3069	+3					627	1310	1500	1949		
ABCB	*Ofabcb7*	Trinity	c25277_g2_i2	3060	+2					446	1297	1487	1936		
ABCB	*Ofabcb7*	CLC	13840	3057	+2					446	1297	1487	1936		
ABCB	*Ofabcb8*	Trinity	c33998_g1_i1	968	-4							968	600		
ABCB	*Ofabcb8*	CLC	5124	681	+2							2	79		
ABCB	*Ofabcb10*	CLC	2826	2980	+1/+2*	542	1366	1705	2001	1741		1556	1807		
ABCB	*Ofabcb10*	Trinity	c24754_g1_i1	2262	+2					542	1366	1556	2014		
ABCB	MDR_Cl_3	CLC	13665	1814	+2					80	901	1097	1558		
ABCB	MDR_Cl_3	Trinity	c20521_g3_i1	983	+2							449	910		
ABCB	MDR_Cl_3	Trinity	c20521_g1_i1	557	+2							1	100		
ABCB	MDR_Cl_3	Trinity	c74772_g1_i1	386											
ABCB	MDR_Cl_4	CLC	23683	1490	+3					6	326	516	968		
ABCB	MDR_Cl_4	Trinity	c18098_g1_i1	1487	-6					1482	1162	972	520		
ABCB	MDR_Cl_5	CLC	20847	663	+3					3	548				
ABCB	MDR_Cl_5	Trinity	c34901_g1_i1	564	-5/-6*	*268*	*38*			*2*	*114*				
ABCB	MDR_Cl_6	CLC	31759	1175	-4			1175	825	407	3				
ABCB	MDR_Cl_6	Trinity	c1359_g1_i1	955	-5					954	802	384	1		
ABCB	MDR_Cl_7	CLC	11526	1430	-4					1430	993	797	336		
ABCB	MDR_Cl_7	Trinity	c12746_g1_i1	1412	+1					1	438	634	1095		

Blastx	Cluster	Assembly	Contig ID	Length [bp]	Frame	TMD		NBD		TMD		NBD		MTABC_N	
						from	to	from	to	from	to	from	to	from	to
ABCB	MDR_Cl_8	CLC	35761	606	-6							604	332		
ABCB	MDR_Cl_8	Trinity	c33615_g1_i1	504	+3							9	173		
ABCC		Trinity	c21756_g1_i1	4475											
ABCC		Trinity	c24340_g1_i2	3928											
ABCC		Trinity	c24340_g1_i3	3849											
ABCC		Trinity	c25303_g1_i3	3841											
ABCC		Trinity	c25303_g1_i4	3840											
ABCC		Trinity	c25303_g1_i2	3822											
ABCC		Trinity	c24340_g1_i4	3725											
ABCC		Trinity	c24340_g1_i8	3645											
ABCC		Trinity	c24340_g1_i6	2934											
ABCC		Trinity	c25303_g1_i1	2712											
ABCC		Trinity	c23997_g1_i2	2293											
ABCC		Trinity	c23997_g1_i1	2233											
ABCC		Trinity	c15290_g1_i1	1739											
ABCC		Trinity	c21129_g1_i3	1694											
ABCC		Trinity	c15290_g1_i2	1636											
ABCC		Trinity	c21129_g1_i2	1611											
ABCC		Trinity	c24340_g1_i5	1547											
ABCC		Trinity	c24340_g1_i7	1289											
ABCC		CLC	8943	5312											
ABCC		CLC	9692	5118											
ABCC		CLC	13364	4428											
ABCC		CLC	9166	3274											
ABCC		CLC	16414	2418											
ABCC		CLC	9679	2252											
ABCC		CLC	23156	1918											
ABCC		CLC	1581	1699											
ABCC		CLC	22366	1664											
ABCC		CLC	11299	1205											

Previous table continued.

Table S 21 Results of the blastx search against the NCBI nr database for putative ABCB contigs found by homology search in the transcriptome of the large milkweed bug assembled by Trinity. The top five blastx hits are given.

ABC subfamily	Contig ID	Hit	Accession Genbank	Taxon	Name	Bit score	Identity [%]	Positives [%]	E-value
B	**1359_g1i1**	**1**	XP_008178172	Hemiptera	PREDICTED: ATP-binding cassette sub-family B member 5-like isoform X3 [Acyrthosiphon pisum]	231,9	42,90	61,73	1,65E-64
		2	XP_008178173	Hemiptera	PREDICTED: multidrug resistance protein 1A-like isoform X4 [Acyrthosiphon pisum]	231,1	41,76	60,59	1,89E-64
		3	XP_001947434	Hemiptera	PREDICTED: ATP-binding cassette sub-family B member 5-like isoform X1 [Acyrthosiphon pisum]	231,1	41,76	60,59	3,36E-64
		4	KFM57969	Araneae	Multidrug resistance protein 1B, partial [Stegodyphus mimosarum]	221,9	45,14	60,19	1,40E-61
		5	XP_002110955	Placozoa	hypothetical protein TRIADDRAFT_54423 [Trichoplax adhaerens]	209,9	44,15	60,23	8,25E-57
B	**12746_g1i1**	**1**	XP_009954582	Aves	PREDICTED: multidrug resistance protein 3-like [Leptosomus discolor]	428,3	49,07	69,30	2,32E-141
		2	XP_010171785	Aves	PREDICTED: multidrug resistance protein 3-like [Caprimulgus carolinensis]	438,3	49,30	70,56	2,56E-141
		3	XP_010150590	Aves	PREDICTED: multidrug resistance protein 3-like [Eurypyga helias]	431,8	49,30	70,09	5,91E-141
		4	KFQ92704	Aves	Multidrug resistance protein 3, partial [Nipponia nippon]	432,6	49,30	69,63	1,69E-140
		5	XP_009968839	Aves	PREDICTED: multidrug resistance protein 3-like [Tyto alba]	429,1	49,07	69,63	6,92E-140
C	**15290_g1i1**	**1**	XP_012274748	Hymenoptera	PREDICTED: probable multidrug resistance-associated protein lethal(2)03659 [Orussus abietinus]	681,4	73,11	86,44	0,00E+00
		2	XP_011301163	Hymenoptera	PREDICTED: probable multidrug resistance-associated protein lethal(2)03659 [Fopius arisanus]	676,4	70,93	86,56	0,00E+00
		3	XP_008561150	Hymenoptera	PREDICTED: probable multidrug resistance-associated protein lethal(2)03659 [Microplitis demolitor]	662,9	69,91	85,40	0,00E+00
		4	XP_011877731	Hymenoptera	PREDICTED: probable multidrug resistance-associated protein lethal(2)03659 [Vollenhovia emeryi]	662,1	71,05	83,11	0,00E+00
		5	XP_011635941	Hymenoptera	PREDICTED: LOW QUALITY PROTEIN: probable multidrug resistance-associated protein lethal(2)03659 [Pogonomyrmex barbatus]	661,8	71,37	83,70	0,00E+00
	15290_g1i2	**1**	XP_011301163	Hymenoptera	PREDICTED: probable multidrug resistance-associated protein lethal(2)03659 [Fopius arisanus]	565,1	73,51	87,57	0,00E+00
		2	XP_008561150	Hymenoptera	PREDICTED: probable multidrug resistance-associated protein lethal(2)03659 [Microplitis demolitor]	560,5	72,51	86,25	0,00E+00
		3	XP_011551880	Lepidoptera	PREDICTED: probable multidrug resistance-associated protein lethal(2)03659 [Plutella xylostella]	533,1	70,49	85,25	1,23E-180
		4	XP_012274748	Hymenoptera	PREDICTED: probable multidrug resistance-associated protein lethal(2)03659 [Orussus abietinus]	556,6	73,77	86,89	2,07E-180
		5	AKC34900	Lepidoptera	ABCC4-like protein [Spodoptera litura]	555,8	71,31	87,16	1,70E-179
B	**18098_g1i1**	**1**	XP_008167865	Testudinata	PREDICTED: multidrug resistance protein 3 isoform X5 [Chrysemys picta bellii]	355,9	50,00	70,98	6,36E-115

ABC subfamily	Contig ID	Hit	Accession Genbank	Taxon	Name	Bit score	Identity [%]	Positives [%]	E-value
		2	XP_011589427	Aves	PREDICTED: multidrug resistance protein 3-like isoform X3 [Aquila chrysaetos canadensis]	355,5	48,28	67,90	2,67E-114
		3	XP_008178172	Hemiptera	PREDICTED: ATP-binding cassette sub-family B member 5-like isoform X3 [Acyrthosiphon pisum]	377,5	50,91	69,09	5,57E-114
		4	XP_008178171	Hemiptera	PREDICTED: multidrug resistance protein 1A-like isoform X2 [Acyrthosiphon pisum]	377,5	50,91	69,09	5,58E-114
		5	XP_001947434	Hemiptera	PREDICTED: ATP-binding cassette sub-family B member 5-like isoform X1 [Acyrthosiphon pisum]	377,5	50,91	69,09	8,37E-114
B	**20521_g1i1**	**1**	AAP92331	Bivalvia	multixenobiotic resistance protein [Crassostrea virginica]	235,0	66,27	83,43	3,63E-73
		2	XP_009974860	Aves	PREDICTED: multidrug resistance protein 3-like, partial [Tyto alba]	227,6	66,07	79,76	6,68E-72
		3	XP_010724661	Aves	PREDICTED: multidrug resistance protein 3-like, partial [Meleagris gallopavo]	227,6	67,26	79,76	1,05E-71
		4	XP_008167865	Testudinata	PREDICTED: multidrug resistance protein 3 isoform X5 [Chrysemys picta bellii]	231,9	65,68	81,66	2,93E-71
		5	XP_010631195	Rodentia	PREDICTED: multidrug resistance protein 1A-like [Fukomys damarensis]	225,7	64,50	80,47	5,28E-71
B	**20521_g3i1**	**1**	EYC12946	Nematoda	hypothetical protein Y032_0045g1172 [Ancylostoma ceylanicum]	288,5	51,69	72,28	5,22E-91
		2	XP_008178172	Homoptera	PREDICTED: ATP-binding cassette sub-family B member 5-like isoform X3 [Acyrthosiphon pisum]	302,0	62,24	77,18	2,90E-89
		3	XP_008178171	Hemiptera	PREDICTED: multidrug resistance protein 1A-like isoform X2 [Acyrthosiphon pisum]	301,6	62,24	77,18	3,54E-89
		4	XP_001947434	Hemiptera	PREDICTED: ATP-binding cassette sub-family B member 5-like isoform X1 [Acyrthosiphon pisum]	301,2	62,24	77,18	4,35E-89
		5	KFM66885	Araneae	Multidrug resistance protein 1, partial [Stegodyphus mimosarum]	277,3	56,85	76,35	4,15E-88
C	**21129_g1i2**	**1**	KDR09980	Isoptera	cGMP-dependent protein kinase, isozyme 1, partial [Zootermopsis nevadensis]	557,4	56,71	74,19	5,41E-175
		2	XP_012273062	Hymenoptera	PREDICTED: ATP-binding cassette sub-family C member Sur [Orussus abietinus]	528,1	55,08	72,56	1,81E-166
		3	XP_012265786	Hymenoptera	PREDICTED: ATP-binding cassette sub-family C member Sur [Athalia rosae]	524,6	52,65	71,12	2,21E-165
		4	XP_012225332	Hymenoptera	PREDICTED: LOW QUALITY PROTEIN: ATP-binding cassette sub-family C member 9 [Linepithema humile]	529,6	54,38	71,31	7,36E-165
		5	XP_006560974	Hymenoptera	PREDICTED: ATP-binding cassette sub-family C member Sur isoform X4 [Apis mellifera]	521,2	53,83	72,78	5,74E-164
	21129_g1i3	**1**	KDR09980	Isoptera	cGMP-dependent protein kinase, isozyme 1, partial [Zootermopsis nevadensis]	557,4	56,71	74,19	1,47E-174
		2	XP_012273062	Hymenoptera	PREDICTED: ATP-binding cassette sub-family C member Sur [Orussus abietinus]	528,1	55,08	72,56	4,86E-166
		3	XP_012225332	Hymenoptera	PREDICTED: LOW QUALITY PROTEIN: ATP-binding cassette sub-family C member 9 [Linepithema humile]	529,6	54,38	71,31	1,97E-164

ABC subfamily	Contig ID	Hit	Accession Genbank	Taxon	Name	Bit score	Identity [%]	Positives [%]	E-value
		4	XP_012265786	Hymenoptera	PREDICTED: ATP-binding cassette sub-family C member Sur [Athalia rosae]	522,7	52,99	71,51	2,73E-164
		5	XP_006560974	Hymenoptera	PREDICTED: ATP-binding cassette sub-family C member Sur isoform X4 [Apis mellifera]	521,2	53,83	72,78	1,53E-163
C	**21756_g1i1**	**1**	XP_008190151	Hemiptera	PREDICTED: probable multidrug resistance-associated protein lethal(2)03659 [Acyrthosiphon pisum]	1357,8	51,1	69,6	0,0
		2	XP_008186883	Hemiptera	PREDICTED: probable multidrug resistance-associated protein lethal(2)03659 [Acyrthosiphon pisum]	1354,7	51,2	69,9	0,0
		3	XP_012274748	Hymenoptera	PREDICTED: probable multidrug resistance-associated protein lethal(2)03659 [Orussus abietinus]	1351,7	50,6	69,7	0,0
		4	KDR22129	Isoptera	putative multidrug resistance-associated protein [Zootermopsis nevadensis]	1347,0	50,0	69,5	0,0
		5	XP_003241113	Hemiptera	PREDICTED: probable multidrug resistance-associated protein lethal(2)03659 [Acyrthosiphon pisum]	1346,6	51,0	70,1	0,0
B	**22616_g1i1**	**1**	KFD70158	Nematoda	hypothetical protein M514_09538 [Trichuris suis]	721,5	45,13	65,61	0,00E+00
		2	KFD49595	Nematoda	hypothetical protein M513_09538 [Trichuris suis]	708,0	44,18	64,36	0,00E+00
		3	KHJ40713	Nematoda	ABC transporter, ATP-binding protein [Trichuris suis]	701,4	45,02	65,46	0,00E+00
		4	XP_007505026	Didelphimorphia	PREDICTED: multidrug resistance protein 1-like isoform X14 [Monodelphis domestica]	689,9	47,22	64,68	0,00E+00
		5	XP_007505014	Didelphimorphia	PREDICTED: multidrug resistance protein 1-like isoform X2 [Monodelphis domestica].1	689,1	47,22	64,68	0,00E+00
B	**23955_g1i1**	**1**	AAP92331	Bivalvia	multixenobiotic resistance protein [Crassostrea virginica]	174,5	72,32	88,39	1,33E-49
		2	XP_009073212	Aves	PREDICTED: multidrug resistance protein 1A-like, partial [Acanthisitta chloris]	168,3	72,73	86,36	1,92E-49
		3	XP_009974860	Aves	PREDICTED: multidrug resistance protein 3-like, partial [Tyto alba]	170,2	73,64	85,45	2,44E-49
		4	XP_010190921	Aves	PREDICTED: multidrug resistance protein 1A-like, partial [Mesitornis unicolor]	167,9	73,64	85,45	3,01E-49
		5	XP_005472826	Pisces	PREDICTED: multidrug resistance protein 3-like, partial [Oreochromis niloticus]	167,9	71,82	86,36	6,82E-49
	23955_g1i2	**1**	XP_008178172	Hemiptera	PREDICTED: ATP-binding cassette sub-family B member 5-like isoform X3 [Acyrthosiphon pisum]	1308,9	51,85	71,71	0,00E+00
		2	XP_011663236	Echinodermata	PREDICTED: multidrug resistance protein 1 [Strongylocentrotus purpuratus]	1104,4	46,50	65,85	0,00E+00
		3	XP_009673196	Aves	PREDICTED: multidrug resistance protein 1-like isoform X2 [Struthio camelus australis]	1094,3	44,76	66,35	0,00E+00
		4	XP_009673195	Aves	PREDICTED: multidrug resistance protein 1-like isoform X1 [Struthio camelus australis]	1094,3	44,66	66,17	0,00E+00
		5	XP_010222846	Aves	PREDICTED: multidrug resistance protein 3 [Tinamus guttatus]	1092,8	45,19	66,17	0,00E+00
C	**23997_g1i1**	**1**	KDR20353	Isoptera	putative multidrug resistance-associated protein [Zootermopsis nevadensis]	277,7	50,80	71,25	2,98E-133
		2	KDR20353	Isoptera	putative multidrug resistance-associated protein [Zootermopsis nevadensis]	228,8	30,94	53,24	2,98E-133

ABC subfamily	Contig ID	Hit	Accession Genbank	Taxon	Name	Bit score	Identity [%]	Positives [%]	E-value
		3	XP_969781	Coleoptera	PREDICTED: probable multidrug resistance-associated protein lethal(2)03659 [Tribolium castaneum]	275,4	52,15	71,29	5,26E-132
		4	XP_969781	Coleoptera	PREDICTED: probable multidrug resistance-associated protein lethal(2)03659 [Tribolium castaneum]	226,9	33,58	54,32	5,26E-132
		5	XP_012169775	Hymenoptera	PREDICTED: LOW QUALITY PROTEIN: probable multidrug resistance-associated protein lethal(2)03659 [Bombus terrestris]	263,1	51,13	69,90	4,93E-131
	23997_g1i2	**1**	KDR20353	Isoptera	putative multidrug resistance-associated protein [Zootermopsis nevadensis]	291,6	47,04	68,01	1,94E-130
		2	KDR20353	Isoptera	putative multidrug resistance-associated protein [Zootermopsis nevadensis]	205,3	30,65	52,47	1,94E-130
		3	XP_969781	Coleoptera	PREDICTED: probable multidrug resistance-associated protein lethal(2)03659 [Tribolium castaneum]	286,6	48,23	67,85	4,29E-129
		4	XP_969781	Coleoptera	PREDICTED: probable multidrug resistance-associated protein lethal(2)03659 [Tribolium castaneum]	205,7	33,78	53,62	4,29E-129
		5	XP_012250545	Hymenoptera	PREDICTED: probable multidrug resistance-associated protein lethal(2)03659 [Athalia rosae]	295,0	48,08	68,96	4,82E-129
B	**24244_g1i1**	**1**	XP_012267076	Hymenoptera	PREDICTED: ATP-binding cassette sub-family B member 6, mitochondrial [Athalia rosae]	457,6	75,3	85,6	0,0
		2	XP_307900	Diptera	AGAP002278-PA [Anopheles gambiae str. PEST]	457,2	74,2	85,8	0,0
		3	KDR08849	Isoptera	ATP-binding cassette sub-family B member 6, mitochondrial [Zootermopsis nevadensis]	454,1	71,7	84,9	0,0
		4	XP_003708301	Hymenoptera	PREDICTED: ATP-binding cassette sub-family B member 6, mitochondrial isoform X1 [Megachile rotundata]	451,1	73,5	85,6	0,0
		5	XP_012342940	Hymenoptera	PREDICTED: LOW QUALITY PROTEIN: ATP-binding cassette sub-family B member 6, mitochondrial [Apis florea]	449,1	73,9	85,6	0,0
	24244_g1i2	**1**	XP_012267076	Hymenoptera	PREDICTED: ATP-binding cassette sub-family B member 6, mitochondrial [Athalia rosae]	901,0	76,4	87,9	0,0
		2	KDR08849	Isoptera	ATP-binding cassette sub-family B member 6, mitochondrial [Zootermopsis nevadensis]	885,9	74,7	85,6	0,0
		3	XP_307900	Diptera	AGAP002278-PA [Anopheles gambiae str. PEST]	884,8	75,4	86,6	0,0
		4	XP_003425259	Hymenoptera	PREDICTED: ATP-binding cassette sub-family B member 6, mitochondrial [Nasonia vitripennis]	884,4	74,1	85,5	0,0
		5	XP_003708301	Hymenoptera	PREDICTED: ATP-binding cassette sub-family B member 6, mitochondrial isoform X1 [Megachile rotundata]	882,1	75,2	87,7	0,0
C	**24340_g1i2**	**1**	XP_001656872	Diptera	AAEL013567-PA, partial [Aedes aegypti]	609,8	45,87	64,34	0,00E+00
		2	EFA03011	Coleoptera	hypothetical protein TcasGA2_TC010434 [Tribolium castaneum]	607,1	47,10	66,67	0,00E+00
		3	XP_008200429	Coleoptera	PREDICTED: probable multidrug resistance-associated protein lethal(2)03659 isoform X1 [Tribolium castaneum]	605,1	46,95	66,72	0,00E+00

ABC subfamily	Contig ID	Hit	Accession Genbank	Taxon	Name	Bit score	Identity [%]	Positives [%]	E-value
		4	XP_008200431	Coleoptera	PREDICTED: probable multidrug resistance-associated protein lethal(2)03659 isoform X2 [Tribolium castaneum]	604,4	46,95	66,72	0,00E+00
		5	XP_012169775	Hymenoptera	PREDICTED: LOW QUALITY PROTEIN: probable multidrug resistance-associated protein lethal(2)03659 [Bombus terrestris]	597,8	44,89	65,06	0,00E+00
	24340_g1i3	**1**	XP_012251875	Hymenoptera	PREDICTED: probable multidrug resistance-associated protein lethal(2)03659 [Athalia rosae]	1031,6	48,90	69,59	0,00E+00
		2	XP_008561150	Hymenoptera	PREDICTED: probable multidrug resistance-associated protein lethal(2)03659 [Microplitis demolitor]	1016,5	48,07	66,64	0,00E+00
		3	EFA03011	Coleoptera	hypothetical protein TcasGA2_TC010434 [Tribolium castaneum]	1015,4	50,81	68,85	0,00E+00
		4	XP_008200431	Coleoptera	PREDICTED: probable multidrug resistance-associated protein lethal(2)03659 isoform X2 [Tribolium castaneum]	1012,3	50,71	68,89	0,00E+00
		5	XP_008200429	Coleoptera	PREDICTED: probable multidrug resistance-associated protein lethal(2)03659 isoform X1 [Tribolium castaneum]	1012,3	50,71	68,89	0,00E+00
	24340_g1i5	**1**	XP_012251875	Hymenoptera	PREDICTED: probable multidrug resistance-associated protein lethal(2)03659 [Athalia rosae]	449,9	58,47	76,23	1,24E-140
		2	XP_003248196	Hemiptera	PREDICTED: probable multidrug resistance-associated protein lethal(2)03659 [Acyrthosiphon pisum]	419,1	54,64	74,32	7,54E-138
		3	XP_012058527	Hymenoptera	PREDICTED: LOW QUALITY PROTEIN: probable multidrug resistance-associated protein lethal(2)03659 [Atta cephalotes]	439,5	58,89	72,68	2,48E-136
		4	EFZ19975	Hymenoptera	hypothetical protein SINV_05651, partial [Solenopsis invicta]	435,6	58,60	71,77	4,76E-136
		5	XP_012058528	Hymenoptera	PREDICTED: probable multidrug resistance-associated protein lethal(2)03659 [Atta cephalotes]	430,3	58,06	72,31	6,97E-136
	24340_g1i6	**1**	XP_002036200	Diptera	GM13023 [Drosophila sechellia]	446,4	42,41	61,85	0,00E+00
		2	AAL39987	Diptera	SD08921p [Drosophila melanogaster]	443,4	42,04	62,04	0,00E+00
		3	NP_609215	Diptera	CG7627, isoform A [Drosophila melanogaster]	443,0	42,22	62,04	0,00E+00
		4	ACD81872	Diptera	RE10805p [Drosophila melanogaster]	442,6	42,22	62,04	0,00E+00
		5	XP_011211256	Diptera	PREDICTED: probable multidrug resistance-associated protein lethal(2)03659 [Bactrocera dorsalis]	441,8	42,40	60,47	0,00E+00
	24340_g1i7	**1**	XP_012251875	Hymenoptera	PREDICTED: probable multidrug resistance-associated protein lethal(2)03659 [Athalia rosae]	412,5	59,71	77,06	6,39E-128
		2	XP_003248196	Hemiptera	PREDICTED: probable multidrug resistance-associated protein lethal(2)03659 [Acyrthosiphon pisum]	383,3	55,29	74,41	3,90E-125
		3	XP_011505353	Hymenoptera	PREDICTED: probable multidrug resistance-associated protein lethal(2)03659 [Ceratosolen solmsi marchali]	402,9	60,86	77,06	3,78E-124
		4	EFZ19975	Hymenoptera	hypothetical protein SINV_05651, partial [Solenopsis invicta]	400,2	59,20	71,55	5,47E-124
		5	XP_011156697	Hymenoptera	PREDICTED: multidrug resistance-associated protein 4-like, partial [Solenopsis invicta]	400,6	59,20	71,55	7,52E-124
	24340_g1i8	**1**	XP_011211256	Diptera	PREDICTED: probable multidrug resistance-associated protein lethal(2)03659 [Bactrocera dorsalis]	475,3	42,13	60,10	0,00E+00

ABC subfamily	Contig ID	Hit	Accession Genbank	Taxon	Name	Bit score	Identity [%]	Positives [%]	E-value
		2	XP_002051547	Diptera	GJ11549 [Drosophila virilis] >gi|194148004|gb|EDW63702.1| GJ11549 [Drosophila virilis]	474,2	40,03	58,72	0,00E+00
		3	XP_011185640	Diptera	PREDICTED: probable multidrug resistance-associated protein lethal(2)03659 [Bactrocera cucurbitae]	473,8	41,19	60,06	0,00E+00
		4	NP_609215	Diptera	CG7627, isoform A [Drosophila melanogaster]	459,5	39,87	60,28	0,00E+00
		5	XP_001961937	Diptera	GF14687 [Drosophila ananassae] >gi|190615634|gb|EDV31158.1| GF14687 [Drosophila ananassae]	459,1	40,56	57,41	0,00E+00
B	**24754_g1i1**	**1**	KDR10680	Isoptera	ATP-binding cassette sub-family B member 10, mitochondrial [Zootermopsis nevadensis]	694,9	60,15	75,11	0,00E+00
		2	XP_008474017	Hemiptera	PREDICTED: ATP-binding cassette sub-family B member 10, mitochondrial-like [Diaphorina citri]	652,5	62,39	80,42	0,00E+00
		3	XP_008186244	Homoptera	PREDICTED: ATP-binding cassette sub-family B member 10, mitochondrial-like [Acyrthosiphon pisum]	637,1	61,86	80,29	0,00E+00
		4	AEE61847	Coleoptera	unknown [Dendroctonus ponderosae]	632,9	55,93	71,81	0,00E+00
		5	ERL89226	Coleoptera	hypothetical protein D910_06600, partial [Dendroctonus ponderosae]	629,4	55,59	71,47	0,00E+00
B	**25277_g2i1**	**1**	XP_003707011	Hymenoptera	PREDICTED: ATP-binding cassette sub-family B member 7, mitochondrial isoform X1 [Megachile rotundata]	867,1	70,27	82,84	0,00E+00
		2	XP_012060794	Hymenoptera	PREDICTED: ATP-binding cassette sub-family B member 7, mitochondrial [Atta cephalotes]	854,7	70,85	84,65	0,00E+00
		3	XP_011060274	Hymenoptera	PREDICTED: ATP-binding cassette sub-family B member 7, mitochondrial isoform X5 [Acromyrmex echinatior]	853,6	70,87	84,58	0,00E+00
		4	XP_011060197	Hymenoptera	PREDICTED: ATP-binding cassette sub-family B member 7, mitochondrial isoform X4 [Acromyrmex echinatior]	853,2	70,87	84,58	0,00E+00
		5	XP_011059970	Hymenoptera	PREDICTED: ATP-binding cassette sub-family B member 7, mitochondrial isoform X1 [Acromyrmex echinatior]	852,4	70,87	84,58	0,00E+00
	25277_g2i2	**1**	XP_003707011	Hymenoptera	PREDICTED: ATP-binding cassette sub-family B member 7, mitochondrial isoform X1 [Megachile rotundata]	867,1	70,27	82,84	0,00E+00
		2	XP_012060794	Hymenoptera	PREDICTED: ATP-binding cassette sub-family B member 7, mitochondrial [Atta cephalotes]	854,7	70,85	84,65	0,00E+00
		3	XP_011060274	Hymenoptera	PREDICTED: ATP-binding cassette sub-family B member 7, mitochondrial isoform X5 [Acromyrmex echinatior]	853,6	70,87	84,58	0,00E+00
		4	XP_011060197	Hymenoptera	PREDICTED: ATP-binding cassette sub-family B member 7, mitochondrial isoform X4 [Acromyrmex echinatior]	853,2	70,87	84,58	0,00E+00

ABC subfamily	Contig ID	Hit	Accession Genbank	Taxon	Name	Bit score	Identity [%]	Positives [%]	E-value
		5	XP_011059970	Hymenoptera	PREDICTED: ATP-binding cassette sub-family B member 7, mitochondrial isoform X1 [Acromyrmex echinatior]	852,4	70,87	84,58	0,00E+00
	25277_g2i3	**1**	XP_003707011	Hymenoptera	PREDICTED: ATP-binding cassette sub-family B member 7, mitochondrial isoform X1 [Megachile rotundata]	869,8	70,06	82,60	0,00E+00
		2	XP_012060794	Hymenoptera	PREDICTED: ATP-binding cassette sub-family B member 7, mitochondrial [Atta cephalotes]	857,4	70,85	84,65	0,00E+00
		3	XP_011060274	Hymenoptera	PREDICTED: ATP-binding cassette sub-family B member 7, mitochondrial isoform X5 [Acromyrmex echinatior]	855,9	70,87	84,58	0,00E+00
		4	XP_011060197	Hymenoptera	PREDICTED: ATP-binding cassette sub-family B member 7, mitochondrial isoform X4 [Acromyrmex echinatior]	855,1	71,03	84,89	0,00E+00
		5	XP_011060112	Hymenoptera	PREDICTED: ATP-binding cassette sub-family B member 7, mitochondrial isoform X3 [Acromyrmex echinatior]	855,1	70,87	84,58	0,00E+00
C	**25303_g1i1**	**1**	XP_012144506	Hymenoptera	PREDICTED: multidrug resistance-associated protein 5-like isoform X6 [Megachile rotundata]	570,9	43,31	62,86	0,00E+00
		2	XP_012144505	Hymenoptera	PREDICTED: multidrug resistance-associated protein 5-like isoform X5 [Megachile rotundata]	569,3	43,31	62,86	8,45E-180
		3	XP_011336487	Hymenoptera	PREDICTED: multidrug resistance-associated protein 5-like isoform X2 [Cerapachys biroi]	569,7	42,43	63,42	9,23E-180
		4	XP_012144503	Hymenoptera	PREDICTED: multidrug resistance-associated protein 5-like isoform X3 [Megachile rotundata]	570,1	43,31	62,86	1,07E-179
		5	XP_012144499	Hymenoptera	PREDICTED: multidrug resistance-associated protein 5-like isoform X2 [Megachile rotundata]	570,1	43,31	62,86	1,16E-179
	25303_g1i2	**1**	XP_012144504	Hymenoptera	PREDICTED: multidrug resistance-associated protein 5-like isoform X4 [Megachile rotundata]	897,5	44,19	62,73	0,00E+00
		2	XP_011336485	Hymenoptera	PREDICTED: multidrug resistance-associated protein 5-like isoform X1 [Cerapachys biroi]	891,7	43,33	62,56	0,00E+00
		3	XP_012144503	Hymenoptera	PREDICTED: multidrug resistance-associated protein 5-like isoform X3 [Megachile rotundata]	886,3	43,82	62,36	0,00E+00
		4	XP_011336487	Hymenoptera	PREDICTED: multidrug resistance-associated protein 5-like isoform X2 [Cerapachys biroi]	883,2	42,96	62,19	0,00E+00
		5	XP_012144506	Hymenoptera	PREDICTED: multidrug resistance-associated protein 5-like isoform X6 [Megachile rotundata]	882,1	42,73	60,66	0,00E+00
	25303_g1i3	**1**	XP_012144504	Hymenoptera	PREDICTED: multidrug resistance-associated protein 5-like isoform X4 [Megachile rotundata]	902,9	43,96	62,76	0,00E+00
		2	XP_012144503	Hymenoptera	PREDICTED: multidrug resistance-associated protein 5-like isoform X3 [Megachile rotundata]	891,3	43,59	62,40	0,00E+00
		3	XP_011336485	Hymenoptera	PREDICTED: multidrug resistance-associated protein 5-like isoform X1 [Cerapachys biroi]	891,0	43,00	62,12	0,00E+00

ABC subfamily	Contig ID	Hit	Accession Genbank	Taxon	Name	Bit score	Identity [%]	Positives [%]	E-value
		4	XP_012144506	Hymenoptera	PREDICTED: multidrug resistance-associated protein 5-like isoform X6 [Megachile rotundata]	886,7	42,51	60,70	0,00E+00
		5	XP_012144499	Hymenoptera	PREDICTED: multidrug resistance-associated protein 5-like isoform X2 [Megachile rotundata]	885,2	42,51	60,70	0,00E+00
B	**25605_g2i1**	**1**	XP_008178173	Hemiptera	PREDICTED: multidrug resistance protein 1A-like isoform X4 [Acyrthosiphon pisum]	434,5	55,65	75,54	5,06E-136
		2	XP_008178172	Hemiptera	PREDICTED: ATP-binding cassette sub-family B member 5-like isoform X3 [Acyrthosiphon pisum]	434,5	55,65	75,54	9,54E-135
		3	XP_008178171	Hemiptera	PREDICTED: multidrug resistance protein 1A-like isoform X2 [Acyrthosiphon pisum]	434,1	55,65	75,54	1,34E-134
		4	XP_001947434	Hemiptera	PREDICTED: ATP-binding cassette sub-family B member 5-like isoform X1 [Acyrthosiphon pisum]	434,1	55,65	75,54	1,73E-134
		5	XP_001943495	Hemiptera	PREDICTED: multidrug resistance protein 1-like [Acyrthosiphon pisum]	431,0	54,16	71,54	2,27E-132
	25605_g2i2	**1**	XP_008178173	Hemiptera	PREDICTED: multidrug resistance protein 1A-like isoform X4 [Acyrthosiphon pisum]	434,5	55,65	75,54	4,53E-131
		2	XP_008178172	Hemiptera	PREDICTED: ATP-binding cassette sub-family B member 5-like isoform X3 [Acyrthosiphon pisum]	434,5	55,65	75,54	8,52E-130
		3	XP_008178171	Hemiptera	PREDICTED: multidrug resistance protein 1A-like isoform X2 [Acyrthosiphon pisum]	434,1	55,65	75,54	1,19E-129
		4	XP_001947434	Hemiptera	PREDICTED: ATP-binding cassette sub-family B member 5-like isoform X1 [Acyrthosiphon pisum]	434,1	55,65	75,54	1,54E-129
		5	XP_001943495	Hemiptera	PREDICTED: multidrug resistance protein 1-like [Acyrthosiphon pisum]	431,0	54,16	71,54	1,94E-127
	25605_g2i5	**1**	XP_008178173	Hemiptera	PREDICTED: multidrug resistance protein 1A-like isoform X4 [Acyrthosiphon pisum]	434,9	55,65	75,54	8,57E-135
		2	XP_008178171	Hemiptera	PREDICTED: multidrug resistance protein 1A-like isoform X2 [Acyrthosiphon pisum]	434,5	55,65	75,54	1,54E-133
		3	XP_008178172	Hemiptera	PREDICTED: ATP-binding cassette sub-family B member 5-like isoform X3 [Acyrthosiphon pisum]	434,5	55,65	75,54	1,62E-133
		4	XP_001947434	Hemiptera	PREDICTED: ATP-binding cassette sub-family B member 5-like isoform X1 [Acyrthosiphon pisum]	434,5	55,65	75,54	2,27E-133
		5	XP_001943495	Hemiptera	PREDICTED: multidrug resistance protein 1-like [Acyrthosiphon pisum]	428,7	56,45	73,92	2,72E-130
	25605_g2i6	**1**	XP_008178173	Hemiptera	PREDICTED: multidrug resistance protein 1A-like isoform X4 [Acyrthosiphon pisum]	434,1	54,48	73,88	9,26E-131
		2	XP_008178172	Hemiptera	PREDICTED: ATP-binding cassette sub-family B member 5-like isoform X3 [Acyrthosiphon pisum]	434,1	55,65	75,54	1,14E-129
		3	XP_008178171	Hemiptera	PREDICTED: multidrug resistance protein 1A-like isoform X2 [Acyrthosiphon pisum]	434,1	55,65	75,54	1,26E-129
		4	XP_001947434	Hemiptera	PREDICTED: ATP-binding cassette sub-family B member 5-like isoform X1 [Acyrthosiphon pisum]	434,5	55,65	75,54	1,58E-129
		5	XP_001943495	Hemiptera	PREDICTED: multidrug resistance protein 1-like [Acyrthosiphon pisum]	430,6	55,33	72,70	3,15E-127

ABC subfamily	Contig ID	Hit	Accession Genbank	Taxon	Name	Bit score	Identity [%]	Positives [%]	E-value
	25605_g2i7	**1**	XP_008178173	Hemiptera	PREDICTED: multidrug resistance protein 1A-like isoform X4 [Acyrthosiphon pisum]	434,5	55,65	75,54	3,86E-130
		2	XP_008178172	Hemiptera	PREDICTED: ATP-binding cassette sub-family B member 5-like isoform X3 [Acyrthosiphon pisum]	434,5	55,65	75,54	7,26E-129
		3	XP_008178171	Hemiptera	PREDICTED: multidrug resistance protein 1A-like isoform X2 [Acyrthosiphon pisum]	434,1	55,65	75,54	1,02E-128
		4	XP_001947434	Hemiptera	PREDICTED: ATP-binding cassette sub-family B member 5-like isoform X1 [Acyrthosiphon pisum]	434,1	55,65	75,54	1,31E-128
		5	XP_001943495	Hemiptera	PREDICTED: multidrug resistance protein 1-like [Acyrthosiphon pisum]	431,0	54,16	71,54	1,63E-126
	25605_g2i8	**1**	XP_008178173	Hemiptera	PREDICTED: multidrug resistance protein 1A-like isoform X4 [Acyrthosiphon pisum]	435,3	54,12	74,48	1,34E-136
		2	XP_008178171	Hemiptera	PREDICTED: multidrug resistance protein 1A-like isoform X2 [Acyrthosiphon pisum]	435,3	54,12	74,48	1,79E-135
		3	XP_008178172	Hemiptera	PREDICTED: ATP-binding cassette sub-family B member 5-like isoform X3 [Acyrthosiphon pisum]	435,3	54,12	74,48	2,27E-135
		4	XP_001947434	Hemiptera	PREDICTED: ATP-binding cassette sub-family B member 5-like isoform X1 [Acyrthosiphon pisum]	435,6	54,12	74,48	2,46E-135
		5	XP_001943495	Hemiptera	PREDICTED: multidrug resistance protein 1-like [Acyrthosiphon pisum]	427,9	54,90	72,42	1,19E-131
	25605_g2i11	**1**	XP_008178173	Hemiptera	PREDICTED: multidrug resistance protein 1A-like isoform X4 [Acyrthosiphon pisum]	434,5	55,65	75,54	2,52E-132
		2	XP_008178172	Hemiptera	PREDICTED: ATP-binding cassette sub-family B member 5-like isoform X3 [Acyrthosiphon pisum]	434,5	55,65	75,54	4,75E-131
		3	XP_008178171	Hemiptera	PREDICTED: multidrug resistance protein 1A-like isoform X2 [Acyrthosiphon pisum]	434,1	55,65	75,54	6,67E-131
		4	XP_001947434	Hemiptera	PREDICTED: ATP-binding cassette sub-family B member 5-like isoform X1 [Acyrthosiphon pisum]	434,1	55,65	75,54	8,61E-131
		5	XP_001943495	Hemiptera	PREDICTED: multidrug resistance protein 1-like [Acyrthosiphon pisum]	431,0	54,16	71,54	1,10E-128
B	**33615_g1i1**	**1**	AFV15804	Bivalvia	P-glycoprotein [Perna viridis]	198,0	69,40	85,07	9,41E-55
		2	XP_008178173	Hemiptera	PREDICTED: multidrug resistance protein 1A-like isoform X4 [Acyrthosiphon pisum]	196,8	59,76	76,83	1,38E-54
		3	XP_001947434	Hemiptera	PREDICTED: ATP-binding cassette sub-family B member 5-like isoform X1 [Acyrthosiphon pisum]	197,2	59,76	76,83	1,86E-54
		4	XP_008178172	Hemiptera	PREDICTED: ATP-binding cassette sub-family B member 5-like isoform X3 [Acyrthosiphon pisum]	196,8	59,76	76,83	1,96E-54
		5	XP_004257047	Ameobozoa	P-glycoprotein, partial [Entamoeba invadens IP1]	185,7	70,08	83,46	2,35E-54
	33998_g1i1	**1**	ABK79935	Crustacea	P-glycoprotein [Lepeophtheirus salmonis]	273,9	65,46	83,51	1,82E-87
		2	AKC42330	Lepidoptera	ABCA8 protein, partial [Spodoptera litura]	275,8	65,10	83,33	1,41E-86
		3	XP_008195551	Coleoptera	PREDICTED: ATP-binding cassette sub-family B member 8, mitochondrial isoform X2 [Tribolium castaneum]	273,5	64,95	82,47	1,89E-84
		4	EHJ71471	Lepidoptera	hypothetical protein KGM_16343 [Danaus plexippus]	278,5	64,06	84,90	3,63E-84

ABC subfamily	Contig ID	Hit	Accession Genbank	Taxon	Name	Bit score	Identity [%]	Positives [%]	E-value
		5	XP_009051635	Mollusca	hypothetical protein LOTGIDRAFT_208936 [Lottia gigantea]	276,9	67,72	82,01	4,56E-84
B	**34901_g1i1**	**1**	XP_001943495	Hemiptera	PREDICTED: multidrug resistance protein 1-like [Acyrthosiphon pisum]	109,8	46,73	71,96	5,09E-37
		2	XP_001943495	Hemiptera	PREDICTED: multidrug resistance protein 1-like [Acyrthosiphon pisum]	71,6	45,57	62,03	5,09E-37
		3	XP_006636066	Pisces	PREDICTED: multidrug resistance protein 1-like [Lepisosteus oculatus]	103,2	44,04	65,14	4,99E-32
		4	XP_006636066	Pisces	PREDICTED: multidrug resistance protein 1-like [Lepisosteus oculatus]	61,6	33,73	57,83	4,99E-32
		5	XP_009906327	Aves	PREDICTED: multidrug resistance protein 3-like [Picoides pubescens]	90,5	40,78	65,05	2,18E-27
B	**74772_g1i1**	**1**	XP_001943495	Hemiptera	PREDICTED: multidrug resistance protein 1-like [Acyrthosiphon pisum]	112,5	49,22	74,22	1,55E-25
		2	XP_008178173	Hemiptera	PREDICTED: multidrug resistance protein 1A-like isoform X4 [Acyrthosiphon pisum]	107,8	52,34	71,09	5,67E-24
		3	XP_008178171	Hemiptera	PREDICTED: multidrug resistance protein 1A-like isoform X2 [Acyrthosiphon pisum]	107,8	52,34	71,09	6,59E-24
		4	XP_001947434	Hemiptera	PREDICTED: ATP-binding cassette sub-family B member 5-like isoform X1 [Acyrthosiphon pisum]	107,5	52,34	71,09	7,33E-24
		5	XP_008178172	Hemiptera	PREDICTED: ATP-binding cassette sub-family B member 5-like isoform X3 [Acyrthosiphon pisum]	107,5	52,34	71,09	7,39E-24

Previous table continued.

Table S 22 Results of the blastx search against the NCBI nr database for putative ABCB contigs found by homology search in the transcriptome of the large milkweed bug assembled by CLC. The top five blastx hits are given.

ABC subfamily	Contig ID	Hit	Taxon	Accession Genbank	Name	Bit score	Identity [%]	Positives [%]	E-value
B	**35761**	**1**	Hemiptera	XP_014294685	multidrug resistance protein 2 [Halyomorpha halys]	251,14	71,43	83,93	1,7E-73
		1	Hemiptera	XP_014294685	multidrug resistance protein 2 [Halyomorpha halys]	195,67	59,63	75,78	4,5E-54
		2	Hemiptera	XP_025195236	multidrug resistance protein 1A-like isoform X1 [Melanaphis sacchari]	249,98	68,45	86,31	5,8E-73
		2	Hemiptera	XP_025195236	multidrug resistance protein 1A-like isoform X1 [Melanaphis sacchari]	204,91	63,13	76,25	3,4E-57
		3	Hemiptera	XP_025195237	multidrug resistance protein 1A-like isoform X2 [Melanaphis sacchari]	249,60	68,45	86,31	6,9E-73
		3	Hemiptera	XP_025195237	multidrug resistance protein 1A-like isoform X2 [Melanaphis sacchari]	204,53	63,13	76,25	4,4E-57
		4	Hemiptera	XP_025418287	multidrug resistance protein 1-like [Sipha flava]	244,59	68,64	84,02	4,6E-71
		4	Hemiptera	XP_025418287	multidrug resistance protein 1-like [Sipha flava]	201,06	63,98	78,88	6,0E-56
		5	Hemiptera	XP_014273830	multidrug resistance protein 1B isoform X2 [Halyomorpha halys]	243,82	64,74	77,89	6,6E-71
		5	Hemiptera	XP_014273830	multidrug resistance protein 1B isoform X2 [Halyomorpha halys]	203,37	62,73	79,50	1,0E-56
B	**31759**	**1**	Hemiptera	XP_024216743	multidrug resistance protein 1-like [Halyomorpha halys]	374,40	60,31	76,34	2,4E-115
		1	Hemiptera	XP_024216743	multidrug resistance protein 1-like [Halyomorpha halys]	176,41	58,12	73,82	1,2E-44
		2	Hemiptera	XP_014294685	multidrug resistance protein 2 [Halyomorpha halys]	293,12	46,73	64,32	1,9E-85
		2	Hemiptera	XP_014294685	multidrug resistance protein 2 [Halyomorpha halys]	179,87	57,89	75,26	6,1E-46
		3	Thysanoptera	XP_026274262	multidrug resistance protein 1B-like isoform X2 [Frankliniella occidentalis]	290,04	47,72	65,23	2,6E-84
		3	Thysanoptera	XP_026274262	multidrug resistance protein 1B-like isoform X2 [Frankliniella occidentalis]	180,64	56,10	68,29	3,5E-46
		4	Thysanoptera	XP_026274261	multidrug resistance protein 1B-like isoform X1 [Frankliniella occidentalis]	289,66	47,72	65,23	5,2E-84
		4	Thysanoptera	XP_026274261	multidrug resistance protein 1B-like isoform X1 [Frankliniella occidentalis]	181,03	56,10	68,29	2,6E-46
		5	Hemiptera	XP_014242218	multidrug resistance protein 1-like isoform X2 [Cimex lectularius]	286,96	45,94	64,72	6,6E-84
		5	Hemiptera	XP_014242218	multidrug resistance protein 1-like isoform X2 [Cimex lectularius]	182,19	58,95	75,26	8,9E-47
B	**23683**	**1**	Hemiptera	XP_024219089	multidrug resistance protein 1A-like [Halyomorpha halys]	523,47	64,10	81,79	6,2E-179
		2	Hemiptera	XP_024218438	phosphatidylcholine translocator ABCB4-like [Halyomorpha halys]	543,50	67,44	83,08	3,7E-178
		2	Hemiptera	XP_024218438	phosphatidylcholine translocator ABCB4-like [Halyomorpha halys]	286,57	41,75	61,60	8,9E-82
		3	Hemiptera	XP_024219088	phosphatidylcholine translocator ABCB4-like [Halyomorpha halys]	524,63	64,87	81,79	5,3E-173
		3	Hemiptera	XP_024219088	phosphatidylcholine translocator ABCB4-like [Halyomorpha halys]	273,09	39,95	61,58	1,3E-77
		4	Hemiptera	XP_014281321	ABC transporter B family member 15-like isoform X2 [Halyomorpha halys]	519,62	63,68	81,07	1,5E-170
		4	Hemiptera	XP_014281321	ABC transporter B family member 15-like isoform X2 [Halyomorpha halys]	279,64	41,60	61,24	8,3E-80
		5	Hemiptera	XP_014281320	ABC transporter B family member 3-like isoform X1 [Halyomorpha halys]	518,85	63,68	81,07	4,8E-169
		5	Hemiptera	XP_014281320	ABC transporter B family member 3-like isoform X1 [Halyomorpha halys]	279,26	41,60	61,24	2,5E-79

ABC subfamily	Contig ID	Hit	Taxon	Accession Genbank	Name	Bit score	Identity [%]	Positives [%]	E-value
B	**22653**	**1**	Hemiptera	XP_014292807	ATP-binding cassette sub-family B member 6, mitochondrial [Halyomorpha halys]	1125,92	75,03	87,52	0,0E+00
		2	Isoptera	XP_021938910	ATP-binding cassette sub-family B member 6, mitochondrial isoform X3 [Zootermopsis nevadensis]	1045,03	71,31	83,76	7,0E-11
		3	Isoptera	XP_021938911	ATP-binding cassette sub-family B member 6, mitochondrial isoform X4 [Zootermopsis nevadensis]	1044,26	71,31	83,76	0,0E+00
		4	Isoptera	XP_021938906	ATP-binding cassette sub-family B member 6, mitochondrial isoform X1 [Zootermopsis nevadensis]	1044,26	71,31	83,76	9,5E-95
		5	Isoptera	XP_023701848	ATP-binding cassette sub-family B member 6, mitochondrial isoform X2 [Cryptotermes secundus]	1043,11	70,85	83,94	9,5E-64
C	**22366**	**1**	Hemiptera	XP_014275641	probable multidrug resistance-associated protein lethal(2)03659 [Halyomorpha halys]	624,01	79,95	91,03	6,2E-63
		1	Hemiptera	XP_014275641	probable multidrug resistance-associated protein lethal(2)03659 [Halyomorpha halys]	76,26	25,25	44,52	6,9E-63
		2	Hemiptera	XP_014275661	probable multidrug resistance-associated protein lethal(2)03659 [Halyomorpha halys]	599,74	80,81	91,35	7,4E-63
		2	Hemiptera	XP_014275661	probable multidrug resistance-associated protein lethal(2)03659 [Halyomorpha halys]	77,03	24,75	43,81	0,0E+00
		3	Hemiptera	XP_014258970	probable multidrug resistance-associated protein lethal(2)03659 isoform X2 [Cimex lectularius]	587,42	74,59	89,19	0,0E+00
		4	Hemiptera	XP_014258968	probable multidrug resistance-associated protein lethal(2)03659 isoform X1 [Cimex lectularius]	587,42	74,59	89,19	0,0E+00
		5	Coleoptera	KRT78583	ABC transporter ATP-binding protein, partial [Oryctes borbonicus]	567,00	73,22	87,70	0,0E+00
		5	Coleoptera	KRT78583	ABC transporter ATP-binding protein, partial [Oryctes borbonicus]	71,25	25,35	46,13	0,0E+00
B	**20847**	**1**	Hemiptera	XP_024216743	multidrug resistance protein 1-like [Halyomorpha halys]	311,23	68,18	86,82	0,0E+00
		2	Hemiptera	XP_025418287	multidrug resistance protein 1-like [Sipha flava]	224,56	50,00	69,09	0,0E+00
		3	Hemiptera	XP_022176200	multidrug resistance protein 1-like isoform X2 [Myzus persicae]	222,25	49,09	69,55	0,0E+00
		4	Hemiptera	XP_022176197	multidrug resistance protein 1B-like isoform X1 [Myzus persicae]	221,86	49,09	69,55	0,0E+00
		5	Hemiptera	XP_022176201	multidrug resistance protein 1B-like isoform X3 [Myzus persicae]	221,86	49,09	69,55	7,9E-91
B	**13840**	**1**	Hemiptera	XP_014283304	ATP-binding cassette sub-family B member 7, mitochondrial [Halyomorpha halys]	1007,67	74,93	86,58	0,0E+00
		2	Hemiptera	XP_014255773	ATP-binding cassette sub-family B member 7, mitochondrial isoform X1 [Cimex lectularius]	874,00	72,54	84,40	3,1E-90
		3	Hymenoptera	XP_015606144	ATP-binding cassette sub-family B member 7, mitochondrial isoform X1 [Cephus cinctus]	870,92	72,83	84,32	1,1E-180
		4	Hymenoptera	XP_017792411	PREDICTED: ATP-binding cassette sub-family B member 7, mitochondrial isoform X1 [Habropoda laboriosa]	869,00	72,27	85,51	0,0E+00
		5	Hymenoptera	KOC70536	ATP-binding cassette sub-family B member 7, mitochondrial [Habropoda laboriosa]	869,00	72,27	85,51	0,0E+00
B	**13665**	**1**	Thysanoptera	XP_026274262	multidrug resistance protein 1B-like isoform X2 [Frankliniella occidentalis]	563,53	54,51	72,57	8,2E-54
		1	Thysanoptera	XP_026274262	multidrug resistance protein 1B-like isoform X2 [Frankliniella occidentalis]	316,24	40,24	58,95	0,0E+00

ABC subfamily	Contig ID	Hit	Taxon	Accession Genbank	Name	Bit score	Identity [%]	Positives [%]	E-value
		2	Thysanoptera	XP_026274261	multidrug resistance protein 1B-like isoform X1 [Frankliniella occidentalis]	562,38	54,51	72,57	0,0E+00
		2	Thysanoptera	XP_026274261	multidrug resistance protein 1B-like isoform X1 [Frankliniella occidentalis]	315,08	39,04	58,46	4,5E-56
		3	Hemiptera	XP_022171476	multidrug resistance protein 1B-like isoform X3 [Myzus persicae]	553,90	57,09	74,36	0,0E+00
		3	Hemiptera	XP_022171476	multidrug resistance protein 1B-like isoform X3 [Myzus persicae]	318,93	37,55	55,05	0,0E+00
		4	Hemiptera	XP_022184709	multidrug resistance protein 1-like [Nilaparvata lugens]	550,82	54,63	72,78	0,0E+00
		4	Hemiptera	XP_022184709	multidrug resistance protein 1-like [Nilaparvata lugens]	323,17	37,27	56,37	3,9E-08
		5	Hemiptera	XP_022171475	multidrug resistance protein 1B-like isoform X2 [Myzus persicae]	553,90	57,09	74,36	0,0E+00
		5	Hemiptera	XP_022171475	multidrug resistance protein 1B-like isoform X2 [Myzus persicae]	318,55	37,55	55,05	0,0E+00
C	**13664**	**1**	Hemiptera	XP_014275641	probable multidrug resistance-associated protein lethal(2)03659 [Halyomorpha halys]	863,60	60,71	75,74	1,1E-148
		1	Hemiptera	XP_014275641	probable multidrug resistance-associated protein lethal(2)03659 [Halyomorpha halys]	452,98	51,22	69,39	4,3E-98
		1	Hemiptera	XP_014275641	probable multidrug resistance-associated protein lethal(2)03659 [Halyomorpha halys]	219,16	67,57	87,16	7,1E-148
		2	Hemiptera	XP_014275661	probable multidrug resistance-associated protein lethal(2)03659 [Halyomorpha halys]	844,34	60,54	76,35	1,4E-103
		2	Hemiptera	XP_014275661	probable multidrug resistance-associated protein lethal(2)03659 [Halyomorpha halys]	439,50	49,28	69,48	1,2E-145
		2	Hemiptera	XP_014275661	probable multidrug resistance-associated protein lethal(2)03659 [Halyomorpha halys]	226,48	72,86	89,29	3,5E-102
		3	Hemiptera	XP_014258970	probable multidrug resistance-associated protein lethal(2)03659 isoform X2 [Cimex lectularius]	806,59	57,48	74,22	1,4E-142
		3	Hemiptera	XP_014258970	probable multidrug resistance-associated protein lethal(2)03659 isoform X2 [Cimex lectularius]	200,29	68,66	84,33	1,8E-142
		3	Hemiptera	XP_014258970	probable multidrug resistance-associated protein lethal(2)03659 isoform X2 [Cimex lectularius]	177,56	49,25	68,66	9,0E-60
		3	Hemiptera	XP_014258970	probable multidrug resistance-associated protein lethal(2)03659 isoform X2 [Cimex lectularius]	70,48	30,77	53,85	3,8E-142
		4	Hemiptera	XP_014258968	probable multidrug resistance-associated protein lethal(2)03659 isoform X1 [Cimex lectularius]	806,59	57,48	74,22	5,9E-142
		4	Hemiptera	XP_014258968	probable multidrug resistance-associated protein lethal(2)03659 isoform X1 [Cimex lectularius]	398,67	45,63	65,63	1,1E-141
		4	Hemiptera	XP_014258968	probable multidrug resistance-associated protein lethal(2)03659 isoform X1 [Cimex lectularius]	200,29	68,66	84,33	1,6E-08
		4	Hemiptera	XP_014258968	probable multidrug resistance-associated protein lethal(2)03659 isoform X1 [Cimex lectularius]	70,09	30,77	53,85	4,5E-141
		5	Hemiptera	XP_022162533	probable multidrug resistance-associated protein lethal(2)03659 isoform X4 [Myzus persicae]	781,17	55,25	72,09	4,7E-141
		5	Hemiptera	XP_022162533	probable multidrug resistance-associated protein lethal(2)03659 isoform X4 [Myzus persicae]	295,05	46,27	66,46	6,8E-141
		5	Hemiptera	XP_022162533	probable multidrug resistance-associated protein lethal(2)03659 isoform X4 [Myzus persicae]	219,55	69,66	84,14	7,2E-141

ABC subfamily	Contig ID	Hit	Taxon	Accession Genbank	Name	Bit score	Identity [%]	Positives [%]	E-value
		5	Hemiptera	XP_022162533	probable multidrug resistance-associated protein lethal(2)03659 isoform X4 [Myzus persicae]	69,71	30,34	51,72	2,5E-15
B	**11526**	**1**	Hemiptera	XP_024216743	multidrug resistance protein 1-like [Halyomorpha halys]	597,82	66,59	80,45	0,0E+00
		1	Hemiptera	XP_024216743	multidrug resistance protein 1-like [Halyomorpha halys]	302,37	42,43	61,47	1,3E-87
		2	Hemiptera	XP_014294685	multidrug resistance protein 2 [Halyomorpha halys]	467,23	52,79	72,33	1,1E-148
		2	Hemiptera	XP_014294685	multidrug resistance protein 2 [Halyomorpha halys]	331,64	40,47	60,47	4,3E-98
		3	Hemiptera	XP_014242218	multidrug resistance protein 1-like isoform X2 [Cimex lectularius]	459,91	52,33	71,40	7,1E-148
		3	Hemiptera	XP_014242218	multidrug resistance protein 1-like isoform X2 [Cimex lectularius]	343,20	45,93	66,93	1,4E-103
		4	Hemiptera	XP_014242217	multidrug resistance protein 1-like isoform X1 [Cimex lectularius]	459,14	52,33	71,40	1,2E-145
		4	Hemiptera	XP_014242217	multidrug resistance protein 1-like isoform X1 [Cimex lectularius]	342,81	45,93	66,93	3,5E-102
		5	Aves	XP_009954582	PREDICTED: multidrug resistance protein 3-like [Leptosomus discolor]	428,33	49,07	69,30	1,4E-142
C	**9692**	**1**	Hemiptera	XP_024216229	multidrug resistance-associated protein 1 isoform X4 [Halyomorpha halys]	1734,54	57,63	75,47	0,0E+00
		2	Hemiptera	XP_014276422	multidrug resistance-associated protein 1 isoform X2 [Halyomorpha halys]	1733,00	57,63	75,40	0,0E+00
		3	Hemiptera	XP_014276421	multidrug resistance-associated protein 1 isoform X1 [Halyomorpha halys]	1732,23	57,57	75,27	0,0E+00
		4	Hemiptera	XP_014276423	multidrug resistance-associated protein 1 isoform X3 [Halyomorpha halys]	1731,07	57,57	75,40	0,0E+00
		5	Hemiptera	XP_014276425	multidrug resistance-associated protein 1 isoform X5 [Halyomorpha halys]	1721,06	57,37	74,89	0,0E+00
C	**9679**	**1**	Hemiptera	XP_014251793	multidrug resistance-associated protein 4-like [Cimex lectularius]	569,31	45,06	64,95	0,0E+00
		1	Hemiptera	XP_014251793	multidrug resistance-associated protein 4-like [Cimex lectularius]	45,05	23,66	45,09	9,1E-01
		2	Hemiptera	AIN44104	multidrug resistance-associated protein 4-like protein [Laodelphax striatella]	498,05	41,47	60,75	3,3E-156
		3	Hemiptera	XP_022194494	probable multidrug resistance-associated protein lethal(2)03659 [Nilaparvata lugens]	493,43	40,66	61,83	1,4E-154
		4	Blattodea	PSN42283	Multidrug resistance-associated protein 4 [Blattella germanica]	491,12	39,22	58,89	1,0E-153
		5	Coleoptera	XP_023310958	multidrug resistance-associated protein 4 [Anoplophora glabripennis]	483,41	41,53	60,08	7,5E-151
C	**9166**	**1**	Hemiptera	XP_014277446	multidrug resistance-associated protein 5-like isoform X7 [Halyomorpha halys]	1095,88	57,32	73,12	0,0E+00
		2	Hemiptera	XP_014277445	multidrug resistance-associated protein 5-like isoform X6 [Halyomorpha halys]	1094,34	57,32	73,12	0,0E+00
		3	Hemiptera	XP_014277441	multidrug resistance-associated protein 5-like isoform X3 [Halyomorpha halys]	1094,34	57,32	73,12	0,0E+00
		4	Hemiptera	XP_014277443	multidrug resistance-associated protein 5-like isoform X5 [Halyomorpha halys]	1093,57	57,32	73,12	0,0E+00
		5	Hemiptera	XP_014277442	multidrug resistance-associated protein 5-like isoform X4 [Halyomorpha halys]	1093,57	57,32	73,12	0,0E+00
C	**8943**	**1**	Hemiptera	XP_014276421	multidrug resistance-associated protein 1 isoform X1 [Halyomorpha halys]	1628,99	61,17	77,51	0,0E+00
		2	Hemiptera	XP_024216229	multidrug resistance-associated protein 1 isoform X4 [Halyomorpha halys]	1628,61	61,29	77,13	0,0E+00

ABC subfamily	Contig ID	Hit	Taxon	Accession Genbank	Name	Bit score	Identity [%]	Positives [%]	E-value
		3	Hemiptera	XP_014276422	multidrug resistance-associated protein 1 isoform X2 [Halyomorpha halys]	1628,61	61,39	77,14	0,0E+00
		4	Hemiptera	XP_014276423	multidrug resistance-associated protein 1 isoform X3 [Halyomorpha halys]	1624,76	61,14	76,98	0,0E+00
		5	Hemiptera	XP_014276425	multidrug resistance-associated protein 1 isoform X5 [Halyomorpha halys]	1616,67	60,95	77,07	0,0E+00
B	**5124**	**1**	Hemiptera	XP_014275581	ATP-binding cassette sub-family B member 8, mitochondrial-like [Halyomorpha halys]	158,30	72,12	86,54	4,6E-41
		2	Hymenoptera	XP_015172529	PREDICTED: ATP-binding cassette sub-family B member 8, mitochondrial, partial [Polistes dominula]	154,45	74,23	91,75	1,1E-39
		3	Hymenoptera	XP_014609654	PREDICTED: ATP-binding cassette sub-family B member 8, mitochondrial [Polistes canadensis]	153,30	73,20	91,75	3,9E-39
		4	Hymenoptera	XP_017886211	PREDICTED: ATP-binding cassette sub-family B member 8, mitochondrial, partial [Ceratina calcarata]	150,98	71,43	87,76	5,7E-39
		5	Coleoptera	XP_008195551	PREDICTED: ATP-binding cassette sub-family B member 8, mitochondrial isoform X2 [Tribolium castaneum]	146,36	68,37	87,76	6,3E-38
		6	Coleoptera	KRT82823	ABC transporter ATP-binding protein, partial [Oryctes borbonicus]	142,51	70,10	85,57	6,8E-38
B	**4439**	**1**	Hemiptera	XP_014294685	multidrug resistance protein 2 [Halyomorpha halys]	1884,38	80,77	90,86	0,0E+00
		2	Hemiptera	XP_014242217	multidrug resistance protein 1-like isoform X1 [Cimex lectularius]	1742,24	75,35	86,59	0,0E+00
		3	Hemiptera	XP_014242218	multidrug resistance protein 1-like isoform X2 [Cimex lectularius]	1643,63	74,59	86,12	0,0E+00
		4	Hemiptera	AIN44097	multidrug resistance protein 1 [Laodelphax striatella]	1234,17	52,85	71,42	0,0E+00
		5	Hemiptera	XP_022184709	multidrug resistance protein 1-like [Nilaparvata lugens]	1229,54	52,50	71,81	0,0E+00
B	**3211**	**1**	Hemiptera	XP_025195237	multidrug resistance protein 1A-like isoform X2 [Melanaphis sacchari]	1275,38	55,08	74,20	0,0E+00
		2	Hemiptera	XP_025195236	multidrug resistance protein 1A-like isoform X1 [Melanaphis sacchari]	1267,68	53,83	72,83	0,0E+00
		3	Hemiptera	XP_022171475	multidrug resistance protein 1B-like isoform X2 [Myzus persicae]	1264,21	54,93	74,67	0,0E+00
		4	Hemiptera	XP_022171474	multidrug resistance protein 1B-like isoform X1 [Myzus persicae]	1258,43	53,71	73,01	0,0E+00
		5	Hemiptera	XP_025409006	multidrug resistance protein 1A-like [Sipha flava]	1256,89	54,13	73,85	0,0E+00
B	**2826**	**1**	Hemiptera	XP_014286386	ATP-binding cassette sub-family B member 10, mitochondrial isoform X1 [Halyomorpha halys]	670,23	71,06	82,93	0,0E+00
		1	Hemiptera	XP_014286386	ATP-binding cassette sub-family B member 10, mitochondrial isoform X1 [Halyomorpha halys]	263,46	83,03	93,94	3,6E-72
		2	Hemiptera	XP_024216596	ATP-binding cassette sub-family B member 10, mitochondrial isoform X2 [Halyomorpha halys]	582,41	77,96	87,70	0,0E+00
		2	Hemiptera	XP_024216596	ATP-binding cassette sub-family B member 10, mitochondrial isoform X2 [Halyomorpha halys]	263,46	83,54	94,51	3,7E-73
		3	Hemiptera	XP_014286387	ATP-binding cassette sub-family B member 10, mitochondrial isoform X3 [Halyomorpha halys]	561,22	77,83	88,41	0,0E+00
		3	Hemiptera	XP_014286387	ATP-binding cassette sub-family B member 10, mitochondrial isoform X3 [Halyomorpha halys]	263,46	83,54	94,51	1,4E-73
		4	Hemiptera	XP_014259484	ATP-binding cassette sub-family B member 10, mitochondrial isoform X1 [Cimex lectularius]	486,49	61,30	75,10	0,0E+00

ABC subfamily	Contig ID	Hit	Taxon	Accession Genbank	Name	Bit score	Identity [%]	Positives [%]	E-value
		4	Hemiptera	XP_014259484	ATP-binding cassette sub-family B member 10, mitochondrial isoform X1 [Cimex lectularius]	226,48	73,62	86,50	0,0E+00
		5	Hemiptera	XP_014259486	ATP-binding cassette sub-family B member 10, mitochondrial isoform X2 [Cimex lectularius]	481,10	64,92	79,04	0,0E+00
		5	Hemiptera	XP_014259486	ATP-binding cassette sub-family B member 10, mitochondrial isoform X2 [Cimex lectularius]	226,87	73,62	86,50	0,0E+00
C	**1581**	**1**	Hemiptera	XP_014276425	multidrug resistance-associated protein 1 isoform X5 [Halyomorpha halys]	744,58	81,02	92,82	0,0E+00
		2	Hemiptera	XP_014276423	multidrug resistance-associated protein 1 isoform X3 [Halyomorpha halys]	744,19	81,02	92,82	0,0E+00
		3	Hemiptera	XP_014276421	multidrug resistance-associated protein 1 isoform X1 [Halyomorpha halys]	744,19	81,02	92,82	0,0E+00
		4	Hemiptera	XP_024216229	multidrug resistance-associated protein 1 isoform X4 [Halyomorpha halys]	743,81	81,02	92,82	0,0E+00
		5	Hemiptera	XP_014276422	multidrug resistance-associated protein 1 isoform X2 [Halyomorpha halys]	743,81	81,02	92,82	0,0E+00
C	**11299**	**1**	Hemiptera	XP_024215330	multidrug resistance-associated protein 4-like isoform X2 [Halyomorpha halys]	443,74	66,88	81,07	3,1E-141
		1	Hemiptera	XP_024215330	multidrug resistance-associated protein 4-like isoform X2 [Halyomorpha halys]	78,57	25,76	46,21	1,0E-11
		2	Hemiptera	XP_024215329	multidrug resistance-associated protein 4-like isoform X1 [Halyomorpha halys]	443,74	66,88	81,07	5,7E-141
		2	Hemiptera	XP_024215329	multidrug resistance-associated protein 4-like isoform X1 [Halyomorpha halys]	78,57	25,76	46,59	9,3E-12
		3	Hemiptera	XP_014275641	probable multidrug resistance-associated protein lethal(2)03659 [Halyomorpha halys]	414,08	61,16	77,68	1,7E-129
		3	Hemiptera	XP_014275641	probable multidrug resistance-associated protein lethal(2)03659 [Halyomorpha halys]	82,03	28,97	50,93	7,2E-13
		4	Coleoptera	XP_012251875	probable multidrug resistance-associated protein lethal(2)03659 [Athalia rosae]	404,83	60,68	78,33	1,7E-126
		5	Blattodea	PNF34546	hypothetical protein B7P43_G10751 [Cryptotermes secundus]	382,10	59,67	77,38	2,6E-126
C	**16414**	**1**	Hemiptera	XP_014276422	multidrug resistance-associated protein 1 isoform X2 [Halyomorpha halys]	991,10	65,90	81,60	0,0E+00
		2	Hemiptera	XP_014276423	multidrug resistance-associated protein 1 isoform X3 [Halyomorpha halys]	988,79	65,63	81,60	0,0E+00
		3	Hemiptera	XP_024216229	multidrug resistance-associated protein 1 isoform X4 [Halyomorpha halys]	987,25	65,49	81,60	0,0E+00
		4	Hemiptera	XP_014276421	multidrug resistance-associated protein 1 isoform X1 [Halyomorpha halys]	961,83	64,55	80,11	0,0E+00
		5	Hemiptera	XP_014276425	multidrug resistance-associated protein 1 isoform X5 [Halyomorpha halys]	961,06	64,55	80,11	0,0E+00
C	**23156**	**1**	Hemiptera	XP_024219052	ATP-binding cassette sub-family C member Sur [Halyomorpha halys]	795,04	71,40	85,79	0,0E+00
		1	Hemiptera	XP_024219052	ATP-binding cassette sub-family C member Sur [Halyomorpha halys]	79,34	27,35	47,53	2,3E-11

ABC subfamily	Contig ID	Hit	Taxon	Accession Genbank	Name	Bit score	Identity [%]	Positives [%]	E-value
		2	Hemiptera	XP_014240366	ATP-binding cassette sub-family C member Sur isoform X4 [Cimex lectularius]	743,04	67,29	81,36	0,0E+00
		2	Hemiptera	XP_014240366	ATP-binding cassette sub-family C member Sur isoform X4 [Cimex lectularius]	72,79	25,00	45,91	2,1E-09
		3	Hemiptera	XP_014240365	ATP-binding cassette sub-family C member Sur isoform X3 [Cimex lectularius]	743,04	67,29	81,36	0,0E+00
		3	Hemiptera	XP_014240365	ATP-binding cassette sub-family C member Sur isoform X3 [Cimex lectularius]	73,17	25,00	45,91	1,8E-09
		4	Hemiptera	XP_014240364	ATP-binding cassette sub-family C member Sur isoform X2 [Cimex lectularius]	743,04	67,29	81,36	0,0E+00
		4	Hemiptera	XP_014240364	ATP-binding cassette sub-family C member Sur isoform X2 [Cimex lectularius]	73,56	25,00	45,91	1,4E-09
		5	Hemiptera	XP_014240361	ATP-binding cassette sub-family C member Sur isoform X1 [Cimex lectularius] >gi|939242205|ref|XP_014240363.1| ATP-binding cassette sub-family C member Sur isoform X1 [Cimex lectularius]	743,04	67,29	81,36	0,0E+00
		5	Hemiptera	XP_014240361	ATP-binding cassette sub-family C member Sur isoform X1 [Cimex lectularius]	73,56	25,00	45,91	1,4E-09

Previous table continued.

Table S 23 Pfam (HmmScan), TMHMM and WoLFPSORT analysis of OfABCB proteins and merged isoforms of *Ofabcb2*. Domain regions given by Pfam analysis refer to nucleotide sequence positions for isoforms. Pfam domains for translated OfABCB proteins (sequenced) and TMHMM regions refer to amino acid (aa) positions. Tri = Trinity. Seq. = sequenced. TMD = transmembrane domain. NBD = nucleotide-binding domain. TH = transmembrane helix. TMHMM analysis is representative of isoforms 1, 2, 5, 7, 8, and 11 because all were predicted to encode the same protein (1088 aa) by sorted six-frame translation. W = WoLFPSORT analysis. Locations: plas = plasma membrane, E.R. = endoplasmic reticulum, per = peroxisome, nuc = nucleus, cyto = cytoplasmatic.

			Ofabcb1		***Ofabcb2***						
Isoform			**Seq.**	**Seq.**	**1**	**2**	**5**	**6**	**7**	**8**	**11**
Contig ID		**Tri**	c23955_g1_i2		c25605_g2_i1	c25605_g2_i2	c25605_g2_i5	c25605_g2_i6	c25605_g2_i7	c25605_g2_i8	c25605_g2_i11
		CLC	3211		4439	4439	4439	4439	4439	4439	4439
Length [bp]			3964	6078	6058	7209	6326	7231	7470	5983	6886
LongestORF			115-3960	97-3807	617-3880	1768-5031	885-4148	1487-5053	2029-5292	542-3805	1445-4708
Protein [aa]			1282	1237	1088	1088	1088	1189	1088	1088	1088
Frame			+1	+1	+2	+1	+3	+2	+1	+2	+2
Pfam/ HmmScan	**TMD1**	**from**	61	38	425	1576	690	1436	1837	272	1253
		to	368	301	1072	2223	1340	2245	2484	997	1900
	NBD1	**from**	435	368	1271	2422	1539	2444	2683	1196	2099
		to	584	517	1720	2871	1988	2893	3132	1645	2548
	TMD2	**from**	718	675	2192	3343	2460	3365	3604	2117	3020
		to	991	949	3016	4167	3284	4189	4428	2941	3844
	NBD2	**from**	1057	1015	3212	4363	3480	4385	4624	3137	4040
		to	1210	1167	3670	4821	3938	4843	5082	3595	4498
TMHMM	**inside**		1-60								
	outside			1-71				1-23		1-22	
	TH1		61-83	72-94				24-46		23-45	
	TH2		139-161	148-170				100-122		103-125	
	TH3		215-237	174-196				126-148		140-162	
	TH4		242-264	252-274				204-226		523-545	
	TH5		319-341	289-311				241-263		565-587	
	TH6		356-378	672-694				624-646		650-667	
	TH7		716-738	714-736				666-688		671-693	
	TH8		758-780	799-816				751-768		749-771	
	TH9		841-858	820-842				772-794		786-808	
	TH10		862-881	898-920				850 -872			
	TH11		940-959	935-957				887-909			
	TH12		979-1001								
	inside		1002-1282	958-1237				910-1189		809-1088	
W	**plas**		27	32				32		30	
	E.R.									2	
	pero		3								
	nucl		1								
	cyto		1								

Table S 24 Sequence of *Ofabcb1* after sequencing. CDS is indicated in black and encodes a 1282 aa protein. Lowercase bases indicate potential variable sites for base exchanges.

>*Ofabcb1*

GAGGAGCGACTGTTATTAGGCTCTGTCGGAGAATGACCGCTGACCCcAGATAAGCCGGAGCGGATATCTGCCCGAC
TCCAGAGGAGATAGGGGAAGATACGCCCTCAGTCAGGCATGGGGAAGCGGCGAAGGGTGTACAGCAGGGAGACCC
AGGAGGATTGCGTTCCTCTGCTCCCGGGGGCCgTCATCACCTACGGTTCTCAGGACAGGCCAGCAGTCGTTAAAAA
GAAAAGGAAGCAAAAGTCAGGAATAATCGGCTTATTCCGTTATGCcAACGGTACAGATATCTGTATGATGCTTcTGGG
AATGTTATTTTCAATGGTGAACGGATCTGCCCTTCCAATTCTCAGTCTTGTCTTTGGACAAATGACTAACACTTTCGTG
ACTGCAACaGTTGACGGCTTTGCTGATTCACCAAACACGAATAACGGTATGCAATTTGATCAGAACAGCAGCTCAGCT
AACTTCAGTGATCTCAGTAACTCAACTTTACTAACAATTGACTCGTTCCTCGTATCAATGAATCAGTATTCTTTGTACTA
CTTGTATATTGGTATAGCAGCATTAGTATCATCATTTTTACAGAATCTCTTTTGGGAACTGTCTTGTGAGAGGCAAGTT
TATCAGCTGAGAAAGCTTTATTTTGCACAAGTTTTAAGACAGGATATTTCCTGGTATGATAAAAACCAAGAAGGAGATC
TCAACTCAAAATTAGCAGATGATATTGAGAGGATAAGAGAAGGAATTGGAGTTAAATTTTCGCTTGTGATTCAGTACTT
AACAACATTCTGGGTTGGTATACTTGTTGGTCTATACGCAGACTGGAGGTTAACgTGTGTCTTGCTGACGACCGGTCC
TTTTGTAATAGGAGCTGCCGCCTACATGGCTTTGTCAACAGCAAGTGGCGCATCAAGGGAACAATTGAAATATTCATA
TGCTGGTGGAGTAGCTGAAGAGGTACTGAATTCcATAAAGACTGTGGCTGCATTTGGTGGAGAAAAAAGAGAAATGG
CAAGGTACGATCATGCTCTTGACGAAGGAAGAAGAGTAGCAATGAAGAAATATCTCCTCATCTCCATAGGATTATTCT
TTGTCTTTTTTACTCTCTATTCCACTTAtGGTCTGGGcTTTTGGGTGGGAACAGGTTTTGTTGAATCTGGGCTCTCAACA
GGCGGCAGTATTATCACAGTATTTTTCAGCGTCATGATGGGGGCATTTTCTCTCGGTGGGATTCTACCATTTATTAGT
CAGGTcAGtGGTGCTGTTGGAGCCTCCAGGAACATATTTGCGATCATAGATCGAATCCCAGATATCGATCCGTATGCT
ACTACTGGGAAAGTGCTTGATAAAATGTCTGGAAACATTACATTTGAAAATGTGTTCTTCAGCTATCCTACCCGACCTG
ATGTAAAGATATTAAAAGGACTCAGTTTGAAAATAAACACTGGACAAACAATAGCTGTTGTTGGTTCgAGTGGAGCTG
GAAAAAGTACGATAGTGAACCTTATTATGAGATTCTATGATGCTACAGATGGAAAGGTACTAATTGACGGTGTTAATAT
TAAGGACTTAAATTTAAAATGGCTGAGAGACAACATCGGTGTAGTTTCACAAGAACCAGTGCTGTTCGGTGTTTCGAT
CCTGGACAACATTAAGTACGGAAGGGATAGAGTTACGCTGGAAGATGTCATATCTGCTGCCATGCTGGCAAACGCCC
ATTCCTTCATCAAACAACTACCCAACGGATATGAAACAATTTTGGGTGATCGTGGCGCCCAGTTATCCGGAGGGCAG
AAGCAACGTATCGCCATTGCAAGAGCTCTTATCCGTCAGCCTAAAATCCTTCTTTTGGACGAAGCTACGTCCGCCCTG
GACTCTCAGAGTGAAGGCGTAGTCCAGGAGGCCCTGGAGAACGCCATGAAAGGAAGAACTACCGTCATTATCGCTC
ATCGGCTCTCCACCATAAGGAACGCCAATGTCATATATGTCATGAAGGATGGCCAAGTGATAGAAGGCGGGACTCAC
GAGCAGCTCATGGCGAAGAAGTCGGCTTACTTCAGCCTGGTCACCACCGAGGCAAAGGCCGCGAAGGAGAGCAAT
GGCTTACCAGTGGTAGTGACACGAGAGAGACCAAAGTCATTGTCTGAATCAAGCTACTCTCTAGTTGAATCAGAGAA
GGATGAAGATGAAGACGTATGCTACGAAGAGGATAAAAGCTTGGTTTTGTGGAGACTGTTAAAGTTAAATGCGAAAGA
ATGGCATCTCTTGCTTTTTGGATTCCTTGCCTCTGCTGTAACTGGAGCGATTCAGCCAATTTTTGCTTTCTTTTACGGC
GAAATATTTTCGACATTTTCTATGACTGGTGATGCTCTGGAGCAGCAACGGACACTCTGGACTTGTATGTTTGTTCTTC
TTGGCGTTGTCTCTGGTTTAGCTTATTGGTTATGGGTTGTTACTATGGCAACATCAGCTGAGTACTTGATCGCCCGCC
TGAGGTCAATGGCTATGGCGAACATTCTGCGTCAGGAGCTGTCTTGGTTTGATGACAAACAGTTCTCTGTTGGGAAAT
TAATCACCAGGCTTACTAGAGATGCACCCGTCATTAGGACTGTGGCTGGAATGAGGATCGCgCAAGTAATTTCATCTA
CTGTTACACTGTTAGTTGCATTGCTTATTGCATTTATTTTTGGTTGGAAGTTAGCTCTTCTTCTCTTGGTTGCAATTCCA
ATTATCATAATAGCAGGATATGAGCAAGTTCACCAGATAAGGAAATTTGCTACCCGAGACATGGCAAGCATGGACATT
GCTGGGAAGGTTGCCTCGGAATGTATACAAAACCTTAAGACTGTACAATCCATTGGAAGAGAGATGAAATTTAGAGAT
GTCTATGTTGAATATTTAAAGCAACCTCATAAGGAATGTAAAAAGCAAGCTTTTATATTTGCATTTATATATTCTATTTGT
CAGGCGATTGTCTACTTCCTATACTCTGGTTCATTCAAATTTGGATCCTTTTTAATTGCTGAAGGAGAAATGAACCCCA
GTGATGTTTTCAGAGTCTTCTTTGCTTTGGCTTTCTCAGCTGTTGCCGTCGGACAGGGAGCTGCATATCTTCAAGACT
ATGCAAAGGGTAAAACTTCCGCACGGATAATATTCTTTCTGATGGATAAAAAATCTGAATTGGATCCTTTAGCTCCTGA
AGGATTGAAACTAACTGTAAAGGGGAAGATAACATTCAATAGCATCTGCTTCTCCTACCCATCAAGGAAAAATGTACA
AATACTAAATGGCTTTGATTTGCGGGTTGAGCCAGGACAGACAGTTGCTCTTGTGGGAGAATCTGGTTGTGGAAAGT
CAACCATCATTCAACTTCTGGAGAGGTTCTATAGACCAGATAGAGGAATCATTCAAATTGATGACATGAACATAGAAA
CATTCAATGTGAGCTGCCTCCGAAGTCAGATTGGCATTGTTACCCAAGAGCCAGTGTTATTCAACTGCACTATAAAGG
AAAATATCATGTACGGAAGTGTCGCCTTGGATAAGGTTCCCTGCGATCAAGAAGTCATCGACGCAGCAAAAGCTGCT
AACATACACGAGTTCATTACTAGCCTTCCTCAGGGATATGATACACCATGCGGGGAAAGAGGTACTCAACTCTCAGG
AGGTCAGAAGCAAAGAATAGCCATTGCCAGGGCACTTATTCGGAACCCGAGAATCCTTCTTCTCGATGAGGCAACTT
CAGCTCTTGACAATGAAAATGAAAAGATTGTTCAAGAGGCCCTGGACAGGGCACGTGAAGGAAGGACTTGCATTGTT
GTTGCTCATAGACTCTCGACCATACAGAATGCGGATAGGATTGCAGTCCTAAGCAAAGGGAGGGTTGCTGAACTTGG
AACTCATCACGATTTGATTGAAAGACAAGGGCTCTACTACCAGTTAGTCAAGAGGCAGCAGCTGTAAT

Table S 25 Sequence of *Ofabcb2* after sequencing. CDS is indicated in black and encodes a 1237 aa protein. Note that the exact sequence is not definitely known. Bases in italics indicate not sequenced sequence regions. Lowercase bases indicate potential variable sites for base exchanges.

>*Of*abcb2

TGTACACACAGGAGGAAATCCTGCTAAGTTAAGGAGGCTCCTCCAAGGATAAGGATTTACGACGAGCATGCACtGGA
CCTGTTGGAGGCCACTCATATGCGCTCACCACTTTGTCTTCTACTGATAcTGTTTCCTTGCCACAAAGTAATCCCACTC
TGTCCACAGGGCTTCAAGGAGTTCAGAAACCAGACATTAAGAGATGGATCCTCCAGCTTCCAGATTGATTTGTCTCCG
TACTGGATCGCTACAGCTGCTAATGAGACTGGTGCTACTGTGACAAGAGAGGAATTCACTAACGCCATGGCTAGTTT
CTCTTACTATTACGTGTACACAGCTGCAGCAGTCTTCGTAGCCGTATACATACAGACTTTtTGCTGGGAGACGGCATG
TGAAAGGCAGGTATTCAGACTCCGTCAGATATTCTTCTCTCAAATCCTTCGCCAGGACATCAGCTGGTATGAtGCCAA
CGAGGAAGGaGATCTCCCTCACAAACTGTCTGATGACCTGGAGCGGATCAGGGAGGGTATTGGAAGCAAGTTCAGC
ATGCTGTCTCAGTACGGCTCTACCTTCCTTACAGGGATCGGAGTCGGCTTCAGtGCTAaCTACAAGATGACTACTGCT
ATGATAGTGATCGCTCCTCTGGTCGTCGCCATGTCTGCTGTTGTcGCCAGGGCTATGAGCGGCTCTGCTGCCAGgGA
ACAGATTAGGTATGGTGTGGCAGGAGGGATCGCATCTGAAGTCCTCAACTCCATTAAGACTGTCGCCTCATTCAGTG
GGGAGCCTCGAGAAATTAAGAGATATGGCGAGGCACTTGAAGAGGGGCGGCGTATAACTTGTGGGAAGTACTATGT
gCTGTCCATAGCAGCTGCCATGATGTTTGTCACGTCATATGGTGCCTTCGCATTTGCGTTCTGGTATGGTTCTCAGCT
GATAAAGGGAGGAGAAGCCTCTCCAGGGAGTATTTTCACTGTCTTCTTCAGCGTGATGGCGGGTGCCTTCACAGTGG
GCAATGCACTGCCCTTCCTGAACACAGTAAGCACCGCCATAGGTTCGGCCTCAACCATTTTCGGGATCATCGACCGA
GTACCAGAGATCGACGCGTACTCCACAGATGGCATCATACCTGACCGCCTCCAGGGGAGGATTCGCTTCGAAGGGG
TGGAGTTCTCGTACCCCACCAGGAAGGAAGTCAAGGTGCTGCGGGGTCTGGACTTTGACTTGGAGTCAGGGAAATC
GGTGGCCCTGGTGGGATCCAGCGGTGCAGGGAAGAGCACAGTGGTCGGTCTGCTACTCCGCTTCTACTCGCCCGA
CAATGGCCGGGTACTCCTGGACGACATCCCCATCGAGGACTACAACCTGCAGTGGCTCCGATCCCAGGTCGGACTT
GTCTCACAGGAGCCAGTATTGTTTGGAGTGAGTATTGCAGAAAACATACGATATGGACGAGAAGGCATTTCAGATATG
GATATAGTGAAGGCTGCCACACTGGCCAATGCCCATTCATTTATCAAATATCTTCCTTTGGGTTATGACACGCATGTC
GGGGACAAGGGCGCAATGCTGTCTGGAGGTCAGAAGCAGCGCATAGCTATAGCACGTGCCCTAGTCCGGGACCCG
AAGATCCTCCTCCTAGATGAAGCCACCTCCGCCCTGGACGCCCACAGTGAGAAAGTGGTACAGGCCGCCCTGGAGA
ATGCAGCTCAAGGAAGGACAACCATCACTATAGCGCACAGGCTCTCCACCGTCAAGAACGTAGACAGGATTTATGCC
CTGAAGGATGGCAAGGTGTACGAATCGGGTAAACATGAAGAGCTGATGGAGAAGGAAGGTCTGTATTACAGCCTTGT
AATGGCACAGAAAGGGCGAGACCAGAAGAAGCAACTCTCGGACGATGAATCGCCAGAAGAAGATGCTCAAGTTAAT
CAGCAACCTAATGTCGTGGAAACGAAAAAACCAGGTTTCTTTTCAAGAATTTCATTAAGGAGGCGAAAGTCTTCAGCA
TTGTCATTACGCAATGTTTTTGTGGGAGCTCCTAAAGACGAAGATTCATCCAAAGAGGAACTTGCTAAGAATGTAAGC
TTTTACAAAATCATCAAAATGAATTTGTCTCTATGGCCTTTCATGCTCCTAACTCTGATTGGTTGTGCCACAGTTGGAA
CCAGCATGCCTCTGTTCTCTTCATTTTATGCTGACGTTTTTTATACCTTCACACTCACAGGCCCAGAATTTGACAGCGC
TGTAATTTTCTGGACTGGGGTGTACGCCACATTTGCTTTGGTTGCTGGTTTAGGAAACTTCACTGCGGCCTTGTGCTC
ATCACTTCTGACTGAGAAGATGATAGTAGTTATGCGATTAAAGGCATTCACCAGCATCATCCGCCAGCAAATTGGGTG
GTTCGACGCAGATGCTCATTCACCTGCCAGACTTGTCACTTCACTTGCAAGGGATCCTCCTCTCATCAAAGCTGCAG
CAGGTTTCAGAGCTGGGCAGATCTTCGTTGCTGGTACTTCTTTGGTGGCAGCAATAGTGATAGCTTTCAGCACTGGA
TGGAAGCTGTCCATCTTGCTCATGCTGGTGGTACCTGTGATAGCAGGTGCTGCTTACAAACAAGCCAGGCTCCTCAG
GCGACATCAGAAAAGGGATGCCAAATACATGGATGATGCTGGCCAGATAGCTACTGAAGGTGTTTTAAATTTGAAGA
CTGTTCAAGCATTGGGAAAAGAAAAACTGTTTATCGAAAAATACAAGAAATGCTTGGATTTACCATTTAAAGAATCTAA
AAAGCAGGCCTATGTTTATGCCTTAGTATTTGCTATTTCACAAGCATTAATTTACATCATGTACGCTGCTGCATTCAGA
TATGGTGCTGCACTTATTTCAAATGGAGATATGGATCCTACATCTGTTTACAGAGTATTTTTTGCTCTGTCGTTCTCAG
CCACTGCAATAGGACAAGCCTCTACGTATTTCCAGGACTTTGCGAAGGCCAAGCTCTCCATCGGCTTTGTCTACAGG
TTAATGCAACTTGAATCTGACGTAGATGTCCTCGATCCAAGTGGACTCAAGCCAACGATCAAAGGCAGAGTTGATTTT
CGCGACATTCATTTTTCATACCCTACAAGGAGAAACATCCCCATCCTCAGAGGTTTAAGTCTCACCATTGAGCCAGGG
CAGACAGTAGCTCTGGTAGGGGGCTCAGGCTGTGGAAAGTCTACTCTCATTGGTCTTCTGGAAAGATTCTACTCACC
AAGCAGTGGAAAAGTGATACTAGATGATACTGATATCTCCGCGATGAACCTCACATGGCTGCGAAGTCACATGGGTC
TTGTGACACAAGAACCGGTACTATTTGATTGCTCCATAAAGGAAAACATTGCATATGGTGCAGCAGACCCATCAGCTG
TCACCCACGAGAATGTTATTGATGCAGCAAAAATTGCTAATATTCATGACTTCATAATCAGCCTTCCTCAGGGATACGA
TACACCTGTTGGGGACCGGGGAGCAAAGCTTTCAGGAGGGCAAAAGCAGAGGTTGGCTATAGCTCGAGCCCTCATA
AGGGACCCCAAAATACTTCTTCTTGATGAGGCAACTTCTGCTTTGGACACCGAGAGTGAAAAGATAGTACAGGAGGC
ACTGGATCGGGCAAGGAAAGGGCGAACCAGCATAGTCATCGCCCACCGTCTATCAACGATCCAGAATGCCGATATG
ATAGCTGTGATCCATAAGGGAAAGGTGGCTGAGCTTGGCACTCATGAGGAGCTCAAGCGACTTGGAGGATTATACTT
TGAACTTATTAAAAACCAATGACCTTATCTAAGGAATGAATCTACTTGACTTCTTCATGGAAGTCTTTGTTTAGCGAAA
GAAGACTTTTACAGCAGCATTTTTTATTGAAATTTTTATGTCTAAACAGCTTATAAATTGTATATAATCTGGATTAAAAAA
AGCCAATCAATTACAATCAAAATGAAAATATTGGCGTGGAAAGTGTATAAGAGGTACTTTGAATTTTTTTTCATTTAGAG
GATCCAAGAGCTTTTTTAAATATTTATATCAATAGATACTTGATAATTTATCTATATTGATTTTATATACATTCAATCAATG
ATTTTGTATATCTTCTTATCAAGCTTTTAATATTGATTTGTATATAAAAAGCATTTAAATTCATCCACTATTTCATGATCTA
TAAATGTTTTCACAGTTCGAAATTTAAATTGAATATTTATAGGTGCTGGCAGGGCTACATCCTGCCTTAAGCCTTAACG
CAAGAGTCCAGGGTAGGTATAGGGTGATACAATTTCATTTAGAATTAGAGTGTGCTCAGTGCTATAGTAATTATAAGAT
CGTGTCCAAATGCCTTCATGTGACCCTGTTGATTGCAAAACTAAACTAAGATATgTAAAACACTTTTTGATGAATTTGAC
TATCTTTTAAAGCTGAATAGTATTACTTAAATTTGATTATTTGCATACATAAATATAAATAAATTAGCATGTATAAATTACT
TATAAAACTTCTCATGAAATTCACCATTTATTAGATATTTTTGAGGTGACCGAGCTACTTACAAGGCAAGTATTTTACTT
CCCTCCAGCATCATATGACCCATCGGTGTCTCACTCTTTAGAAAAAGAAAACTGTAATAACGATATACACTGATTTACT
AACAGCATTAATAGAGATAGTCTAAGCTGAAACTTAATCAATAAATGAAATTCATTTAAAAATTTTCATGAAAACAGATG

>*Of*abcb2

GATTCTTTTCTCAACAACAATTTTTTCCTTGTAAGGGGGAAATAAGCAGATGATTCTCGAACATTTAAATGTGGAAGGT
AATTGATTTAATTATTATATATGAAAGTGTGCTTCATATAATTTAAAGTTAGTTTTTGGTTAGGTTTTTATGGAAGAAGTT
AAATATTCTCCAAGATTCTCAGTCTAAGTAAAGTCTCTGTATTTATATTTTTTATCCAGCAACTCTTACTATACAGAGCC
ATTGATAAGGGACCCGGGGAAACTAGGGCATGTTGCATAGATATGGCTTTGCATATATTTATCTTGAGCAAATACTTTT
GATAAAGTACCTCATCTGCTGTTAGTAGTATAGCAGTGGTGATCAACTCTTTCTCATAATAGTCTAAACTATTACTATCA
TTACTGATCTGCACTTAGCAGCATATGACTTGCTTCATCAACTTCTTTCATTACTAGGTGCCTGAAGGAAGCAGTTATA
CAAGTCCTGCCGAGGCAAACCTAATTCGCCTAAAACATTTGACACCAATGCTCATGACTTCCAATGTTCATGATGCAg
TATTTTTATCCCTAATTCTTGGTAACCACAATTGAGAAGGAGCTTTAAAAAATGAAAAGTCGAGGTCCTGCCAACGACA
ACTGTGGGCCTTACAGCTGCCTTCTGATTTGTCAAACTAAACCTACCCAATTACTTTCAATTCCACTGGTATAGAATAT
ACAGAAAATTACTTGTGTCAAGGGGGTGAAAACTCTCTGCACCCGATCCATAAGAAGCCGTCGGAGATAAAAGTTGT
CTTGCGGTTTGAATCAACTCAATTTGAATCAAATATGTTACCTCATATTTAATATAGAACTTTACAATATACATATATATA
TCGAAGTTTTAATAAACTCTACTGGAAATACTCTGAGAGAATGTTAAAAATTTTTTAAAGATGCCGGGATCTATTGTTTT
TATTCATTAAGTTTCCCATAAATTCACCCTAAAAAATAATTAAAGTGAACAACATGAAAACTGCTATTGTAGATGACACC
ATATACCTATAAAAAATGCTGTTGCTAAAGTCTGAAGCTTTATGAGCTCAATTAGTATTATTAATGGGTATTTTGAATTT
GTGAAAAGAATATCTGGTCAATCTTGGAAAAAAGGTATTTATAA*TTTGTATTTATTTGCATTTAGAGATATTTCCAGTCT*
TAACAAATTTTGATTCAATCCATAATCAATTGGGTTTTTTTTTATACTGTAAATACTTAGATTTAAGTGTGTAGATATTTA
TTTATAAAGAAAGTGATCTAACAAGTATTTAATTTTTCGGTTTAAAGTGGAGTG

Table S 26 Summary of gene structure analysis and prediction for *Ofabcb2* by different approaches. Gene structure analysis for the *Ofabcb2* sequence based on amplified or cloned PCR amplicons or *Ofabc2* isoforms predicted in silico after manual curation was conducted by comparing them with the genomic scaffold (214) using splign software. A second gene prediction was conducted using FGENESH+. Star (= start) and stop refer to the exon position on the scaffold. Junction gives the two intronic bases flanking the predicted exonic region.

	Version		Exon length	*Ofabcb2* sequenced			Isoform 1			Isoform 2			Isoform 5			Isoform 6			Isoform 7			Isoform 8			Isoform 11			FGENESH+		
				star	stop	junction	star	stop	junction	star	stop	junction	star	stop	junction	star	stop	junction	star	stop	junction	star	stop	junction	star	stop	junction	star	stop	junction
Exon 1			71																					352169	352239	<exon>GT			
Exon 2			89																					354826	354914	AG<exon>GT			
Exon 3			338																		357456	357793	GG<exon>CT						
Exon 4		a	671							358061	358731	<exon>GT																	
		b	685										358061	358745	<exon>TA														
		c	149																					358583	358731	TT<exon>GT			
		d	159																								358573	358731	TA<exon>GT
Exon 5			654													359933	360586	GG<exon>NN	359933	360586	GG<exon>NN								
Exon 6	1	a	41																								360876	360916	AG<exon>GT
	2	a	246	361034	361279	<exon>GT																								
	2	b	94				361186	361279	<exon>GT																					
	3	a	753													361110	361862	GG<exon>GT											
	3	b	106	361757	361862	AG<exon>GT																								
	3	c	85																								361778	361862	AG<exon>GT
	4	a	1126																361110	362235	GG<exon>GT								
	4	b	1051							361185	362235	AG<exon>GT													361185	362235	AG<exon>GT			
	4	c	479				361757	362235	AG<exon>GT																					
	4	d	153										362082	362235	CA<exon>GT															
	4	e	153																			362083	362235	AC<exon>GT						
	4	g	134	362102	362235	AG<exon>GT										362102	362235	AG<exon>GT									362102	362235	AG<exon>GT
Exon 7		a	177	363464	363640	AG<exon>TC	363464	363640	AG<exon>TC	363464	363640	AG<exon>TC	363464	363640	AG<exon>TC	363464	363640	AG<exon>TC	363464	363640	AG<exon>TC	363464	363640	AG<exon>TC	363464	363640	AG<exon>TC			
		b	172																								363464	363635	AG<exon>GT
Exon 8		a	176	365810	365985	GC<exon>GT	365810	365985	GC<exon>GT	365810	365985	GC<exon>GT	365810	365985	GC<exon>GT	365810	365985	GC<exon>GT	365810	365985	GC<exon>GT	365810	365985	GC<exon>GT	365810	365985	GC<exon>GT			

	Version		Exon length	*Ofabcb2* sequenced			Isoform 1			Isoform 2			Isoform 5			Isoform 6			Isoform 7			Isoform 8			Isoform 11			FGENESH+		
				star	stop	junction	star	stop	junction	star	stop	junction	star	stop	junction	star	stop	junction	star	stop	junction	star	stop	junction	star	stop	junction	star	stop	junction
		b	162																									365 824	365 985	AG<exon>GT
Exon 9		a	227	367 222	367 448	AG<exon>AA	367 222	367 448	AG<exon>AA	367 222	367 448	AG<exon>AA	367 222	367 448	AG<exon>AA	367 222	367 448	AG<exon>AA	367 222	367 448	AG<exon>AA	367 222	367 448	AG<exon>AA	367 222	367 448	AG<exon>AA			
		b	225																									367 222	367 446	AG<exon>GT
Exon 10		a	131	373 181	373 311	TT<exon>GT	373 181	373 311	TT<exon>GT	373 181	373 311	TT<exon>GT	373 181	373 311	TT<exon>GT	373 181	373 311	TT<exon>GT	373 181	373 311	TT<exon>GT	373 181	373 311	TT<exon>GT	373 181	373 311	TT<exon>GT			
		b	129																									373 183	373 311	AG<exon>GT
Exon 11			252	373 652	373 903	AG<exon>GT	373 652	373 903	AG<exon>GT	373 652	373 903	AG<exon>GT	373 652	373 903	AG<exon>GT	373 652	373 903	AG<exon>GT	373 652	373 903	AG<exon>GT	373 652	373 903	AG<exon>GT	373 652	373 903	AG<exon>GT	373 652	373 903	AG<exon>GT
Exon 12			122	374 277	374 398	AG<exon>GT	374 277	374 398	AG<exon>GT	374 277	374 398	AG<exon>GT	374 277	374 398	AG<exon>GT	374 277	374 398	AG<exon>GT	374 277	374 398	AG<exon>GT	374 277	374 398	AG<exon>GT	374 277	374 398	AG<exon>GT	374 277	374 398	AG<exon>GT
Exon 13			48	374 889	374 936	AG<exon>GT	374 889	374 936	AG<exon>GT	374 889	374 936	AG<exon>GT	374 889	374 936	AG<exon>GT	374 889	374 936	AG<exon>GT	374 889	374 936	AG<exon>GT	374 889	374 936	AG<exon>GT	374 889	374 936	AG<exon>GT			
Exon 14			112	375 023	375 134	AG<exon>GT	375 023	375 134	AG<exon>GT	375 023	375 134	AG<exon>GT	375 023	375 134	AG<exon>GT	375 023	375 134	AG<exon>GT	375 023	375 134	AG<exon>GT	375 023	375 134	AG<exon>GT	375 023	375 134	AG<exon>GT	375 023	375 134	AG<exon>GT
Exon 15			144	376 228	376 371	AG<exon>GT	376 228	376 371	AG<exon>GT	376 228	376 371	AG<exon>GT	376 228	376 371	AG<exon>GT	376 228	376 371	AG<exon>GT	376 228	376 371	AG<exon>GT	376 228	376 371	AG<exon>GT	376 228	376 371	AG<exon>GT	376 228	376 371	AG<exon>GT
Exon 16			102	376 987	377 088	AG<exon>GT	376 987	377 088	AG<exon>GT	376 987	377 088	AG<exon>GT	376 987	377 088	AG<exon>GT	376 987	377 088	AG<exon>GT	376 987	377 088	AG<exon>GT	376 987	377 088	AG<exon>GT	376 987	377 088	AG<exon>GT			
Exon 17			162	377 964	378 125	AG<exon>GT	377 964	378 125	AG<exon>GT	377 964	378 125	AG<exon>GT	377 964	378 125	AG<exon>GT	377 964	378 125	AG<exon>GT	377 964	378 125	AG<exon>GT	377 964	378 125	AG<exon>GT	377 964	378 125	AG<exon>GT	377 964	378 125	AG<exon>GT
Exon 18			204	379 706	379 909	AG<exon>GC	379 706	379 909	AG<exon>GC	379 706	379 909	AG<exon>GC	379 706	379 909	AG<exon>GC	379 706	379 909	AG<exon>GC	379 706	379 909	AG<exon>GC	379 706	379 909	AG<exon>GC	379 706	379 909	AG<exon>GC	379 706	379 909	AG<exon>GT
Exon 19			101	381 667	381 767	AG<exon>GT	381 667	381 767	AG<exon>GT	381 667	381 767	AG<exon>GT	381 667	381 767	AG<exon>GT	381 667	381 767	AG<exon>GT	381 667	381 767	AG<exon>GT	381 667	381 767	AG<exon>GT	381 667	381 767	AG<exon>GT	381 667	381 767	AG<exon>GT
Exon 20			141	381 848	381 988	AG<exon>GT	381 848	381 988	AG<exon>GT	381 848	381 988	AG<exon>GT	381 848	381 988	AG<exon>GT	381 848	381 988	AG<exon>GT	381 848	381 988	AG<exon>GT	381 848	381 988	AG<exon>GT	381 848	381 988	AG<exon>GT	381 848	381 988	AG<exon>GT
Exon 21			157	383 164	383 320	AG<exon>GT	383 164	383 320	AG<exon>GT	383 164	383 320	AG<exon>GT	383 164	383 320	AG<exon>GT	383 164	383 320	AG<exon>GT	383 164	383 320	AG<exon>GT	383 164	383 320	AG<exon>GT	383 164	383 320	AG<exon>GT	383 164	383 320	AG<exon>GT
Exon 22			195	388 431	388 625	AG<exon>GT	388 431	388 625	AG<exon>GT	388 431	388 625	AG<exon>GT	388 431	388 625	AG<exon>GT	388 431	388 625	AG<exon>GT	388 431	388 625	AG<exon>GT	388 431	388 625	AG<exon>GT	388 431	388 625	AG<exon>GT	388 431	388 625	AG<exon>GT
Exon 23			210	392 394	392 603	AG<exon>GT	392 394	392 603	AG<exon>GT	392 394	392 603	AG<exon>GT	392 394	392 603	AG<exon>GT	392 394	392 603	AG<exon>GT	392 394	392 603	AG<exon>GT	392 394	392 603	AG<exon>GT	392 394	392 603	AG<exon>GT	392 394	392 603	AG<exon>GT
Exon 24			147	393 829	393 975	AG<exon>GT	393 829	393 975	AG<exon>GT	393 829	393 975	AG<exon>GT	393 829	393 975	AG<exon>GT	393 829	393 975	AG<exon>GT	393 829	393 975	AG<exon>GT	393 829	393 975	AG<exon>GT	393 829	393 975	AG<exon>GT	393 829	393 975	AG<exon>GT
Exon 25			2364	396 880	399 336	AG<exon>	396 880	399 243	AG<exon>	396 880	399 243	AG<exon>	396 880	399 243	AG<exon>	396 880	399 243	AG<exon>	396 880	399 243	AG<exon>	396 880	399 243	AG<exon>	396 880	399 243	AG<exon>	396 880	397 068	AG<exon>GT
Total exon number				22			21			21			21			22			21			21			23			21		

Previous table continued.

Table S 27 Expression stabilities of the tested reference gene candidates across different treatments. The lower the Normfinder stability value or geNorm averaged M-value, the more stable the expression of the reference gene or candidate gene combination is. GeNorm V-value gives the minimal gene number required for normalization. For details on algorithms see Chapter 1. Tissues included three biological replicates of seven milkweed bug tissues as follows: male and female gonads, salivary glands, thoracic region, Malpighian tubules, nervous system and gut. Diet: milkweed bugs fed either sunflower seeds only or additionally *A. syriaca* seeds (n = 3 each). RNAi 7d: Animals injected with RNAi (*Ofabcb1* (700 ng) or *Ofabcb2* (700 ng or 1.17 µg) or control (700 ng *egfp*). Experimental groups for Normfinder analysis were not defined here because of small sample size (n = 2 each). RNAi + ouabain: Animals injected with 700 ng RNAi each (*Ofabcb1* or *Ofabcb2* or combination of both) and controls (700 ng *egfp* or buffer) followed by injection with 10 µg ouabain after seven days. Most stable gene is ranked first. BC SV = best gene combination stability value.

		Normfinder						GeNorm		
		No experimental groups			Experimental groups					
Treatment	**Gene name**	**Stability value**	**Standard error**	**Rank**	**Stability value**	**Rank**	**BC SV**	**Averaged M-value**	**Rank**	**V(2/3)-value**
Tissue	*Ofef1a*	0.120	0.206	1	0.220	1		0.347	1	0.320
	Ofrp49	0.314	0.094	2	0.253	2		0.347	1	
	Oftactin5C	0.654	0.107	3	0.408	3		0.764	2	
	Oftactin5C|*Ofrp49*						0.158			
Diet	*Ofef1a*	0.035	0.165	1	0.094	1		0.1024	1	0.122
	Ofrp49	0.099	0.068	2	0.148	2		0.1024	1	
	Oftubulin	0.251	0.080	3	0.206	3		0.2803	2	
	Ofef1a|*Oftubulin*						0.092			
RNAi 7d	*Ofef1a*	0.041	0.032	1				0.115	1	0.040
	Ofrp49	0.073	0.025	3				0.127	2	
	Oftubulin	0.068	0.025	2				0.115	1	
	Ofef1a|*Oftubulin*									
RNAi + ouabain	*Ofef1a*	0.026	0.045	1	0.021	1		0.146	1	0.057
	Ofrp49	0.107	0.019	3	0.059	3		0.171	2	
	Oftubulin	0.098	0.018	2	0.049	2		0.146	1	
	Ofef1a|*Oftubulin*						0.027			

Table S 28 Results of multi-level calibration with two different HPLC systems. RT = retention time. M = regression slope of the multi-level calibration used for ouabain quantification with coefficient of determination (R^2). IRF = Internal response factor = ratio of analyte (ouabain) to the internal standard (digitoxin). 1 - 5 denotes different standards differing in their ouabain to digitoxin ratios ((1) 2:1, (2) 1:1, (3) 1:2, (4) 1:4 and (5) 1:8). IRF ratio gives the ratio of different peak-specific IRFs.

	HPLC system					
	I			**II**		
Peaks [RT min]	2.07	4.25	both	12.06	12.23	both
m	0.5290	0.5407	1.0698	0.2569	0.7483	1.0052
R^2	0.999	0.999	1.000	0.990	0.994	0.999
IRF 1	1.82	1.92	0.93	3.68	1.40	1.01
IRF 2	1.95	1.80	0.94	4.74	1.18	0.94
IRF 3	1.98	1.82	0.95	4.60	1.18	0.94
IRF 4	1.84	1.89	0.93	4.69	1.18	0.94
IRF 5	1.70	1.96	0.91	4.59	1.19	0.94
IRF ratio 1			0.95			2.63
IRF ratio 2			1.08			4.03
IRF ratio 3			1.09			3.90
IRF ratio 4			0.97			3.96
IRF ratio 5			0.87			3.87

Table S 29 Run conditions used for ouabain quantification optimization in HPLC system II. ACN = percentage of organic solvent acetonitrile. Italicized numbers = rate of ACN % increase per min in the first gradient section. Injection volumes were 15 µl.

OUABAIN_TEST2.M		**OUABAIN_TEST3.M**		**OUABAIN_TEST4.M**	
Min	**ACN %**	**Min**	**ACN %**	**Min**	**ACN %**
0	10	0	13	2	8
2	10	2	13	11.4	30
10.5	30	9.2	30	16.4	95
15.5	95	14.2	95	22.4	95
20.5	95	19.2	95	22.5	8
20.6	10	19.3	13	32.5	8
30.5	10	29.3	13		
	2.35		*2.36*		*2.34*
OUABAIN_TEST5.M		**OUABAIN_TEST6.M**		**OUABAIN_TEST7.M**	
Min	**ACN %**	**Min**	**ACN %**	**Min**	**ACN %**
2	8	2	5	2	2
28.5	70	12.7	30	14	30
33.5	95	17.7	95	19	95
38.5	95	22.7	95	22	95
38.6	8	22.8	8	24.1	2
53	8	32.8	8	34.1	2
	2.34		*2.34*		*2.33*

Table S 30 Exploratory general and generalized linear model summary for modelling released defensive fluid volume as a function of diet history, biomass, and sex. The model coefficients are given in the rows, the standard error is shown below in italics. Abbreviations are as follows: Df = degrees of freedom. AIC = Akaike information criterion. GOF = goodness of fit. Nvc = Non-constant Variance Score Test. * p < 0.1; ** p < 0.05; *** p < 0.01.

	Dependent variable																	
	log(dfv)	Defensive fluid (dfv)																
	LM	*glm: quasipoisson link = log*	*glm: Gamma link = log*	*glm: Gamma link = identity*	*glm: Gamma link = log*	*glm: Gamma link = identity*	*glm: Gamma* *link = log*											
	(1)	(2)	(3)	(4)	(5)	(6)	(7)	(8)	(9)	(10)	(11)	(12)	(13)	(14)	(15)	(16)	(17)	(18)
Biomass	0.050***	0.045***	0.052***	0.025***	0.050***	0.023***	0.047***	0.044***	-0.024***	-0.026***			0.057***	0.053***	0.052***	0.046***	0.052***	0.050***
	-0.009	*-0.009*	*-0.01*	*-0.005*	*-0.008*	*-0.004*	*-0.009*	*-0.008*	*-0.007*	*-0.007*			*-0.011*	*-0.009*	*-0.011*	*-0.009*	*-0.01*	*-0.008*
Sex	1.678***	1.513***	1.634***	1.008***	1.661***	1.006***	1.563***	1.570***			0.828***	0.891***	2.462***	2.214***	1.634***	1.658***	1.576***	1.657***
	-0.153	*-0.177*	*-0.17*	*-0.095*	*-0.144*	*-0.083*	*-0.163*	*-0.145*			*-0.112*	*-0.101*	*-0.787*	*-0.677*	*-0.171*	*-0.144*	*-0.193*	*-0.167*
Diet	0.229**	0.216**	0.194*	0.097	0.246***	0.116**			-0.012	0.023	0.054	0.116	0.173*	0.231**	0.185	-0.054	0.132	0.243**
	-0.091	*-0.092*	*-0.101*	*-0.06*	*-0.086*	*-0.05*			*-0.125*	*-0.122*	*-0.112*	*-0.101*	*-0.101*	*-0.088*	*-0.456*	*-0.386*	*-0.138*	*-0.12*
Biomass x diet															0.0002	0.007		
															-0.011	*-0.009*		
Biomass x gender													-0.022	-0.015				
													-0.021	*-0.018*				
Diet x sex																	0.126	0.007
																	-0.191	*-0.166*
Constant	-3.373***	-2.985***	-3.318***	-0.728***	-3.301***	-0.666***	-2.974***	-2.886***	0.781**	0.829***	-0.703***	-0.796***	-3.579***	-3.471***	-3.313***	-3.130***	-3.303***	-3.300***
	-0.435	*-0.496*	*-0.482*	*-0.216*	*-0.41*	*-0.184*	*-0.44*	*-0.393*	*-0.306*	*-0.299*	*-0.097*	*-0.088*	*-0.53*	*-0.455*	*-0.533*	*-0.45*	*-0.481*	*-0.414*
Observa-tions	80	80	80	80	79	79	80	79	80	79	80	79	80	79	80	79	80	79
R^2	0.668																	
Adjusted R^2	0.655																	
Log Likelihood			-9.764	-10.152	-0.923	-2.271	-12.109	-5.368	-43.007	-40.01	-24.4	-17.478	-9.081	-0.551	-9.764	-0.565	-9.491	-0.922
AIC			27.528	28.303	9.846	12.543	30.217	16.736	92.013	86.019	54.8	40.956	28.162	11.102	29.527	11.129	28.982	11.844
Residual Std. Error	0.388 (df = 76)																	
F Statistic	50.912*** (df = 3; 76)																	
Ncv Test χ2	4.744**																	
Shapiro-Wilk test (residuals) W	0.983																	

	Dependent variable																	
	log(dfv)	Defensive fluid (dfv)																
	LM	*glm: quasipoisson link = log*	*glm: Gamma link = log*	*glm: Gamma link = identity*	*glm: Gamma link = log*	*glm: Gamma link = identity*						*glm: Gamma link = log*						
	(1)	(2)	(3)	(4)	(5)	(6)	(7)	(8)	(9)	(10)	(11)	(12)	(13)	(14)	(15)	(16)	(17)	(18)
McFadden's pseudo R2		0.616	0.609															
Dispersion estimate check			0.185															
Residual Deviance test			0.833															
	Dependent variable defensive fluid																	
Distribution	Normal	Lognormal	Gamma	Weibull	Poisson	Negativ Binomial												
GOF AIC	848.125	841.781	836.446	835.473	2668.758	836.610												

Previous table continued.

Table S 31 Exploratory general and generalized linear model summary for modelling released defensive fluid volume as a function of diet history, biomass, female age, and the total number of releasing sites. The model coefficients are given in the rows, the standard error is shown below in italics. Abbreviations are as follows: Df = degrees of freedom. AIC = Akaike information criterion. GOF = goodness of fit. Nvc = Non-constant Variance Score Test. *p<0.1; **p<0.05; ***p<0.01.

	Dependent variable																					
	log(dfv)	Defensive fluid (dfv)																				
	LM	*glm: quasipoisson link = log*	*glm: Gamma link = log*	*glm: Gamma link = identity*	*glm: Gamma link = log*	*glm: Gamma link = identity*	*glm: Gamma link = log*															
	(1)	(2)	(3)	(4)	(5)	(6)	(7)	(8)	(9)	(10)	(11)	(12)	(13)	(14)	(15)	(16)	(17)	(18)	(19)	(20)	(21)	(22)
Biomass	0.051***	0.052***	0.055***	0.022***	0.051***	0.021***			0.051***	0.047***	0.051***	0.050***	0.054***	0.046***	0.045***	0.037***	0.053***	0.049***	0.055***	0.051***	0.056***	0.052***
	-0.01	*-0.011*	*-0.009*	*-0.004*	*-0.008*	*-0.004*			*-0.009*	*-0.008*	*-0.009*	*-0.009*	*-0.01*	*-0.009*	*-0.013*	*-0.011*	*-0.009*	*-0.008*	*-0.009*	*-0.008*	*-0.009*	*-0.008*
Diet	0.214*	0.218	0.215*	0.085*	0.233**	0.083**	0.046	0.093			0.251**	0.288**	0.216*	0.248**	-0.678	-1.063	0.239**	0.239**	0.505	0.23	0.224*	0.252**
	-0.121	*-0.133*	*-0.113*	*-0.048*	*-0.098*	*-0.04*	*-0.171*	*-0.148*			*-0.12*	*-0.115*	*-0.117*	*-0.099*	*-0.833*	*-0.682*	*-0.107*	*-0.1*	*-0.33*	*-0.303*	*-0.114*	*-0.102*
Age 1	-0.056	0.002	-0.017	-0.016	-0.093	-0.024	-0.204	-0.289**	-0.065	-0.141*			0.137	0.847	-0.034	-0.122*	-0.406*	-0.173	-0.031	-0.093	0.055	-0.058
	-0.089	*-0.104*	*-0.083*	*-0.03*	*-0.074*	*-0.026*	*-0.124*	*-0.11*	*-0.083*	*-0.077*			*-0.707*	*-0.603*	*-0.085*	*-0.071*	*-0.218*	*-0.213*	*-0.083*	*-0.076*	*-0.106*	*-0.097*
Age 2	0.221***	0.212**	0.214***	0.107***	0.256***	0.109***	0.215*	0.276***	0.239***	0.280***			0.084	-0.367	0.220***	0.266***	0.23	0.092	0.220***	0.256***	0.247**	0.311***
	-0.077	*-0.083*	*-0.072*	*-0.034*	*-0.063*	*-0.028*	*-0.113*	*-0.099*	*-0.073*	*-0.066*			*-0.582*	*-0.495*	*-0.072*	*-0.06*	*-0.218*	*-0.208*	*-0.07*	*-0.064*	*-0.103*	*-0.093*
Releasing sites	0.207***	0.201***	0.228***	0.099***	0.171***	0.078***	0.248***	0.173***	0.218***	0.163***	0.242***	0.197***	0.229***	0.171***	0.225***	0.162***	0.200***	0.156***	0.258***	0.171***	0.216***	0.165***
	-0.048	*-0.049*	*-0.045*	*-0.022*	*-0.041*	*-0.018*	*-0.069*	*-0.063*	*-0.046*	*-0.044*	*-0.049*	*-0.049*	*-0.048*	*-0.042*	*-0.045*	*-0.039*	*-0.045*	*-0.044*	*-0.055*	*-0.053*	*-0.045*	*-0.042*
Biomass x age 1													-0.003	-0.021								
													-0.015	*-0.013*								
Biomass x age 2													0.003	0.014								
													-0.012	*-0.01*								
Biomass x diet															0.018	0.027*						
															-0.017	*-0.014*						
Age 1 x Releasing sites																	0.111*	0.024				
																	-0.058	*-0.059*				
Age 2 x Releasing sites																	-0.001	0.048				
																	-0.059	*-0.057*				
Diet x Releasing sites																			-0.085	0.001		
																			-0.091	*-0.084*		
Diet x Age 1																					-0.168	-0.077
																					-0.161	*-0.145*
Diet x Age 2																					-0.035	-0.089
																					-0.142	*-0.127*
Constant	-4.170***	-4.120***	-4.359***	-0.952***	-4.029***	-0.871***	-1.662***	-1.480***	-4.018***	-3.681***	-4.205***	-4.056***	-4.316***	-3.811***	-3.862***	-3.300***	-4.189***	-3.909***	-4.486***	-4.028***	-4.407***	-4.069***
	-0.498	*-0.565*	*-0.463*	*-0.199*	*-0.407*	*-0.169*	*-0.278*	*-0.246*	*-0.439*	*-0.4*	*-0.482*	*-0.462*	*-0.524*	*-0.447*	*-0.645*	*-0.534*	*-0.459*	*-0.434*	*-0.473*	*-0.433*	*-0.458*	*-0.411*
Observations	40	40	40	40	39	39	40	39	40	39	40	39	40	39	40	39	40	39	40	39	40	39
R^2	0.663																					
Adjusted R^2	0.614																					

	Dependent variable																					
	log(dfv)	Defensive fluid (dfv)																				
	LM	*glm: quasipoisson link = log*	*glm: Gamma link = log*	*glm: Gamma link = identity*	*glm: Gamma link = log*	*glm: Gamma link = identity*		*glm: Gamma link = log*														
	(1)	(2)	(3)	(4)	(5)	(6)	(7)	(8)	(9)	(10)	(11)	(12)	(13)	(14)	(15)	(16)	(17)	(18)	(19)	(20)	(21)	(22)
Log Likelihood			21.443	20.408	26.823	25.863	7.082	11.894	19.53	24.012	16.567	19.518	21.484	28.374	22.122	28.69	23.359	27.427	21.902	26.823	22.328	27.551
AIC			-30.887	-28.815	-41.647	-39.726	-4.164	-13.788	-29.06	-38.024	-25.134	-31.036	-26.967	-40.747	-30.244	-43.381	-30.719	-38.854	-29.805	-39.647	-28.656	-39.101
Residual Std. Error	0.355 (df = 34)																					
F Statistic	13.399*** (df = 5; 34)																					
Ncv Test $\chi 2$	4.706**																					
Shapiro-Wilk test (residuals) W	0.955																					
McFadden's pseudo R2		0.635	0.692																			
Dispersion estimate check																						
Residual Deviance test *P* value		0.504	0.336																			

	Dependent variable defensive fluid					
Distribution	Normal	Lognormal	Gamma	Weibull	Poisson	Negativ Binomial
AIC	394.051	372.912	376.189	380.730	902.861	376.644

Previous table continued.

Table S 32 Post hoc analysis results for the interaction between HPLC quantification method and peak integration using emmeans. Abbreviations are as follows: MLC = multi-level calibration. IRF.e = empirically determined response factor, IRF.h = hypothetical internal response factor (= 1), Asymp.LCL = asymptotic lower confidence limit, Asymp.UCL = asymptotic upper confidence limit. SE = standard error. Pairwise contrasts of p-values: 1st block row: MLC-IRF.e, 2nd block row: MLC-IRF.h, 3rd block row: IRF.e-IRF.h

Peak	Diet	Method	Emmean	SE	Df	Asymp.LCL	Asymp.UCL	Estimate	SE	Df	Z.ratio	*P* value
1	sunflower	MLC	1.43	0.19	Inf	1.05	1.81	-0.05	0.28	Inf	0.168	0.985
		IRF.e	1.48	0.20	Inf	1.08	1.87	0.67	0.22	Inf	3.075	*0.006*
		IRF.h	0.76	0.10	Inf	0.56	0.96	0.72	0.22	Inf	3.206	*0.004*
2	sunflower	MLC	1.58	0.21	Inf	1.16	2.00	0.04	0.30	Inf	0.129	0.991
		IRF.e	1.55	0.21	Inf	1.13	1.96	0.73	0.24	Inf	2.984	0.008
		IRF.h	0.86	0.12	Inf	0.63	1.08	0.69	0.24	Inf	2.880	*0.011*
both	sunflower	MLC	1.51	0.20	Inf	1.11	1.91	-0.01	0.29	Inf	0.023	1.000
		IRF.e	1.51	0.21	Inf	1.11	1.92	-0.11	0.30	Inf	0.359	0.932
		IRF.h	1.61	0.22	Inf	1.19	2.04	-0.10	0.30	Inf	0.336	0.940
1	milkweed	MLC	3.89	0.55	Inf	2.82	4.96	-0.13	0.79	Inf	0.165	0.985
		IRF.e	4.02	0.56	Inf	2.92	5.13	1.83	0.62	Inf	2.967	*0.008*
		IRF.h	2.06	0.29	Inf	1.49	2.63	1.96	0.63	Inf	3.096	*0.006*
2	milkweed	MLC	2.33	0.33	Inf	1.69	2.97	0.06	0.46	Inf	0.121	0.992
		IRF.e	2.27	0.32	Inf	1.65	2.89	1.07	0.37	Inf	2.882	*0.011*
		IRF.h	1.26	0.18	Inf	0.91	1.60	1.01	0.36	Inf	2.784	*0.015*
both	milkweed	MLC	3.10	0.44	Inf	2.25	3.96	-0.01	0.62	Inf	0.015	1.000
		IRF.e	3.11	0.44	Inf	2.26	3.97	-0.22	0.64	Inf	0.337	0.939
		IRF.h	3.32	0.47	Inf	2.41	4.23	-0.21	0.64	Inf	0.322	0.944

Table S 33 Post hoc analysis results for the interaction between sample origin in terms of diet history and peak integration using emmeans. Abbreviations are as follows: MLC = multi-level calibration. IRF.e = empirically determined response factor, IRF.h = hypothetical internal response factor (=1), Asymp.LCL = asymptotic lower confidence limit, Asymp.UCL = asymptotic upper confidence limit. SE = standard error.

Diet	Method	Peak	Emmean	SE	Df	Asymp.LCL	Asymp.UCL	Contrast	Estimate	SE	Df	Z.ratio	*P* value
sunflower	MLC	1	1.43	0.19	Inf	1.05	1.81	1 - 2	-0.15	0.29	Inf	-0.533	0.8553
		2	1.58	0.21	Inf	1.16	2.00	1 - both	-0.08	0.28	Inf	-0.272	0.9599
		both	1.51	0.20	Inf	1.11	1.91	2 - both	0.08	0.30	Inf	0.261	0.9631
milkweed	MLC	1	3.89	0.55	Inf	2.82	4.96	1 - 2	1.57	0.64	Inf	2.466	*0.0364*
		2	2.33	0.33	Inf	1.69	2.97	1 - both	0.79	0.70	Inf	1.133	0.4935
		both	3.10	0.44	Inf	2.25	3.96	2 - both	-0.78	0.54	Inf	-1.429	0.3259
sunflower	IRF.e	1	1.48	0.20	Inf	1.08	1.87	1 - 2	-0.07	0.29	Inf	-0.237	0.9695
		2	1.55	0.21	Inf	1.13	1.96	1 - both	-0.04	0.29	Inf	-0.128	0.9910
		both	1.51	0.21	Inf	1.11	1.92	2 - both	0.03	0.29	Inf	0.109	0.9934
milkweed	IRF.e	1	4.02	0.56	Inf	2.92	5.13	1 - 2	1.75	0.65	Inf	2.705	*0.0187*
		2	2.27	0.32	Inf	1.65	2.89	1 - both	0.91	0.71	Inf	1.278	0.4078
		both	3.11	0.44	Inf	2.26	3.97	2 - both	-0.84	0.54	Inf	-1.557	0.2643
sunflower	IRF.h	1	0.76	0.10	Inf	0.56	0.96	1 - 2	-0.10	0.15	Inf	-0.646	0.7945
		2	0.86	0.12	Inf	0.63	1.08	1 - both	-0.86	0.24	Inf	-3.553	*0.0011*
		both	1.61	0.22	Inf	1.19	2.04	2 - both	-0.76	0.25	Inf	-3.062	*0.0062*
milkweed	IRF.h	1	2.06	0.29	Inf	1.49	2.63	1 - 2	0.80	0.34	Inf	2.374	*0.0463*
		2	1.26	0.18	Inf	0.91	1.60	1 - both	-1.26	0.55	Inf	-2.295	0.0565
		both	3.32	0.47	Inf	2.41	4.23	2 - both	-2.06	0.50	Inf	-4.141	*0.0001*

Table S 34 Results of HPLC analysis of milkweed bug defensive fluids, mature and maturing seeds from seed pods of *A. syriaca*. Median retention times (RT) and relative retention times (RRT) are given and were determined across all HPLC runs. Abundance gives the relative quantity of a certain cardenolide in relation to total cardenolide amount. N ≥ 5 % gives number of dominant cardenolides, n ≥ 1 % gives number of subdominant cardenolides. Quantifications were conducted for common cardenolides (frequency ≥ 3) in defensive fluids (n = 15).

Carde-nolide	median RT	RRT median	ΔRT	ΔRRT	Defensive fluid					Milkweed (*A. syriaca*)			Abundance [%]				
					Fre-quen-cy	Concentration [µg/µl]		Quantity [µg]		Concentration [mg/g dry weight]			Defensive fluid		Mature seeds		Seed pods
						Mean	SE	Mean	SE	Mature seeds Mean	Mature seeds SE	Seed pods	Mean	SE	Mean	SE	
1	12.94	2.09	0.02	0.00						0.015	0.002				0.44	0.06	
2	13.17	0.05	0.08	0.01	14	0.05	0.01	0.05	0.01	0.025	0.001		0.29	0.03	0.76	0.03	
3	13.38	2.02	0.04	0.01	15	0.23	0.04	0.17	0.03	0.241	0.016		1.43	0.24	7.31	0.29	
4	13.53	1.99	0.04	0.01	15	1.43	0.28	1.11	0.26	1.142	0.080	0.076	8.77	1.34	34.6	0.9	8.16
5	13.86	1.95	0.02	0.00						0.068	0.005				2.08	0.09	
6	13.99	1.93	0.05	0.01	13	0.23	0.05	0.19	0.05	0.406	0.024	0.027	1.16	0.10	12.33	0.49	2.90
28	14.28	1.89	0.04	0.01	6	0.05	0.01	0.04	0.01				0.19	0.02			
7	14.41	1.87	0.02	0.01	10	0.19	0.03	0.18	0.05				1.13	0.25			
37	14.49				1												
29	14.64	1.84	0.00	0.00	4	0.01	0.00	0.01	0.00				0.04	0.01			
8	14.92	1.81	0.05	0.01	15	0.30	0.05	0.24	0.04	0.085	0.011		1.84	0.08	2.59	0.40	
9	15.14	1.78	0.04	0.00	15	7.97	1.34	6.46	1.26				46.99	1.02			
30	15.41	1.75	0.02	0.00	4	0.03	0.00	0.03	0.00				0.31	0.10			
10	15.51	1.74	0.04	0.00	15	1.52	0.22	1.25	0.23	0.298	0.015		9.62	0.64	9.08	0.45	
11	15.81	1.71	0.02	0.00						0.024	0.002				0.72	0.08	
12	15.91	1.70	0.07	0.01	15	2.40	0.42	1.96	0.38	0.089	0.008	0.049	13.70	0.77	2.70	0.12	5.31
13	16.21	1.67	0.09	0.01	14	0.14	0.02	0.12	0.03	0.287	0.021	0.506	0.83	0.08	8.71	0.21	54.61
14	16.53	1.63	0.08	0.01	15	0.43	0.06	0.35	0.06	0.036	0.014		2.69	0.08	1.12	0.44	
31	16.74	1.61	0.04	0.01	8	0.02	0.00	0.01	0.00				0.08	0.00			
15	17.06	1.58	0.04	0.00	1					0.008	0.000				0.24	0.02	
16	17.20	1.57	0.09	0.01	10	0.17	0.02	0.15	0.03	0.009	0.001		0.86	0.06	0.28	0.04	
17	17.46	1.55	0.07	0.00	15	0.52	0.09	0.43	0.10	0.016	0.004		3.37	0.46	0.48	0.11	
38	17.55				2												
18	17.75	1.52	0.03	0.00	2					0.073	0.013				2.23	0.41	
39	17.84				1												
32	17.97	1.50	0.04	0.00	6	0.03	0.01	0.04	0.01				0.21	0.02			
19	18.12	1.49	0.07	0.00	15	0.86	0.13	0.71	0.14	0.161	0.020	0.019	5.31	0.33	4.93	0.77	2.03
20	18.26	1.48	0.06	0.00	5	0.17	0.10	0.12	0.05				1.38	0.82			
33	18.46	1.46	0.04	0.00	10	0.08	0.02	0.07	0.02				0.45	0.06			
21	18.57	1.45	0.03	0.00						0.008	0.001				0.25	0.03	
34	18.71	1.44	0.04	0.00	9	0.03	0.01	0.03	0.01				0.14	0.02			
22	18.98	1.42	0.08	0.00	10	0.12	0.02	0.09	0.01	0.090	0.006		0.62	0.05	2.73	0.13	
27	19.69	1.37	0.05	0.00						0.004	0.001	0.007			0.14	0.03	0.72
24	19.93	1.35	0.08	0.00	10	0.04	0.01	0.03	0.01	0.022	0.004		0.24	0.07	0.68	0.14	
40	20.30				1												
25	20.67	1.31	0.08	0.00	11	0.21	0.03	0.14	0.02				1.37	0.20			

Carde-nolide	median RT	RRT median	ΔRT	ΔRRT	Defensive fluid Frequ-ency	Concentration [µg/µl] Mean	SE	Quantity [µg] Mean	SE	Milkweed (*A. syriaca*) Concentration [mg/g dry weight] Mature seeds Mean	SE	Seed pods	Abundance [%] Defensive fluid Mean	SE	Mature seeds Mean	SE	Seed pods
Calotropin	20.79																
41	20.98				2												
35	21.05	1.29	0.03	0.01	3	0.05	0.02	0.04	0.00				0.38	0.16			
26	21.38	1.26	0.02	0.00	1					0.025	0.006				0.75	0.14	
Calactin	21.79																
42	22.20				2												
36	22.64	1.19	0.08	0.00	5	0.03	0.01	0.02	0.01				0.24	0.13			
27	23.08	1.17	0.02	0.00						0.160	0.014	0.244			4.83	0.18	26.28
∑					36					23		7	27		23		7
Mean						16.7		13.6		3.2							
SE						6.0		5.8		0.2							
MIN						5.1		1.4									
MAX						38.7		40.3									
n ≥ 5 %													5		5		4
n ≥ 1 %													13		13		6
Polarity index						15.51	0.04			14.11	0.07	17.79					
Diversity index						0.80	0.01			0.93	0.01	0.55					

Previous table continued.

Table S 35 Summary of multiple regression models explored to study the effect of sequestered cardenolide concentration and sequestration time on sequestered ouabain amount. The model coefficients are given in the rows, the standard error is shown below in italics. Abbreviations are as follows: AIC = Akaike information criterion. GOF = goodness of fit. Nvc = Non-constant Variance Score Test. * p < 0.1; ** p < 0.05; *** p < 0.01.

	Dependent variable (stored ouabain amount)				
Model	(1)	(2)	(3)	(4)	(5)
I(1/sequestration time)	-1.855***				
	-0.493				
Log(sequestration time		0.396***	0.472***		0.389***
		-0.103	*-0.124*		*-0.107*
Cardenolide concentration	0.053**	0.052**		0.070**	
	-0.019	*-0.018*		*-0.025*	
Log(cardenolide concentration)					0.879**
					-0.333
Constant	2.326***	0.763*	1.433***	1.541***	-0.673
	-0.408	*-0.401*	*-0.404*	*-0.497*	*-0.866*
Observations	15	15	15	15	15
R^2	0.711	0.718	0.527	0.37	0.701
Adjusted R^2	0.663	0.671	0.491	0.322	0.651
Residual Std. Error	0.700 (df = 12)	0.692 (df = 12)	0.861 (df = 13)	0.993 (df = 13)	0.713 (df = 12)
F Statistic	14.773*** (df = 2; 12)	15.287*** (df = 2; 12)	14.478*** (df = 1; 13)	7.644** (df = 1; 13)	14.041*** (df = 2; 12)
Ncv test χ2	0.329	0.347			0.377
Shapiro-Wilk test (residuals) W	0.861**	0.904			0.834**
	Dependent variable				
Distribution	normal	lognormal	gamma	weibull	
GOF: AIC	51.154	52.326	51.277	50.325	

Table S 36 Summary of exploratory generalized linear models for modelling sequestered ouabain concentration as a function of diet history and sequestration time. Sequestration time intervals were treated either as a continuous or factorial variable. The model coefficients are given in the rows, the standard error is shown below in italics. Abbreviations are as follows: AIC = Akaike information criterion. *p<0.1; **p<0.05; ***p<0.01.

	Dependent variable (ouabain concentration)							
Model type	*glm: Gamma link = identity*	*glm: Gamma link = log*	*glm: Gamma link = inverse*	*OLS*	*glm: Gamma link = identity*	*glm: Gamma link = log*	*glm: Gamma link = inverse*	*glm: Gamma link = identity*
Model	(1)	(2)	(3)	(1)	(2)	(3)	(4)	(5)
Time as numeric	0.016*	0.004*	-0.001*					
	-0.008	*-0.002*	*-0.001*					
Diet history	-0.658*	-0.205*	0.055*					
	-0.378	*-0.11*	*-0.031*					
Constant	2.836***	1.039***	0.344***					
	-0.454	*-0.156*	*-0.052*					
Time point 1				-2.537***	-2.503***	-1.037***	0.529***	-2.525***
				-0.78	*-0.432*	*-0.199*	*-0.161*	*-0.436*
Time point 2				-0.111	-0.091	0.095	-0.087	-0.099
				-0.78	*-0.726*	*-0.199*	*-0.066*	*-0.716*
Time point 3				0.981	0.981	0.311	-0.152**	0.993
				-0.78	*-0.89*	*-0.199*	*-0.058*	*-0.945*
Time point 4				1.071	1.214	0.373*	-0.154**	1.067
				-0.841	*-1.003*	*-0.215*	*-0.059*	*-0.956*
Diet history				-0.665*	-0.026	-0.129	0.046*	-0.677*
				-0.386	*-0.22*	*-0.099*	*-0.026*	*-0.392*
Constant				3.642***	3.619***	1.168***	0.378***	0.873*
				-0.386	*-0.386*	*-0.099*	*-0.045*	*-0.436*
Diet history x time point 1								0.479
								-0.716
Diet history x time point 2								-1.429
								-0.945
Diet history x time point 3								-0.068
								-0.956
Diet history x time point 4								3.630***
								0.392
Observations	32	32	32	32	32	32	32	32
R^2				0.358				
Adjusted R^2				0.235				
					-61.444	-60.611	-59.812	-58.023
AIC	-67.632	-67.707	-67.941		134.888	133.222	131.625	136.047
Residual Std. Error	141.263	141.414	141.883	2.143 (df = 26)				
F Statistic				2.900** (df = 5; 26)				

Table S 37 Summary of exploratory general and generalized linear models for modelling the released defensive fluid volume as a function of sequestration time, diet history, and sequestered ouabain amount. The model coefficients are given in the rows, the standard error is shown below in italics. Abbreviations are as follows: dfv = defensive fluid volume, Df = degrees of freedom, AIC = Akaike information criterion. * p < 0.1; ** p < 0.05; *** p < 0.01. All explored GLMs showed a variance inflation of the residuals in diagnostic plots. All LMs showed a p-value > 0.05 for their F-statistics indicating a low goodness of fit.

	Dependent variable								
	dfv	log (dfv)	dfv						
Model type	*LM*	*LM*	*glm: gaussian*	*glm: inverse. gaussian*	*glm: Gamma*		*glm: Gamma*	*glm: Gamma*	*gam: log-normal*
			link = inverse	*link = log*	*link = log*		*link = identity*	*link = inverse*	
Model	(1)	(2)	(3)	(4)	(5)	(6)	(7)	(8)	(9)
Time point 1	0.119	0.412*	-0.738*	0.560***	0.113	0.567**	0.344**	-0.823**	0.412
	-0.15	*-0.239*	*-0.394*	*-0.19*	*-0.202*	*-0.211*	*-0.14*	*-0.339*	*0.211*
Time point 2	-0.081	-0.016	0.12	-0.068	-0.109	-0.074	-0.059	0.094	-0.016
	-0.15	*-0.189*	*-0.309*	*-0.148*	*-0.202*	*-0.167*	*-0.103*	*-0.262*	*0.167*
Time point 3	0.013	-0.071	0.129	-0.073	0.061	-0.064	-0.06	0.069	0.071
	-0.15	*-0.192*	*-0.273*	*-0.162*	*-0.202*	*-0.17*	*-0.123*	*-0.237*	*0.170*
Time point 4	-0.098	-0.236	0.338	-0.360**	-0.134	-0.332*	-0.215*	0.42	-0.236
	-0.162	*-0.214*	*-0.335*	*-0.166*	*-0.218*	*-0.189*	*-0.111*	*-0.294*	*0.189*
Dietary history	-0.074	-0.006	0.081	0.027	-0.094	0.023	0.017	-0.024	-0.006
	-0.074	*-0.103*	*-0.141*	*-0.084*	*-0.1*	*-0.091*	*-0.062*	*-0.129*	*0.091*
Ouabain		0.253**	-0.266	0.316***		0.289***	0.188***	-0.384**	0.253**
		-0.101	*-0.195*	*-0.081*		*-0.089*	*-0.057*	*-0.154*	*0.0894*
Constant	0.727***	-1.028***	2.060***	-1.083***	-0.328***	-1.020***	0.290**	2.345***	-1.028***
	-0.074	*-0.25*	*-0.537*	*-0.186*	*-0.1*	*-0.221*	*-0.122*	*-0.415*	*0.221*
Observations	32	32	32	32	32	32	32	32	32
R^2	0.07	0.238							
Adjusted R^2	-0.109	0.055							
Log Likelihood			-11.749	-5.866	-10.59	-6.074	-5.947	-6.637	
AIC			37.498	25.732	33.179	26.149	25.893	27.274	28.059
Residual Std. Error	0.412 (df = 26)	0.518 (df = 25)							
F Statistic	0.391 (df = 5; 26)	1.302 (df = 6; 25)							

Supplementary figures

The supplementary figures Figure S 1, Figure S 2, Figure S 3, Figure S 4, Figure S 5, Figure S 6, Figure S 7, Figure S 8, Figure S 9, Figure S 10, and Figure S 11 have been published and are accessible online at the following link: https://doi.org/10.1016/j.gene.2019.05.032.

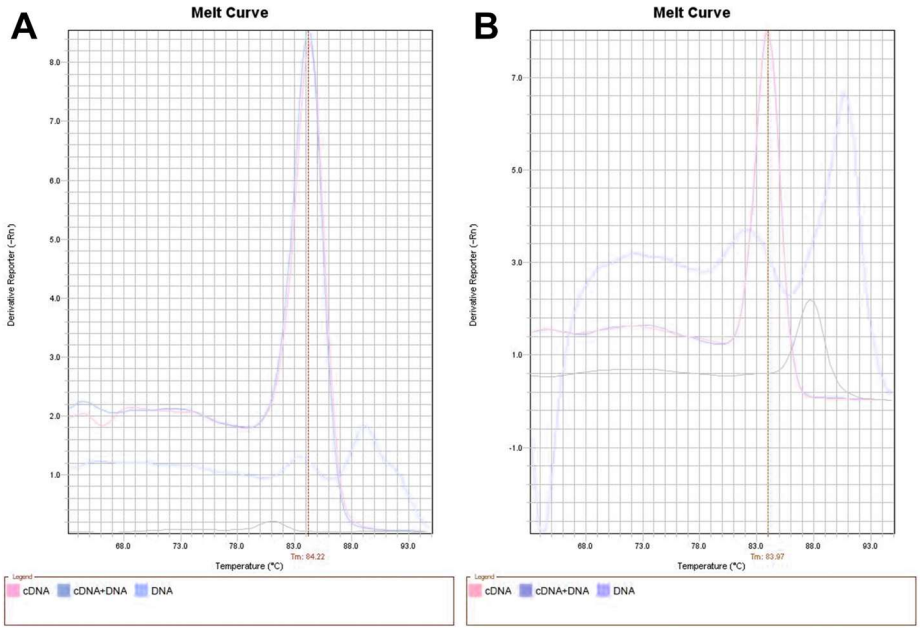


Figure S 12 Melt curve analysis of *Ofabcb* primer specificity testing. A: RT-qPCR primer for *Ofabcb1*, B: RT-qPCR primer for *Ofabcb2*. Grey = NTC.

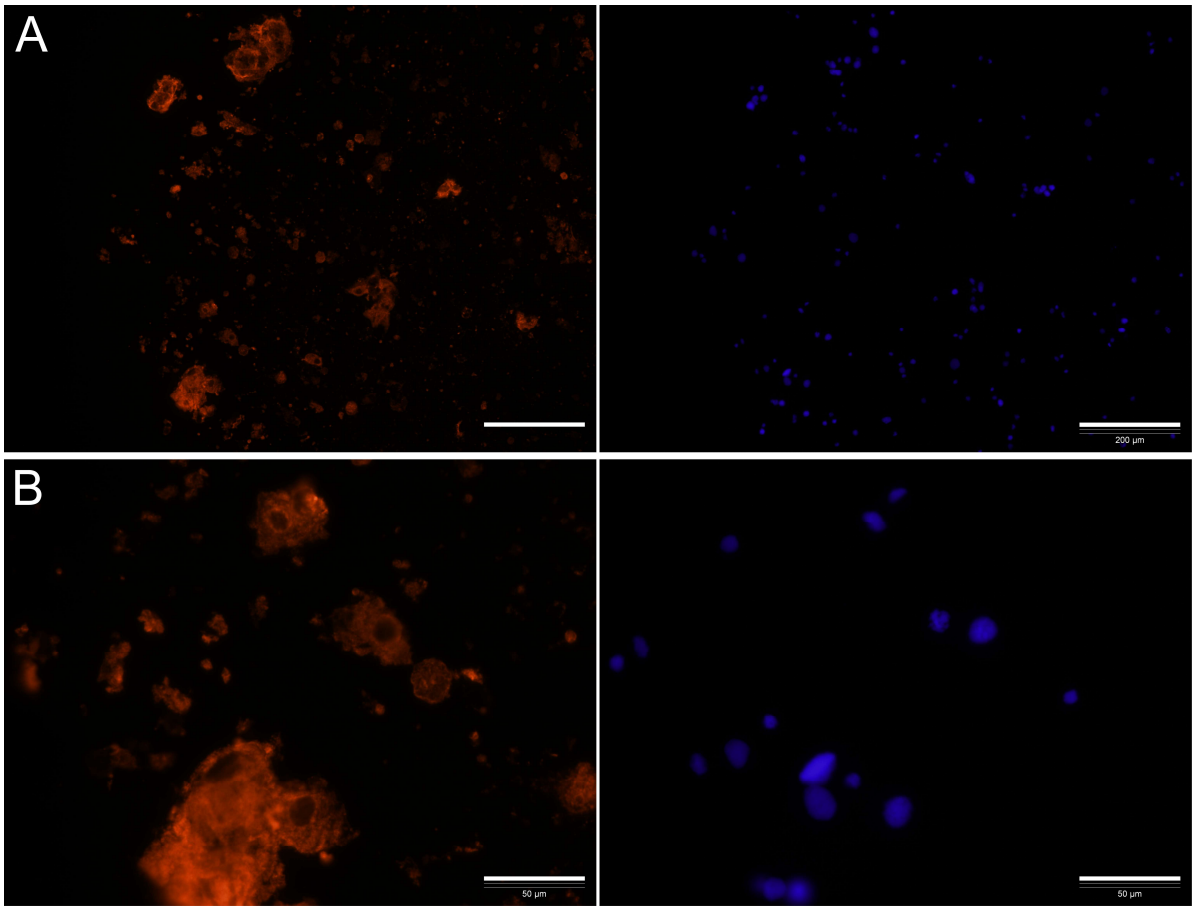


Figure S 13 Unmerged immunofluorescence stainings of defensive fluids with mAb C219 related to Figure 7. A: Cy3 left: 100 ms, DAPI right: 20 ms, scale bar = 200 µm, 10x magnification. B: Cy3 left: 50 ms, DAPI right: 10 ms, scale bar = 50 µm, 40x magnification. Additional scale bars were added for better visualization.

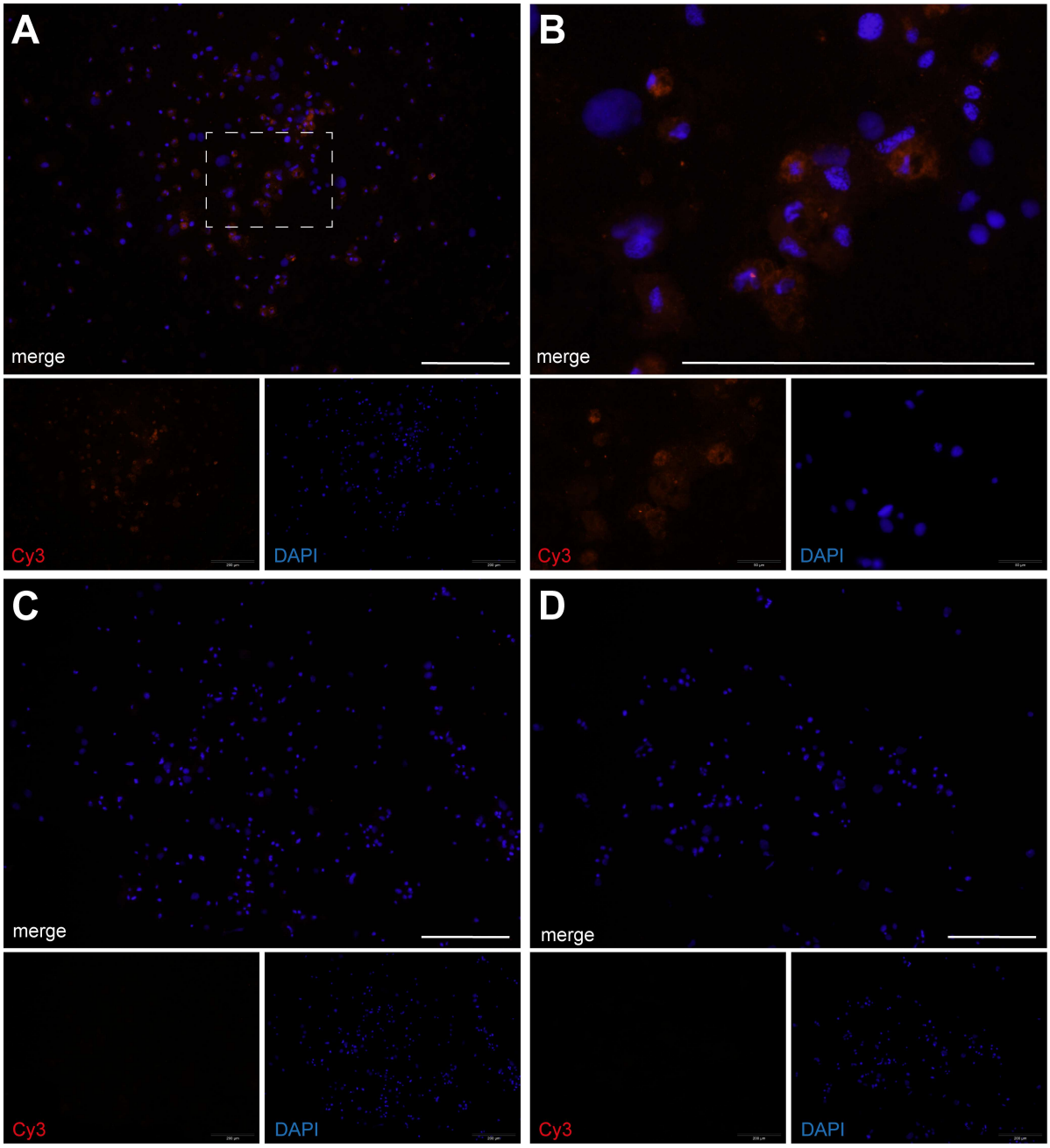


Figure S 14 Sampled defensive fluids of *O. fasciatus* individuals stained with two different commercially available anti-ABCB transporter monoclonal antibodies. A - B: mAb C494; increasing magnification shown in B is indicated by the dashed square in A. C: JSB-1. D: Control staining; the primary antibody was omitted. Positive staining is indicated by red fluorescence (Cy3 secondary antibody; exposure time: 100 ms). Nuclei are stained by DAPI and appear blue (exposure time: 20 ms). Merged images were cropped and scale bars adjusted to 100 µm for illustrative purposes. Original images are illustrated below.

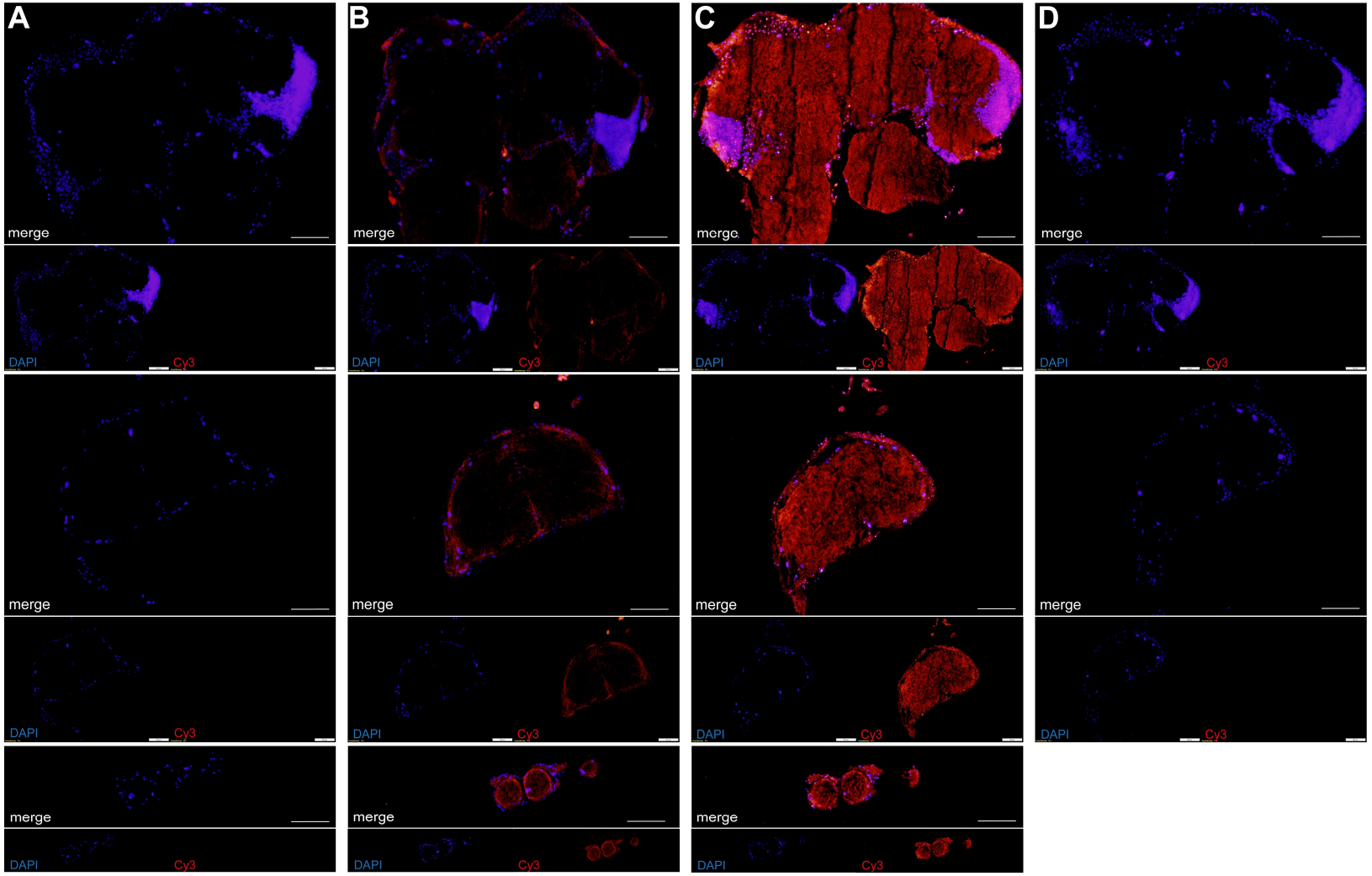


Figure S 15 Transverse sections of the large milkweed bug's nervous system stained with anti-ABCB transporter monoclonal antibodies. A: Control, B: mAb C219, C: mAb C494, D: mAb JSB-1. Positive staining is indicated by red fluorescence (Cy3 secondary antibody, 500 ms). Nuclei are stained by DAPI (blue, 20 ms). Scale bars are equivalent to 100 µm and were adjusted in merged images for illustration purposes. Original images are shown below.

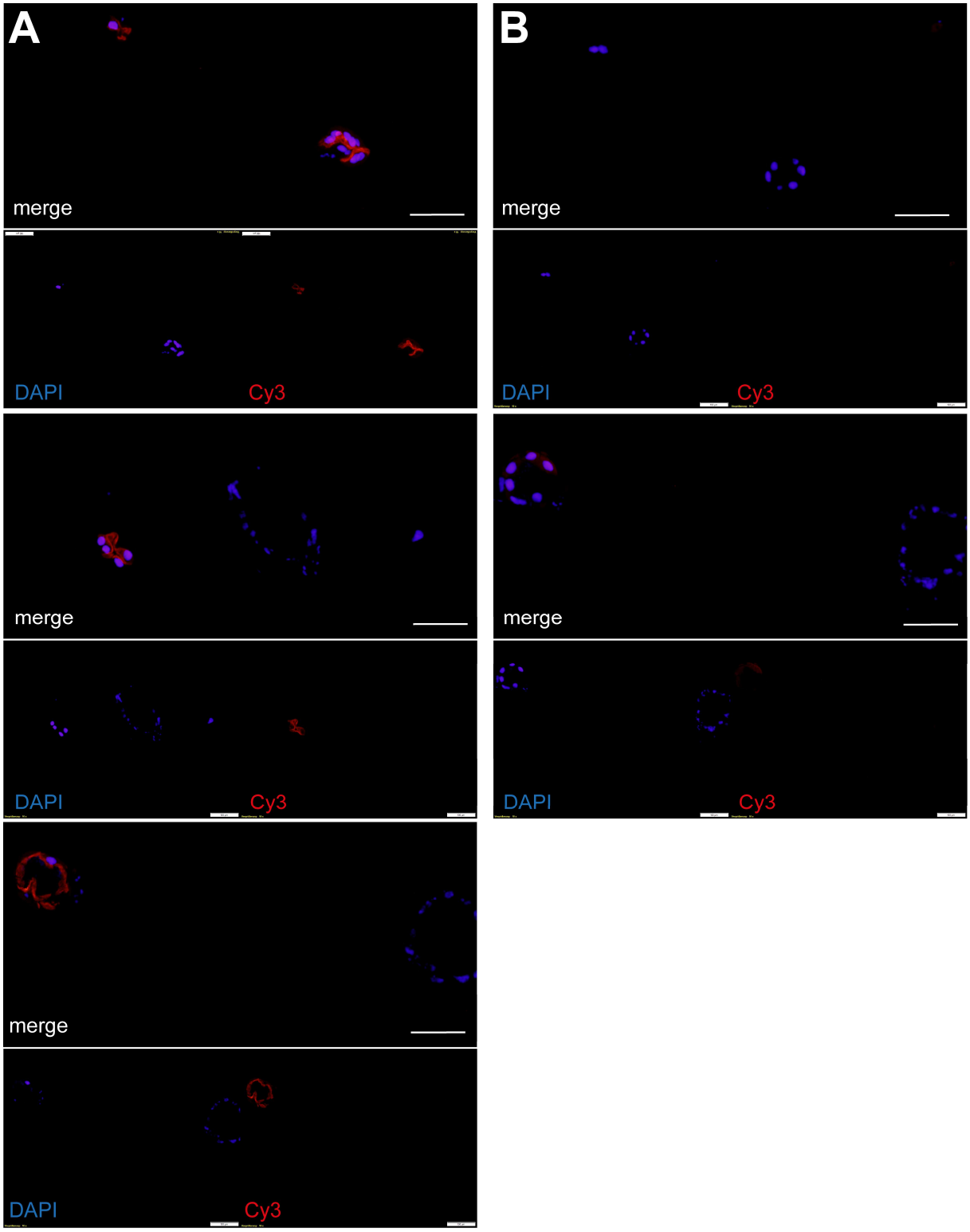


Figure S 16 Transverse sections of the large milkweed bug's Malpighian tubules stained with an anti-ABCB transporter monoclonal antibody. A: mAb C219, B: control without primary monoclonal antibody C219. Positive staining is indicated by red fluorescence (Cy3 secondary antibody, 500 ms). Nuclei are stained by DAPI (blue, 20 ms). Merged images were cropped and scale bars, equivalent to 100 µm, adjusted for illustrative purposes. Original images are shown below.

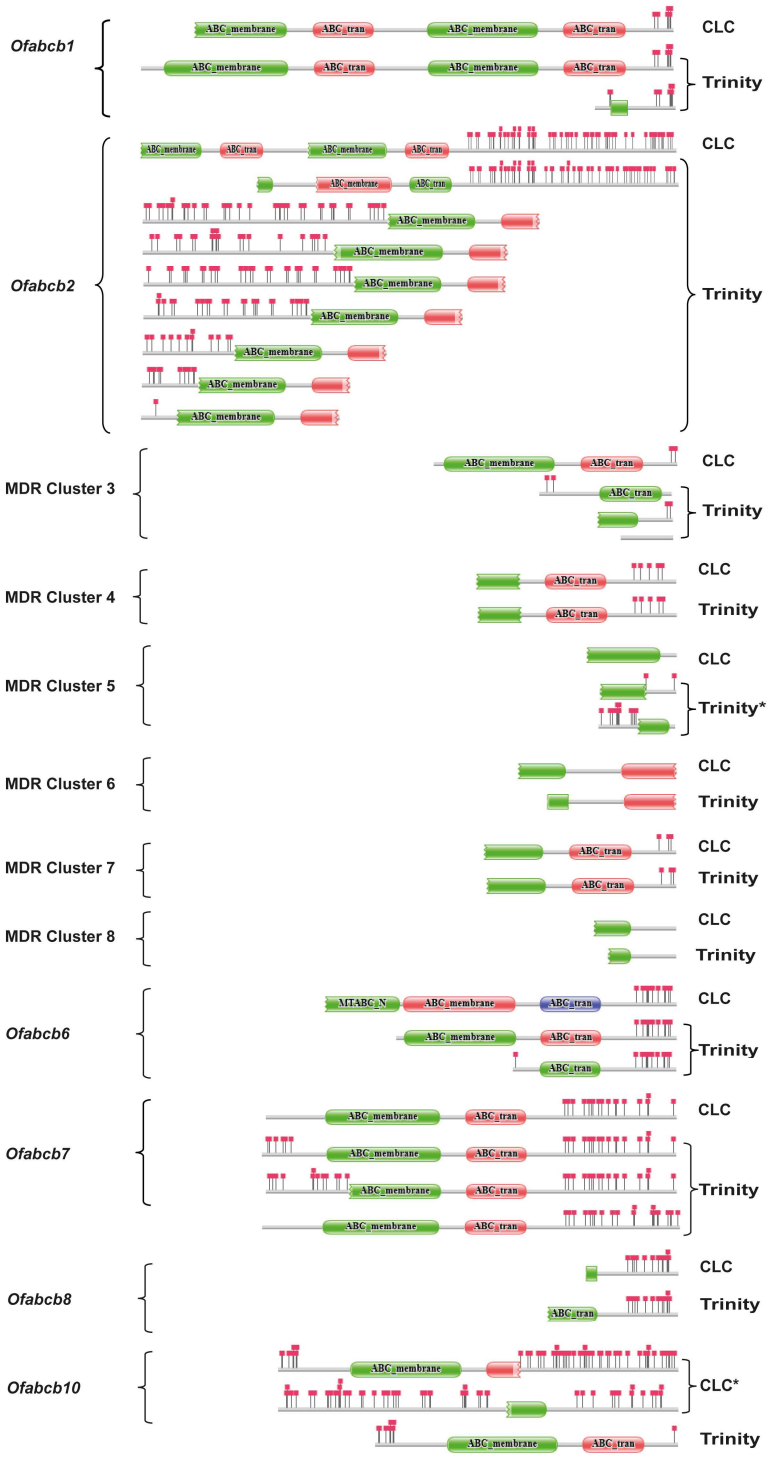


Figure S 17 Identification of potential protein domains in putative ABCB-like transcript sequences identified in two different transcriptome assemblies (Trinity and CLC) by Pfam. Sequences were classified according to preceding blastx analysis (full transporters: *Ofabcb1, Ofabcb2* and MDR clusters; half transporters: *Ofabcb6* - *Ofabcb10*) and blastn of assemblies against each other. Nucleotide sequences were translated in all six frames and searched for functional protein regions by Pfam on the EMBL-EBI webserver. Frames exhibiting those are displayed. Multiple sequences for the Trinity assembly correspond to analyses of different isotigs. Asterisks indicate presence of frame shifts within a contig sequence. Stemmed red squares represent stop codons in respective frames. ABC_membrane: transmembrane (TM) domain PF00664, Clan CL0241; ABC_tran: nucleotide-binding domain PF00005, CL0023; MTABC_N: mitochondrial ABCB-transporter N-terminal five TM region PF16185.

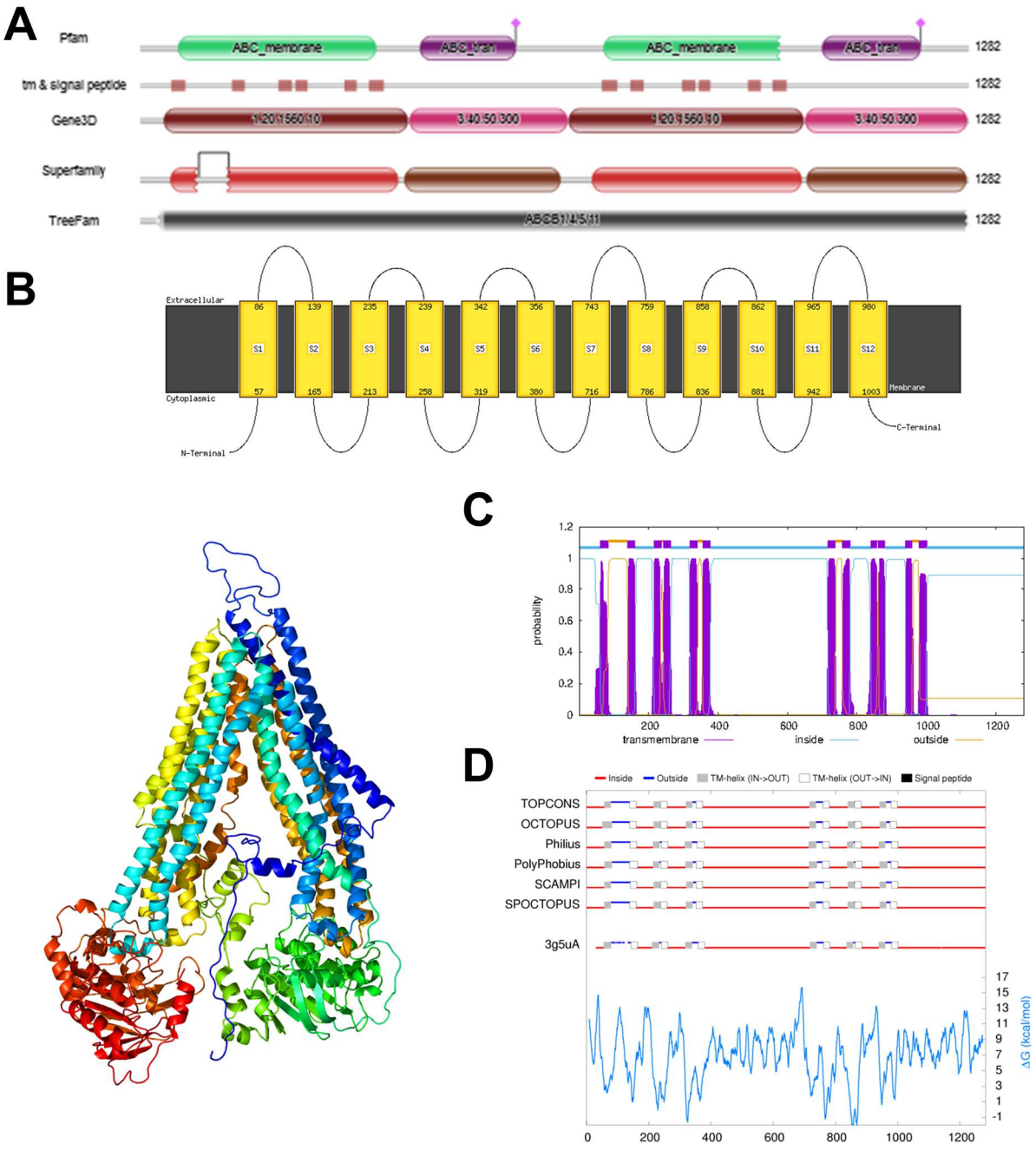


Figure S 18 Structure prediction of OfABCB1 (1282 aa) by different software. A: HmmScan with protein families (Pfam, TIGRFAM, Gene3D, PIRSF and TreeFam). B: Phyre^2 3D model (97 % modeled with 90 % confidence based on templates c4f4cA, c3g5uB, c6c0vA). C: TMHMM. D: TOPCONS.

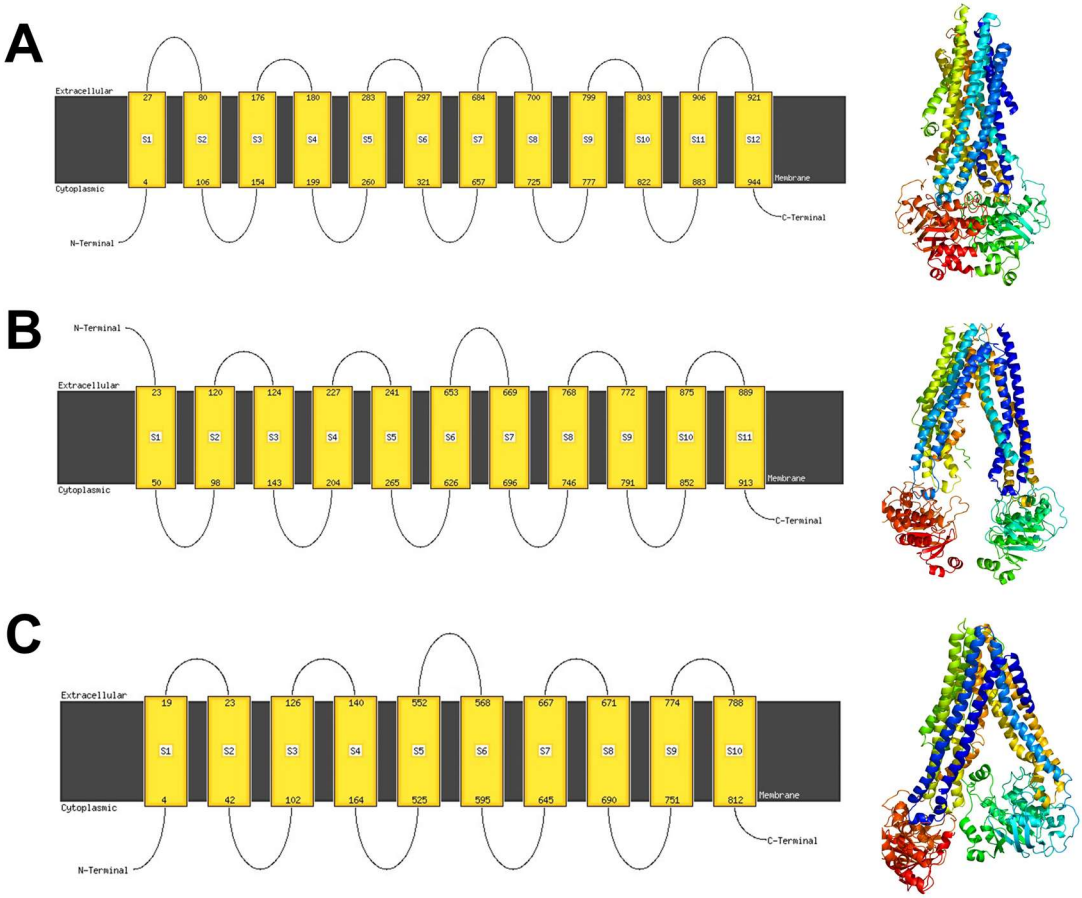


Figure S 19 3D structure modelling by Phyre[2] for different OfABCB2 isoforms and partial OfABCB1. A: partial OfABCB1 (1223 aa) modelled with > 90 % confidence. B: OfABCB2 isoform 6 (1189 aa) modelled with > 90 % confidence. C: Other OfABCB2 isoforms (1088 aa; 1, 2, 5, 7, 8, 11), 96 % of residues modelled with > 90% confidence.

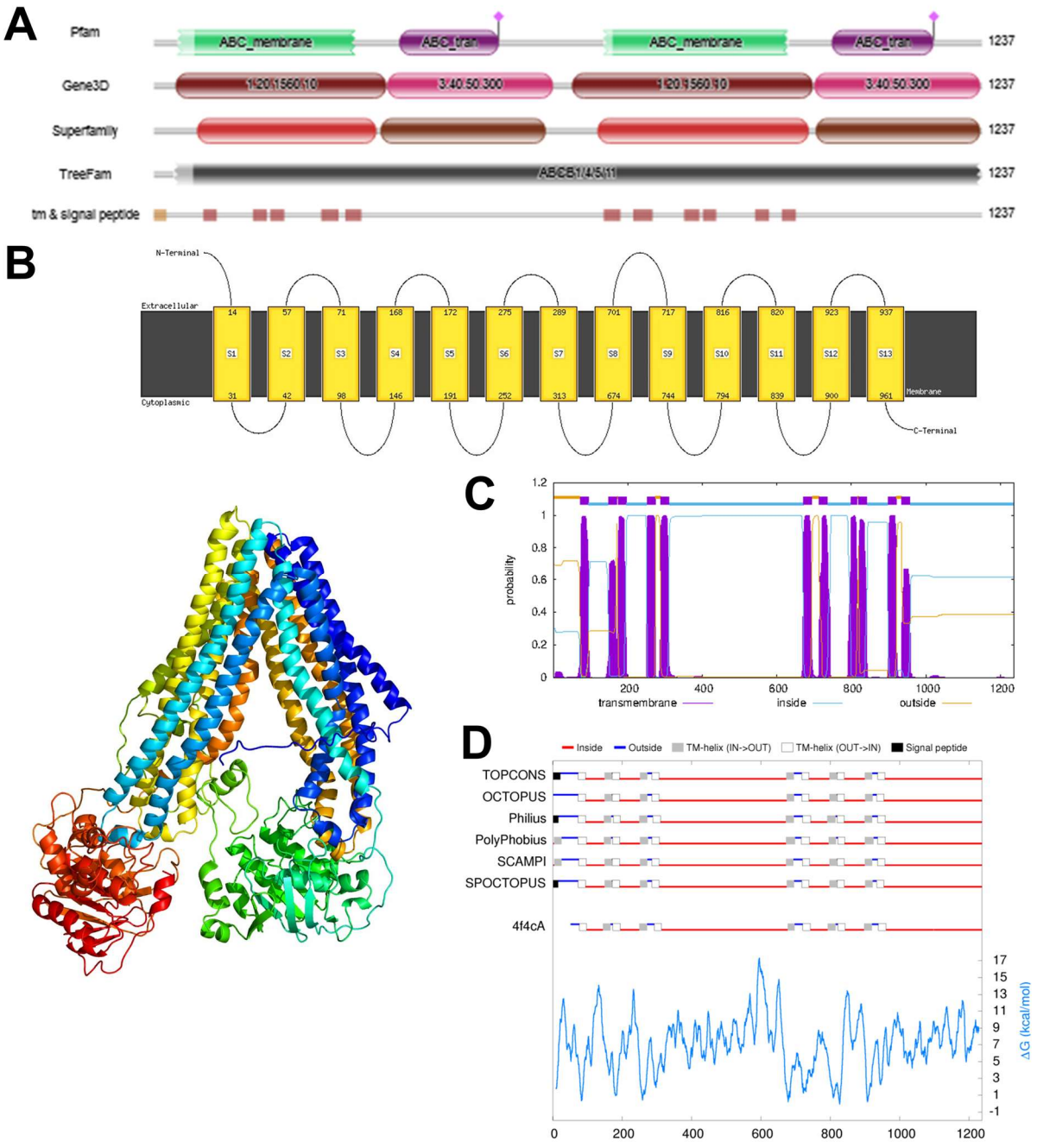


Figure S 20 Structure prediction of OfABCB2 (1237 aa) by different software. A: HmmScan with protein families (Pfam, TIGRFAM, Gene3D, PIRSF and TreeFam). B: Phyre^2 3D model (96 % modeled with 90 % confidence based on templates c4f4cA, c3g5uB, c6c0vA). C: TMHMM. D: TOPCONS.

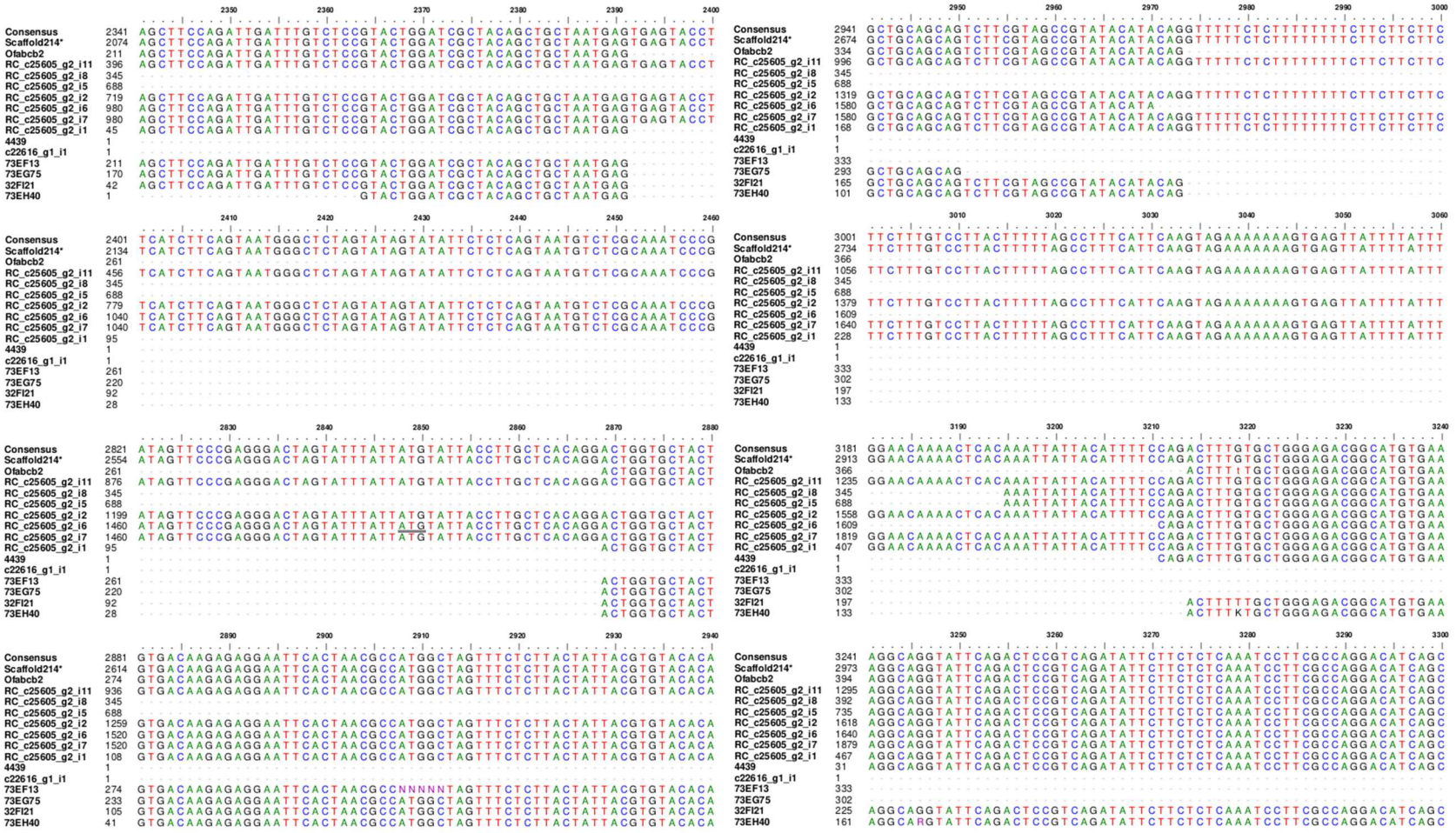


Figure S 21 Section of the alignment of *Ofabcb2* contigs with sequenced PCR fragments of the *Ofabcb2* five prime end. Consensus: consensus sequence of the alignment of *Ofabcb2* contigs (Trinity: c25605_g2_i11, c25605_g2_i8, c25605_g2_i5, c25605_g2_i2, c25605_g2_i6, c25605_g2_i7, c25605_g2_i1, c22616_g1_i1; CLC: 4439) with scaffold region (214) of the *O. fasciatus* genome. Scaffold214* refers to region 352159 - 373268. RC = reverse complement. Sequenced amplified or cloned PCR fragments: 73EF13, 73EG75, 32FI21, 73EH40. Grey line marks start codon for isoform 6.

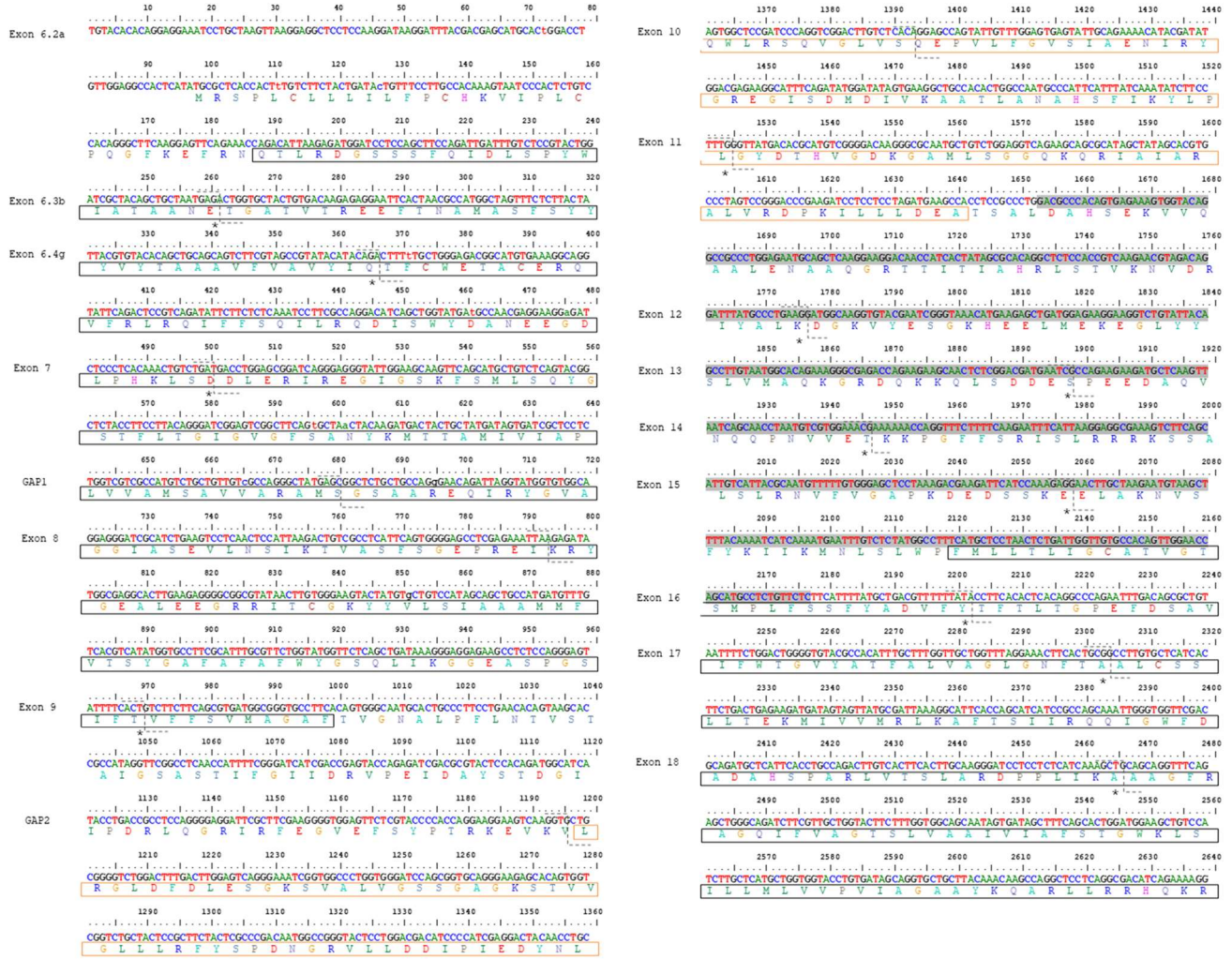


Figure S 22 Nucleotide and predicted protein sequence of *Ofabcb2*. Predicted splice junctions are indicated by dotted lines. Asterisks indicate consensus splice sites. Black boxes indicate predicted transmembrane domains, orange boxes indicate predicted nucleotide-binding domains. GAP refers to sequences not matched to the genomic scaffold 214. Bases marked in yellow give primer sequences used for expression quantification. Bases marked in grey give the sequence used for RNAi. Note that not the complete *Ofabcb2* sequence is shown.



Previous figure continued.

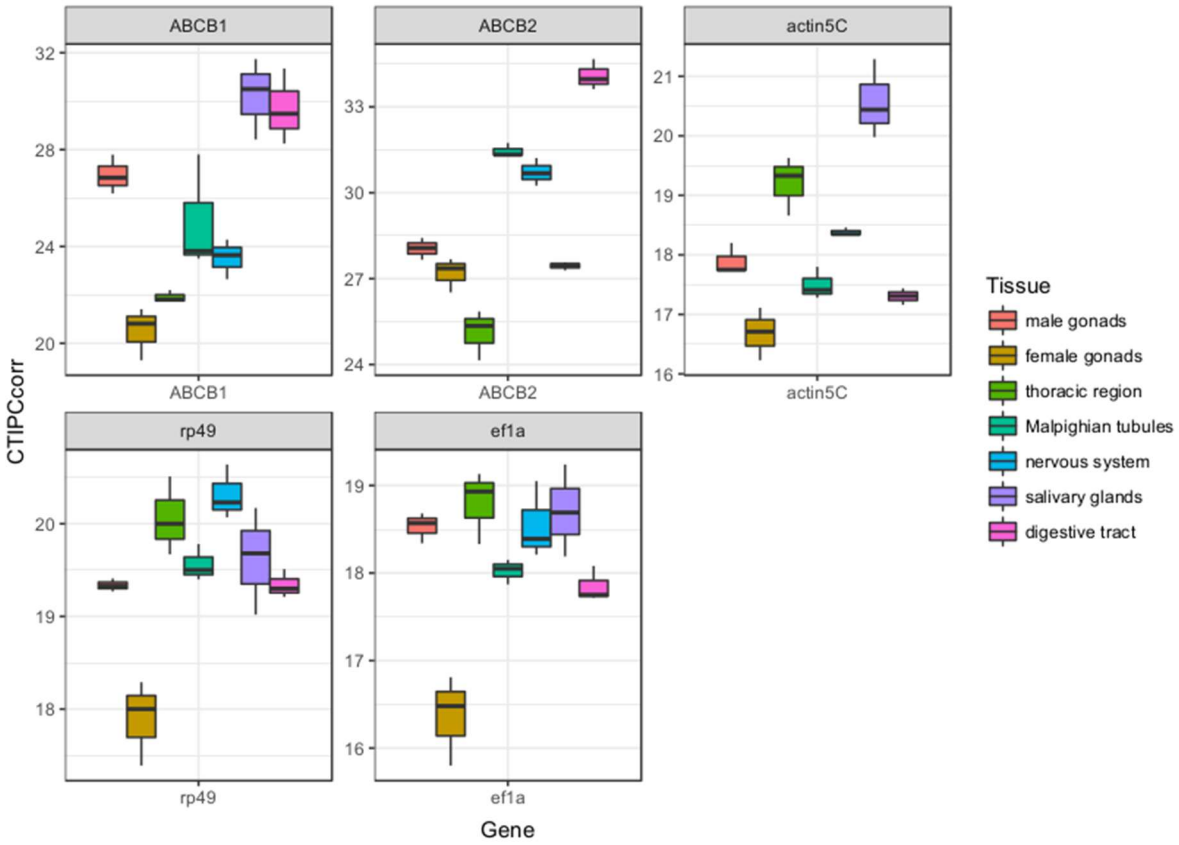


Figure S 23 Raw expression values of *Ofabcb* and reference genes in different tissues. CTIPCcorr = interplate corrected Cp value.

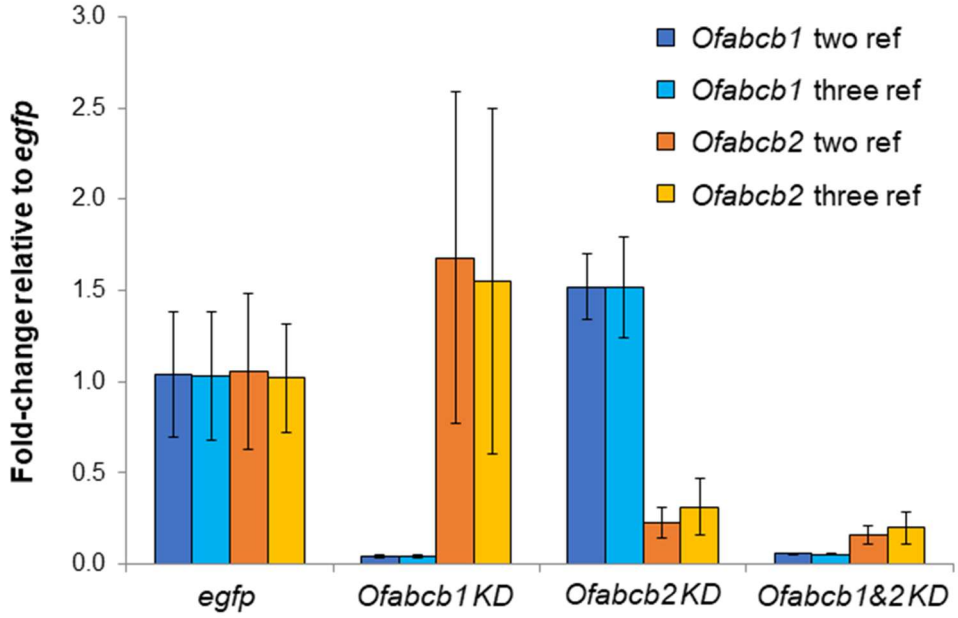


Figure S 24 Gene expression of *Ofabcb1* and *Ofabcb2* in RNAi knockdowns ten days *post* injection compared to control (*egfp*). Gene expression was normalized either by two reference genes (ref) (*Ofef1a* + *Oftubulin*) or three reference genes (*Ofef1a* + *Oftubulin* + *Ofrp49*) as given in the legend.

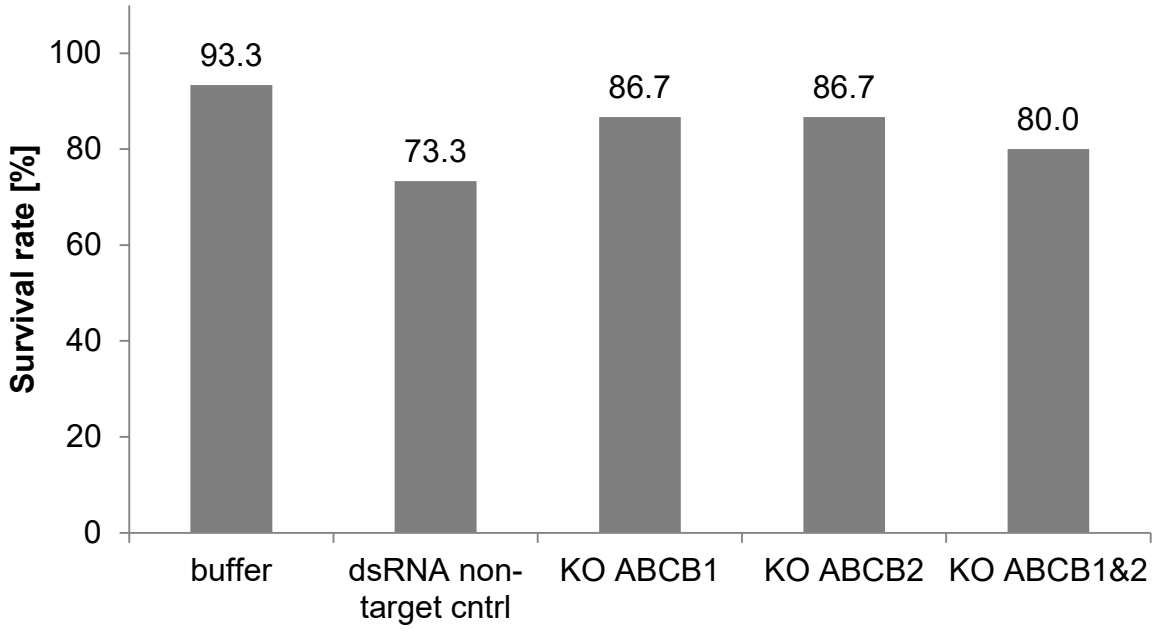


Figure S 25 Survival rate of adult milkweed bugs seven days after injection with dsRNA or buffer. *Egfp* = dsRNA non-target control, KO = knockdown. Observations from 15 biological replicates in each treatment.

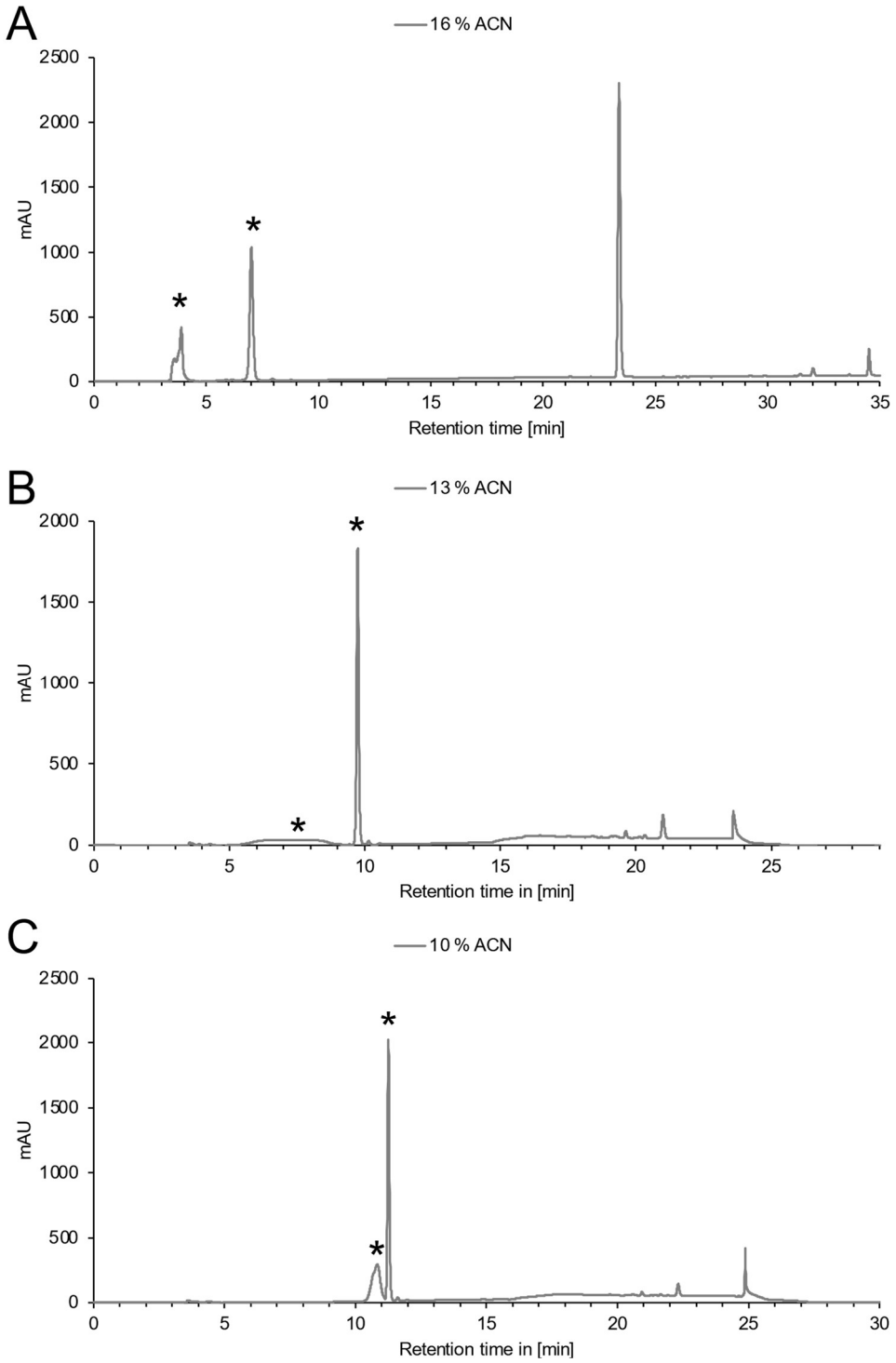


Figure S 26 HPLC chromatograms of ouabain standards in HPLC system II with different acetonitrile starting concentrations. A: 16 %, B: 13 %, C: 10 %. Asterisks mark peaks corresponding to ouabain (0.1 µg/µl). Peak in A = ITSD (0.1 µg/µl).

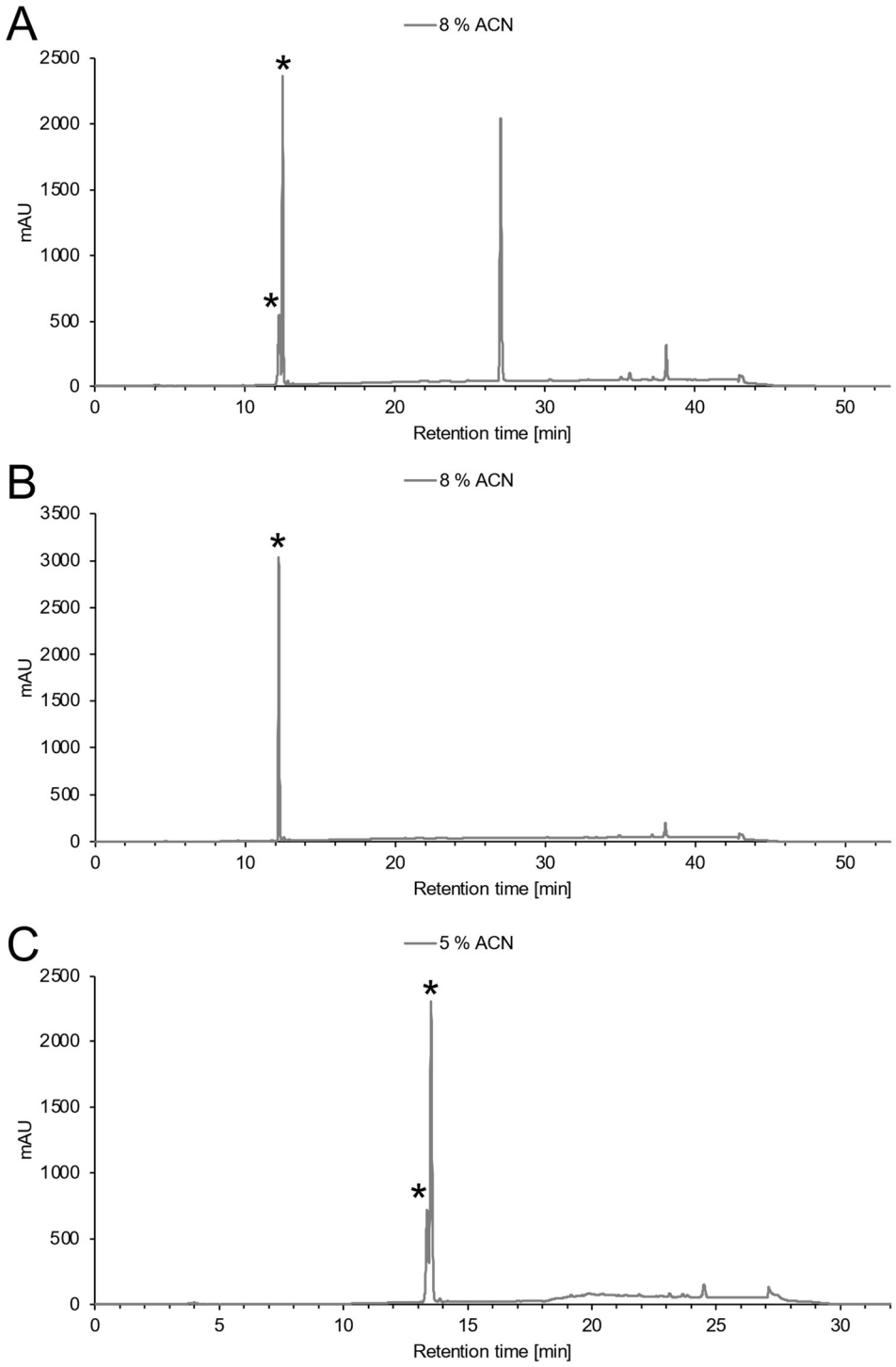


Figure S 27 HPLC chromatograms of ouabain standards in HPLC system II with different acetonitrile starting concentrations. A: 8 %, B: 8 %, C: 5 %. Asterisks mark peaks corresponding to ouabain (0.1 µg/µl). Peak in A = ITSD (0.1 µg/µl). In contrast to A, ouabain was dissolved in water instead of methanol in B.

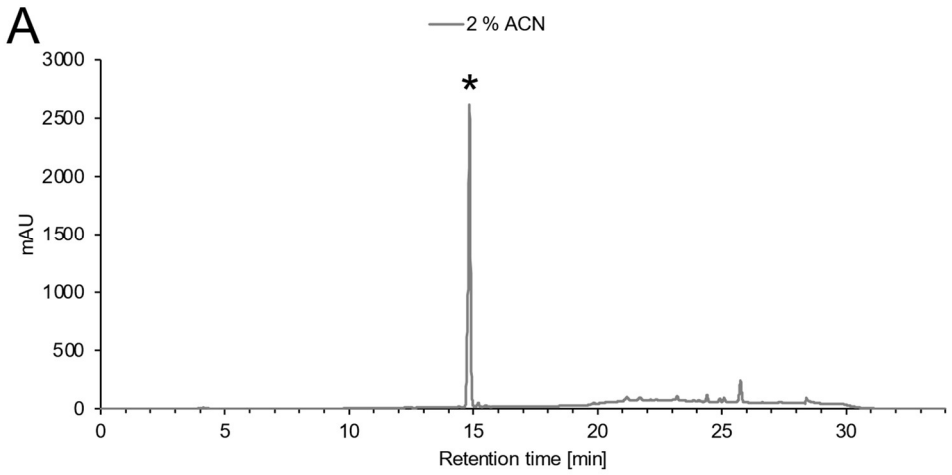


Figure S 28 HPLC chromatogram of ouabain standard (0.1 µg/µl) in HPLC system II with 2 % acetonitrile (ACN) as starting percentage. Asterisk marks the peak corresponding to ouabain.

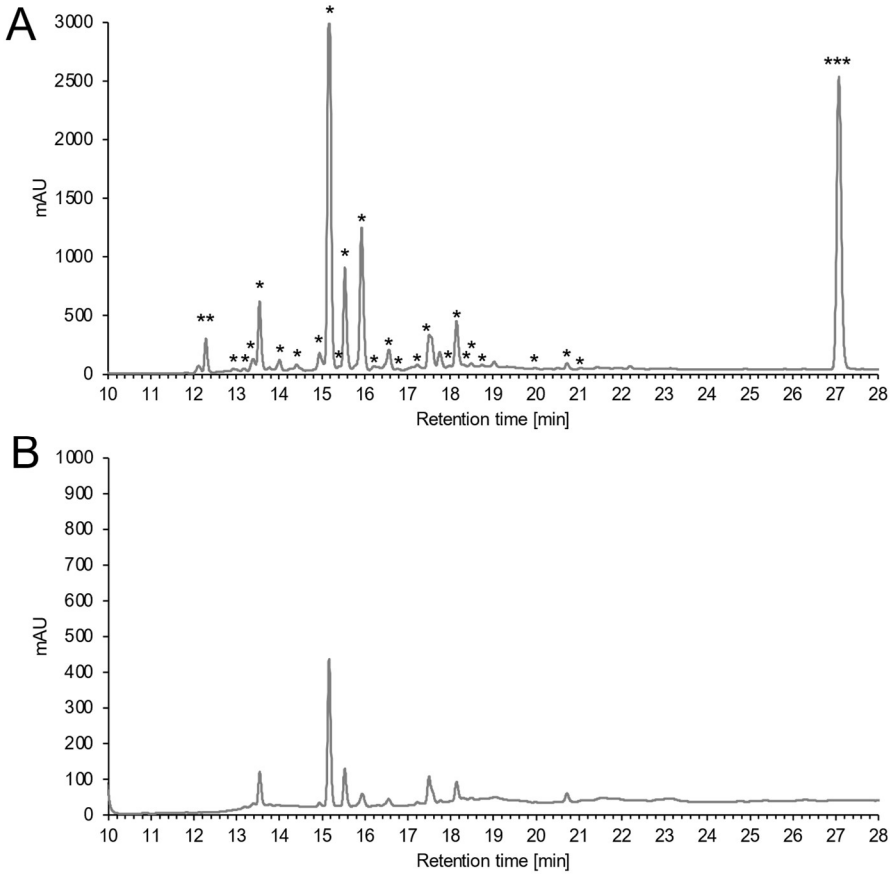


Figure S 29 HPLC chromatograms of defensive fluids sampled from adult animals fed on milkweed seeds. A: Individual that was allowed to sequester injected ouabain for one hour *prior* to sampling. B: Non-injected individual to confirm absence of coeluting compounds within the elution time range of ouabain (**) and digitoxin (ITSD: ***). Asterisks mark peaks which were inferred to be cardenolides based on absorbance spectra.

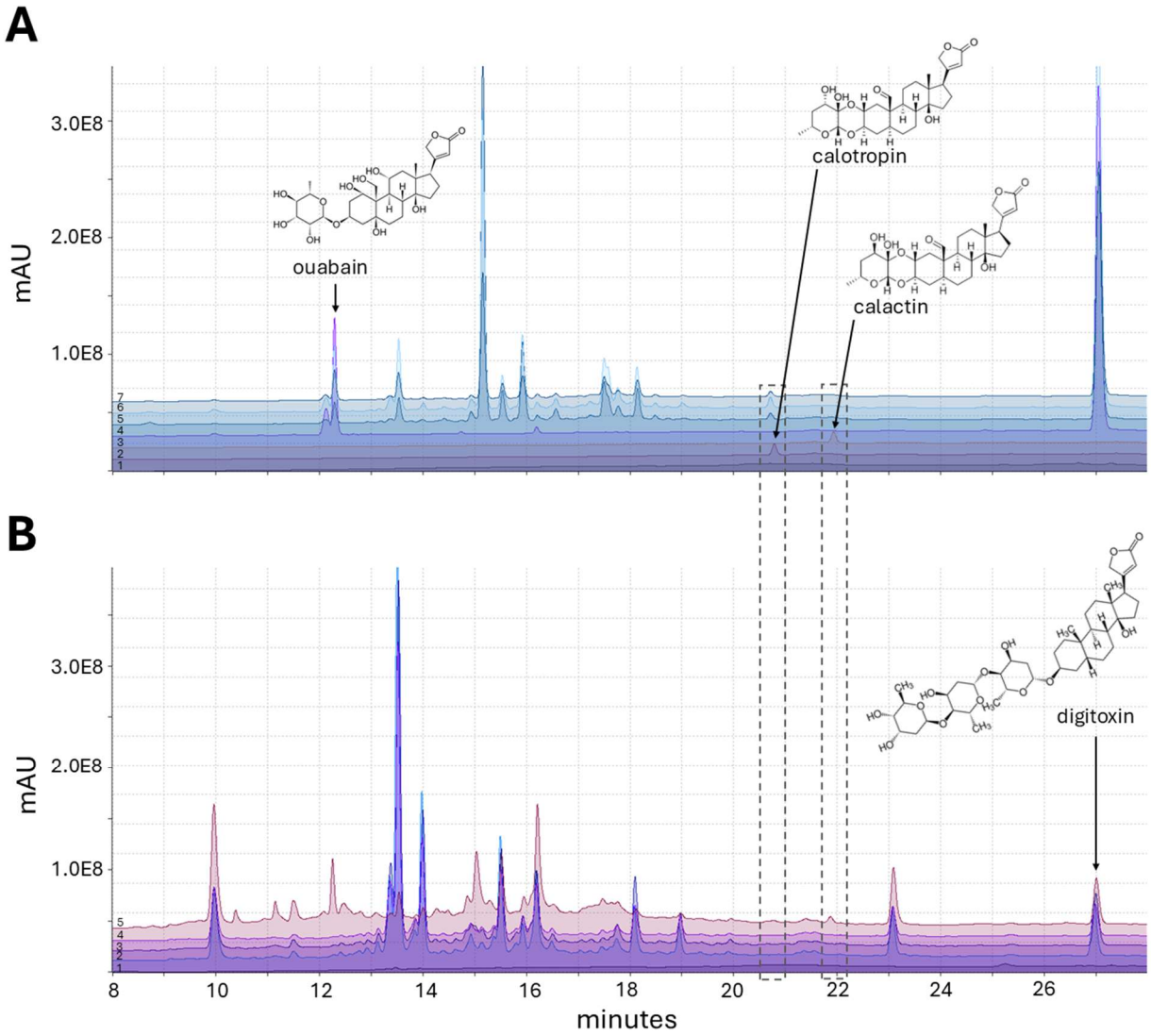


Figure S 30 HPLC chromatograms of defensive fluids, isolated calotropin and calactin (A), and mature and maturing milkweed seeds (B). A: Lane 1: blank, Lane 2: Isolated calotropin, Lane 3: Isolated calactin, Lane 4: defensive fluid from sunflower seed fed bugs injected with ouabain, Lane 5 to 7: defensive fluids from milkweed seed fed bugs injected with ouabain. B: Lane 1: blank, Lane 2 to 4: mature milkweed seeds from the USA, Lane 5: maturing milkweed seeds from seed pods from Germany. Digitoxin was used as internal standard.

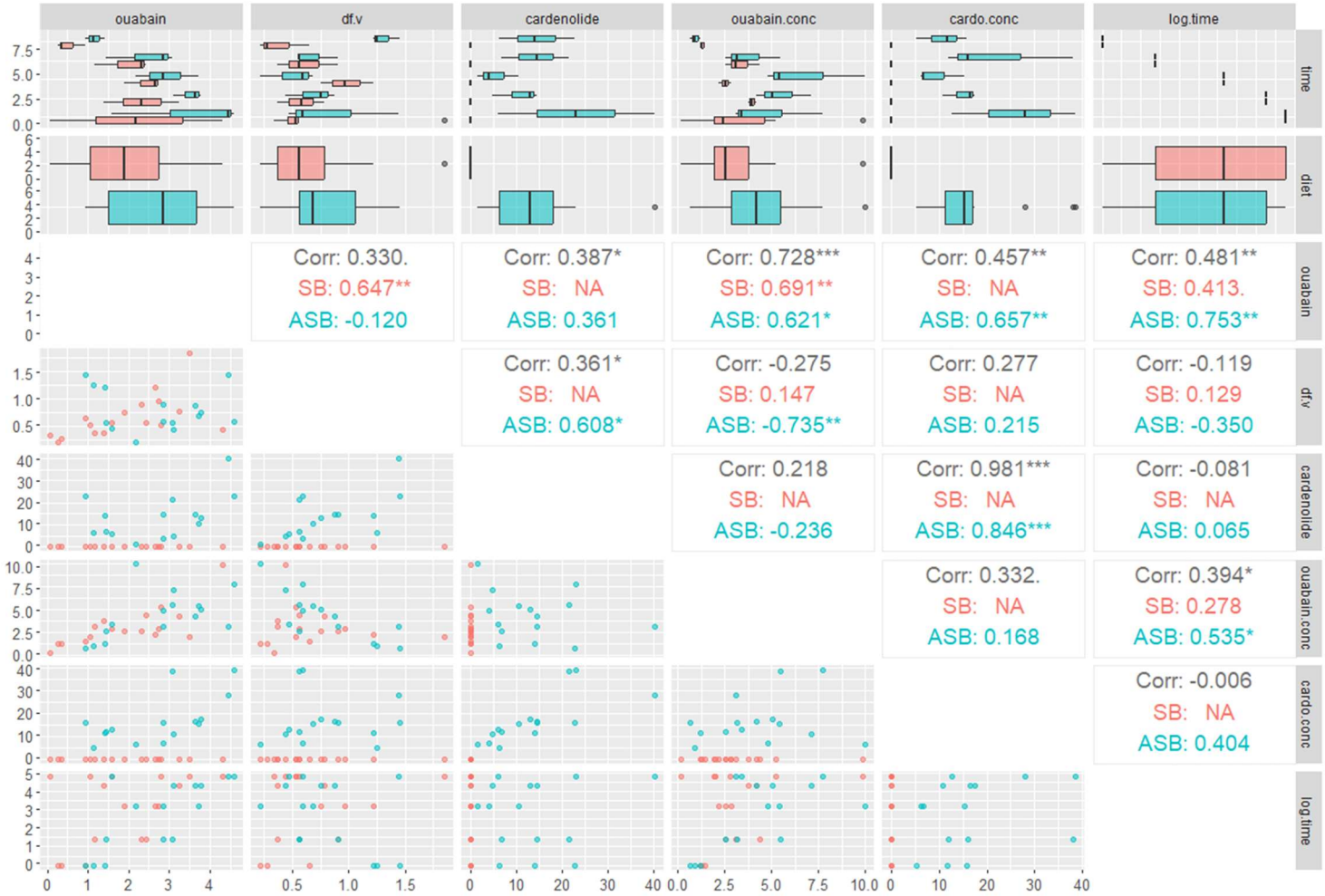


Figure S 31 Graphical exploratory analysis and pairwise Spearman correlations of parameters determined in animals of different diet lines. Abbreviations are as follows: SB = sunflower diet line animals (red). ASB = milkweed seed diet line animals (turquoise). Df.v = released defensive fluid. Conc. = concentration [µg/µl]. Cardo = natural cardenolide amount sequestered [µg]. Log.time: log-transformed sequestration time (h). Entries above the diagonal are Spearman's rank correlation coefficients for subsets and complete data: *p < 0.05, **p < 0.01, *** p < 0.001.

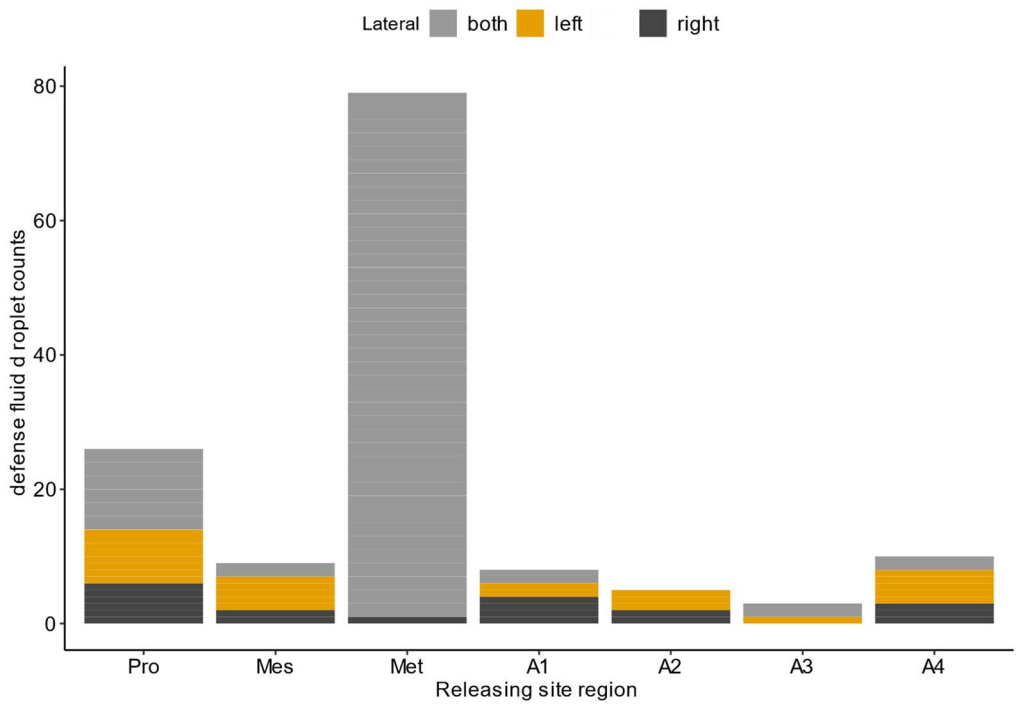


Figure S 32 Number of released fluid droplets from different cardenolide storage compartment regions. Pro = prothorax, Mes = mesothorax, Met = metathorax, A1 to A4 = abdominal segments I to IV. Legend indicates whether fluid release was observed at both or single lateral sides of the compartment (n = 40 individuals).

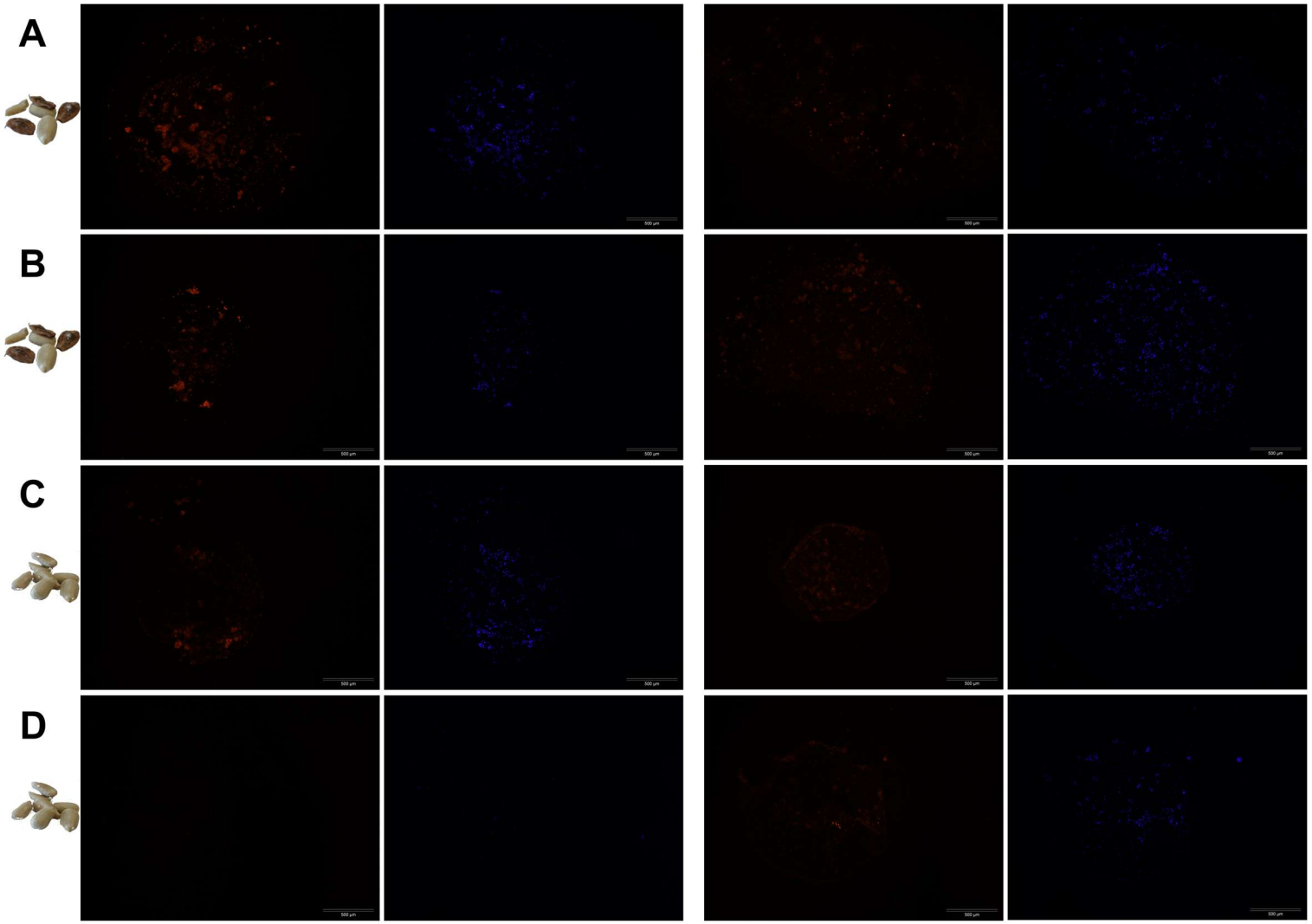


Figure S 33 Immunofluorescence staining of defensive fluids from animals of different diet histories used for ABCB full transporter fluorescence quantifications. A - B: milkweed seed line. C - D: sunflower seed diet line. Each row represents one individual. Blocks show fluids from different metathoracic flanges stained with either mAb C219 (left panel) or mAb C494 (right panel). Red fluorescence: Cy3 160 ms, blue fluorescence: DAPI 100 ms. Scale bars are equivalent to 500 µm.

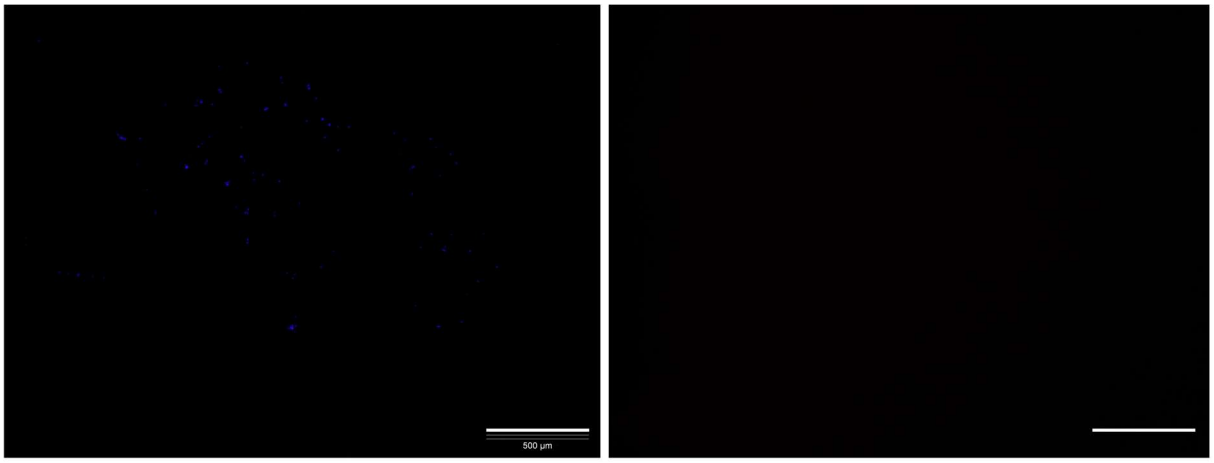


Figure S 34 Secondary antibody control staining of defensive fluid from a metathoracic flange of a milkweed seed line animal. Left: DAPI, 100 ms. Right: Cy3, 200 ms. Additional scale bars equivalent to 500 µm were added for illustrative purposes.

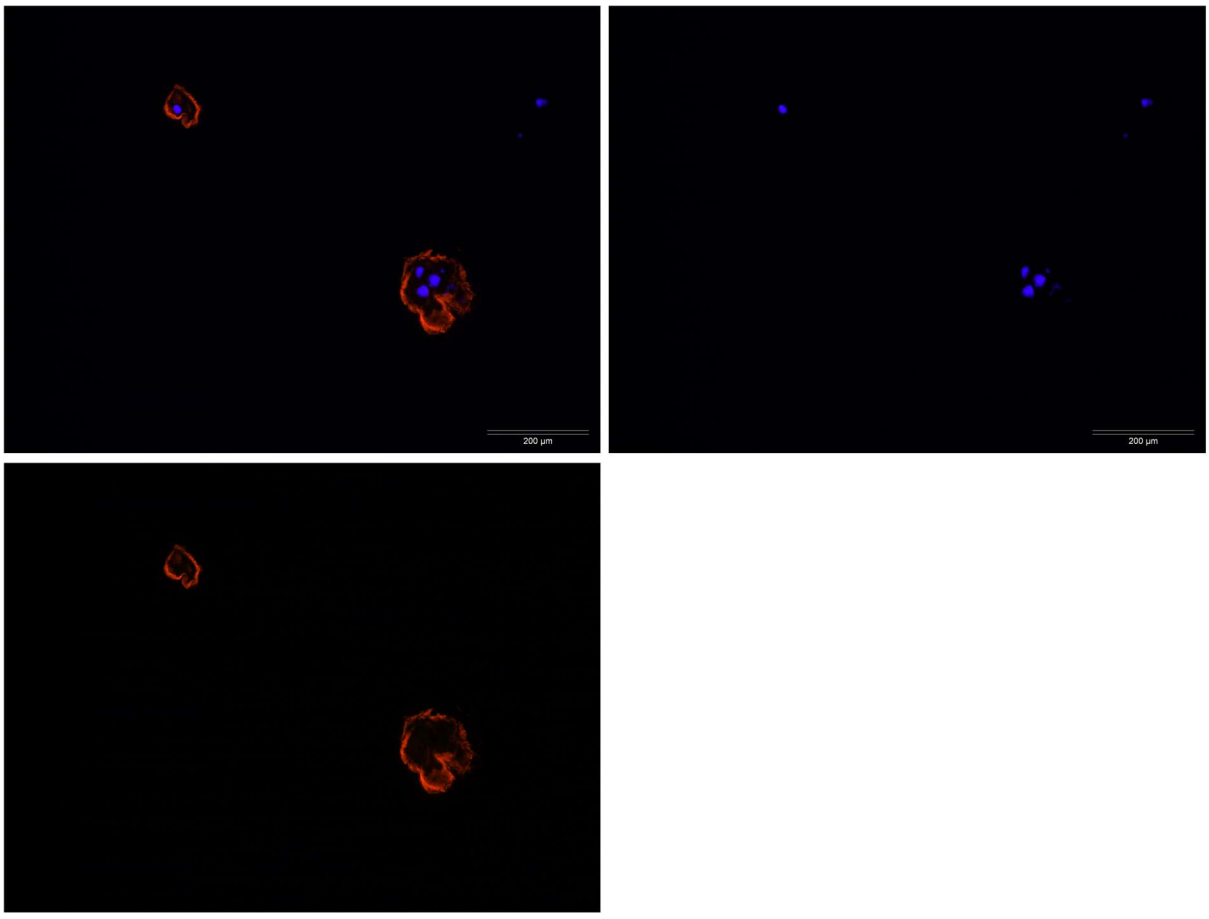


Figure S 35 Immunofluorescence staining of the Na,K-ATPase α-subunit in transverse sections of the Malpighian tubules of *O. fasciatus.* Upper panel left: merged fluorescence images (negative multiplication), upper panel right: DAPI 2.889 ms, lower panel left: Cy3, 10 ms. 10x magnification, scale bar is equivalent to 200 µm.

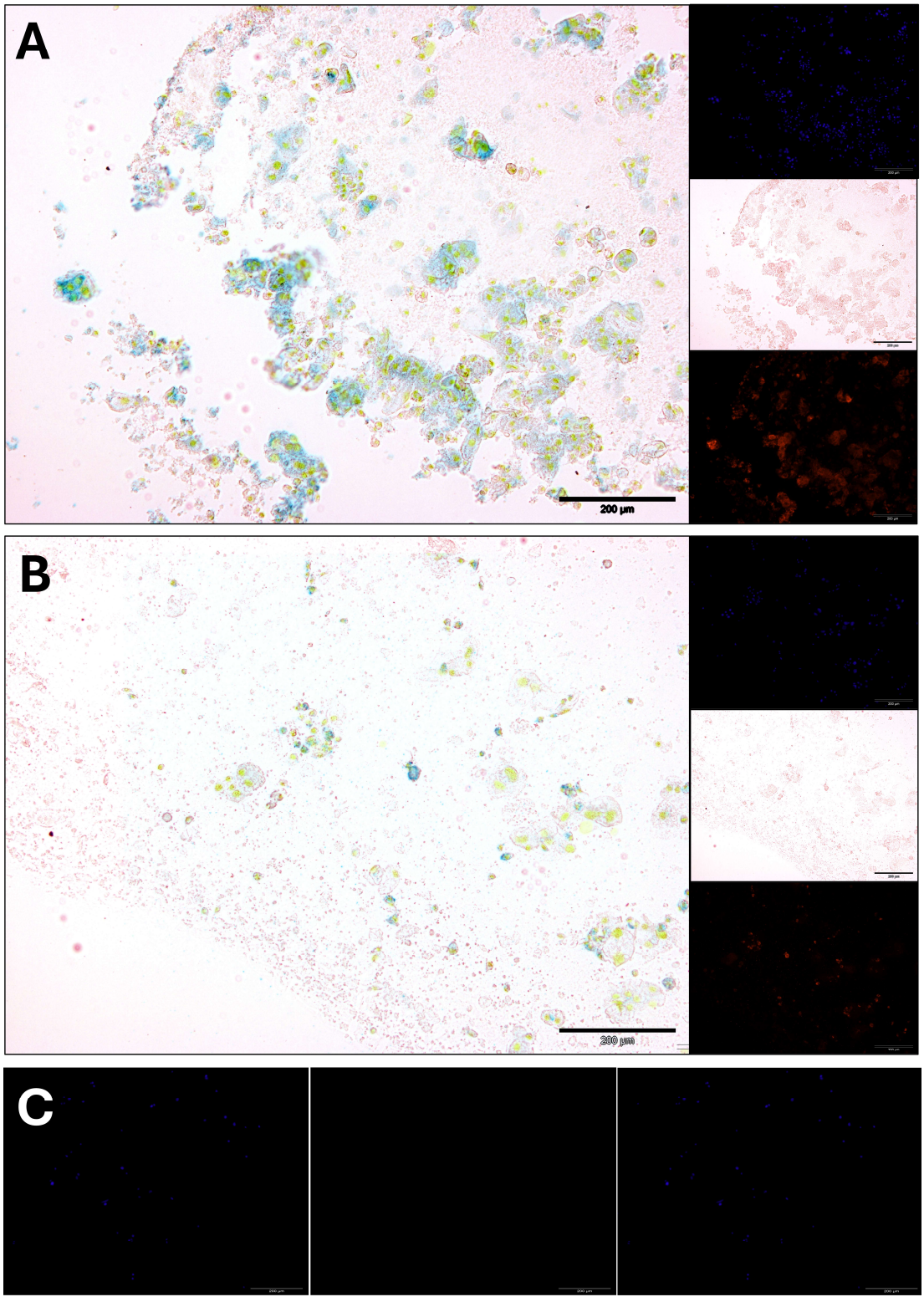


Figure S 36 ABCB transporter immunofluorescence staining of defensive fluids of *O. fasciatus* adults from the laboratory milkweed seed line. A: mAb C219. B: mAb C494. C: Secondary antibody control (primary mAb was omitted). Exposure times were 100 ms for Cy3 and 20 ms for DAPI. Tonal value correction was conducted for brightfield images which then were merged by subtraction with fluorescence images. The blue DAPI fluorescence therefore appears yellow and the red Cy3 fluorescence appears blue.

Additional files

The additional files S1 and S2 have been published and are accessible online at the following link: https://doi.org/10.1016/j.gene.2019.05.032.

List of publications

Lohr, J.N., Meinzer, F., Dalla, S., Romey-Glüsing, R., Dobler, S., 2017. The function and evolutionary significance of a triplicated Na,K-ATPase gene in a toxin-specialized insect. BMC Evolutionary Biology 17, 256. https://doi.org/10.1186/s12862-017-1097-6.

Meinzer, F., Dobler, S., Donath, A., Lohr, J.N., 2019. Robust reference gene design and validation for expression studies in the large milkweed bug, *Oncopeltus fasciatus*, upon cardiac glycoside stress. Gene 710, 66–75. https://doi.org/10.1016/j.gene.2019.05.032.

Dobler, S., Wagschal, V., Pick, N., Dahdouli, N., Meinzer, F., Romey-Glüsing, R., Petschenka, G., Schuette, K., 2019. New ways to acquire resistance to cardiac glycosides: pyrgomorphid grasshoppers do it differently. Proceedings of the Royal Society B: Biological Sciences. https://doi.org/10.1098/rspb.2019.0883.

Röpcke, M., Lu, S., Plate, C., Meinzer, F., Lisiecki, A., Dobler, S., 2024. Substrate Specificity of ABCB Transporters Predicted by Docking Simulations Can Be Confirmed by Experimental Tests. Molecules 29. https://doi.org/10.3390/molecules29225272.

Acknowledgments

I want to express my gratitude to the many people who helped, motivated, encouraged, inspired, and supported me during this thesis in my native language, so that my thanks come directly and without detours from my heart.

Als aller erstes und ganz besonders möchte ich meiner Betreuerin Susanne Dobler danken. Ich danke ihr dafür, dass sie mir dieses Thema nicht nur anvertraut hat, sondern mich dabei und darüber hinaus stets unterstützt hat. Sei es durch ihre immer offene Tür mit offenem Ohr, das Teilen ihrer Expertise und Erfahrung, Finanzierungen für meine Forschung, der Selbstverständlichkeit von Konferenzteilnahmen bis hin zu weiteren Schritten in meinen beruflichen Lebensweg. Ganz besonders möchte ich ihr danken, dass sie immer an mich geglaubt hat und mir geholfen hat, es auch zu tun. Ich bin sehr dankbar, dass ich vieles von ihr lernen durfte, beruflich, wie auch menschlich. Christian Lohr danke ich für die Bereitschaft und für die Zeit diese Dissertation zu begutachten, sowie den weiteren Kommissionsmitgliedern dafür, ein Teil der Prüfungskommission zu sein. Der ehemaligen „AG Burmester“ möchte ich für die Bereitstellung und Unterstützung bei der Fluoreszenzmikroskopie danken. Auch danke ich Annika Herwig für die Bereitstellung des

verwendeten Kryostats und die Einführung in Gefriergewebeschnitte. Ebenso möchte ich mich bei der ehemaligen „AG Cordellier“ bedanken, besonders bei Mathilde für die Einführung in die Transkriptomassemblierung mittels CLC. Alexander Donath (Zoologisches Forschungsmuseum Alexander Koenig) danke ich sehr für die Assemblierung mittels Trinity. Ein weiteres Dankeschön richtet sich an Anurag Agrawal von der Cornell University und den Botanischen Garten Hamburg für die Bereitstellung der *Asclepias*-Samen und -Samenstände. Ganz herzlich bedanken möchte ich mich bei den Menschen der „AG Dobler“, besonders bei Safaa, Jenny, Paulina, Micha, Renja, Christiane, Marlena, Shab, Kim, Karin, Semra und Vera. Sie haben die Arbeit für mich zu einem Ort des Wachstums und der Freundschaft gemacht. Jenny danke ich besonders für die Einführung in die RNAi- und HPLC-Technik, die Mitbegleitung durch meinen ersten Publikationsprozess und die Hilfe bei der Wanzenzucht. Sie ist, wie Safaa, für mich nicht nur eine brillante Wissenschaftlerin, sondern auch Freundin und Vorbild. Safaa danke ich für die vielen schönen und unterstützenden Momente, Diskussionen und Tipps. Ihre molekularbiologischen Fähigkeiten sind herausragend und ich danke ihr für die Einführung in verschiedene Labortechniken, wie beispielsweise zur Klonierung. Paulina möchte ich besonders für ihre grenzenlose Hilfsbereitschaft, die Motivations- und Frusthelfer, das Teilen ihres Wissens und ihres Zimmers auf Konferenzen, ihre Offenheit und unsere endlosen Gespräche danken. Sie war mir, wie viele andere auch, nicht nur eine unterstützende Kollegin, sondern auch Freundin. Dafür danke ich auch meinem lieben Büronachbarn Micha, der immer ein offenes Ohr und Tipps hatte, ebenso wie das gewisse Süddeutsche-Flair, das sich nach Zuhause anfühlte. Renja danke ich besonders für ihre Expertise und Tipps bezüglich quantitativer real-time PCR, die mir die Etablierung dieser Technik in meine Forschung erleichterten. Christiane danke ich für das Teilen ihres Wissens und ihrer Leidenschaft zu den Lygaeidae, was den Einstieg in das Thema dieser Dissertation nicht nur erleichtert, sondern auch mit Begeisterung und Tatendrang erfüllt hat. Vera, dem Herz des Labors, danke ich für die Hilfe dort, besonders bei den Sequenzierungen und Klonierungen, für ihre unermessliche Problemlösungskompetenz und ihre einzigartige Fähigkeit alles zu finden, besser als die berühmteste Suchmaschine der Welt. Marlena danke ich besonders für ihre Hilfsbereitschaft gerade am Ende dieser Dissertation, die Übernahme der Wanzenzucht in so fähige Hände und, ebenso wie Shab, für Ihre Freundschaft und für unsere wertvollen Gespräche. Semra danke ich besonders für ihre Energie, ihre stetige Hilfe in administrativen Bereichen und die Einführung in die Welt der Kunst. Ein Dankeschön möchte ich auch an Sam dafür richten, dass ich dieses tolle Wanzenfoto verwenden durfte. Ein weiterer Dank geht an die vielen Menschen der Universität Hamburg, mit denen ich während meiner Lehrtätigkeiten zusammengearbeitet habe, besonders an Martin H., Martin

K., Stefanie, Jakob, Ilka, Claudia, Julian, und an die Studenten und BTA-Schüler, die ich auf einem Teil ihrer Reise etwas begleiten durfte. Besonders an Antonia, Nadja, Stefanie und Sebastian. Sebastian danke ich auch, dass er sich mit beeindruckender Expertise mit um die HPLC gekümmert hat. Am Schluss möchte ich von Herzen Lena, Tanja und meiner Familie danken. Meinen Eltern für ihre Unterstützung meinen eigenen Weg zu gehen. Meinem Mann, Sebastian, für mehr als sich in Worten ausdrücken lässt und meiner Tochter, Eleonora, die mich die Welt neu entdecken lässt.

Contribution and Declaration on Oath

Chapter 1: The work presented in Chapter 1 was published in the journal Gene (https://doi.org/10.1016/j.gene.2019.05.032) by Fee Meinzer, Susanne Dobler, Alexander Donath and Jennifer N. Lohr. The authors contributions were as follows: The research was designed by Jennifer N. Lohr, Susanne Dobler and me; I performed the research, analyzed the data and wrote the manuscript; Alexander Donath contributed the transcriptome assembly; all co-authors revised the manuscript.

Chapter 2: The *Ofabcb1* transporter 5' completion and cloning presented in Chapter 2 was performed by Antonia Lisiecki as part of her master's thesis. Sequencing of cloned *Ofabcb1* was conducted by Antonia Lisiecki and Vera Wagschal. Part of the 5' completion of *Ofabcb2* was also performed by Vera Wagschal and David Naubereit as well as cloning of 3’ strand PCR fragments. The Western blot shown was performed together with Paulina Kowalski. Primer for generation of dsRNA were designed by Jennifer N. Lohr and me. A preliminary dsRNA probe testing (data not shown) was conducted by Jennifer N. Lohr.

Chapter 3: The isolation and purification of calactin and calotropin described in Chapter 3 was carried out by Sebastian Gathemann as part of his bachelor's thesis. One biological replicate from mature milkweed seeds for HPLC analysis was extracted by Jennifer N. Lohr.

Artificial intelligence in the form of UHHGPT-4.1 was used to translate sentences and draft sections on defensive fluids and HPLC optimization in Chapter 3 (Dokumentation UHHGPT: Translation Discussion parts chapter 3, 2025). Likewise, a proofreading of the introduction and discussion of the third chapter was carried out (Dokumentation UHHGPT: Proofreading Diskussion Chapter 3, 2025; Dokumentation UHHGPT: Proofreading Introduction Chapter 3, 2025), and the AI was used for brainstorming the content of the introduction of Chapter 3. (Dokumentation UHHGPT: Brainstorming Introduction Chapter 3, 2025). It was further used to generate specific pubmed search strings for literature search during the writing of the general

discussion (Dokumentation UHHGPT: Pubmed strings for literature search for general discussion, 2025) and ChatGPT was used for initial literature overview on two topics (Dokumentation ChatGPT: Literature search topics general discussion, 2025). DeePL was occasionally used to translate or check words/sentences for proper spelling and grammar. The dissertation was section-wise proofread by UHHGPT-5.1 to confirm the correctness of the use of English language (Dokumentation UHHGPT, 2026).

Eidesstattliche Versicherung:

Hiermit versichere ich an Eides statt, die vorliegende Dissertationsschrift selbst verfasst und keine anderen als die angegebenen Hilfsmittel und Quellen benutzt zu haben.
Sofern im Zuge der Erstellung der vorliegenden Dissertationsschrift generative Künstliche Intelligenz (gKI) basierte elektronische Hilfsmittel verwendet wurden, versichere ich, dass meine eigene Leistung im Vordergrund stand und dass eine vollständige Dokumentation aller verwendeten Hilfsmittel gemäß der Guten wissenschaftlichen Praxis vorliegt. Ich trage die Verantwortung für eventuell durch die gKI generierte fehlerhafte oder verzerrte Inhalte, fehlerhafte Referenzen, Verstöße gegen das Datenschutz- und Urheberrecht oder Plagiate.

Affidavit:
I hereby declare and affirm that this doctoral dissertation is my own work and that I have not used any aids and sources other than those indicated.
If electronic resources based on generative artificial intelligence (gAI) were used in the course of writing this dissertation, I confirm that my own work was the main and value-adding contribution and that complete documentation of all resources used is available in accordance with good scientific practice. I am responsible for any erroneous or distorted content, incorrect references, violations of data protection and copyright law or plagiarism that may have been generated by the gAI.

18.01.2026 _____

Haag an der Amper, den Unterschrift